The Early Proterozoic Makganyene Glacial Event In South Africa: Its implication In Sequence Stratigraphy Interpretations, Paleoenvironmental Conditions And Iron And Manganese Ore Deposition.

A thesis submitted in fulfilment of the requirements
for the degree of
DOCTOR OF PHILOSOPHY
of
RHODES UNIVERSITY

By

Stéphane Polteau

December 2004

DECLARATION

All material contained in this thesis represents the original work of the author, except where specific acknowledgement is made to the work of others.

<u>Signed</u>

S. POLTEAU :

December 2004

ABSTRACT

The Makganyene Formation forms the base of the Postmasburg Group in the Transvaal Supergroup in the Griqualand West Basin. It consists of diamictites, sandstones, banded iron-formations (BIFs), shales, siltstones and carbonates. It is generally accepted that the Makganyene Formation rests on an erosive regional unconformity throughout the Northern Cape Province. However this study demonstrates that this stratigraphic relationship is not universal, and conformable contacts have been observed. One of the principal aims of this study is to identify the nature of the Makganyene basal contact throughout the Griqualand West Basin.

Intensive fieldwork was carried out from Prieska in the south, to Danielskuil in the north. In the Sishen and Hotazel areas, only borehole material was available to assess the stratigraphy. The Griquatown Fault Zone delimits the boundary between the deep basin and platform facies. The Koegas Subgroup is only present south of the Griquatown Fault Zone, where it pinches out. However, the transition Griquatown BIFs-Koegas Subgroup occurs in lacustrine deposits on the Ghaap platform (Beukes, 1983). The Griquatown Fault Zone represents the edge of the basin, which corresponds to a hinge rather than a fault zone. The Makganyene Formation rests with a conformable contact on the Koegas Subgroup south of the Griquatown Hinge Zone, and north of it the Makganyene Formation lies unconformably on the Asbestos Hills Subgroup.

The Makganyene Formation displays lateral facies changes that reflect the paleogeography of the Griqualand West Basin, and the development of ice sheets/shelves. The Ghaap platform is characterised by coarse immature sand interbedded with the diamictites. The clasts in this area contain local Asbestos Hills material and no dropstones are present. Such settings are typical of sediments that are being deposited below a grounded ice mass. At the Griquatown Hinge Zone, the sandstone lenses are smaller, and the clasts consist of chert, of which a great number are striated and faceted. In the Matsap area, the presence of dropstones is strong evidence for the presence of a floating ice shelf that released its material by basal melting. Further south, the Makganyene Formation contains stromatolitic bioherms that only form if clastic contamination is minimal and therefore the ice that transported the detritus to the basin did not extend far into open sea conditions.

The base of the Hotazel Formation also contains diamictite levels. Dropstones have been identified, implying a glacial origin. The Hotazel diamictites are interbedded with hyaloclastites and BIFs. The Makganyene glacial event, therefore, was not restricted to the Makganyene Formation, but also included the Ongeluk Formation, through to the base of the Hotazel Formation.

Petrographic studies of the Makganyene Formation and the base of the Hotazel Formation reveal mineral assemblages that are diagnostic of early to late diagenetic crystallisation and of low-grade metamorphism not exceeding the very low green-schist facies. The facies identified display the same sense of basin deepening, from shallow high-energy Hotazel area on the Ghaap platform, to the deep basin in the Matsap area.

Whole-rock geochemical analyses reveal that the elemental composition of the Makganyene Formation is very similar to that of the Asbestos Hills BIFs, which were the most important source of clastic detritus for the Makganyene Formation. However, minor amounts of carbonates of the Campbellrand Subgroup, as well as a felsic crustal input from the Archean granitoid basement, made contributions. On the Ghaap platform, the Makganyene diamictite is enriched in iron, calcium, and magnesium, while in the deeper parts of the basin the diamictites are enriched in detrital elements, such as titanium and aluminium, which occur in the fine clay component. The Hotazel diamictite displays a distinct mafic volcanic input, related to the extrusion of the Ongeluk basaltic andesites, which was incorporated in the glacial sediments.

Sequence stratigraphy is based on the recognition of contacts separating the different systems tracts that compose a depositional sequence. However, because the basal contact of the Makganyene Formation has not been properly identified in previous work, no correct model has been proposed so far. Therefore correlations between the Griqualand West and the Transvaal basins, based on lithostratigraphic similarities and extrapolations of unconformities, have to be reviewed, especially since the publication of new radiometric ages contradict all previously proposed correlations. It is proposed here that the Transvaal Supergroup in the Griqualand West Basin represents a continuous depositional event that lasted about 200 Ma.

The Makganyene glacial event occurred during changing conditions in the chemistries of the atmosphere and ocean, and in the continental configuration. A Snowball Earth event

has been proposed as the causative process of such paleoenvironmental changes. However, evidence presented here of less dramatic glacial conditions, with areas of ice-free waters, implies an alternative to the Snowball Earth event. The paleoenvironmental changes are thought to represent a transition from an anaerobic to aerobic atmosphere, that was responsible for the global cooling of the surface of the Earth. Such a glacial event may have aided in the large-scale precipitation of iron and manganese in areas of intense upwellings.

Table of contents

Acknowledgements

"The credit belongs to the man who is actually in the arena, whose face is marred by dust and sweat and blood; who strives valiantly; who errs and comes short again and again, who knows the great enthusiasms, the great devotions, and spends himself in a worthy cause; who at best, knows the triumph of high achievement; and who, at the worst, if he fails, at least fails while daring greatly, so that his place shall never be with those cold and timid souls who know neither victory nor defeat."

Theodore Roosevelt
"Citizen in a Republic", April 23, 1910

CHAPTER I
Introduction

I.1. Generalities

The rock record of glaciations, although imperfect and incomplete (Eyles and Young, 1994), provides critical paleoclimatic data of the long-term climatic changes (Deynoux, 1994), which reflect thermal perturbations experienced on the surface of the Earth (Young, 1991). The understanding of the present climate, and the climate of the Pleistocene, will some day reveal the complex interplay of astronomic, oceanic, atmospheric, biospheric and lithospheric processes (Deynoux et al., 1994; Eriksson et al., 1998).

Different glacial epochs may have had different triggering and ending causes (Young, 1991). The internal and external processes controlling the climate may have been different during the Proterozoic from those of the Quaternary (Dreimanis, 1983). Still, local or global climatic conditions permitted the formation of mountain glaciers, ice-sheets and ice-shelves during the Proterozoic (Hambrey and Harland, 1981; Dreimanis, 1983). Even if the causes of glaciations during the Proterozoic were different, the general physical rules governing the behaviour of glaciers must have been the same during various times of Earth's history (Dreimanis, 1983; Eriksson et al., 1998). As pointed out by Dreimanis (1983), the only difference between Proterozoic and Quaternary glacial deposits is the nature of sediments interfingering with the glacial sediments.

Only two main periods of glaciation were recorded during the Proterozoic: the 2.4-2.2 Ga Early Proterozoic and the 0.75-0.6 Ga Late Proterozoic. One puzzling aspect is the apparent absence of glacial deposits in the Mesoproterozoic. The Early Proterozoic record includes the oldest widespread glacial event in Earth history on almost all the continents. Glacial sediments have been identified in:

- North America (Symons, 1975; Morris, 1977; Young and McLennan, 1981; Houston et al., 1981; Kurtz, 1981; Young and Nesbitt, 1985; Miall, 1985; Mustard and Donaldson, 1987; and Aspler and Chiarenzelli, 1997),
- Western Australia (Trendall, 1976, 1981),
- South Africa (Visser, 1971; De Villiers and Visser, 1977; and Evans et al., 1997),
- India (Young, 1991; Eriksson et al., 1999),
- Scandinavia (Marmo and Ojakangas, 1984; Young, 1991; Strand and Laajoki, 1993).

Figure I.1 (from Polteau, 2000) shows the distribution of glacial deposits of Early Proterozoic age.

According to Young (1991), the Gowganda Formation, part of the Huronian Supergroup in Canada, is the best known and the most clearly exposed glacial deposit (Miall, 1985; Young and Nesbitt, 1985; Eyles and Young, 1994). In the well preserved Huronian Supergroup of Ontario, Canada, three glacial events have been defined from about 2.5 to 2.2 Ga, each separated by periods of intense chemical weathering (Eyles and Young, 1994).

Thick glacial sequences (from 1000 to 3000 metres), like the Gowganda Formation, have been deposited during periods of continental rifting (Young and Nesbitt, 1985; Young, 1991) whereas thin glacial sequences (300 metres) such as the glacial sediments of Australia and South Africa are more enigmatic.

Rocks commonly associated with Proterozoic glacial deposits are banded iron-formations and carbonates in the Transvaal Supergroup (Beukes, 1983) and in the Rapitan Iron-Formation in Canada (Klein and Beukes, 1993), and manganese ore such as Urucum in Brazil (Urban et al., 1992), Otjosondu in Namibia (Bühn et al., 1992) and the Kalahari Manganese Field in South Africa (Tsikos and Moore, 1998; Tsikos, 1999), which make these glacial deposits significant in metallogenic terms. In this context, there are important questions to be addressed in this study:

> What is, if any, the relationship between the glacial rocks and the stratigraphically associated BIFs, carbonates and manganese deposits?
> How does this relationship compare to younger glacial settings?

The four critical questions of Eyles and Young (1994) in relation with the Earth's glacial record can also be addressed in this study:

> What are the factors that can trigger cold climatic conditions on the planet?
> Why is the record of Precambrian glaciation sporadic?
> Did the Proterozoic glaciers extend to sea level in equatorial latitudes?
> Why do the rocks associated with glacial deposits apparently suggest warm climatic conditions?

Figure I.1. World distribution map of diamictites for the Early Proterozoic (from Polteau, 2000).

I.2. Previous work

Early work in the Griqualand West Basin referred to the existence of a "Griquatown Glacial Member" in the Griqualand West Area (Nel, 1929; Visser, 1944, 1958; Visser, 1971) and it is since 1980 (SACS) that the Makganyene Formation has acquired its current name.

The Makganyene outcrops are truncated by a basal thrust fault, where the Makganyene Formation overlies the Gamagara Formation. A lack of recognition of this thrust led to stratigraphic misinterpretations: such tectonic contact was initially interpreted as a major erosional unconformity (Visser, 1971, 1981; De Villiers and Visser, 1977) and the Gamagara Formation was included in the Transvaal Supergroup succession although the former is younger than the latter. Beukes and Smit (1987) clarified this problem further by demonstrating the existence of a thrust fault (the Blackridge Thrust Fault) and re-establishing the Transvaal Supergroup stratigraphy. However little attention has been brought to the nature of the basal contact of the Makganyene Formation with the underlying strata.

Polteau (2000) agrees with early work (Nel, 1929; Truter et al., 1938; Visser, 1944, 1958) in the presence of a conformable contact at the base of the Makganyene Formation. The nature of this contact (i.e. conformable or unconformable) is crucial for a better understanding of the depositional processes for the Transvaal rock succession.

Five papers (Visser, 1971, 1981, 1994, 1999; De Villiers and Visser, 1977) have been published on the sedimentological and petrographical attributes of the Makganyene Formation during the last 30 years, and were recently followed up by one unpublished M.Sc. thesis (Polteau, 2000). Visser (1971) observed that the Makganyene Formation displays extreme thickness variations, from 3 metres near the Orange River, to 70 metres near Kuruman and to 500 metres in a borehole near Lohatla.

The Makganyene Formation contains a variety of rock types ranging from diamictite to sandstone, iron-formation, shale and stromatolite bioherms. According to Hambrey and Harland (1981), a diamictite is a non-sorted mixture of clasts with or without a muddy matrix. The term "diamictite" does not carry any genetic implication. In the case of the Makganyene diamictite, all previously mentioned authors agreed on a glacial origin due to the presence of faceted and striated pebbles, as well as dropstones. The diamictite units are generally massive to bedded, with subordinate lenses of sandstone and shale. On average, the clasts within the diamictite are heterogeneously distributed within the matrix and are 0.5 to 30 cm in diameter, though larger clasts can also be found (Polteau, 2000). Only the large clasts have striations (Visser, 1999).

The associated lithologies with the diamictite are interpreted as glacial advances/retreats during glacial/interglacial stages of the Makganyene ice age (Visser, 1971; 1981, 1999; De Villiers and Visser, 1977). It is also proposed that glaciation originated on land in the far north (De Villiers and Visser, 1977), probably on the Vryburg rise (Visser, 1971), the sediments were transported towards the south by piedmont glaciers, and that the glaciation was terminated by the onset of volcanism (Ongeluk lava).

The significance of a glacial deposit in the Transvaal Supergroup carries important genetic implications for associated iron and manganese deposits in the Griqualand West Basin, but also in the Precambrian in general. As shown by Klein and Beukes (1993), banded iron-formations (BIFs) were deposited during two major periods; the Early and Late Proterozoic, and both periods contain glaciogenic deposits. In the Rapitan Iron-Formation of Canada, but also in the Makganyene Formation, dropstones are present in the banded iron-formations (Klein and Beukes, 1993; Polteau, 2000), which make them coeval with glaciation. Tsikos (1998, 1999), Polteau (2000) and Moore et al. (2001) stressed the role played by a glacial event in the formation of the Kalahari Manganese Field in the Griqualand West Basin.

Evans et al. (1997) demonstrated that the Makganyene Formation was deposited in equatorial latitudes. Most of the other glaciogenic deposits of Precambrian age around the world were also deposited, as a rule, at low latitudes (Williams, 1993). This is an apparent paradox in Precambrian glacial climate which could be explained either by unusually high obliquity of the Earth (over 54°) (Williams, 1993), or by the Earth frozen from pole to pole, commonly known as the Snowball Earth hypothesis (Kirschvink, 1992).

I.3. Aims of this study

This project represents a regional extension of the work done by Polteau (1999, 2000), Moore et al. (2001) and Polteau and Moore (2002). The study undertaken by Polteau (1999, 2000) was restricted to the Rooinekke Mine area.

This field-based project consists of mapping of the Makganyene Formation between its southern occurrences near Prieska, and its northern outcrops observed in the vicinity of Danielskuil and Boshoek. One emphasis has been the assessment of the basal contact of the Makganyene Formation throughout the Griqualand West Basin, since it is crucial to determine the relationship of the Makganyene diamictite with the underlying rocks of the Koegas Subgroup and the Griquatown Formation, and to confirm the presence of a major unconformity or not (Beukes, 1983; Moore et al., 2001). Borehole core intersections of the

Makganyene Formation at the Sishen and Hotazel mines (where the Kalahari sand covers outcrops) were also examined in this regard.

Petrographic studies of the Makganyene Formation were undertaken in order to assess the mineral composition of the different rock types of the Makganyene Formation, and thus provide insight into the various metamorphic, diagenetic and depositional processes. Some fine-grained diamictites immediately overlying the Ongeluk lava were investigated in order to identify whether or not these have a glacial origin and are thus related to the same cold-climate event.

The geochemical signature of the Makganyene Formation was assessed using both major and trace elements of selected samples to evaluate elemental affiliations in the minerals forming the Makganyene Formation; potential source rocks; sorting processes; and physico-chemical conditions during formation and diagenesis. Certain chemical characteristics of the depositional environment were evaluated using stable isotope geochemistry (C,O), in order to examine changes in depositional conditions across the entire Transvaal Supergroup.

This Early Proterozoic glaciation, also present in other parts of the world, is proposed to have appeared during a global oxygen rise that was associated with the sudden deposition of iron as BIFs, as well as the world-class deposit of the Kalahari Manganese Field (Tsikos, 1999). The Late Proterozoic glacial event was also accompanied by the deposition of iron and occasionally manganese, and was followed by dramatic changes in biosphere evolution in the Phanerozoic (Williams, 1994). Both Proterozoic glacial events can provide clues to these major changes in the geological environment. The environmental control of the Makganyene glacial event in the Early Proterozoic will similarly be assessed, with emphasis on the deposition of iron and manganese-rich chemical sediments on the Kaapvaal Craton.

I.4. Geology of the Transvaal Supergroup

I.4.1. The Transvaal Supergroup

As shown in figure I.2, the Late Archean-Early Proterozoic Transvaal Supergroup is preserved in the Transvaal and Griqualand West Basins in South Africa, and in the Kanye Basin in southern Botswana (Eriksson et al., 1995). These structural basins (Eriksson et al., 1995) developed between 2.7 to 2.1 Ga on the northeastern and western parts of the Kaapvaal Craton (Tsikos, 1999).

Stratigraphic correlations between these three basins have been made to some degree (Cheney et al., 1990; Eriksson et al., 1993; Cheney and Winter, 1995; Cheney, 1996). Recent studies led to the replacement of the name "Griqualand West Supergroup" with that of the "Transvaal Supergroup in the Griqualand West Basin" (Geobulletin, 1995).

For the purposes of this study, the stratigraphy of the Transvaal Supergroup in the Griqualand West and Transvaal structural basins will be described.
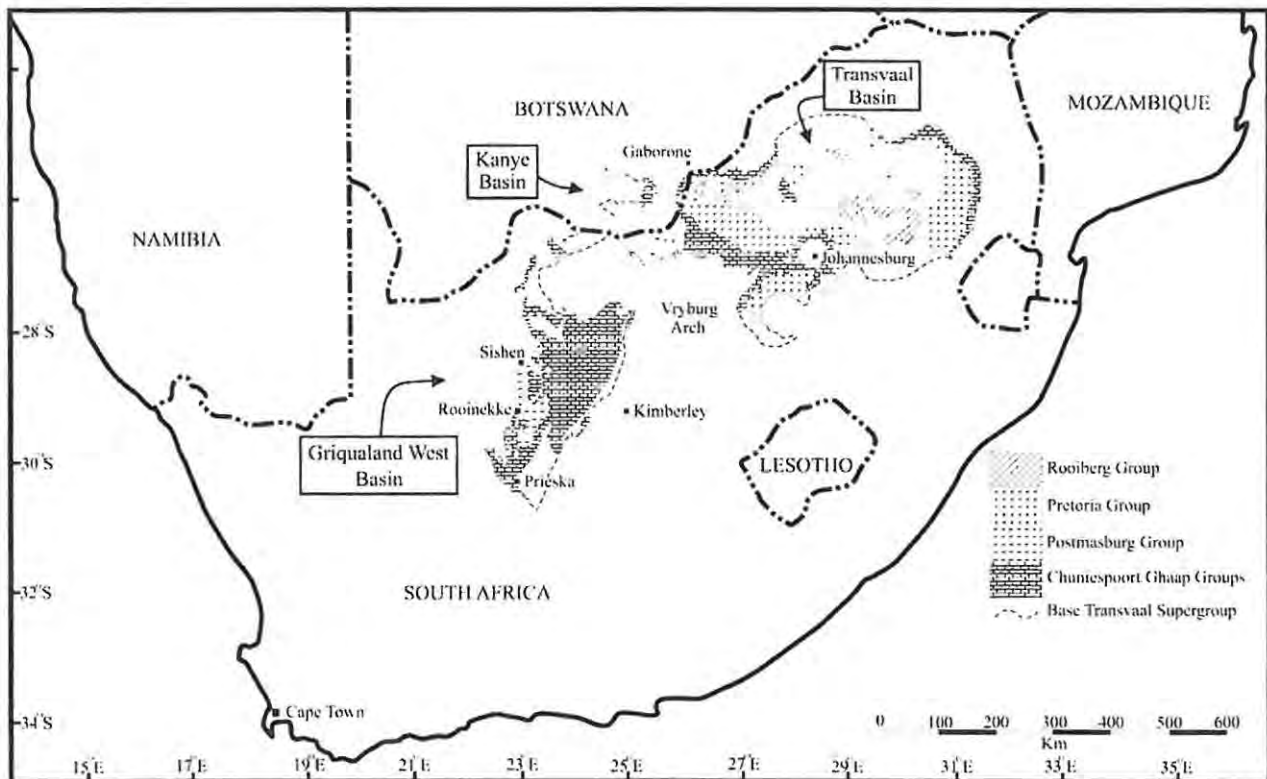
Figure I.2. Distribution of the Transvaal Supergroup on the Kaapvaal Craton (Moore et al., 2001)

I.4.2. The Transvaal Supergroup in the Griqualand West Basin

The Transvaal Supergroup in the Griqualand West Basin is delimited to the west by a sharp tectonic contact that separates it from the easternmost tectonic block of the Namaqualand Metamorphic Province, also known as the Kheis Province (Stowe, 1986). This contact represents the western margin of the Kaapvaal Craton. To the south, the Transvaal Supergroup is overlain by the Paleozoic-Mesozoic Karoo Supergroup along a regional unconformity. To the east, the Transvaal Supergroup has been extensively eroded down to Archean basement. The geographical extent of the Griqualand West Basin is shown in figure I.2 (from Moore et al., 2001).

Table I.1 (after Beukes and Smit, 1987) shows the main stratigraphic subdivisions of the Transvaal Supergroup. The names of formations of the Campbellrand and Schmidtsdrif Subgroups have been omitted for simplicity, as this study focuses on the Koegas Subgroup and Postmasburg Group. The colours have been added to emphasize the symmetrical nature of carbonates and BIFs, stratigraphically above and below the Makganyene and Ongeluk Formations.

Supergroup	Group	Subgroup	Formation	Lithology	Approx. thickness in m.
Transvaal	Postmasburg	Voëlwater	Mooidraai (2.394 Ga)	Carbonate, chert	300
			Hotazel	BIFs, Mn	250
			Ongeluk	Andesitic lava	900
			Makganyene	diamictite	50-150
	Ghaap	Koegas	Rooinekke	BIFs, dolomite	100
			Naragas	Shale, siltstone	240-600
			Kwakwas	Riebeckite slate	
			Doradale	BIF	
			Pannetjie	Quartz wacke, shale	
		Asbesheuwels	Griquatown (2.432 Ga)	Clastic-texture BIFs	200-300
			Kuruman (2.465 Ga)	Microbanded BIFs	150-750
		Campbellrand	(2.557 Ga)	Carbonate, shale, chert	1500-1700
		Schmidtsdrif	(2.642 Ga)	Shale, quartzite, lava, carbonate	10-250

Table I.1. Simplified stratigraphic subdivisions of the Transvaal Supergroup in the Griqualand West Basin (modified after Beukes and Smit, 1987; ages from Cheney and Winter, 1995; Eriksson et al., 1993, 1995; Cheney, 1996; Romer and Bau, 1998; Bau et al., 1999; Martin et al., 1998). The colours (light orange=carbonate, red=BIFs, blue=diamictites/volcanics) refer to lithologies, and emphasise the symmetrical nature of the Transvaal Supergroup.

According to Grobbelaar et al. (1995), and as shown in table I.1, the Transvaal Supergroup in the Northern Cape Province consists of clastic and chemical sediments of the Ghaap Group, followed by a silicilastic-volcanic sequence at the base of the Postmasburg Group, and chemical sediments of the Voëlwater Subgroup at the stratigraphic top.

The base of the Ghaap Group (Schmidtsdrif Subgroup) directly overlies either crystalline Archean basement or lavas of the Ventersdorp Supergroup along a regional unconformity (Beukes, 1983). The predominantly clastic nature of the Schmidtsdrif Subgroup is in contrast with the rest of the Ghaap Group. In this study, the Schmidtsdrif Subgroup is excluded from the Transvaal Supergroup because these protobasinal rocks are more related to the Ventersdorp and Limpopo events even if others regard it as basal part of the Transvaal Supergroup (Catuneanu and Eriksson, 1999, Eriksson et al., 2001).

The Campbellrand Subgroup consists of a thick succession of stromatolitic carbonates, which are in turn overlain by a transgressive Asbestos Hills Subgroup (or in Afrikaans, the Asbesheuwels Subgroup) (Grobbelaar et al., 1995). The Asbestos Hills Subgroup is composed of iron-formations divided into two different formations: the orthochemical Kuruman Formation, and the allochemical Griquatown Formation (Beukes, 1983). Developed only in the south and southwestern parts of the basin, the Koegas Subgroup consists of a mixed sequence of terrigeneous clastic sediments with subordinate iron-formations, dolomite bioherms and lavas (Beukes, 1983).

The base of the Postmasburg Group is developed throughout the basin and is represented by the Makganyene Formation. The latter consists of a glacial diamictite unit resting conformably on the Koegas Subgroup in the Rooinekke Mine area (Polteau, 2000), and unconformably on the Griquatown Formation elsewhere. The Makganyene Formation is draped by a thick succession of continental flood-type basaltic andesites of the Ongeluk Formation (Grobbler and Botha, 1976; Tsikos, 1999). The Voëlwater Subgroup, conformably overlying the Ongeluk Formation is developed only in the northern part of the Griqualand West Basin. It is divided into two distinct formations; namely the Hotazel and Mooidraai Formations. The Hotazel Formation comprises three manganese ore beds interbedded with iron-formations, with the lowermost manganese bed being extensively mined (Dunn et al., 1980; Beukes, 1983; De Villiers, 1983; Kleyenstrüber, 1984; Dixon, 1985; Nel et al., 1986; Miyano and Beukes, 1987; Beukes et al., 1995; Gutzmer and Beukes, 1996, 1997; Gutzmer et al., 1997; Tsikos, 1994, 1999; Tsikos and Moore, 1997, 1998). A gradational contact separates the Hotazel Formation from the Mooidraai Formation (Bau et al., 1999; Tsikos, 1999). The Mooidraai Formation consists of limestone, dolomite and chert (Tsikos, 1999).

This formation is the topmost preserved part of the Transvaal Supergroup present in the Griqualand West Basin and is overlain unconformably by the Gamagara and Mapedi Formations of the Olifantshoek Supergroup.

The full sequence of the Transvaal Supergroup in the Griqualand West Basin was deposited over about 200 Ma, as demonstrated by radiometric age constrains displayed in Table I.1.

I.4.3. The Transvaal Supergroup in the Transvaal Basin

The Transvaal Supergroup is preserved in the Transvaal Basin on the Kaapvaal Craton as shown in figure I.2 (Eriksson et al., 1993). The simplified stratigraphy of the Transvaal Supergroup in the Transvaal Basin is shown in table I.2 (modified after Catuneanu and Eriksson, 1999; and Polteau, 2000).

Supergroup	Group	Formation	Lithology	Approx. Thickness in m.
Transvaal	Pretoria	Steenkampsberg/Houtenbek	Sandstone, shale, lavas	1500
		Lakenvlei/Nederhorst		
		Magaliesberg/Vermont		
		Silverton		
		Daspoort		
		Strubenkop		
		Dwaalheuwel/Droogedal		
		Hekpoort (2.224 Ga)	Andesitic lava	250-900
		Boshoek	Conglomerate, sandstone, shale, lavas	1000
		Timeball Hill (2.35 Ga)		
		Rooihoogte/Duitschland		
	Chuniespoort	Penge (2.432 Ga)	Iron formations	0-500
		Malmani (2.552 Ga)	Carbonate, shale, chert	1500-1700
		Black Reef (2.642 Ga)	Shale, quartzite, lava, carbonate	10-100

Table I.2. Simplified stratigraphic subdivisions of the Transvaal Supergroup in the Transvaal Basin (modified after Catuneanu and Eriksson, 1999; Polteau, 2000; ages from Cheney and Winter, 1995; Eriksson et al., 1993, 1995; Cheney, 1996; 1999; Martin et al., 1998). The colours (light orange=carbonate, red=BIFs, blue=diamictites/volcanics, green=clastics) refer to lithologies, and emphasise the unsymmetrical nature of the Transvaal Supergroup in the Transvaal Basin.

The base of the Transvaal Supergroup in the Transvaal Basin is represented by the clastic Black Reef Formation, which unconformably overlies Archean basement rocks. The Black Reef Formation grades into the chemical Chuniespoort Group, which consists of a carbonate platform (Malmani Subgroup) draped by iron-formations (Penge Formation). The Penge Formation is erratically preserved (Button, 1986) due to the presence of a major

erosional unconformity along which the clastic Rooihoogte/Duitschland Formations rest, in places, directly on the dolomites of the Malmani Subgroup (Button, 1986). The Rooihoogte/Duitsland Formations are lateral equivalents (Coetzee, 2002) and form the basal unit of the Pretoria Group although in the Duitschland type area it is unconformably overlain by the Rooihoogte Formation, which onlaps onto older units laterally. A gradational contact separates the Rooihoogte/Duitsland Formations from the clastic Timeball Hill Formation (Catuneanu and Eriksson, 1999, Eriksson et al., 2001). A total of another two erosional unconformities are present in the Pretoria Group. The first separates the Timeball Hill Formation from the Boshoek and Hekpoort Formations, and the second separates the Hekpoort Formation from the rest of the Pretoria Group (Coetzee, 2001).

As shown by the radiometric ages displayed in table I.2 (modified after Catuneanu and Eriksson, 1999; Polteau, 2000), the base of the Transvaal Supergroup in the Transvaal Basin is dated at 2.642 Ga. The topmost part of the Transvaal Supergroup is estimated to be older than 2.053 Ga which is the age of the mafic igneous rocks of the Bushveld Complex (Beukes, 1983), but younger than the 2.224 Ga Hekpoort Formation (Cornell and Schütte, 1995; Reczko et al., 1995). Therefore, deposition of the Transvaal Supergroup in the Transvaal Basin appears to have lasted approximately 550 Ma.

Chapter II
Geology of the Makganyene Formation

II.1. Introduction

The Makganyene Formation is frequently not well exposed (Rogers and du Toit, 1909). Thus field localities were carefully selected using a combination of the South African Geological maps (1/250 000 scale of the 2922 Prieska and 2822 Postmasburg sheets) and aerial photographs (1/50 000 scale). The following steps were followed:

> identification of all outcrops of the Makganyene Formation present on the Prieska and Postmasburg geological maps;

> location of those outcrops on the flight plan (Job 844 and Job 962, 1981 and 1993 respectively);

> identification and location of the Makganyene Formation outcrops on the aerial photographs using the geological maps;

> selection of localities suitable for the study of the Makganyene Formation.

Field localities were selected from the aerial photographs when hills were obviously composed of the Makganyene Formation and over/under-lying formations. Most of the outcrops mapped on the Prieska and Postmasburg sheets was sufficiently well exposed to allow for objective interpretations. Fieldwork completed by the author for his M.Sc. (Polteau, 2000) will not be described here, but will be included in the conclusions.

The best outcrops of the Makganyene Formation are generally located at the foot of prominent escarpments formed by the Ongeluk beds, usually situated at the closures of synclinal folds. Using the above procedure, a total of six localities were selected:

> the Folmink 38, Klooffontein 332 and Naragas 333 farms form locality A, situated at the closure of the southern most syncline along the Orange River between Prieska and Koegas;

> the Juanana 145, Heynskop 342 and Grassmead 336 farms form locality B, situated 15 km west of Niekerkshoop at the foot of Die Rooiberg;

> the Kloof 143 farm forms locality C, situated 15 km north of Niekerkshoop on the Griquatown road;

> the Punt 128, Dunmore 131 and Schans 127 farms form the locality D, situated approximately mid-way between Griquatown and Niekerkshoop;

➤ the Taaibosch Fontein 2, Middelplaats 6, 5, Koertje Smits Dam 3, Annex Taaibosch, Griquatown Erf 261, Moos Fontein 18, 55, Reliance 347 farms form locality E, situated 10km west of Griquatown;

➤ the farm Humansrus 469 forms locality F, situated approximately 35 km east of Postmasburg on the Kimberley road.

Besides these six localities, other outcrops were investigated, but they were not described in great detail because of their lack of suitable exposure. These additional localities are:

➤ the farms Stinkwater 161 and Eland 162 form locality W, situated 30 km north of locality A along the same north-south elongated syncline;

➤ the Prairie 98 and Eden 97 farms form locality X, situated 40 km west of Griquatown;

➤ the Kameelhoek 478 farm forms locality Y, located 20 km west of Postmasburg;

➤ the Skeitfontein 252 farm forms locality Z, situated 20 km northwest of Danielskuil.

An additional two localities were logged and sampled for analytical work from boreholes kindly made available by the Sishen Iron Mine (Kumba Resources) and the Hotazel Manganese Mine. All these localities have been located in the regional geological map of the Griqualand West Basin as illustrated in figure II.1. The following paragraph describes field observations made at these localities. This was necessary for correlations between the different localities, in order to formulate a depositional model for the Makganyene Formation.

II.2. Field Observations

II.2.1. Introduction

Fieldwork started in mid-2000 and was finally completed by the end of 2001. Descriptions of the different localities follow the outcrop patterns of the encountered Makganyene and other formations, from the south to the north. Maps and profiles are presented for each locality.
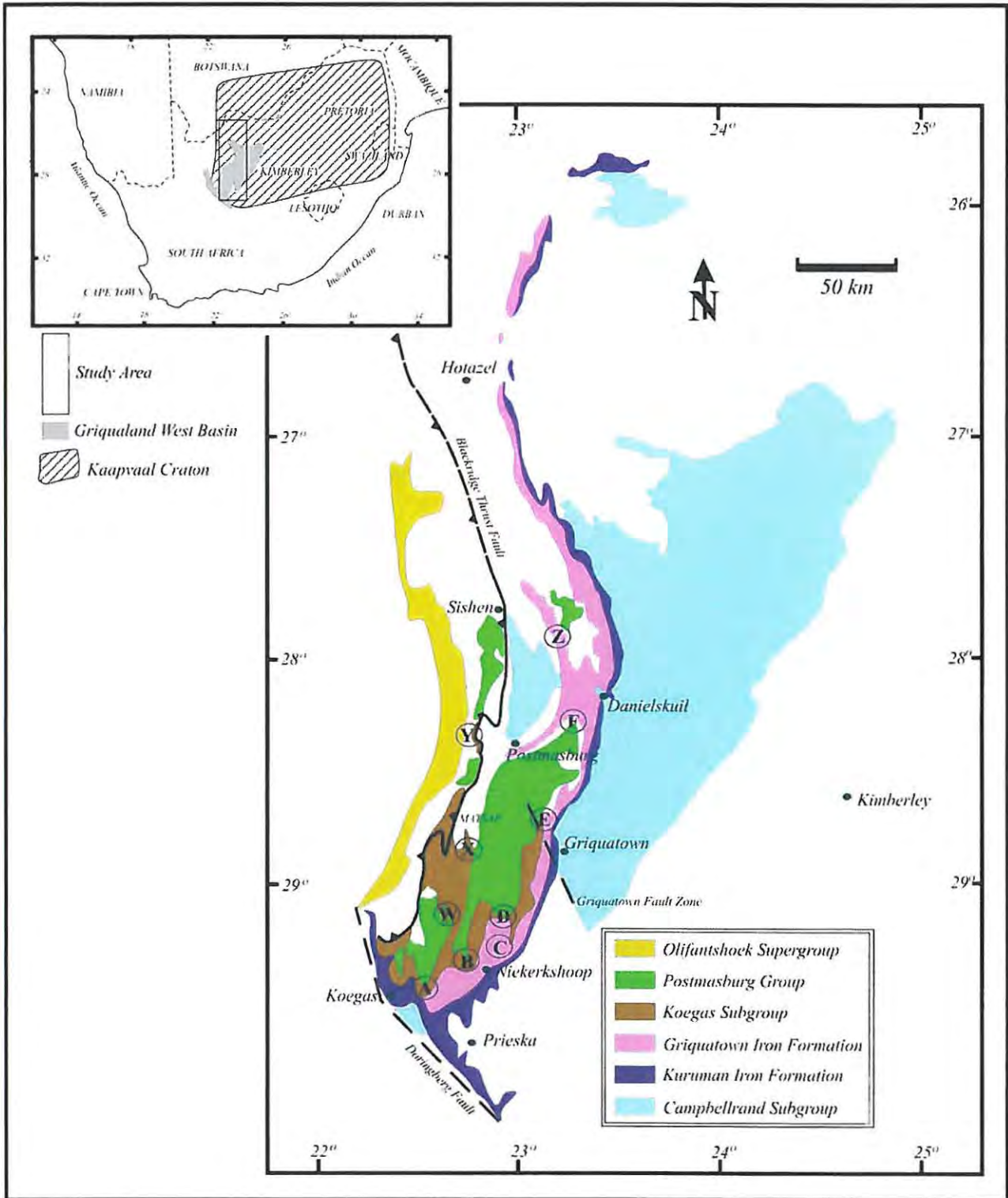
Figure II.1. Geological sketch map showing the outcrop distribution of the Ghaap and Postmasburg Groups over the Griqualand West Basin. Localities investigated are the circled letters from A to F and W to Z. Map after Horstmann and Hälbich (1995).

II.2.2. Locality A

The locality A, shown on figure II.1, is situated along the Orange River between Niekerkshoop and Koegas at the closure of a syncline formed by the Ongeluk Formation.

Figure II.4 is a representation of the geology at locality A. The succession consists (from older to younger) of the Doradale, Naragas, Rooinekke, Makganyene and Ongeluk Formations. All formations dip at about 25° towards the axis of the syncline along its flanks. At the fold closure, the strata are sub-horizontal and have an average plunge of 5° to the north.

A total of five faults has been mapped. Three of them have a general NNW-SSE direction, with a maximum displacement of 10 meters. They were later utilised as conduits for dolerite dyke emplacements of Karoo age. The two most significant faults show white recrystallised quartz, enhancing the fault contour in aerial photographs, with strikes of approximately E-W for one and NNW-SSE for the other. The first fault displaced the Doradale Formation to a higher level than the Rooinekke Formation, indicating that the vertical displacement exceeds a 100 meters. The second fault does not have a significant displacement, but shows strong brecciation effects on the country rock.

In locality A, the Doradale Formation crops out along the Orange River on its northern bank. The Doradale Formation consists essentially of yellowish/brown laminated shale. No stromatolitic bioherms were observed in this locality. Its basal contact was not observed, so the true thickness of this formation could not be deduced.
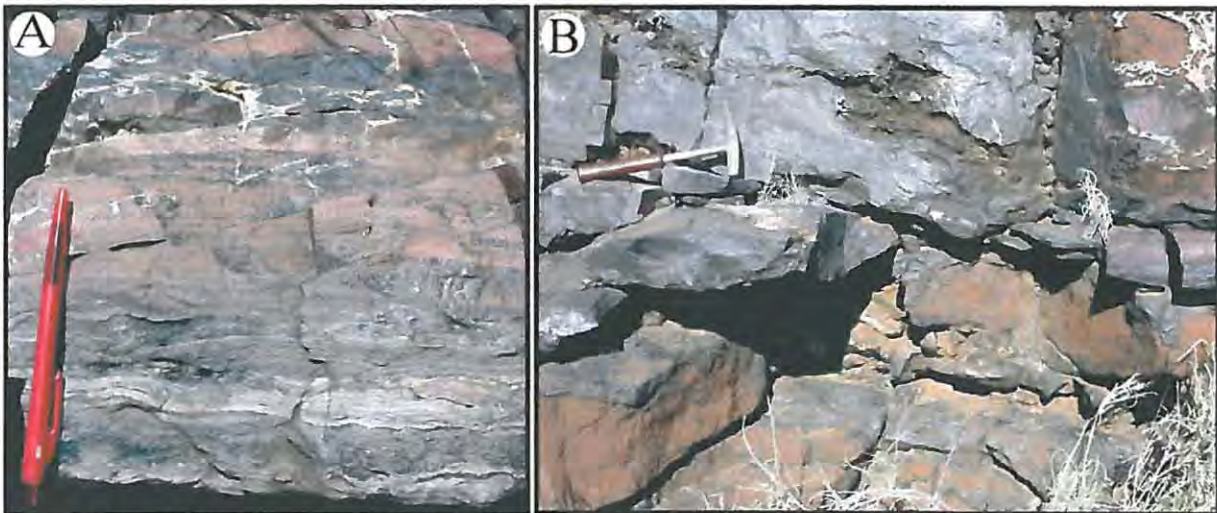
Figure II.2. A: mixed origin of the Rooinekke Iron Formation: the base has wavy, silty laminations grading into planar silty laminations and finally into chemically precipitated red Fe-lutite. **B**: calcareous pods, consisting almost entirely of calcite, have been compacted and deformed during burial by the black-coated band-lutite.

The Naragas Formation is poorly exposed in the area, except where the more weathering-resistant Rooinekke Formation overlies it. The Naragas Formation consists of yellow-green shales with interbedded grey siltstone beds. Its thickness is approximately 130 meters.

The Rooinekke Formation starts at the first iron formation, which is usually a hematite band-lutite with a clear clastic influence (see figure II.2.A). The Rooinekke Formation in this area, consists of thin stromatolitic bioherms (50 centimetres or less in thickness), which have been compacted and deformed by the interbedded black-coated band-lutite during burial (see figure II.2.B). On the aerial photographs, the Rooinekke Formation has a distinctive cream colour due to the presence of abundant stromatolitic bioherms that form half of the formation thickness at locality A. Towards the top of the Rooinekke Formation, disc-lutites and shale beds start to appear, followed by thin tuffaceous beds. The total thickness of the Rooinekke Formation is approximately 100 meters.

The Makganyene Formation in this locality is generally well exposed. The base of the Makganyene Formation is taken at the first level of diamictite encountered. At locality A, the first level of diamictite occurs above a cherty bed of the Rooinekke Formation, and the contact is conformable. The rest of the Makganyene Formation consists of orange shale, jasperoid, calcareous/stromatolitic diamictites followed by manganiferous domal structures finally overlain by another 2 meter-thick diamictite at the top.

The calcareous diamictite resembles stromatolitic bioherms when not bearing any clasts (see figure II.3.C), displaying sharp bottom contact with the clast-bearing diamictite (shown in figure II.3.A, B, C, D) and occurs as domal structures (shown in figure II.3.A). When the calcareous domes contain clasts, they are commonly brecciated (see figure II.3.D).

The manganiferous domes have a characteristic dark colour (shown in figure II.3A, E, and F). They appear folded (see figure II.3.E) with alternating calcite/manganese/iron-rich bands interpreted as primary features formed on the basin floor because they are found as reworked clasts in the overlying diamictite bed at the top of the Formation (see picture F from figure II.3).

Just below the Ongeluk Formation, one tuff bed containing stacked graded cycles (2 to 3cm thick) is present. The clasts within the Makganyene Formation are generally angular chert pebbles with a maximum diameter of 20 centimetres. The Makganyene Formation at locality A is 14.5 meters thick.
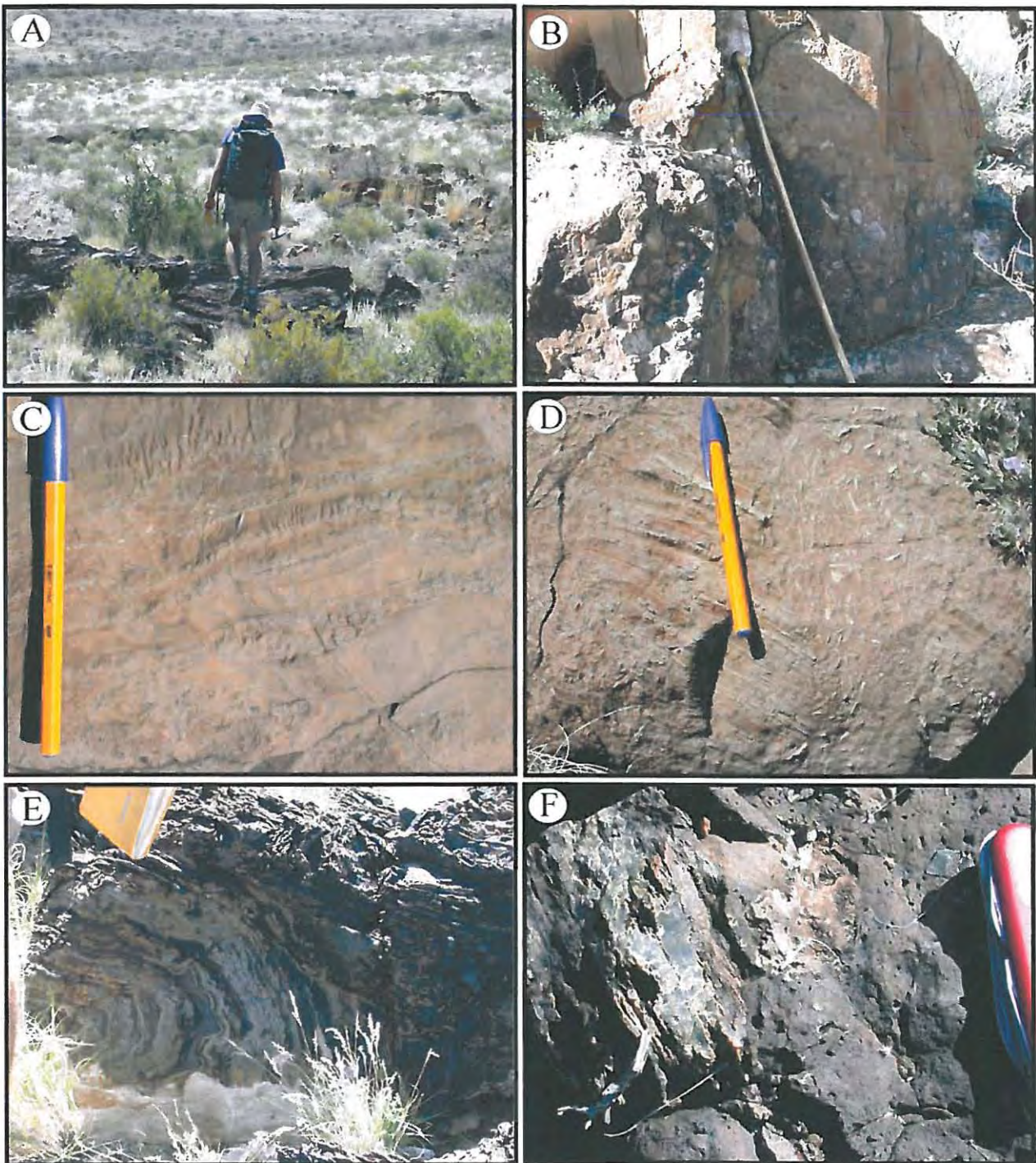
Figure II.3. A: stromatolitic (cream) and manganiferous domes (dark) are present within the diamictites. **B**: sharp contact between the diamictites and the overlying calcareous dome. **C**: possible biogenic laminations. **D**: brecciated stromatolitic material. The displacement has been very small due to the stickiness of the matrix. **E**: folding of the manganiferous dome overlying the stromatolitic domes. **E**: clast from the manganiferous dome found in the immediately overlying diamictite.

The Ongeluk Formation consists of monotonous, massive greyish-green amygdaloidal andesitic lava that is approximately 900 meters thick. Its appearance is fairly uniform in the field and it forms most of the prominent escarpments. According to Grobler and Botha (1976), hyaloclastic units composed of large, massive lava fragments and smaller angular glass fragments have been described, but have not been encountered during this study.

A Makganyene Formation-like outcrop was mapped within the Doradale Formation, in the southern part of locality A (see figure II.4). This outcrop corresponds to a lens of diamictite two meters thick in its thickest part, and about one hundred meters long. This lens is black-coated and contains cherty angular clasts up to 15 centimetres in diameter, similar to the diamictites below the Ongeluk lava. The presence of diamictite in the Doradale Formation is not due to faulting or thrusting, but is part of the sedimentary package of the Koegas Subgroup, indicating possible glacial conditions during its development.
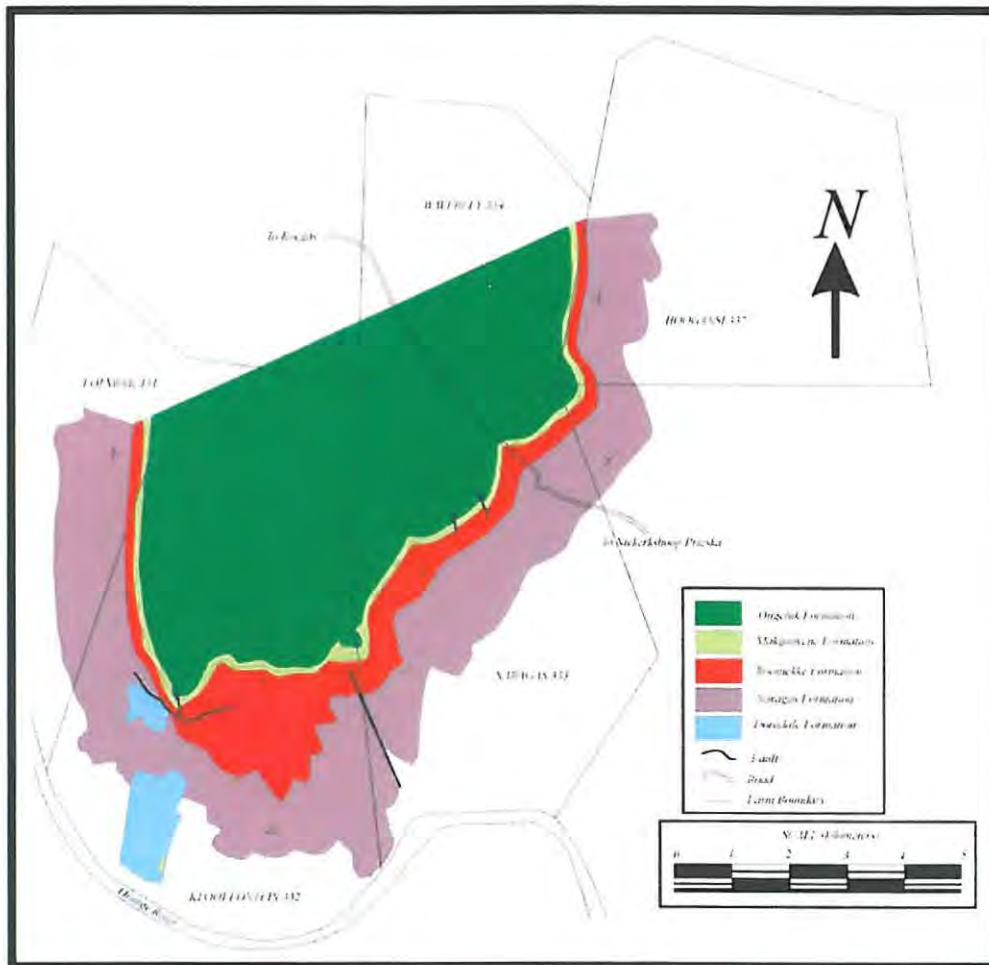
Figure II.4. Geology of locality A.
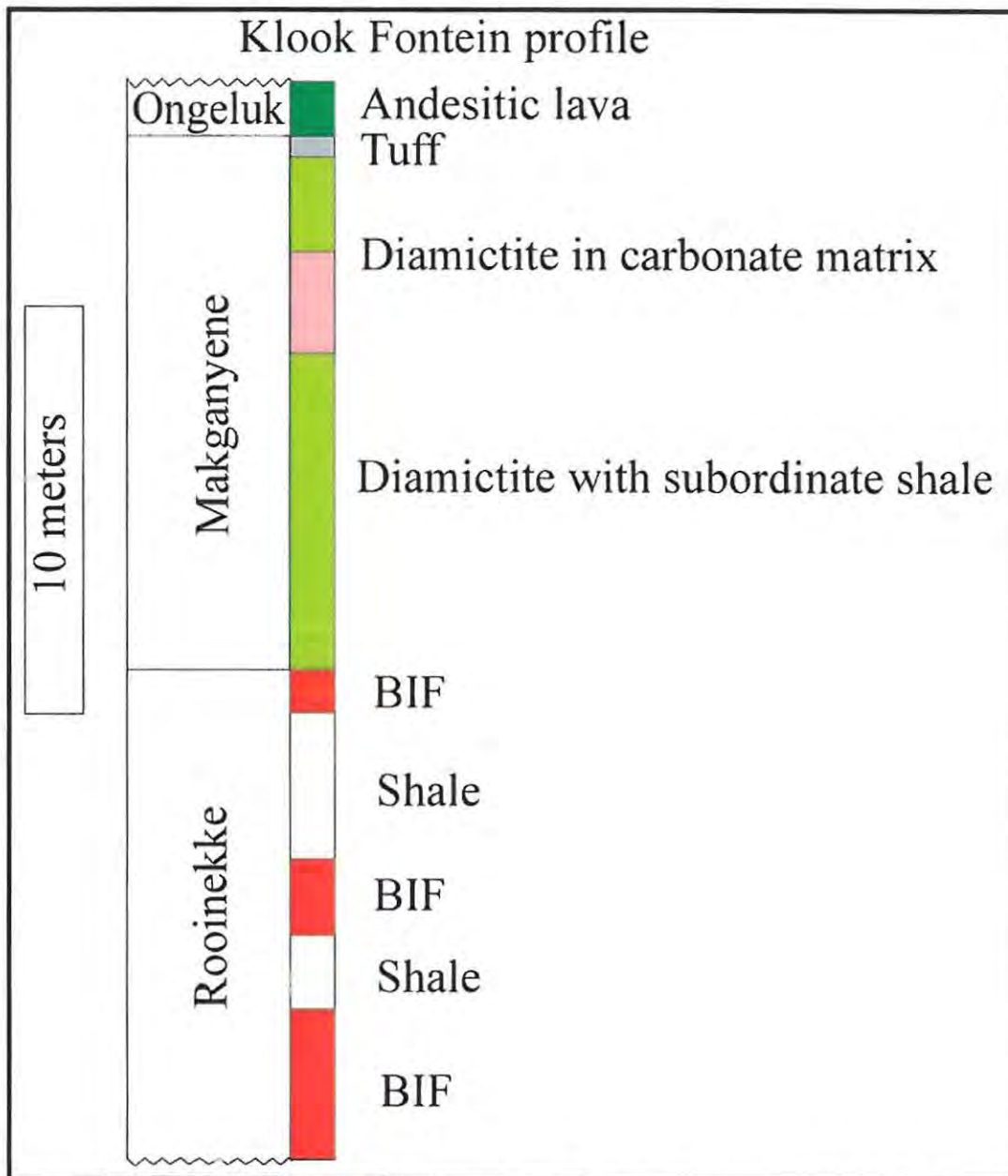
Figure II.5. Typical section of the Makganyene Formation at locality A. Note that the Rooinekke Formation has not been completely represented, and its true thickness is about 100m.

Figure II.5 shows the details of a typical section through the Makganyene Formation and the uppermost 10 meters of the Rooinekke Formation from locality A. The base of this section is underlain by about 80 meters of thin, interbedded stromatolitic bioherms with black-coated hematite-band-lutite/silty units of the Rooinekke Formation.

II.2.3. Locality B

As shown in figure II.1, locality B is situated in a similar setting to locality A, at a closure of a syncline capped by the Ongeluk Formation. The hill formed by the lava was named Die Rooiberg (red hill) with an elevation of 1360 meters, compared to the 1100 meters elevation for the surrounding plain. The geology of locality B is illustrated in the map shown in figure II.7. The beds dip gently towards the lava, generally sub-horizontally. This succession of strata has only been disturbed by one fault situated on Omdraai 139 that has a NW-SE strike, bringing the Rooinekke Formation into contact with the Ongeluk Formation. The vertical displacement is therefore approximately 50 meters.

The Naragas Formation is similar to the Naragas lithologies of locality A. At all localities, it consists of generally one-meter-thick, massive to parallel- and cross-laminated beds of grey-blue siltstone (see figure II.6.A), interbedded with reddish-green laminated shales (see figure II.6.B). At locality B, the Naragas Formation contains two stromatolite bioherms, 70 cm thick, interbedded with 6 meters of green shales. The upper stromatolite bioherms is overlain by black shale which are stratigraphically situated below the first manganese-coated (black) hematite band-lutite of the Rooinekke Formation.

The Rooinekke Formation resembles the Rooinekke outcrops of locality A. It comprises mainly thin stromatolitic bioherms (less than 50 cm thick) interbedded with black-coated hematite band-lutite associated with silty units, implying synchronous, mixed chemical and clastic conditions. The top of the formation differs from locality A, as black-coated conglomeratic beds are found just below the Makganyene Formation. In these conglomerates, well rounded and flattened chert clasts were originally composed of calcite (ghost structures present) which were subsequently entirely silicified probably before the formation of the conglomerate. The thickness of the Rooinekke Formation is similar to locality A (100 meters).

The Makganyene Formation is 10 meters and thick overlies the Rooinekke Formation conformably. In this locality, massive diamictite beds represent the bulk of the Makganyene Formation. Stromatolite bioherms are present (shown in figure II.6.C), as well as diamictite with a calcareous matrix (see figures II.6.D and E). These calcareous bodies are bioherms that incorporated ice-rafted debris (see figure II.6.C and E) suggesting a quiet environment with periods of high clastic input. All the beds are massive, lacking internal sedimentary structures, besides one graded bed of diamictite near the base. The top of the Makganyene Formation is overlain by a one-meter thick bed of graded cycles of volcaniclastic origin, each cycle being one to three centimetres thick, but at locality B, it is interbedded with thin calcareous layers.
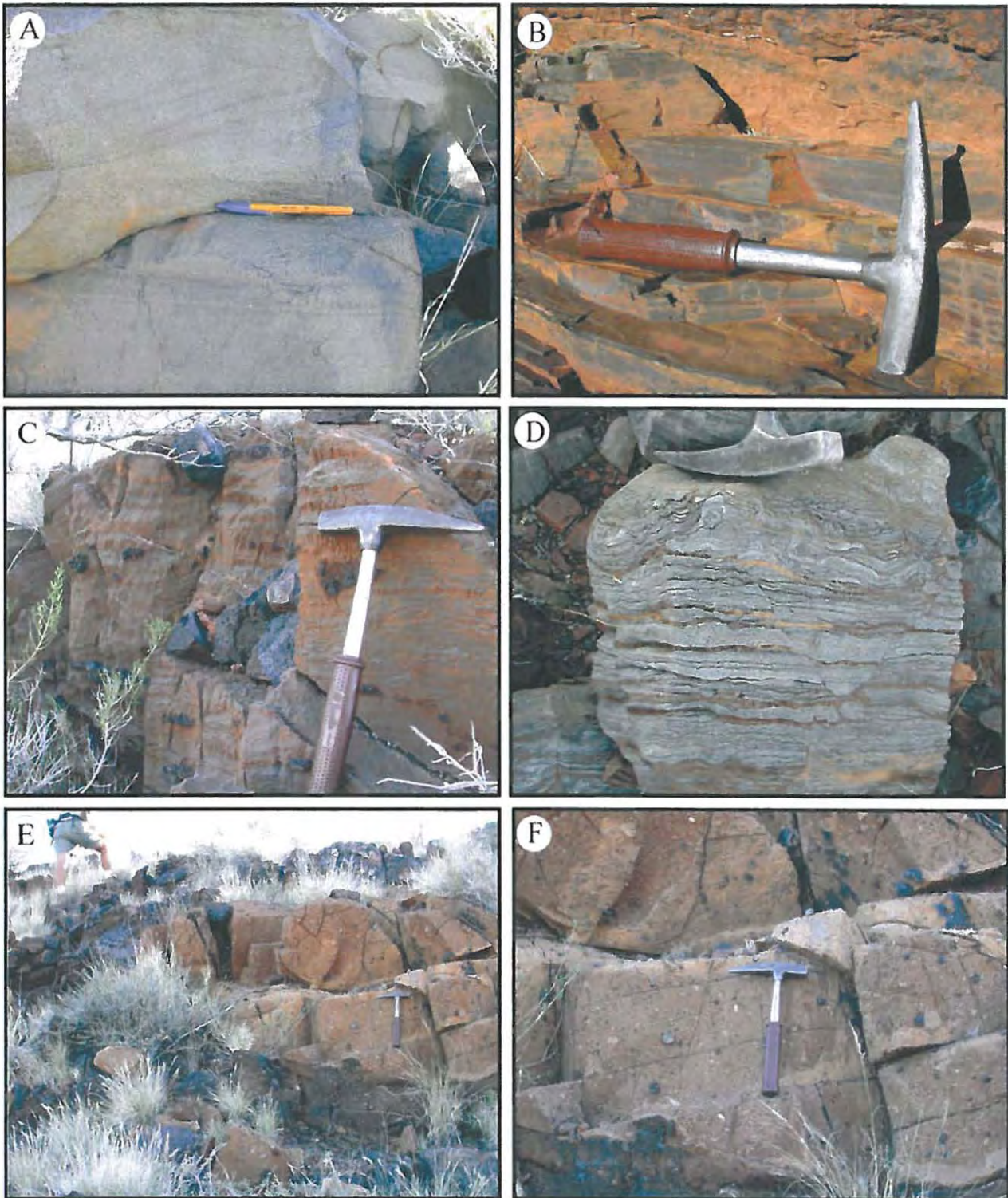
Figure II.6. A: planar- and cross-laminations in Naragas siltstone. **B**: typical aspect of the reddish-green Naragas shales. **C**: stromatolitic bioherm with no clasts. **D**: diagenetically transformed stromatolite. **E**: occurrence of clast-bearing stromatolitic bioherms within the diamictites of the Makganyene Formation **F**: close-up of E with the chert and carbonate clasts.

Conformably overlying the Makganyene Formation is the Ongeluk Formation, which is a monotonous, 900 meters-thick massive andesitic lava throughout the project area.

A typical section of rocks from locality B is presented in figure II.8.
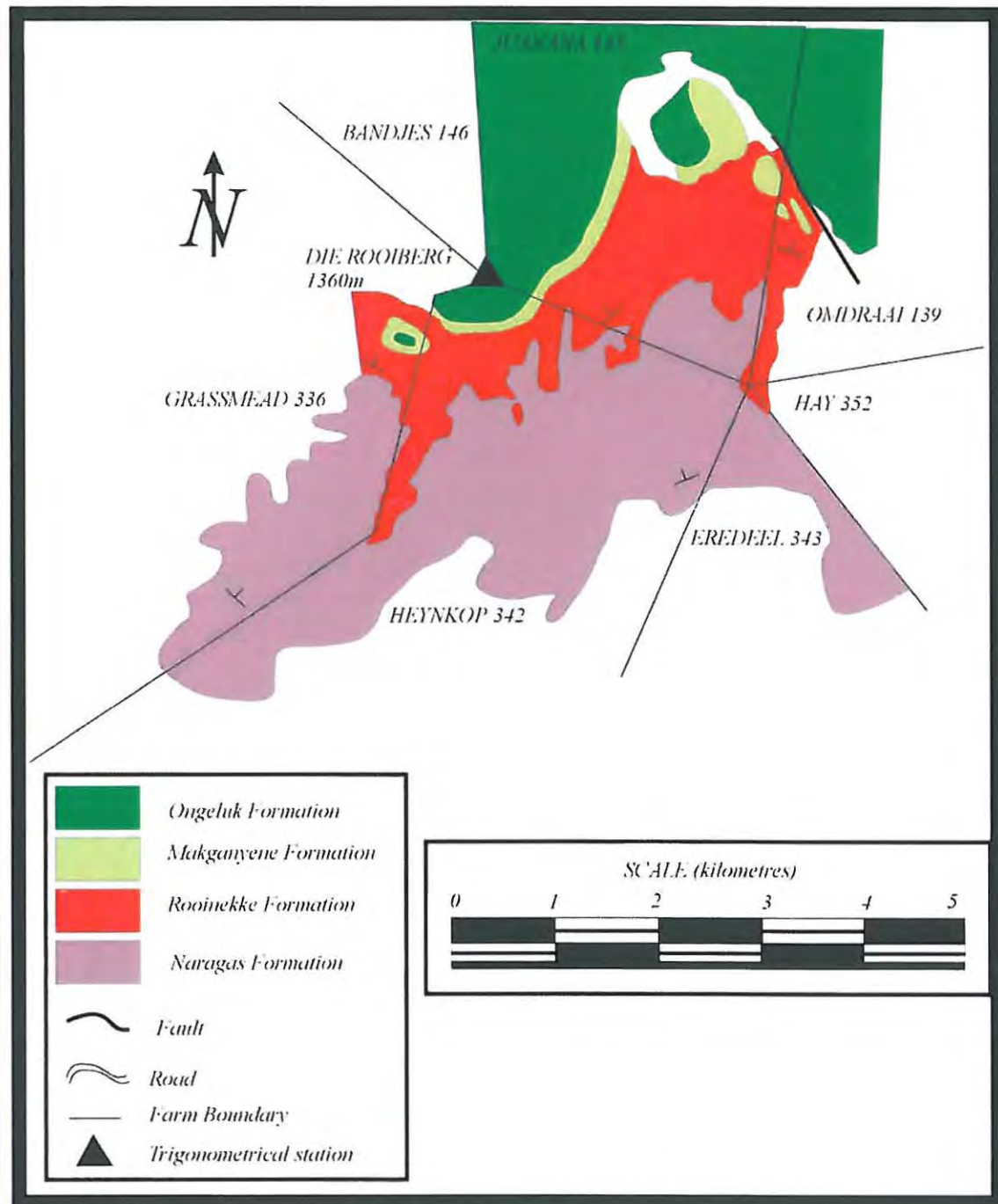
Figure II.7. Geology of locality B.
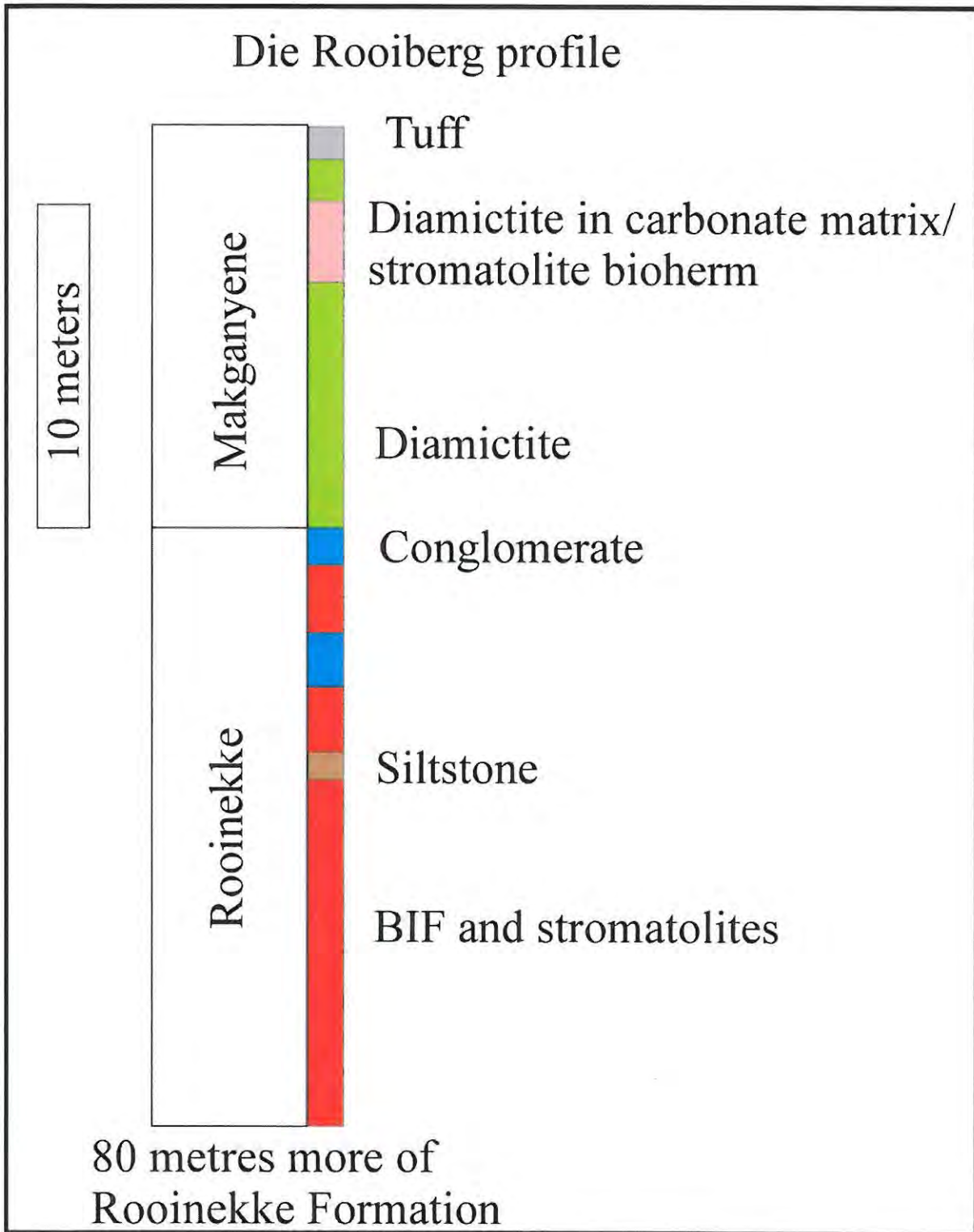
Figure II.8. Typical section from locality B.

II.2.4. Locality C

Locality C, shown in figure II.1, is situated in the Griquatown Iron Formation. On the 2922 Prieska geological map, outcrops of the Makganyene Formation are reported directly overlying the Griquatown Iron Formation. However after further investigation by the author, no such outcrop was confirmed. Therefore at this locality, only the Griquatown Iron Formation is reported. The absence of the Makganyene Formation directly lying on top of the Griquatown Iron Formation also indicates that no high angle unconformity is present at the base of the Postmasburg Group south of the Griquatown Fault Zone (Beukes, 1980, 1983).

II.2.5. Locality D

Locality D, shown in figure II.1, is situated at the closure of a syncline with the Ongeluk Formation in its core. All formations are well exposed, except for the Naragas Formation, which lies in the surrounding plain. In this locality, the strata dip gently towards the Ongeluk lava between $5°$ to $10°$. No faulting was observed.

The Naragas Formation consists of grey-blue siltstone interbedded with green shale. This formation is poorly exposed, but is similar to the Naragas Formation examined at the other localities, with no stromatolitic bioherms observed.

The Rooinekke Formation is thin, about 20 meters thick and consists of black-coated Fe-lutite, hematite band-lutite and brown jasper. Again no stromatolitic bioherms were observed.

The Makganyene Formation rests conformably on the Rooinekke Formation. At locality D, it consists of 15 meters of matrix-supported massive diamictite containing a thick (6 meters thick) white sandstone lens. This sandstone lens contains small clasts and has no apparent internal sedimentary structure, though thin cherty clast horizons (up to 3 cm diameter clasts, 5 cm thick layers) define the bedding in some places. This sandstone lens has been mapped as Ongeluk lava on the 2922 Prieska sheet. The matrix of the massive diamictite is composed of reddish-brown shale while the clasts consist of chert fragments, up to 10 cm in diameter. Near the top of the Makganyene Formation, above the massive diamictite lies a 1.5 meter thick diamictite with large clasts up to 20 cm in diameter enclosed in a carbonate-rich matrix. This is overlain by more massive diamictite (maximum 1 meter thickness) and finally by the graded tuffaceous cycles described in locality A and B.

Amygdaloidal Ongeluk andesitic lava conformably overlies the graded cycles. Figure II.9 represents the geology, while figure II.10 represents a typical section of locality D.
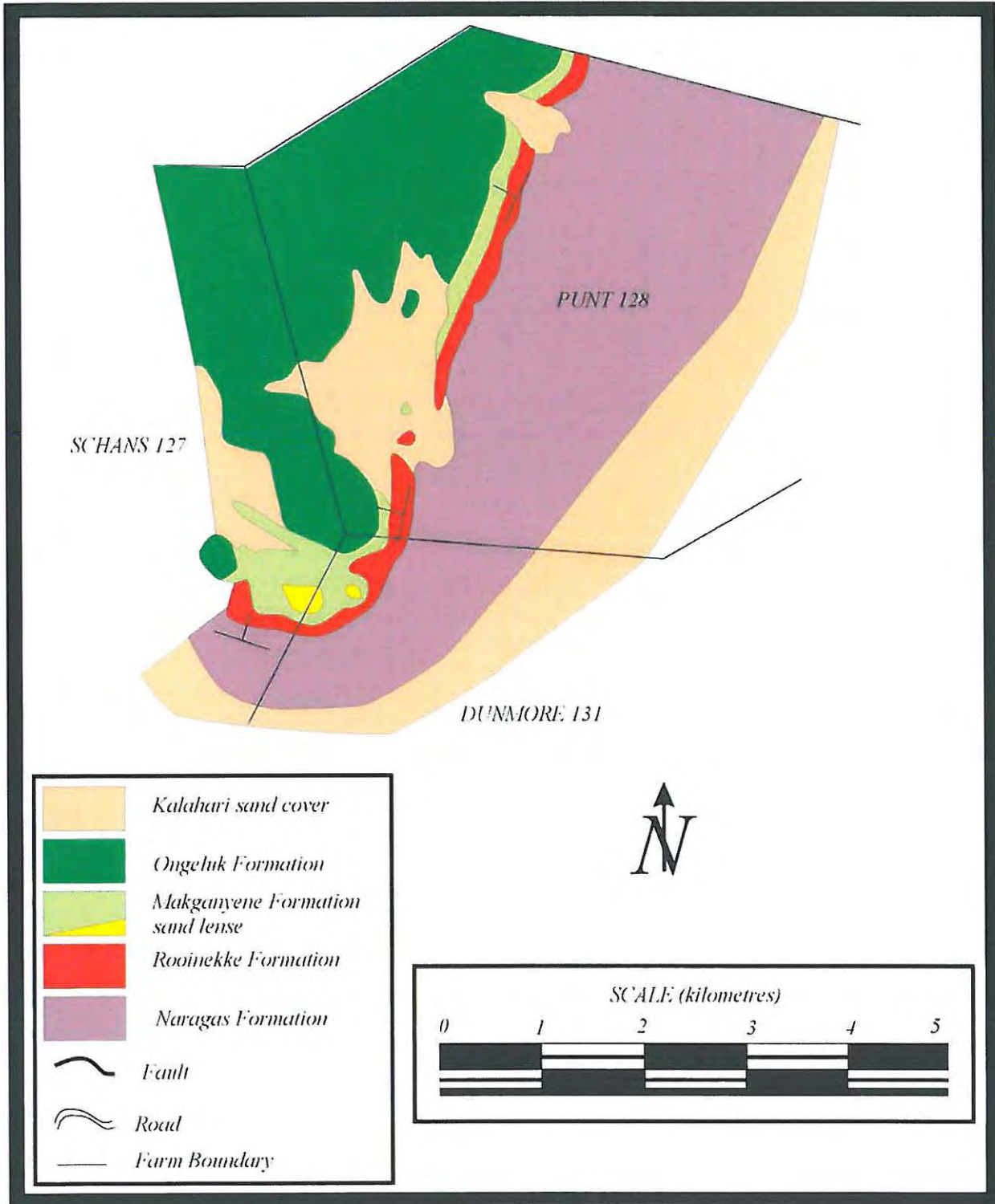
Figure II.9. Geology of locality D.
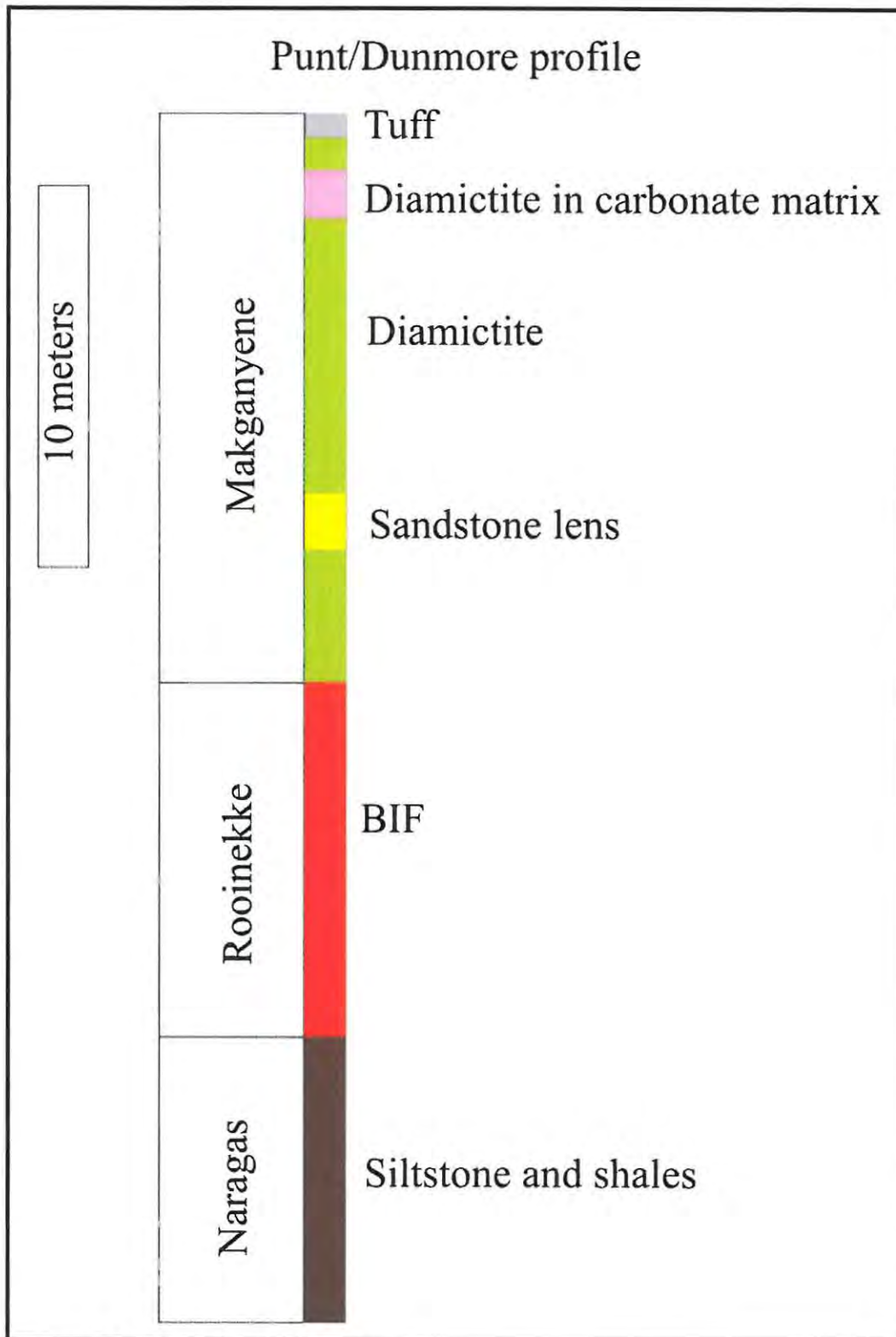
Figure II.10. Typical section of locality D.

II.2.6. Locality E

Locality E, shown in figure II.1, is the most significant locality, since it is situated where the Koegas Subgroup pinches out completely, placing the Makganyene Formation on top of the Griquatown Iron Formation along a major high-angle erosional unconformity. This is also the place where a fault zone (Beukes, 1983) or a hinge zone (Altermann, 1997) separates the Ghaap Platform facies from the more basinal Prieska facies. Figure II.12 illustrates the geology at locality E.

The strata at locality E are gently folded, with dips varying from sub-horizontal to a maximum of 25°. The bedding is very regular and tracing of the strata is obvious from aerial photographs in the southern part of this locality. On the other hand, outcrops from the northern section of Taaibosch Fontein 2 are poor, and this basically includes most of the Makganyene exposures and the underlying formations.

Three faults have been mapped at locality E. The first fault has a NNE-SSW direction, is vertical and obvious in the field, as it has developed breccia and quartz veining. It displaces the Rooinekke Formation to the level of the Naragas Formation, hence its vertical displacement was estimated to be around 30 meters. The second fault, running in a similar NNE-SSW direction is more difficult to examine, but was assumed since the Naragas strata do not correlate with the Doradale beds. It also separates a lens of sandstone from the Makganyene diamictite at the northern end of the fault. Its vertical displacement is less at its northern end (5 to 10 meters) than at its southern end (20 meters at least). The third fault has a WNW-ESE direction and is easily observed on aerial photographs, but not as clearly on the ground. This fault has a very small displacement in the order of few meters, and follows the orientation of valleys. A fourth fault is present on the published geological map (2822 Postmasburg 1/250.000) and is situated along the dirt road from Griquatown to Lime Acres with a WNW-ESE direction. This fourth fault was not assessed herein, but appears to be present on the aerial photograph and therefore is included in figure II.12.

The Griquatown Iron Formation, in general, has good exposures. At locality E, it consists of brown Fe-rhythmite (or microbanded chert). Disc-lutite horizons have been observed on Moos Fontein 18 farm, in a trench, but the weathered aspect of the Griquatown Iron Formation may be mistaken for yellow shales. On Reliance 347 farm, strike-slip structures are present in the Griquatown Iron Formation with a general displacement of top to southeast, but these most probably occurred during the deformation event that caused the gentle folding.

The Doradale Formation is present in the southern part of Taaibosch Fontein 2. It contains, from base to top, of some stromatolitic bioherms about 1 meter thick, a 40 cm thick conglomerate, and intercalated band-lutite and shale horizons.

The Naragas Formation has excellent outcrops in Taaibosch Fontein 2 since it forms prominent escarpments when capped by the Rooinekke Formation. Two Fe-lutite beds of a thickness of 1 meter are present. The remainder is invariably composed of a gray-blue siltstone bed, up to 2 meters thick, interbedded with laminated reddish-green shale. Near the top of the formation, the siltstone beds become black and are similar to the Rooinekke Formation. The Naragas Formation is not present beneath the Makganyene Formation in the northern part of Taaibosch Fontein 2 (see figure II.12).
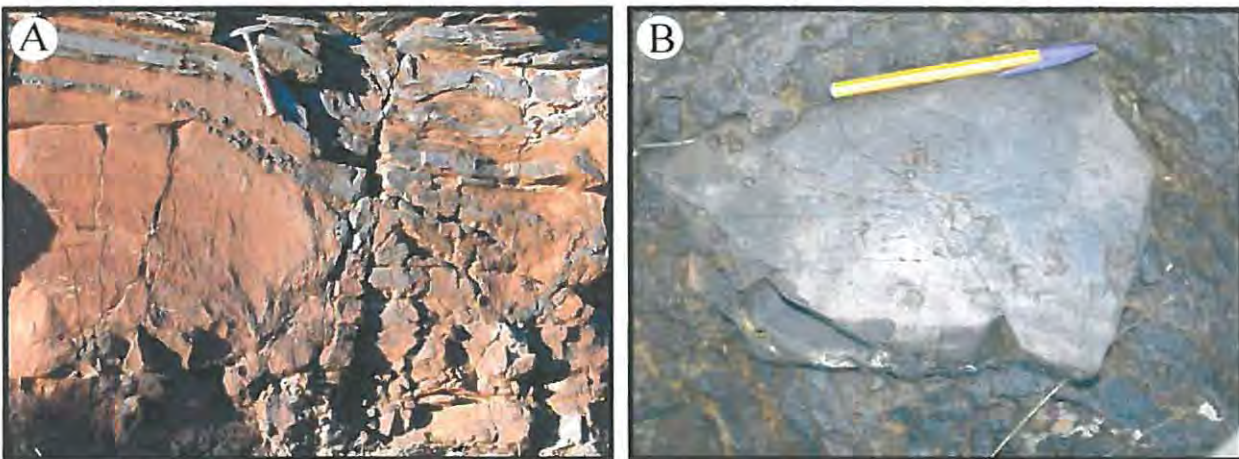
Figure II.11. A: layer consisting of stromatolitic bioherm persistent throughout locality E in the Rooinekke Formation. **B:** striated clast from the Makganyene diamictite showing three different orientations, such clasts are abundant at locality E and the localities further north and are diagnostic of a glacial origin.

The Rooinekke Formation is 10.5 meters thick and consists of hematite band-lutite with pillows in places, consistent stromatolitic bioherms throughout this locality (see figure II.11.A) and Fe-lutite at the top showing onionskin weathering, overlain by red shales. The unit mapped as "Top Rooinekke" in figure II.12 contains black shales and stromatolite bioherms.

The Makganyene Formation contains diamictites with a red shaly matrix, forming the bulk of the formation. Sandstone lenss were also observed. The latter generally consist of coarse sand, and may have some clasts, and sometimes show cross-bedding. These sandstone lenss are concentrated in the northern part of Taaibosch Fontein 2, Moos Fontein 18 and Griquatown Erf 261.

The clasts within the diamictite are generally chert, but striated nodules of Fe-rhythmite have been found. Towards the top of the Makganyene Formation, carbonate clasts derived from stromatolite have been found. The clast size varies from sand grain size to 15 centimetres in diameter. The Makganyene Formation at Locality E, compared with the other previously described locations, contains abundant striated and faceted clasts (see figure II.11.B).

Due to the stratigraphic configuration in this locality, an unconformity could be assumed, even though in the field the Makganyene Formation has not been observed cutting the underlying formations.

The Makganyene Formation rests on top of the Rooinekke Formation with what appears to be a conformable contact. Evidence of the presence of a stratigraphic pinch-out rather than an unconformity is that the Naragas cuts out completely beneath the Makganyene Formation. This is observed on aerial photographs where the Naragas siltstone layers pinch-out beneath the Makganyene diamictite. Where this occurs, a very red Fe-rhythmite is in contact with the diamictite, the two being separated by 50 centimetres of a slumped/brecciated Fe-rhythmite. The strata are parallel and there is no evidence of a major unconformity between the two, since this red Fe-rhythmite can be followed for more than 5 kilometres, from the northern part of Taaibosch Fontein 2 to the northern part of Moos Fontein 18. The basal contact of the red Fe-rhythmite with the Griquatown Iron Formation is not exposed, so the exact stratigraphic position of the red Fe-rhythmite is unclear, i.e. whether it belongs to the Rooinekke or Griquatown Formation. The Makganyene Formation, on the farms Griquatown Erf 261, Reliance 347 and the eastern part of Moos Fontein 18 lies on the Griquatown Iron Formation. The contact is not exposed and it is not evident from aerial photographs that an unconformity separates the Makganyene from the Griquatown Formation.

If the red Fe-rhythmite is a correlative of the Rooinekke Formation, then two hypotheses might explain the disappearance of the Naragas Formation where no intense folding is present. The first involves a normal fault that was active during late-Naragas/pre-Rooinekke times. However, since no fault was observed, and the red Fe-rhythmite continues beyond the inferred fault, this seems unlikely. Instead of the Griquatown Fault Zone of Beukes (1980, 1983), the second explanation assumes the presence of a hinge zone (see figure II.12.B) separating the platform facies to the north, and the deep basin to the south. The Koegas Subgroup is then confined to the deeper parts of the basin and wedges out north of the Griquatown Hinge Zone.
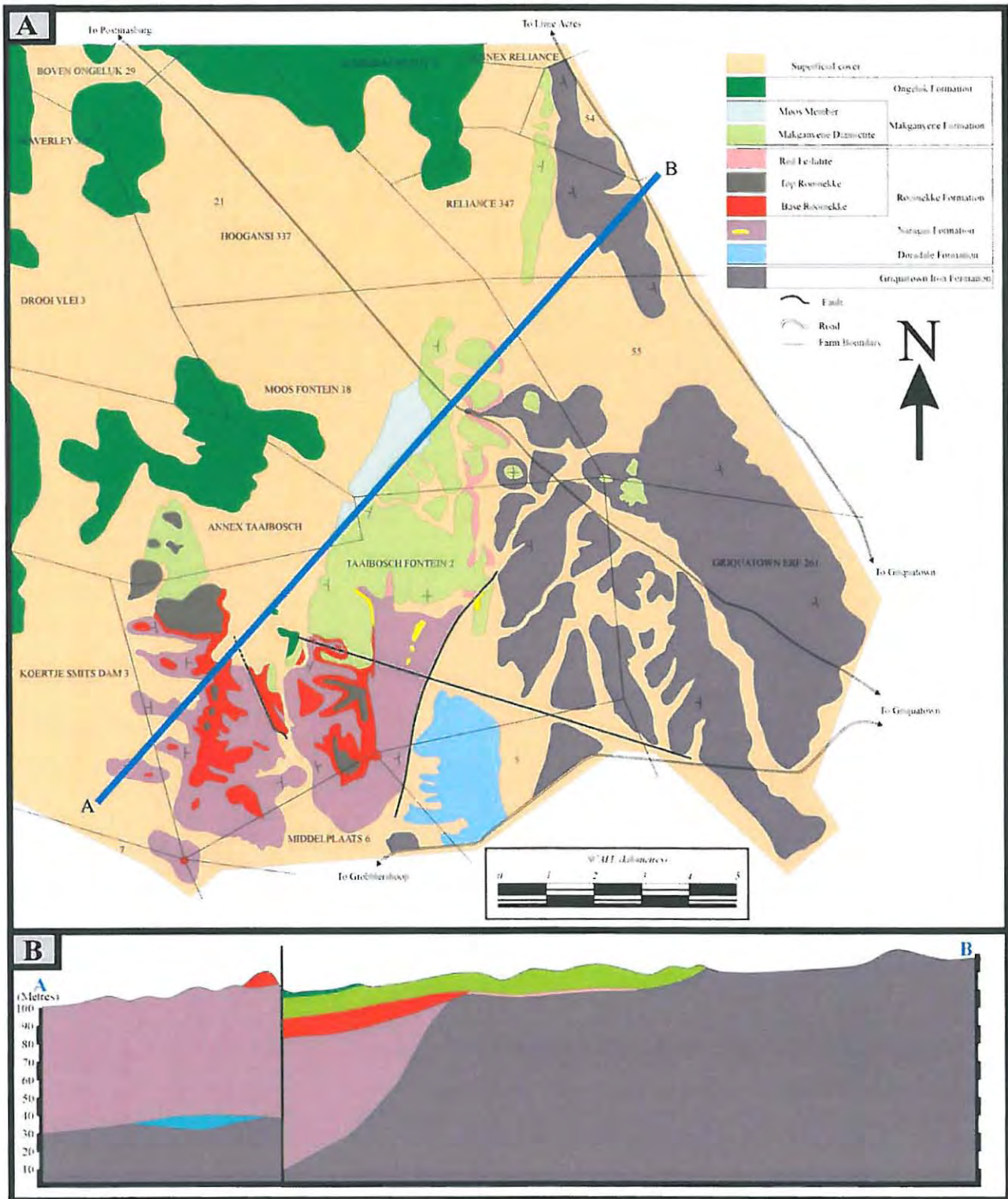
Figure II.12. A. Geology of locality E. The blue line A-B corresponds to the profile drawn in figure B where the Hinge Zone is clearly represented. The color scheme is identical for the map and the profile.

Three selected sections are illustrated in figure II.13 that display stratigraphic variations from the southern to the northern parts of locality E. Essentially three main points can be outlined from such profiles: (1) the transgressive nature of the Makganyene Formation in this locality tied with the pinch-out of the Koegas Subgroup (see figure II.12.B), (2) the increased amount of sandstone lenss associated with the disappearance of the large calcareous bodies within the diamictite and (3) a northward increase in thickness of the Makganyene Formation.

II.2.7. Locality F

Locality F, as shown in figure II.1, is situated along the Postmasburg-Kimberley road. There, the Makganyene Formation lies unconformably on the Griquatown Iron Formation. The beds have different dips in the Makganyene Formation and underlying Griquatown Iron Formation: the Makganyene beds are sub-horizontal while the Griquatown beds are gently folded (fold frequency is about 10 meters). No faults have been mapped at locality F.

The Griquatown Iron Formation at locality F consists predominantly of brown Fe-rhythmite with numerous interbedded disc-lutite and conglomeratic layers. The clastic units are very similar to the Makganyene diamictite because they contain similar shaped clasts. The difference is the brown jasperoidal matrix of the Griquatown Iron Formation, in contrast with the red shaly matrix of the Makganyene Formation.

At locality F, the Makganyene Formation is not totally exposed since the Kalahari sand covers its upper part. Nevertheless, diamictite was the only type of rock observed. The clasts consist of angular black chert, 5 cm in diameter in general. The Makganyene rests on the Griquatown Iron Formation in an unconformable manner. This was deduced from the different attitudes of both the Griquatown and Makganyene Formations, even where the contact was not directly examined. The geological map of locality F is provided in figure II.14. A corresponding section is not shown, as it is similar to the one presented in figure II.13 (C: Reliance section).

32
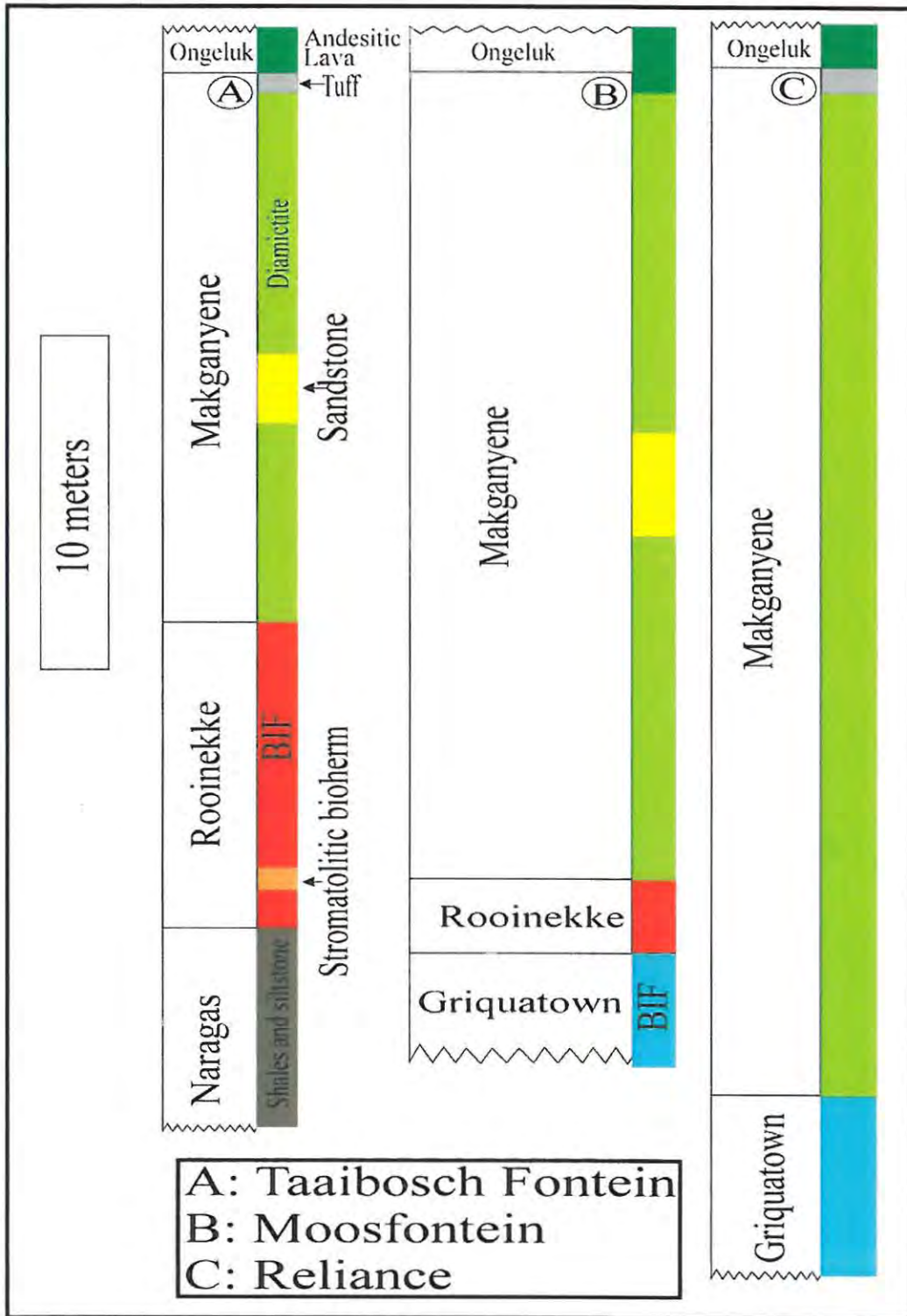
Figure II.13. Most representative sections from south (Taaibosch Fontein) to north (Reliance). Note that the Naragas Formation is not totally represented in profile A, and is totally absent from the other profiles further north.
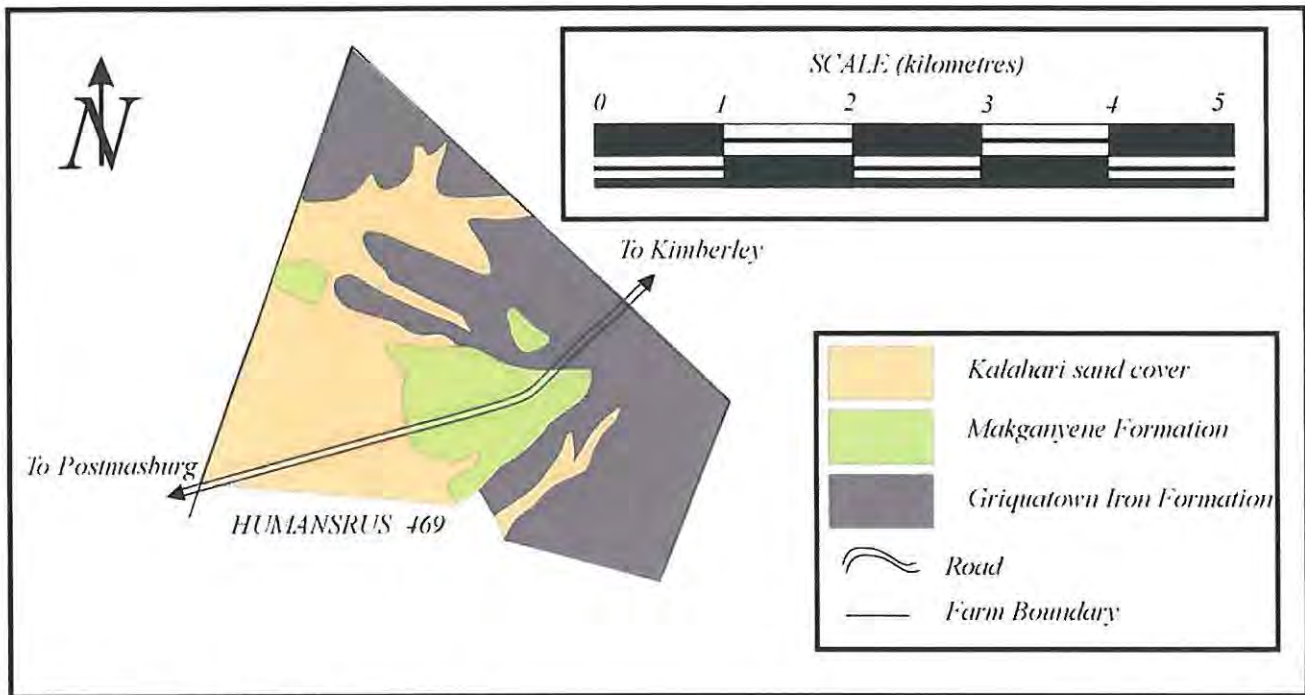
Figure 14. Geology of locality E.

II.2.8. Localities with poor exposures

The localities W, X, Y and Z have outcrops mostly covered by the Kalahari sand and are situated, as shown in figure II.1, west of the traverse A to F previously described.

As shown in figure II.1, locality W is situated near the closure of a syncline with the Ongeluk Formation in its core. Outcrops were good enough to be able to provide a basic geological map. The problem here was the difficulty in following individual beds along strike, especially when facies changes occur. For example, as is illustrated in figure II.15, the Rooinekke Formation changes over short distances (three kilometres) from red hematite-band-rhythmite, to stromatolitic bioherms, to green banded chert, to finally black manganiferous shales. The contact between the Rooinekke Formation and the Makganyene Formation may or may not be conformable. The Makganyene Formation consists of a red matrix containing chert clasts. Calcareous bodies were not observed. However, since the contact with the Ongeluk Formation does not crop out, such calcareous bodies might still be present under the Kalahari cover.
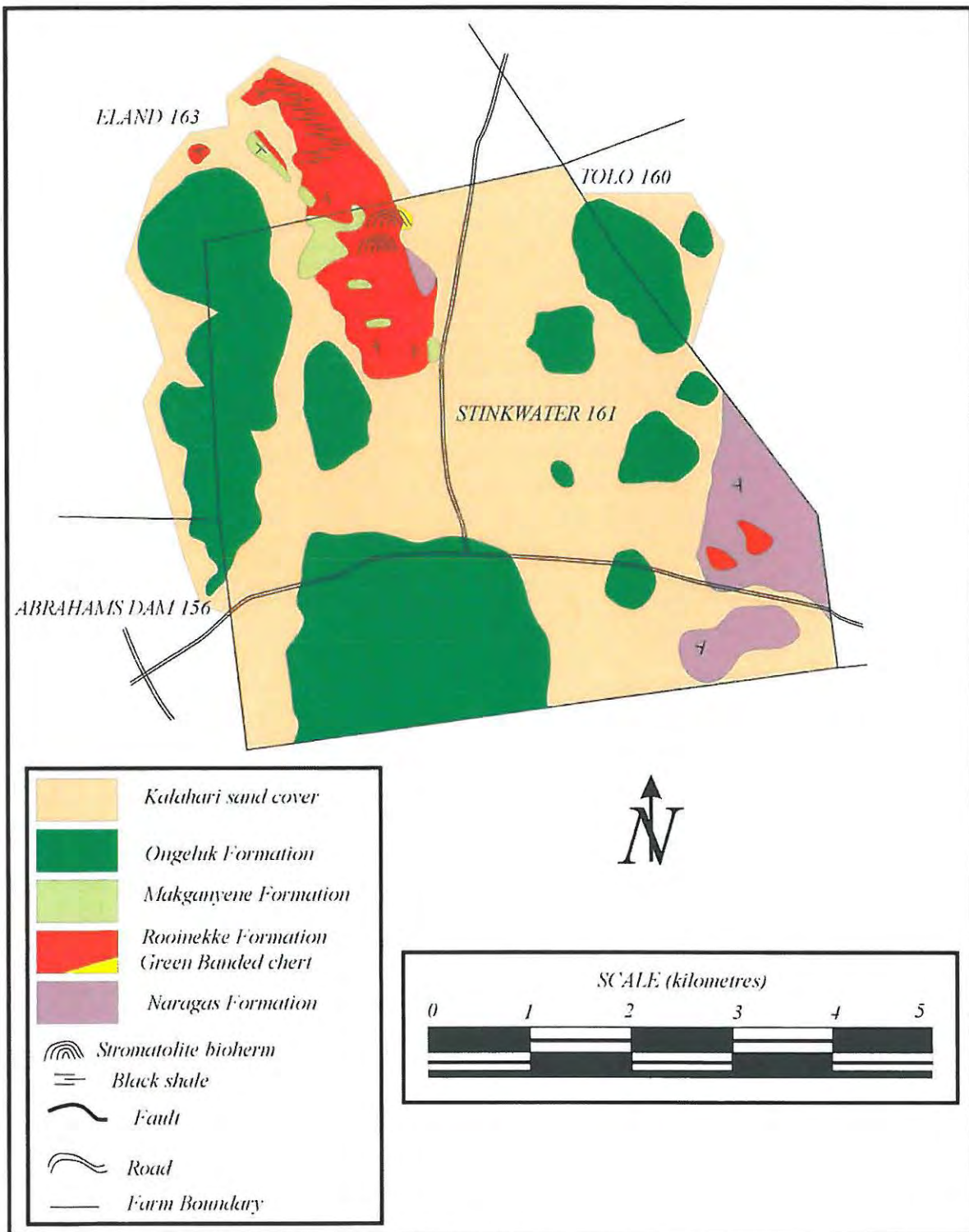
Figure II.15. Approximate geology of locality W.

Locality X, as shown in figure II.1, is situated 20 km south of the Rooinekke area. The important observation worth noting at this locality is the well-exposed and conformable contact between the Makganyene Formation and the Rooinekke Formation. Regarding lithologies, the Rooinekke Formation does not contain any stromatolitic bioherms, but consists essentially of black-coated hematite-band-rhythmite. The Makganyene Formation contains, besides diamictites, sandstone beds or lenss with parallel laminations and cross-beddings.

The Rooinekke area, investigated by the author for his M.Sc. studies (Polteau, 2000) comprises the farms Paauvlei 190 (above the thrust fault), Koodooskloof 96 and Vaalwater 84 (both beneath the thrust fault). At Paauvlei 190 and Koodooskloof 96, the basal contact between the Makganyene and the underlying Rooinekke Formation is conformable and sharp (Polteau, 2000). On the other hand, the same contact at Vaalwater 84 is gradational and displays a transition over 8 meters where Makganyene diamictite horizons are intimately interbedded with BIFs and shales of the underlying Rooinekke Formation (see figure II.16; after Polteau, 2000).

Locality Y, as shown in figure II.1, is situated on the northern outcrop of the Koegas Subgroup, just west of Postmasburg. There, the Koegas Subgroup is particularly well exposed and consists of hematite-band-rhythmite with occasional stromatolitic layers. The Makganyene Formation is exposed as débris, and consists of the usual red diamictite. As no contact was exposed, the stratigraphic relationship with the underlying formation is too speculative.

Locality Z, as shown in figure II.1, is situated west of Danielskuil. At this locality, the outcrops of the Makganyene Formation are poor and no contact with the underlying Griquatown Iron Formation was observed. What can be noted from this locality is that the Makganyene Formation contains beds/lenss of very coarse sand containing clasts.
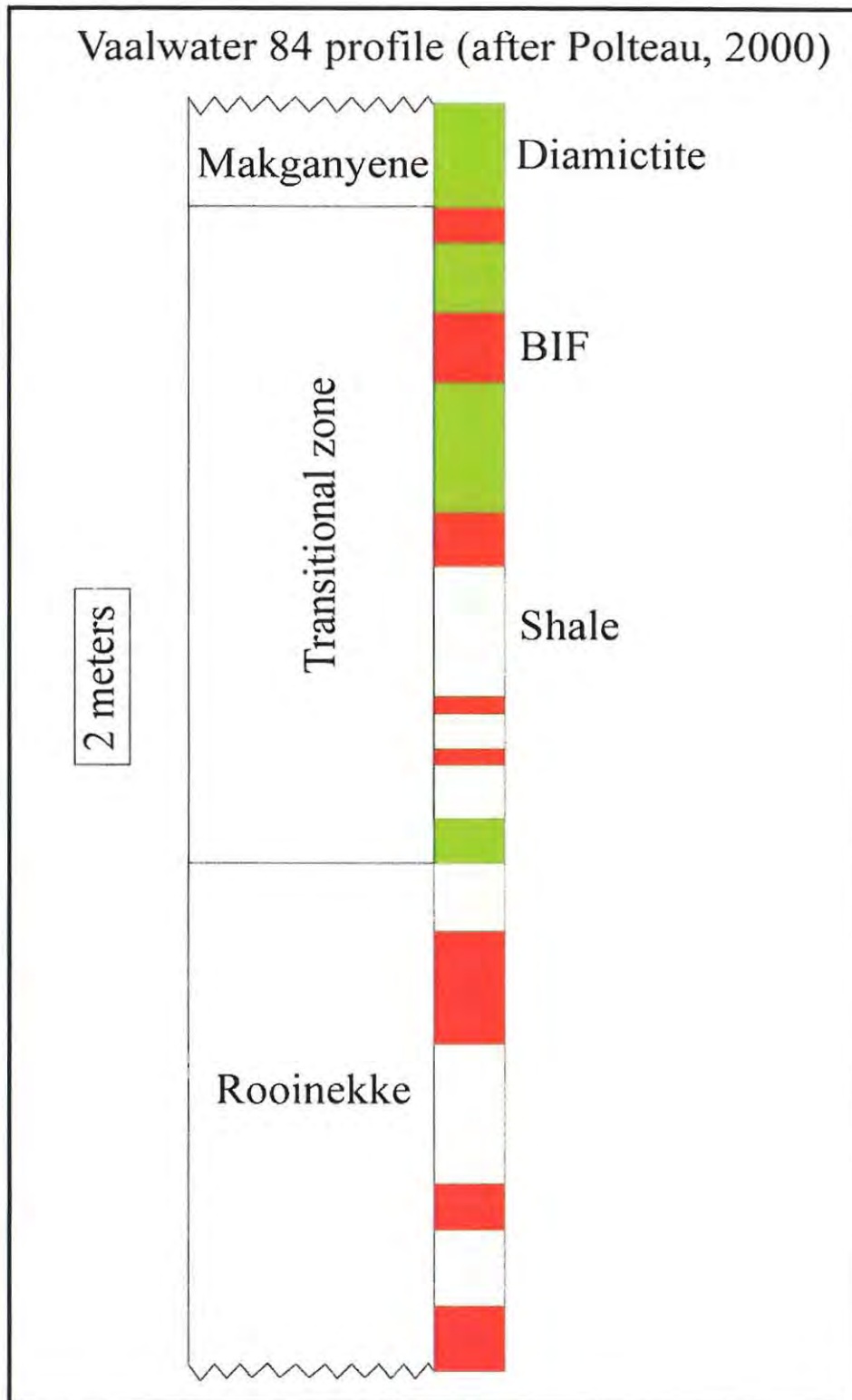
Figure II.16. Typical profile from the Rooinekke mine area.

II.2.9. Borehole data

Where the Kalahari sand blankets all exposures, outcrops of the Makganyene Formation are extremely rare and poor. However, borehole material is available from the Sishen and Hotazel areas due to mining activities. Both localities are shown in figure II.1. They are situated where thrusting, often misinterpreted as erosional unconformities (de Villiers, 1967), has duplicated the Transvaal Supergroup upon itself (Visser, 1944; Beukes, 1987), and thus led to confusions in stratigraphic interpretations, particularly around Sishen (see paragraph I.2). The stratigraphic succession established in these complicated areas has also been, rather erroneously, extrapoled to the whole Griqualand West Basin (de Villiers, 1967, 1977; SACS, 1980).

The Gamagara Formation has two conflicting interpretations that have a direct influence on the understanding of the stratigraphy of the Transvaal Supergroup.

- ➤ de Villiers (1967, 1977) and SACS (1980) consider that the Gamagara Formation belongs to the Transvaal Supergroup. It is sandwiched between the Ghaap Group and the Postmasburg Group along 2 major regional unconformities (see table II.1). This interpretation is still used at the Sishen mine.

- ➤ However Beukes and Smit (1987) consider the Gamagara Formation as being the correlative of the Mapedi Formation of the Olifantshoek Supergroup (from 1.9 to 1.8 Ga; Cheney, 1996), and it is therefore not part of the Transvaal Supergroup. The basal contact of the Gamagara Formation with the underlying Transvaal Supergroup is a major regional unconformity, and the Postmasburg Group overlies the Gamagara Formation on a thrust fault (see table II.1).

Fresh borehole samples are comparably fresher and thus more suitable than the deeply weathered field samples. Therefore, grouping of similar facies of the borehole samples was carried out to facilitate correlations between field and borehole data. Descriptions of the different facies described in the core samples are presented in chapter III. The colour of the matrix of the diamictite has not been differentiated and the hematitic mudstone and banded iron-formations (all types of facies) have been grouped together.

Other borehole material is available, for example in the Matsap area (for descriptions, see Polteau, 2000).

SACS (1980)				Beukes and Smit (1987)				
Sequence	Group	Formation	Member	Supergroup	Group	Subgroup	Formation	Thickness
Olifantshoek	Volop	Groblershoop		Olifantshoek		Volop	Groblershoop	>2000
							Top Dog	
		Brulsand					Verwater	
							Glen Lyon	
							Ellies Rus	3500
							Fuller	
		Hartley					Hartley	700
		Lucknow					Lucknow	450
		Mapedi					Mapedi	10-1500
Griqualand West	Cox		Mooidraai	Transvaal	Postmasburg	Voëlwater	Mooidraai	250
			Hotazel				Hotazel	
		Ongeluk					Ongeluk	900
		Makganyene	Hartebeeshoek				Makganyene	50-150
			Bolham					
			Magoloring		Ghaap	Koegas	Rooinekke and Nelani	300
		Gamagara	Paling	Olifantshoek			Gamagara (Correlative of Mapedi)	290
			Marthaspoort					
			Sishen					
	Griquatown	Koegas	Kwakwas	Transvaal	Ghaap	Koegas	Rooinekke	100
							Naragas	240-600
							Kwakwas	
							Doradale	
			Middlewater				Pannetjie	
		Asbestos Hill	Danielskuil			Asbestos Hill	Griquatown	200-300
			Kuruman				Kuruman	150-170
		Ghaap Plateau					Campbellrand	1500-1700
		Schmidtsrif					Schmidtsrif	10-250

═══ Unconformity ═══════ Thrust fault

Table II.1. Stratigraphic subdivisions of SACS (1980) compared with Beukes and Smit (1987) for the Sishen and Hotazel areas.
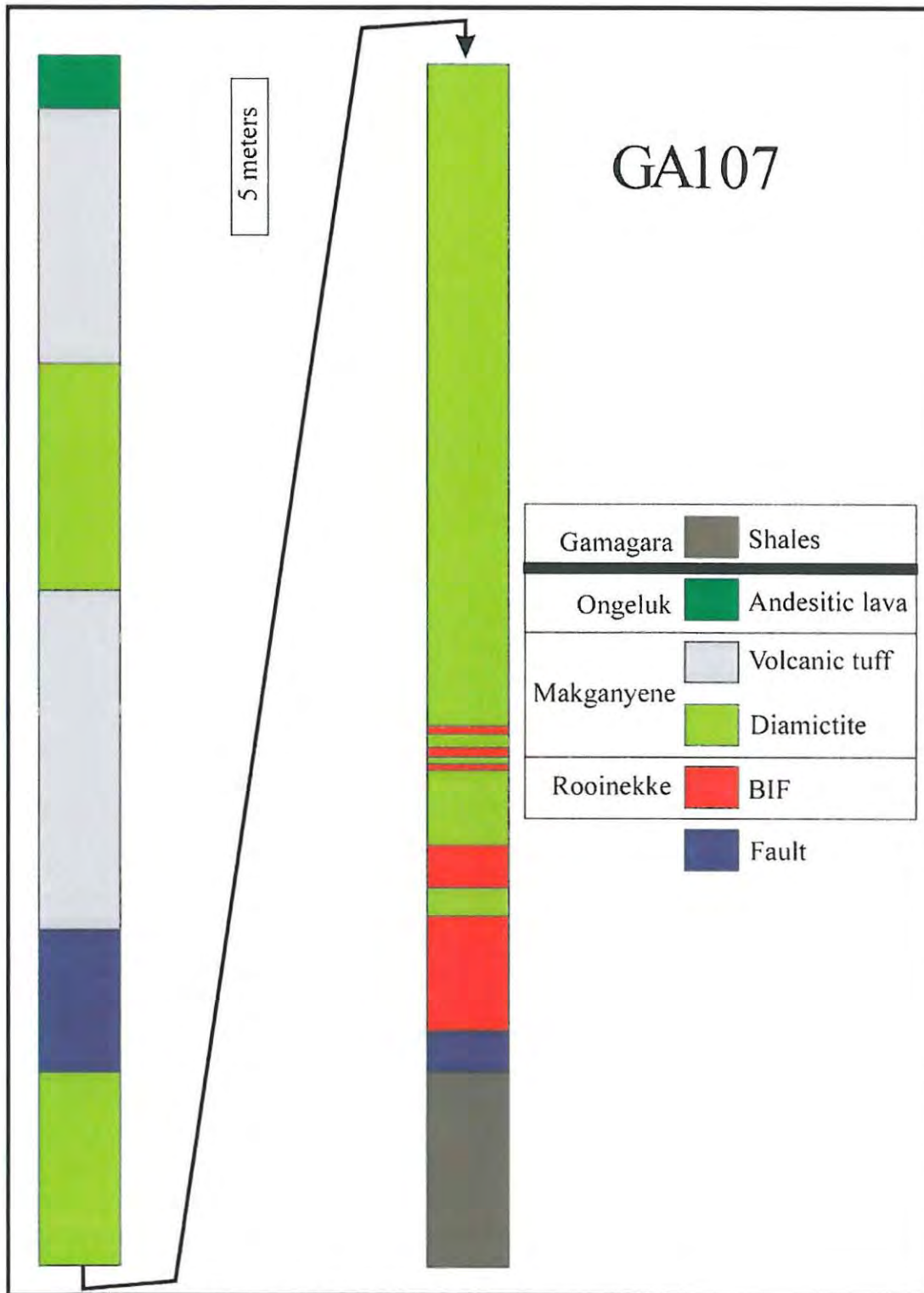
Figure II.17. Log of borehole GA107 from Sishen

II.2.9.1. Borehole data from Sishen

Intersections of the Makganyene Formation, displaying basal and top contacts, are difficult to obtain at Sishen, despite the available computerised borehole dataset. This is because most borehole cores from mined out areas of the open pit are disposed of to reduce storage costs. Borehole GA107 (X = 733332.35; Y = 846069.53; Z = 1192.66) was the only preserved borehole located during this study that displayed both contacts and a substantial thickness of the Makganyene diamictite, as well as a limited thickness of underlying BIFs due to the presence of a thrust fault that placed the Transvaal Supergroup lithologies above the younger Gamagara shales of the Olifantshoek Supergroup (see figure II.17).

As shown in figure II.17, the base of the borehole GA107 consists of breccia caused by faulting. Immediately overlying this tectonic zone, hematitic banded iron-formations are present. The contact with the overlying Makganyene Formation is gradational with interbedded BIFs within the diamictites. Therefore the Makganyene Formation in the Sishen area is conformable on the underlying formation. Because only the Rooinekke Formation (topmost part of the Koegas Subgroup) has been observed in the field as being conformable with the Makganyene Formation, the interbedded BIFs would logically belong to the Koegas Subgroup. The same gradational basal contact between the Rooinekke and the Makganyene Formations was also observed at the Rooinekke mine locality and on two other boreholes (GA171 and GA129; Polteau, 2000). The rest of the borehole GA107 consists of massive diamictites that are truncated by another fault. The top of the Makganyene Formation contains two volcanic tuff units consisting of stacked graded cycles 2-3 centimetres thick interbedded with diamictites. The volcanic tuff is a distinctive unit (referred to as the "Moos Member" at locality E) that has been observed over the entire outcrop area of the Griqualand West Basin. Andesitic lavas of the Ongeluk Formation overlie the Makganyene Formation conformably.

The Makganyene Formation displayed in this borehole section is approximately 50 meters thick, containing almost half diamictite and half volcanic tuff, but including a fault in the middle of the succession. However it is assumed that the section observed is thinner than the real thickness of the Makganyene Formation due to a normal fault that is superposing the uppermost portion of the Makganyene Formation (the tuffaceous graded cycles) with the diamictites.

II.2.9.2. Borehole data from Hotazel

Boreholes from the Hotazel area have intersected a significantly greater part of the Postmasburg Group and contain units both immediately above and below the Ongeluk Formation. The two boreholes BG5 and BH171/93, shown in figure II.18, represent the succession below the Ongeluk lava, while figure II.20 displays the sequence occurring above the lava, by correlating individual boreholes (REX40, REX41, REX43, REX48, REX51, and REX56).

Borehole BG5 develops a thinner Makganyene Formation compared to borehole BH171/93 (figure II.18, and figure II.19 for borehole localities), about 20 and 55 meters respectively. Another difference is that the BG5 diamictites rest on allochemical BIFs while the BH171/93 diamictites rest on orthochemical BIFs. The basal contacts of the Makganyene diamictites of both boreholes are sharp, unlike the gradational ones observed in the Sishen area, and together with the variable footwall lithologies, place the Makganyene Formation unconformably on the Griquatown Formation at the Hotazel localities. The observations of the BIFs below the Makganyene Formation in borehole BH171/93 are restricted due to the presence of a fault that places the entire package on to the Ongeluk Formation (figure II.18).

Another difference between these two boreholes is that BH171/93 does not contain any evidence of the volcanic tuff ("Moos Member"), which has been present in all the Griqualand West Basin outcrops at this particular stratigraphic position, i.e. at the contact between the Makganyene and the Ongeluk Formations.

Since the first manganese ore horizon of the Kalahari manganese field is situated a few meters immediately above the Ongeluk lavas, abundant boreholes of this stratigraphic level are available. As a result, most boreholes from the Hotazel area show the contact between the Ongeluk and the Hotazel Formations. It was therefore possible to carry out correlations between certain boreholes (REX40, REX41, REX43, REX48, REX51, REX56), resulting in the representation of sections B and C in figure II.20. Figure II.19 displays borehole coordinates forming the sections B and C of figure II.20, but locates also boreholes BG5 and BH171/91. Both sections are situated stratigraphically above the Ongeluk lava and contain diamictites as reported by Kirschvink et al. (2000).
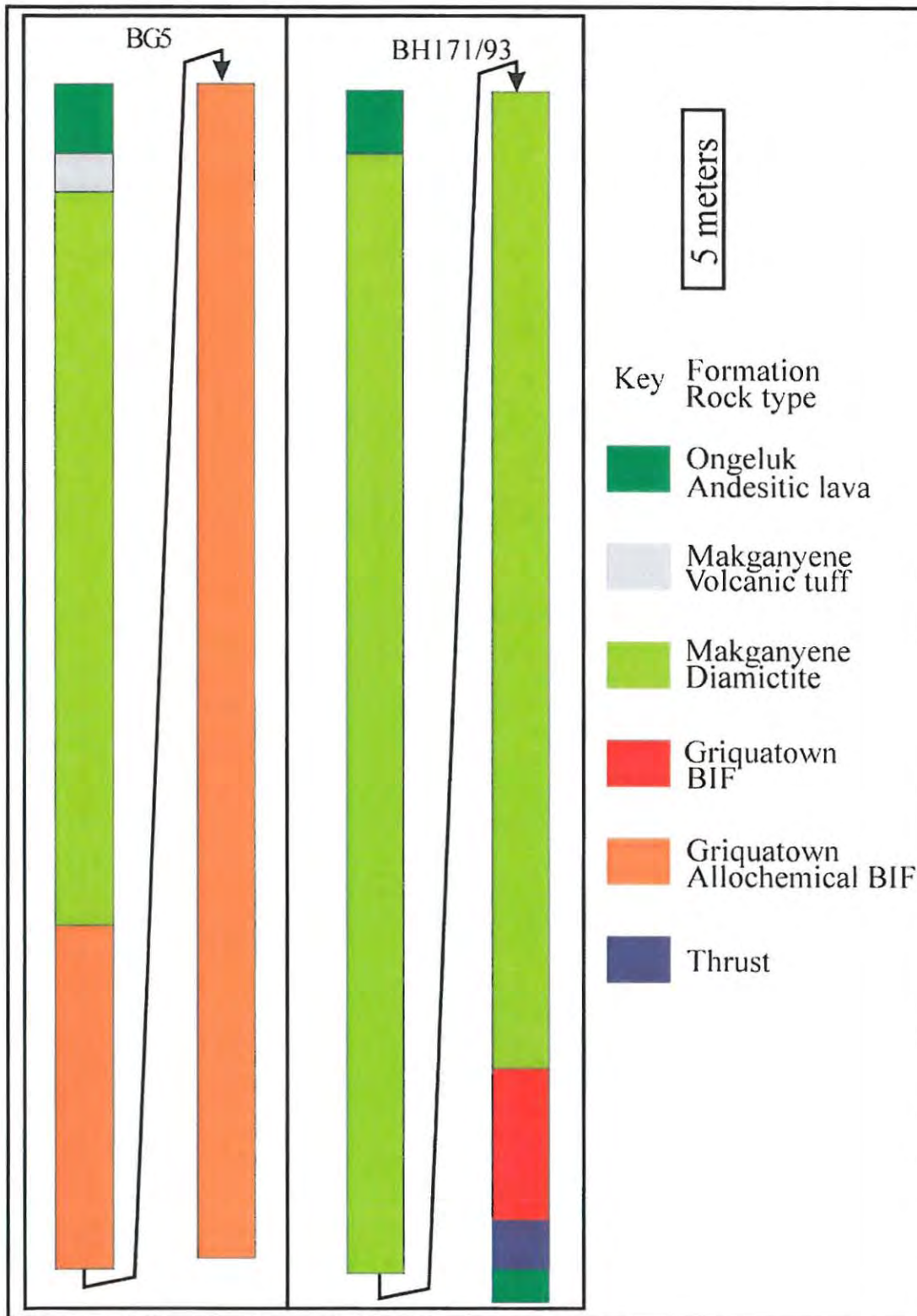
Figure II.18. Boreholes BG5 and BH171/93 from the Hotazel area.
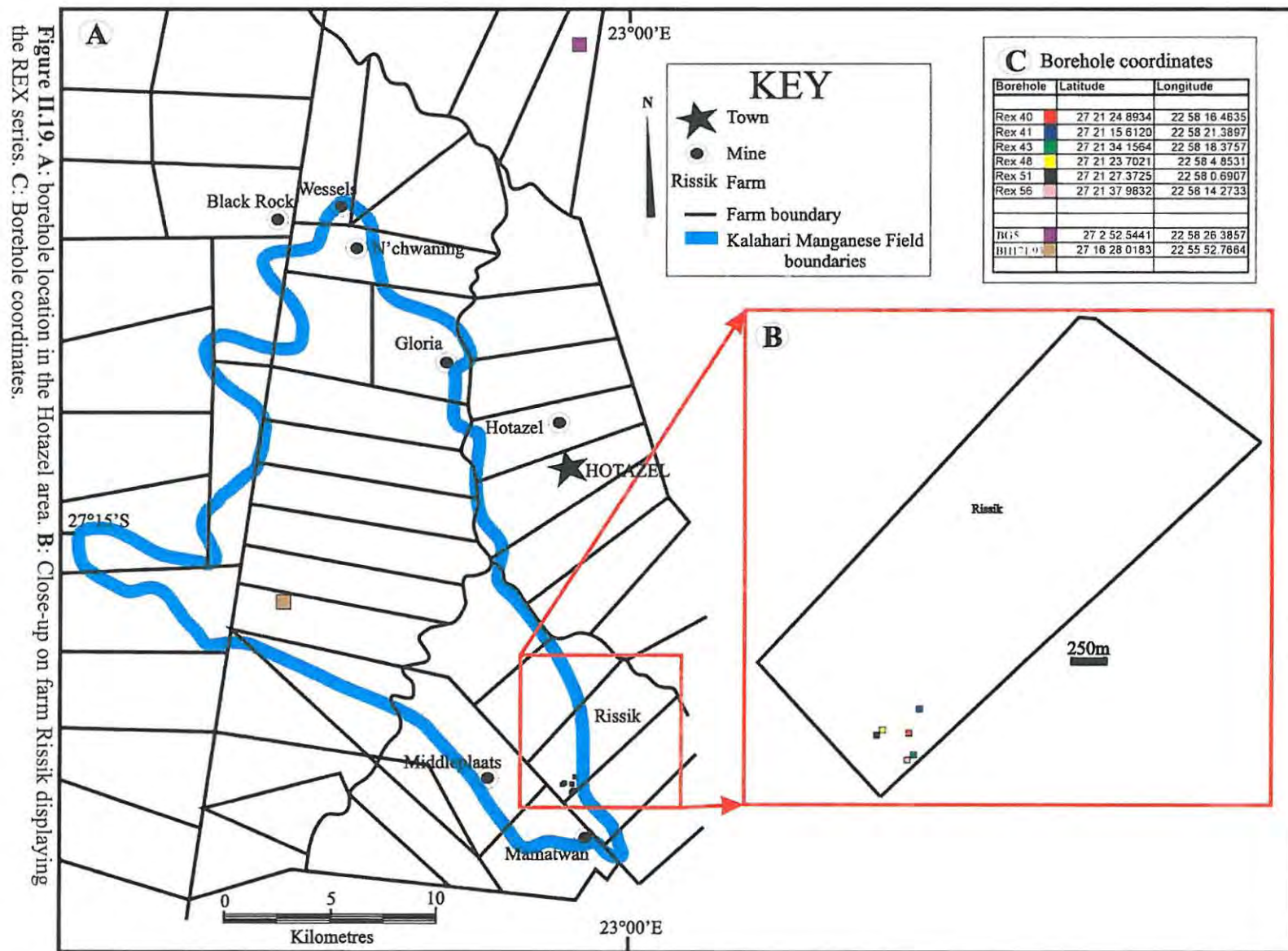
Figure II.19. A: borehole location in the Hotazel area. B: Close-up on farm Rissik displaying the REX series. C: Borehole coordinates.

KEY

★ Town
● Mine
Rissik Farm
— Farm boundary
▬ Kalahari Manganese Field boundaries

C Borehole coordinates

Borehole		Latitude	Longitude
Rex 40		27 21 24.8934	22 58 16.4635
Rex 41		27 21 15.6120	22 58 21.3897
Rex 43		27 21 34.1564	22 58 18.3757
Rex 48		27 21 23.7021	22 58 4.8531
Rex 51		27 21 27.3725	22 58 0.6907
Rex 56		27 21 37.9832	22 58 14.2733
BGS		27 2 52.5441	22 58 26.3857
BH1219		27 16 28.0183	22 55 52.7664

43
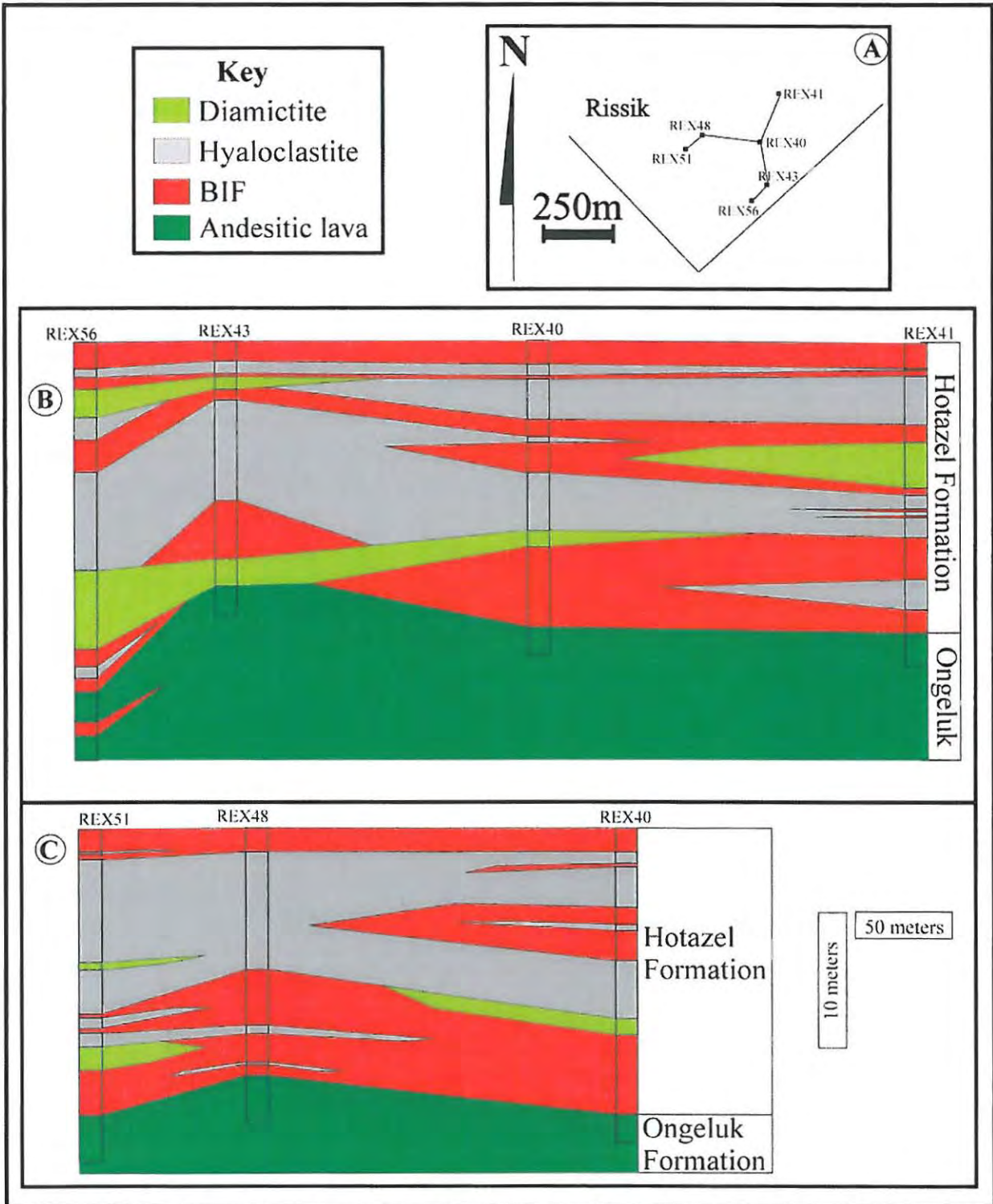
Figure II.20. A: Borehole location at Rissik. **B**: Section of boreholes REX56, REX43, REX41, REX40. **C**: Section of boreholes REX51, REX48, REX40.

The main characteristic of sections B and C (see figure II.20) is that facies changes are significant and occur over short distances (less than 100 meters) towards the base of the sections. Towards the top of the same sections, the strata become continuous and extensive with no facies changes. The Hotazel Formation apparently rests on an undulating surface of the Ongeluk lava (Kirschvink et al., 2000). The latter may contain some interbedded BIFs as in borehole REX56. Some BIFs or diamictites that are both developed as lenss overlie the Ongeluk Formation. The diamictites are relatively fine grained and contain small rounded clasts, with a maximum diameter of 2 centimetres (figure II.22.E). The BIFs have different facies, from hematitic, to greenalitic, to calcareous. The black volcanic tuff (figure II.22.E), containing angular clasts, is prominent in the central part of the sections (figure II.20). The top of the sections consists of the hematitic BIFs typical of those associated with the manganese beds (Tsikos, 1999). These facies will be described in detail in the next chapter (see chapter III on petrography).

II.3. Conclusions

Major aims of the fieldwork were to assess both changes in facies in the Makganyene Formation as well as its relationship with the Koegas and Asbestos Hills Subgroup. All sections from the different localities have been juxtaposed in a single profile (figure II.21). This does not include the sections from above the Ongeluk Formation because they were observed only at the Hotazel localities. A description of figure II.21 follows, proceeding from south to north, from the deep basin around Prieska to the shallow Ghaap platform.

The Koegas Subgroup was deposited conformably on the Asbestos Hills Subgroup during a regression that marked the end of the deposition of the Griquatown Iron Formation (Beukes, 1983; Catuneanu and Eriksson, 1999). The sea level was low during formation of the Koegas Subgroup and saline lakes (Beukes, 1983) developed on the Ghaap platform while deeper in the Prieska basin a submarine fan accumulated off the shelf edge. The Griquatown Hinge Zone, which was an active fault zone during the Campbellrand times, separated these two different depositional environments. The Koegas Subgroup is well developed in the southern part of the basin (240-600 meters thick), and pinches out at the hinge zone beneath the Makganyene Formation. North of the hinge zone, an erosional surface developed during the deposition of the Koegas Subgroup. Therefore the Griquatown Hinge Zone separates an erosional surface from conformable basinal sediments.
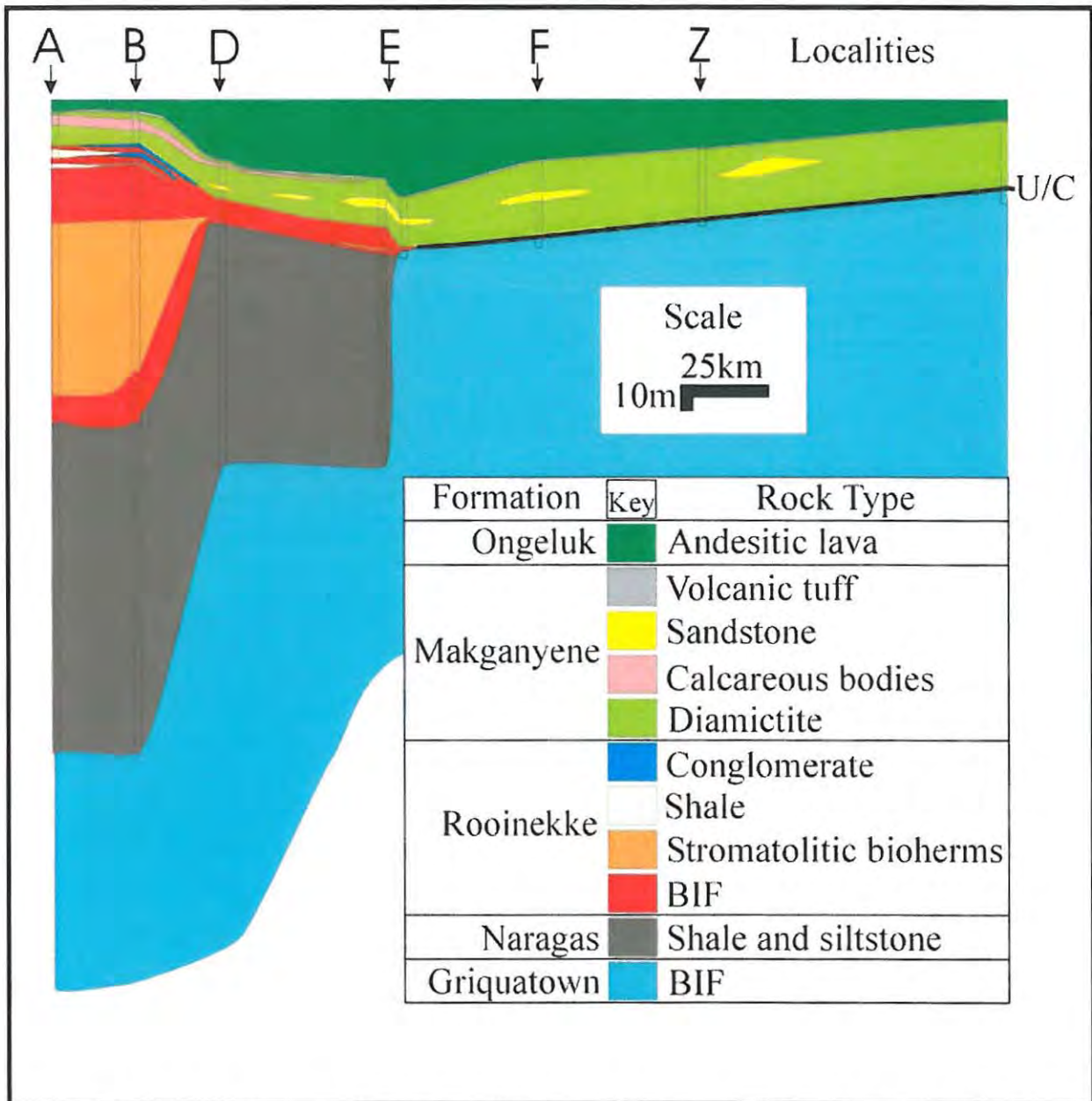
Figure II.21. Hypothetical section correlating all the localities previously described (localities A, B, D, E, F, and Z) during this field campaign. Note that the unconformity at the base of the Makganyene Formation grades into a conformity at the Griquatown Hinge Zone where all the Koegas subgroup wedges out.

The basal contact separating the Makganyene Formation from the underlying formations is not of the same nature at every locality. Generally, the Makganyene Formation rests clearly conformably on top of the Koegas Subgroup south of the Griquatown Hinge Zone. The contacts are displayed in figure II.22 (A, B, C, and D) where they were sufficiently

well exposed. North of the Griquatown Hinge Zone, the Makganyene Formation rests unconformably on the Griquatown Iron Formation of the Asbestos Hills Subgroup. This unconformity corresponds to the erosional event (possibly subglacial ice scouring, because diamictites have been observed at the base of the Koegas Subgroup at locality A) that has affected the Vryburg Arch during Koegas times. The unconformity present on the Ghaap platform represents the entire Koegas package.

In a major regional seismic study of the Griqualand West Basin, Tinker et al. (2002) did not identify any major unconformity at the base of or within the Postmasburg Group. The fact that the Makganyene Formation is conformable to the south of the Griquatown Hinge Zone, and mostly unconformable to the north on the Ghaap platform, as well as the behaviour of the Koegas Subgroup wedging out at the Hinge Zone, shows that basin morphology and relative sea level changes were controlling sedimentation of the entire Transvaal Supergroup in the Griqualand West Basin.

The calcareous bodies within the Makganyene diamictite are only present south of the Griquatown Hinge Zone. They are best preserved in the southern localities as bioherms with/without clasts. Further north, these calcareous bodies thin out and are developed as clastic sheets until they completely disappear about 20 kilometres south of the Griquatown Hinge Zone.

Evidence that volcanism related to the development of the Ongeluk Formation started before the end of the Makganyene times is seen in the basin-wide presence of volcanic tuff in the uppermost part of the glacial deposit. Kirschvink et al. (2000) observed beds of jaspilite and diamictites up to the top of the Ongeluk Formation. The Ongeluk Formation blanketed all sedimentary deposits, leaving a smooth undulating and unweathered surface on which deposition of the Hotazel Formation took place.

It can be deduced that volcanism continued during the deposition of the BIFs and diamictites of the Hotazel Formation due to the latters' intimate association with hyaloclastites. Initially after the Ongeluk stage, volcaniclastic and chemical sediments were being deposited while the diamictites, preserved in channels, locally cut the BIFs causing the latter to be impersistant. Subsequently chemical sedimentation developed extensive and continuous beds of BIFs and manganese, marking a transgression. Finally, the regressive carbonates of the Mooidraai Formation mark the end of the Transvaal Supergroup deposition in the Griqualand West Basin.
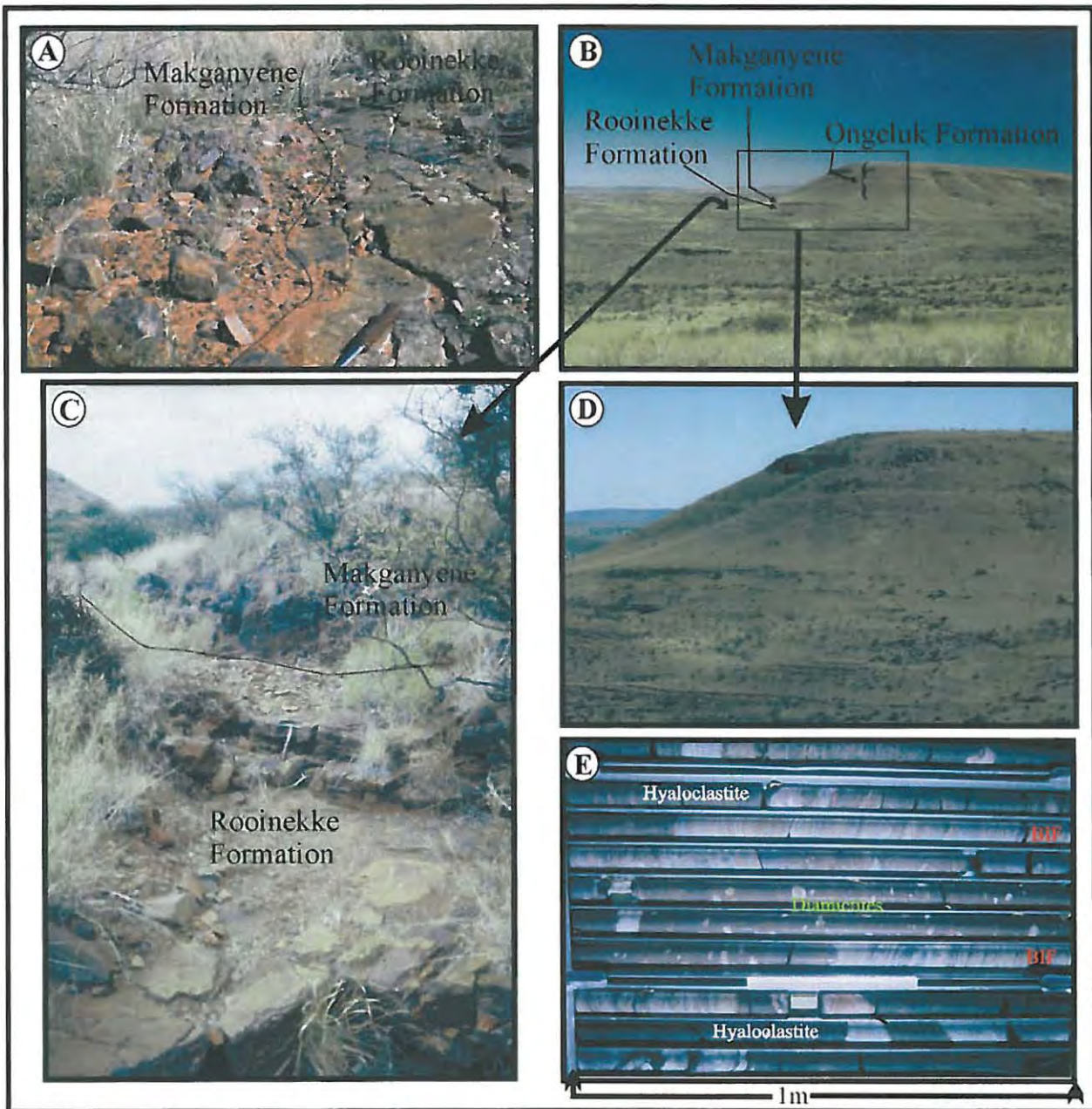
Figure II.22. A. conformable flat contact of the Makganyene Formation with the Rooinekke Formation. Note that the top surface of the Rooinekke Formation is not striated. **B.** Locality B, where Die Rooiberg is shown, at the foot of which the Makganyene Formation is conformably sandwiched between the Rooinekke and Ongeluk Formations. **C** is a conformable contact between the Rooinekke Formation and the Makganyene Formation. **D** is a close up of Die Rooiberg, showing the conformable nature of the Makganyene Formation above the Rooinekke Formation. **E**: photograph of a portion of borehole REX41 exhibiting central diamictites, together with BIFs, and volcaniclastic horizons.

Chapter III
Petrography

III.1. Introduction

The only previous petrographic studies of the Makganyene Formation were undertaken by de Villierss and Visser (1977) and Polteau (2000). The present study substantially expands the macroscopic and microscopic descriptions of the Makganyene Formation. Different rock types (see Chapter II) were examined, corresponding to BIFs, diamictites and volcanic tuffs, and are described in their stratigraphic order.

Diamictites form the main rock type of the Makganyene Formation, and consist of clasts of heterogeneous sizes set in a very fine-grained matrix. The main characteristics of the BIFs interbedded within the diamictites, and also of unmetamorphosed Proterozoic BIFs, are in general their very fine-grained nature and their typical rhythmic iron-poor/iron-rich banding. The volcanic tuffs in this study consist of 2 to 3 cm thick stacked graded cycles below the Ongeluk lavas, and of massive black pyroclastites above the lavas. This chapter describes in more detail each of the different main rock types.

III.2. Sample selection and methods

Samples selected for petrographic studies were collected from boreholes from the Matsap, Sishen and Hotazel areas, and from the field at locality E. A combination of standard microscopic investigations and x-ray diffraction (XRD) was conducted to determine the mineralogical composition of each sample analysed for whole-rock and isotopic geochemistry (see Chapter IV). Microscopic studies were conducted on thin sections under refracted light. Identification of minerals by XRD was carried out on powdered samples using a Philips Standard Water-Cooled Diffractometer using the following procedure: the powdered samples were packed onto aluminium slide holders. $CoK\alpha_1$ radiation was used with variable instrumental settings (30-40 kV, 20-30 mA) and a scan rate of $2°/1$ mn. Minerals were identified using their diffraction patterns and compared with the d-spacing values given in the "Powder data file", published by the International Center of Diffraction Data (JCPDS, 1974, 1980).

III.3. Mineralogy and petrography

BIFs, diamictites and volcanic tuffs were encountered both above and below the Ongeluk Formation, and their respective mineral compositions are presented in table III.1. All

the minerals identified are of a diagenetic to very low-grade metamorphic environment (James, 1954; Klein and Bricker, 1977; Tsikos, 1999).

The BIFs contain minerals typical of other Proterozoic BIFs (Tsikos, 1999). The difference between the BIFs below and above the Ongeluk lava is that hematite is more abundant above the lavas, whereas dolomite/ankerite and siderite are completely absent from the BIFs stratigraphically located above the lava.

The diamictites are lacking in diagnostic minerals of an igneous origin, for example plagioclase. Instead, they have bulk mineral compositions similar to the BIFs.

The volcanic tuffs are mineralogically more simple, and consist mainly of quartz, stilpnomelane and greenalite, and conspicuous glass shards.

	Below Ongeluk				Above Ongeluk		
	G-BIF	R-BIF	diam	tuff	BIF	diam	tuff
Quartz	XXX	XXX	XXX	XXX	XXX	XXX	XXX
Magnetite	XX	XXX	XX	X	XXX	XX	X
Hematite	X	X	X		XX	X	X
Calcite	XX	X	X	X	XXX	XXX	XX
Dolomite/ankerite	XX	X	XX				
Siderite	XX	X	XX				
Greenalite	XX	XX	X	XX	XX	X	XXX
Minnesotaite					XX	X	XX
Riebeckite			X				
Stilpnomelane	XX	XX	XX	XXX	XX	XXX	XXX
Pyrite	X	X	X		X	X	

Table III.1. Bulk mineralogical composition of the different rock types present in the Makganyene Formation. (G-BIF: Griquatown BIF; R-BIF: Rooinekke BIF; XXX: abundant phase >20%; XX: common phase >5%; X: accessory phase observed but not detected by XRD means).

III.3.1. BIF petrography

The three stratigraphically different BIFs (i.e. Griquatown, Rooinekke and Hotazel BIFs) are described separately in order to aid comparaisons. Corresponding sample names are included in the legend of each photomicrograph.

III.3.1.1. Petrography of BIFs below the Makganyene Diamictite
III.3.1.1.1. Petrography of the Griquatown BIFs

The BIFs below the Makganyene Formation belong to the Griquatown BIFs, and two different facies can be described: clastic-textured allochemical BIFs and microbanded

autochtonous/orthochemical BIFs according to the classification of Beukes (1980, 1983, 1984).

The clastic textured BIFs occur mainly in the northern part of the Griqualand West Basin, in the Hotazel area. The main corresponding lithofacies is a peloidstone consisting of micritic ankerite and siderite peloids set in a micritic chert matrix (see figure III.1), with occasional chert intraclasts (as shown in figure III.1, C1 and C2). The peloids generally have a unimodal grain size, but larger grains are also present. The shape of the peloids is spheroidal and flattened, and is occasionally elongate. The peloids usually lie parallel to the bedding plane. Generally, the ankerite and siderite have been partly or wholly replaced by magnetite, and to a lesser extent by greenalite, outlining the contours of the peloids (see figure III.1, A1 and A2). The positive identification of the very fine-grained carbonate minerals was accomplished by means of the XRD technique with reflections of dÅ=2.90 for ankerite and dÅ=2.80 for siderite. The peloidstones are organised in mesobands, which consist of graded cycles, 2 to 3 cm thick.

The presence of stilpnomelane in the peloidstones was revealed by its typical reflection dÅ=12.20 in the XRD patterns. As shown in figure III.1, C1 and C2, intraclastic microbands of peloids could be present within a micritic to microsparitic chert mesoband. In this particular example, the peloids are stilpnomelane-rich (brown colour) and well rounded chert grains are associated with the intraclastic microbands. Stilpnomelane under the microscope consists of brown needles arranged in an acicular fashion (Tsikos, 1999), but in the peloidstones, it was not observed due to its very fine-grained nature. Stilpnomelane needles are practically always associated with carbonate minerals (Tsikos, 1999), and would therefore probably be present within the peloids where ankerite and siderite minerals occur.

The matrix of the peloidstone consists of micritic chert and greenalite (see figure III.1, A1 and A2). Greenalite was positively identified by standard petrographic studies (very fine, green disseminated flakes, strong pleochroism as shown in figure III.1, A1 and A2) and by its characteristic reflection of dÅ=7.20 in XRD patterns. Not all peloidstone samples contained greenalite, but when present, it occurred with micritic chert and to a lesser degree carbonate minerals. As shown in figure III.1, B1 and B2, stylolites are present and are of a late diagenetic origin. Stylolitic joints usually occur in limestones and well-cemented sandstones (Conybeare and Crook, 1968).
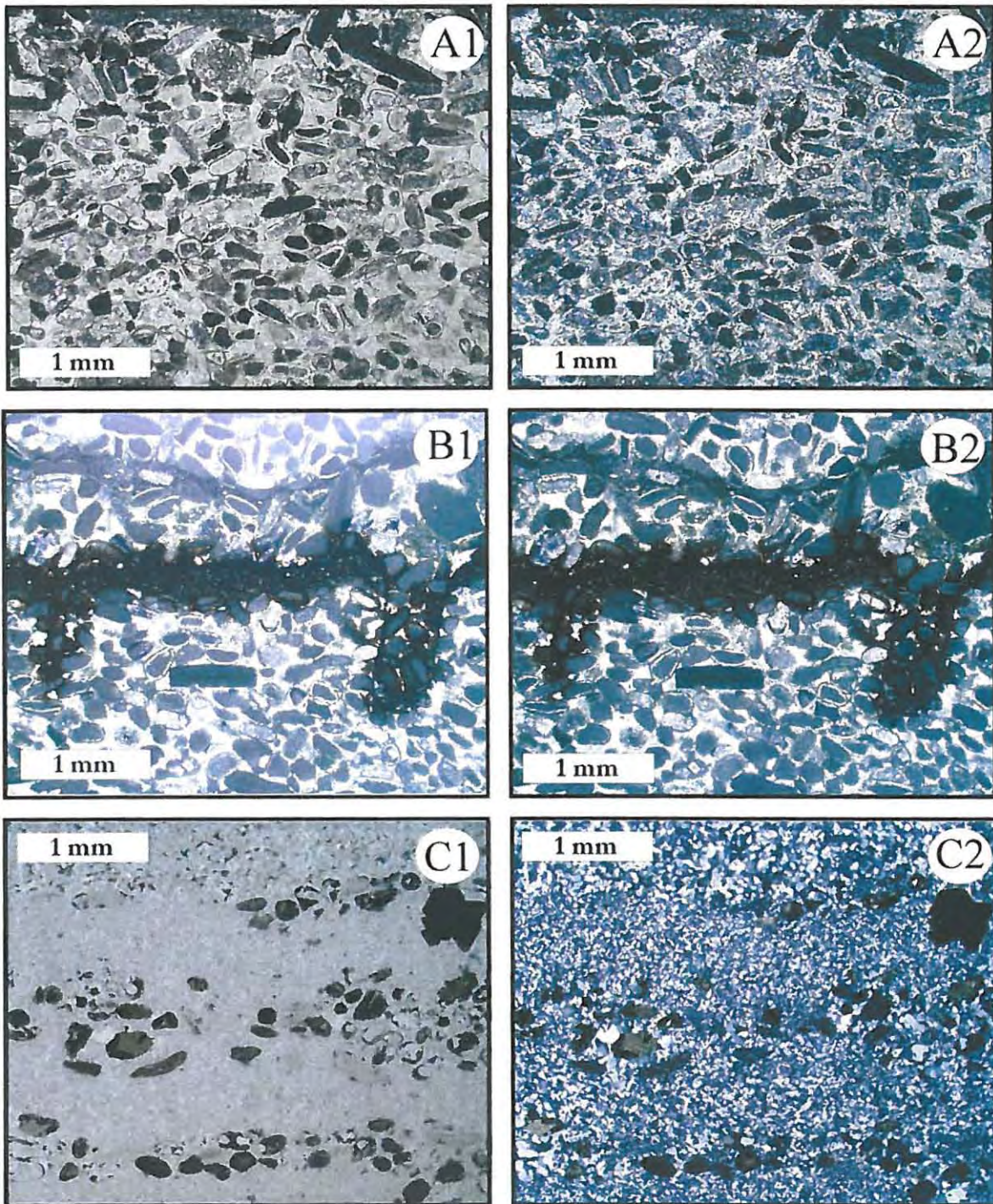
Figure III.1. A1 (plain polarized light) and **A2** (cross polarized light): peloidstone (BG5-163.50). **B1** (plain polarized light) and **B2** (cross polarized light): peloidstone with stylolite (BG5-163.50) .**C1** (plain polarized light) and **C2** (cross polarized light): intraclastic peloids in a chert matrix (BG5-128.20).

This could be an indication that chert cementation took place at a very early diagenetic stage, and later underwent differential dissolution, forming the stylolitic joints. The occurrence of hematite along the stylolitic joint enhances this post-depositional structure.

Pyrite can be seen with the naked eye in hand-samples. It appears throughout the stratigraphy, with no specific concentration gradient. Pyrite usually occurs as anhedral to subhedral grains.

The autochtonous BIFs (Beukes, 1980, 1983, 1984) occur to a lesser extent in the Hotazel area, but are generally well developed from the Sishen area southward into the Griqualand West Basin. Their varve-like aspect (Kimberley, 1989) is their principal characteristic, with alternating chert and iron-rich bands. According to the classification of Beukes (1980, 1983, 1984), the corresponding main lithofacies are banded ferruginous chert and rhythmic iron-formations.

Photomicrographs shown in figure III.2 (A1 and A2) represent the other type of BIF existing in the Hotazel area. It is stratigraphically located at about two meters below the Makganyene diamictite, and is markedly different from the previously described underlying peloidstones. Because of the high content in magnetite within this sample, this BIF belongs to the magnetite-chert band-lutite lithofacies of Beukes (1980, 1983, 1984). The figure III.2 (A1 and A2) shows disseminated euhedral opaque magnetite grains within a chert/stilpnomelane micritic matrix. Other mineral phases were identified in this sample using the XRD technique, and these are small amounts (less than 5%) of ankerite and siderite. These carbonate minerals are associated with stilpnomelane which is invariably intimately related with the carbonate phase. The magnetite is disseminated throughout the hand-sample, but also shows higher concentrations forming magnetite microbands. The magnetite may form from a precursor consisting of hematite (Tsikos, 1999) or could have replaced carbonate minerals (Beukes, 1980). No evidence could be drawn to differentiate the origin of the magnetite here.

III.1.1.2. Petrography of the Rooinekke BIFs

Further south, in the Sishen area, the BIFs are typically laminated with alternating iron-rich and chert bands. In the photomicrographs shown in figure III.2 (B1 and B2), euhedral rhombs form a central ankerite-rich band. Each ankerite rhomb has a brown "cloudy" centre consisting of stilpnomelane (Beukes, 1980; Tsikos, 1999). The background of this ankerite-rich band consists of microcrystalline chert and dusty hematite associated with minor opaque and euhedral magnetite. The euhedral ankerite rhombs seem to float in this

background, clearly indicating a late diagenetic recrystallisation or replacement of pre-existing minerals (Tsikos, 1999). According to Beukes (1980), the ankerite rhombs replace both chert and siderite, but this is not evident here. On both sides of the ankerite-rich band, ankerite rhombs are disseminated and are finer grained, and not as well developed as in the band itself. There, the opaque microcrystalline hematite phase is disseminated and more abundant and forms part of the matrix mainly consisting of microcrystalline chert. Therefore, what seems to create banding is the alternation of higher concentrations of ankerite and hematite set in a cherty matrix. Therefore the rock type corresponds to a banded ferruginous chert or more precisely hematite-ankerite banded chert.

The photomicrographs shown in figure III.2 (C1 and C2) display another lithofacies of BIFs. This consists of a microband of euhedral magnetite grains within a mainly microcrystalline cherty matrix. This lithofacies would be described as magnetite-microbanded chert (Beukes, 1980, 1983, 1984). Within the magnetite microband, high birefringence minerals can be seen, that correspond to ankerite of the carbonate phase. Along the contact between the magnetite microband and the matrix, brownish minerals are concentrated comprising stilpnomelane and hematite. It is assumed that micritic ankerite must be present, hosting the stilpnomelane phase. Away from the magnetite microband, stilpnomelane (with micritic ankerite) and hematite are evenly disseminated within the microcrystalline chert matrix.

The last lithofacies encountered within the BIFs underlying the Ongeluk lava in the Sishen area corresponds to the pillow-rhythmites of Beukes (1980, 1983, 1984). The pillows consist of microcrystalline chert occurring with green flakes of greenalite (see figure III.3). They may contain ankerite that is invariably associated with brown needles of stilpnomelane. The edges of the pillows are generally coated with ankerite and stilpnomelane (not shown in figure III.3). The pillows are set in a microcrystalline chert-hematite-greenalite matrix (as shown in figure III.3). The banding is outlined by a concentration of very thin bands of hematite dust, and flat and elongated patches of greenalite. This particular sample contains quartz veining, which is associated with greenalite.
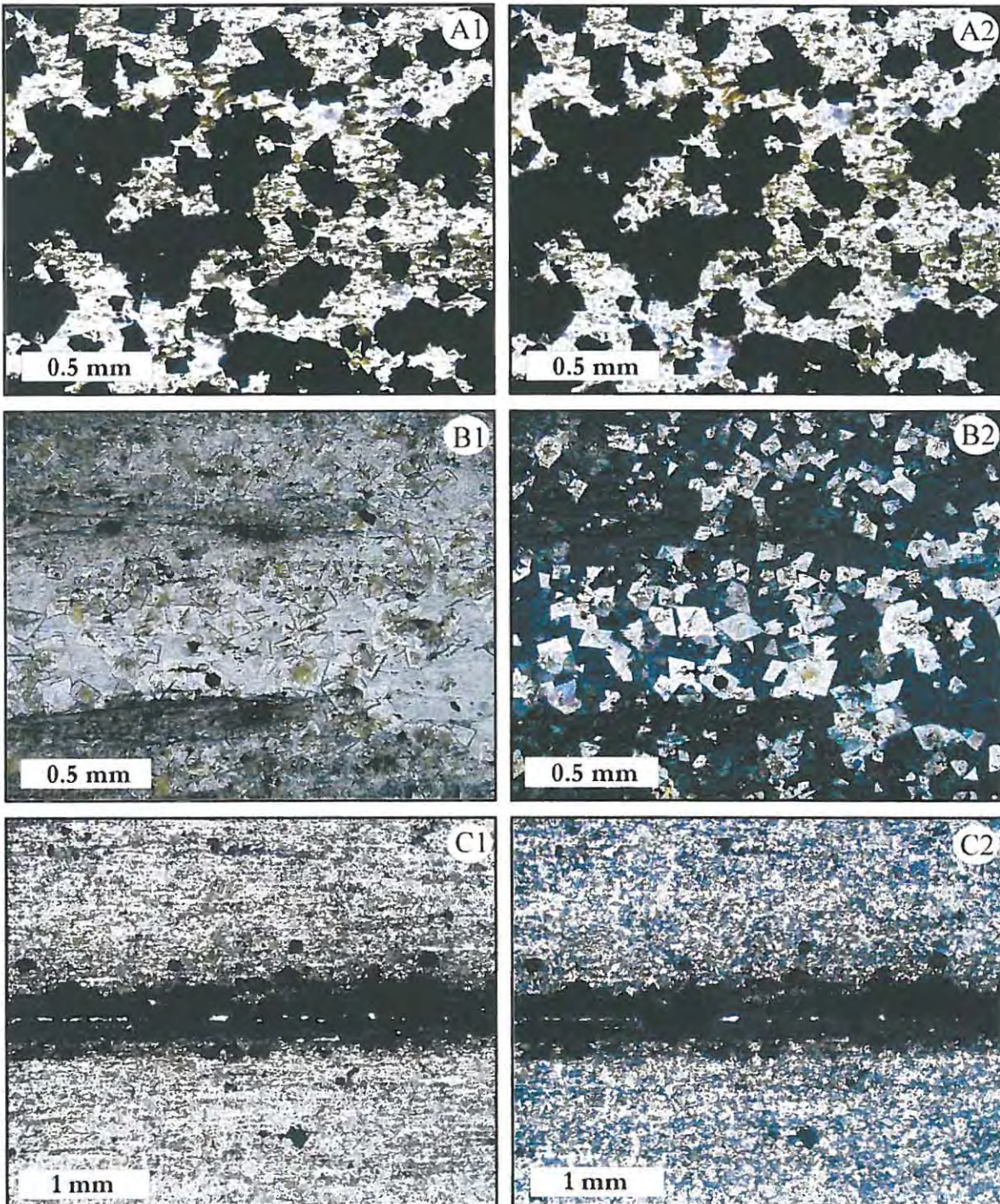
Figure III.2. A1 (plain polarized light) and **A2** (cross polarized light): magnetite-chert lutite from the Hotazel area (BG5-125.40). **B1** (plain polarized light) and **B2** (cross polarized light): hematite-ankerite banded chert from the Sishen area (GA129-26). **C1** (plain polarized light) and **C2** (cross polarized light): magnetite microbanded chert from the Sishen area (GA129-26).
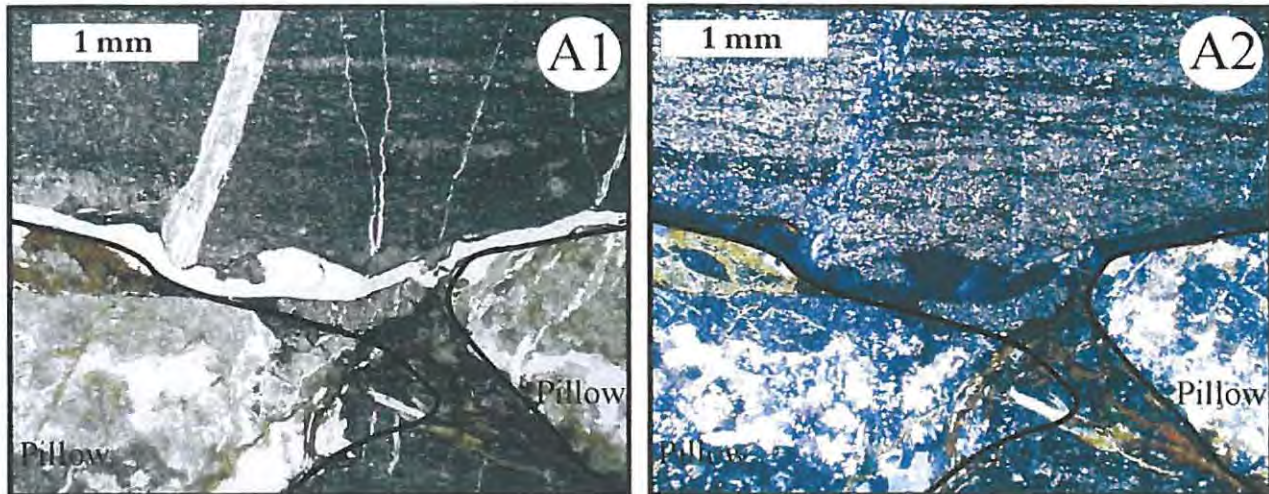
Figure III.3. A1 (plain polarized light) and **A2** (cross polarized light): pillow-rhythmite from the Sishen area, the pillows are outlined (GA107-337.2).

In the Hotazel area, no BIFs were interbedded with the diamictites. But in the Sishen area, especially at the base of the Makganyene Formation, thin horizons of BIFs are present and correspond to the facies described in figure III.2 and III.3. The BIF facies interbedded with the Makganyene diamictite are identical to the facies of the Rooinekke Formation underlying the diamictites.

III.3.1.2. Petrography of BIFs above the Ongeluk Formation

The BIFs located above the Ongeluk lava, belonging to the lowermost part of the Hotazel Formation, are texturally and mineralogically different from the BIFs below the Ongeluk lava described in the previous paragraphs. They are only preserved in the Hotazel area and have been eroded away elsewhere in the Griqualand West Basin. These BIFs are interbedded with volcanic tuffs and diamictites, and define the following cycle of deposition: hematite band-rhythmite – greenalite-magnetite rhythmite – calcite-magnetite rhythmite – hematite band-rhythmite.

The first lithofacies, shown in figure III.4 (A1 and A2), corresponds to the hematite band-rhythmite. This lithofacies consists of alternating chert-rich and hematite-rich bands. The chert bands also contain hematite, and the overall colour of this rock type is red. As shown in figure III.4 (A1 and A2), some of the microcrystalline chert is not in banded form, but rather in the form of irregular patches.
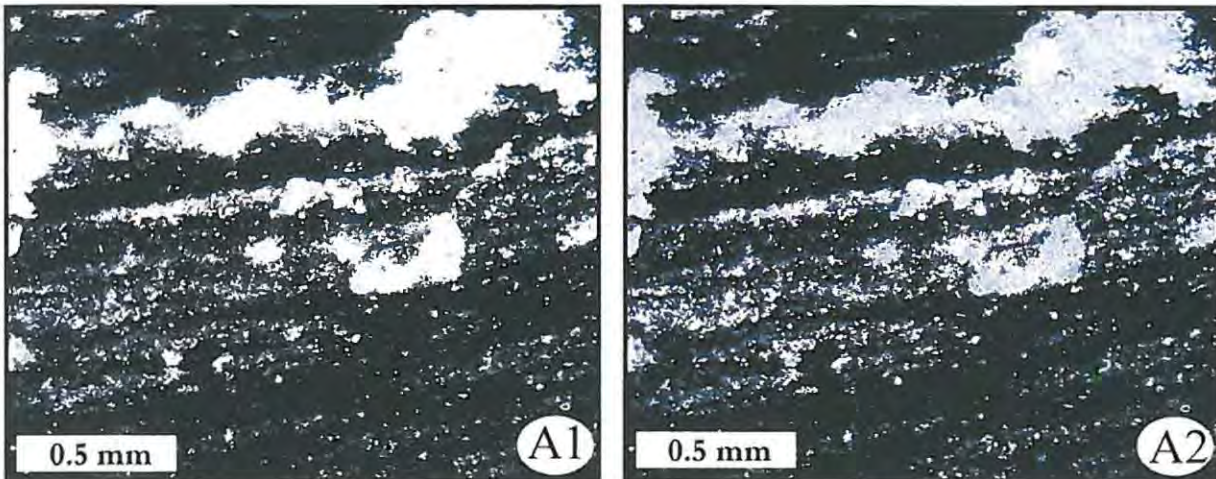
Figure III.4. A1 (plain polarized light) and **A2** (cross polarized light): photomicrographs of hematite band-rhythmite (REX41-144.9).

The second lithofacies encountered above the Ongeluk lava, at the base of the Hotazel Formation, is shown in figure III.5 (C1 and C2) and consists of alternating bands of chert-greenalite-calcite-stilpnomelane-magnetite and calcite-stilpnomelane. Since greenalite is usually associated with microcrystalline chert, and stilpnomelane with carbonate minerals, the simplified mineral assemblage would be chert-calcite-magnetite alternating with calcite bands. The bands of calcite are not bands as such, but are present as irregular pods (see figure III.5, C1 and C2 where A represents the chert-magnetite bands and B the irregular calcite pods) which are soft-sedimentary structures similar to the ones observed by Gross (1972) and Tsikos (1997).

The photomicrographs A1 and A2 from figure III.5 are a close-up view of a magnetite-rich band. It consists of a microcrystalline homogeneous mixture of chert and calcite (calcite is easily identified in picture A2 due to its high birefringence compared to the quartz) associated with euhedral grains of magnetite that are disseminated or concentrated along a magnetite band. Where hematite is present, it is associated with microcrystalline chert and not with calcite (see figure III.5.C1, band labelled "C" with its reddish colour). The contact with the irregular calcite pods is sharp and marked by a thin envelope of micritic calcite without any stilpnomelane (see figure III.5. B1, B2, C1 and C2). The rest of the irregular calcite pods consist of sparitic calcite, very rich in stilpnomelane, which gives these pods a typical brown colour. As shown in figure III.5 (C1 and C2), the basal contact of the calcite pods could be erosive, since it truncates the underlying magnetite-rich bands.
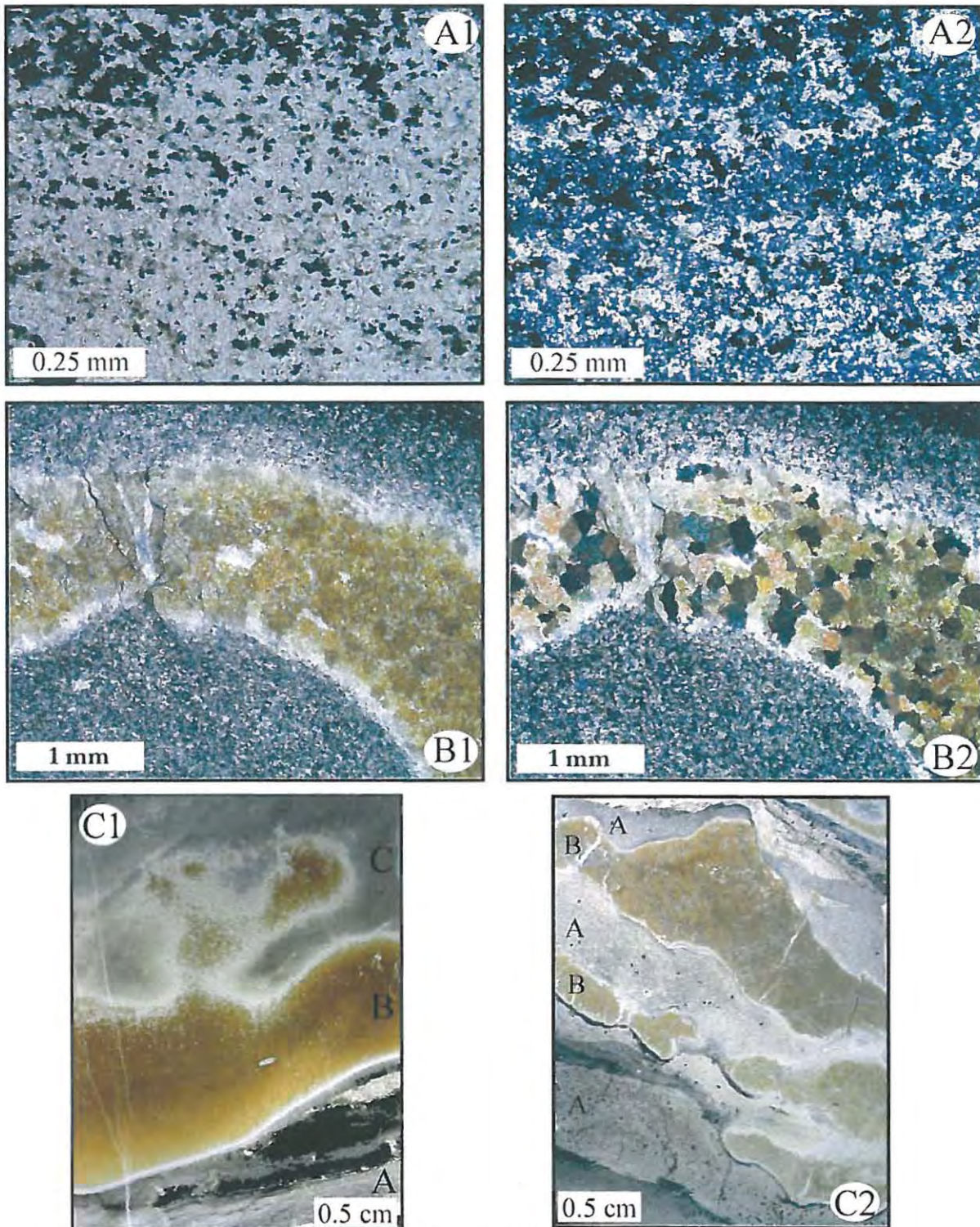
Figure III.5. A1 (plain polarized light) and **A2** (cross polarized light): magnetite-chert-carbonate band (REX41-129.90). **B1** (plain polarized light) and **B2** (cross polarized light): carbonate-stilpnomelane band(REX41-129.90). **C1** (REX41-134.30) and **C2** (REX41-129.90): magnetite-chert mesobands alternating with intraclastic calcite mesobands (A: chert-magnetite band; B: irregular calcite pod; C: chert-hematite band).

According to Beukes (1980, 1983, 1984), this lithofacies would be assigned to magnetite-chert mesobands, alternating with softly-deformed calcite mesobands.

The third lithofacies encountered above the Ongeluk lava, at the base of the Hotazel Formation and shown in figure III.6, consists of alternating bands of greenalite-chert and magnetite-rich bands. This lithofacies corresponds to a greenalite-magnetite rhythmite (Beukes, 1980, 1983, 1984) that belongs to the silicate-facies rhythmites.
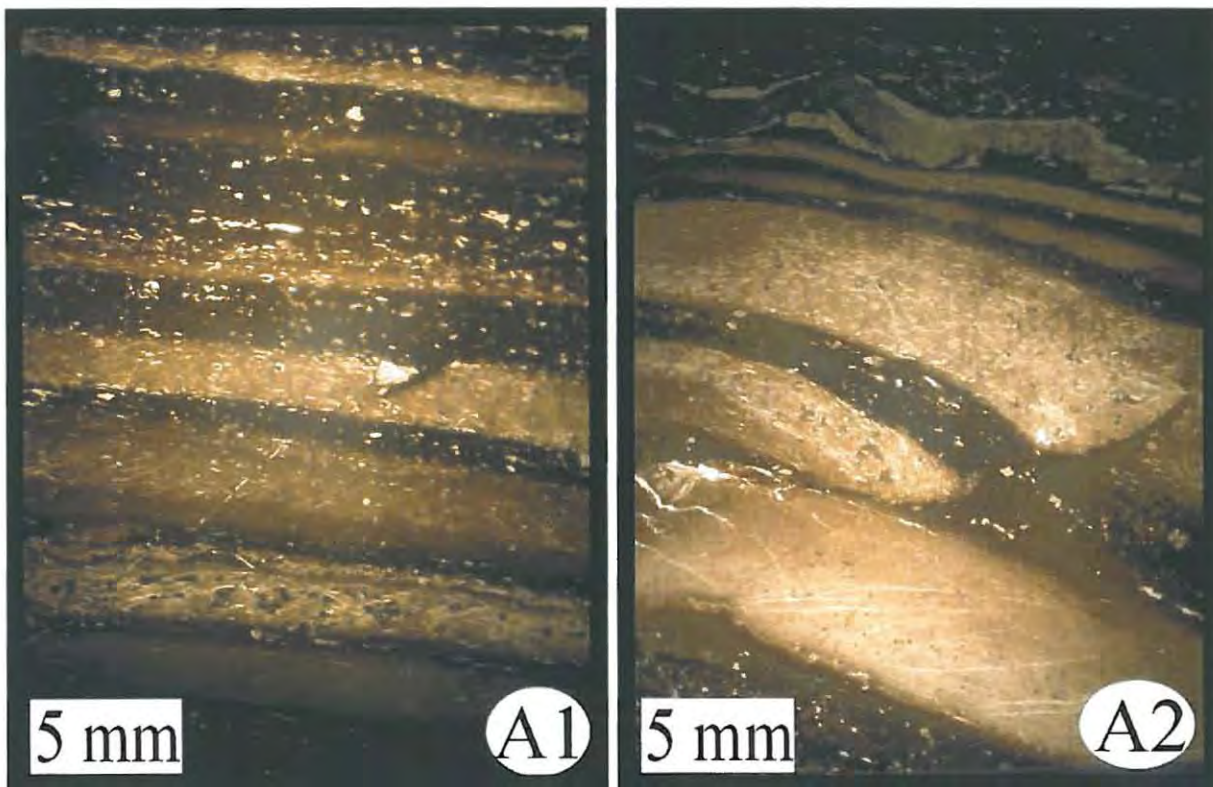
Figure III.6. A1 and **A2** represent the greenalite-magnetite rhythmite. Note in A2 soft-sediment deformation resulting probably from slumping (REX41-138.70).

Figure III.6.A1 clearly shows the rhythmic alternance of opaque magnetite-rich bands with greenalite-chert bands. The disseminated white grains are calcite associated with stilpnomelane. The overall colour of such lithofacies is green, which is a good indication for the presence of the mineral greenalite. The figure III.6.A2 shows soft-sedimentation deformation structures such as microfolding and microfaulting, probably caused by slumping.

In the figure III.7.A1 and A2, the magnetite-rich band is very well defined, with sharp bottom and top contacts. The magnetite-rich bands contain disseminated calcite grains (white), but also microcrystalline chert occurring with greenalite. The magnetite crystals occur in two different phases, i.e. a microcrystalline phase, and as coarse euhedral grains. The chert bands are composed of microcrystalline chert associated with greenalite and disseminated anhedral calcite grains, which are in places, flattened parallel to the bedding.

Within the greenalitic facies, some samples are laminated. The laminations are enhanced by greenalite flakes, which are parallel to the bedding, as shown in figure III.7 (B1 and B2). The rest of the matrix consists of microcrystalline chert, calcite, and minor minnesotaite. The latter is only found associated with greenalite-rich samples. A microband consisting of euhedral grains of magnetite is also present. The thickness of magnetite-rich bands in the greenalitic facies vary from about 5mm to less than 1mm.

Clastic contamination occurred in the greenalitic BIFs, and this is shown in figure III.7.C1 and C2. In this instance a fairly rounded clast 2x1mm is observed, consisting of chert, greenalite and calcite. Such an outsized clast disturbing and draped over by an otherwise fine and regular laminated sediments is interpreted as a dropstone (Hart and Roberts, 1994).

III.3.1.3. Petrogenetic constraints

According to Klein (1983) and Tsikos (1999), Fe-silicate minerals are the most diagnostic of the degree of burial metamorphism, whereas quartz, Fe-oxides and carbonates are of very little significance in assessing metamorphic grade.

In all the BIFs observed and described in the present study, all Fe-silicate minerals are characteristic of early to late diagenetic crystallisation (Klein and Bricker, 1977), and low-grade metamorphism is interpreted as not exceeding the very low green-schist facies due to the absence of the amphibole grunerite-cummingtonite (Tsikos, 1999). The BIFs below the Ongeluk lava are less calcareous (ankerite and siderite) than the ones above (only calcite). There are basically two kinds of diagenetic reactions that could form the same mineral assemblages observed depending on the Fe-precursor materials. One involves no valence changes if the Fe-precursor compounds were hydrous materials (i.e. hydromagnetite) (Tsikos, 1999). The second involves reduction processes of ferric precursor materials by concomitant organic matter oxidation to form ferrous Fe-silicates (greenalite), carbonate (ankerite), or magnetite (Tsikos, 1999).
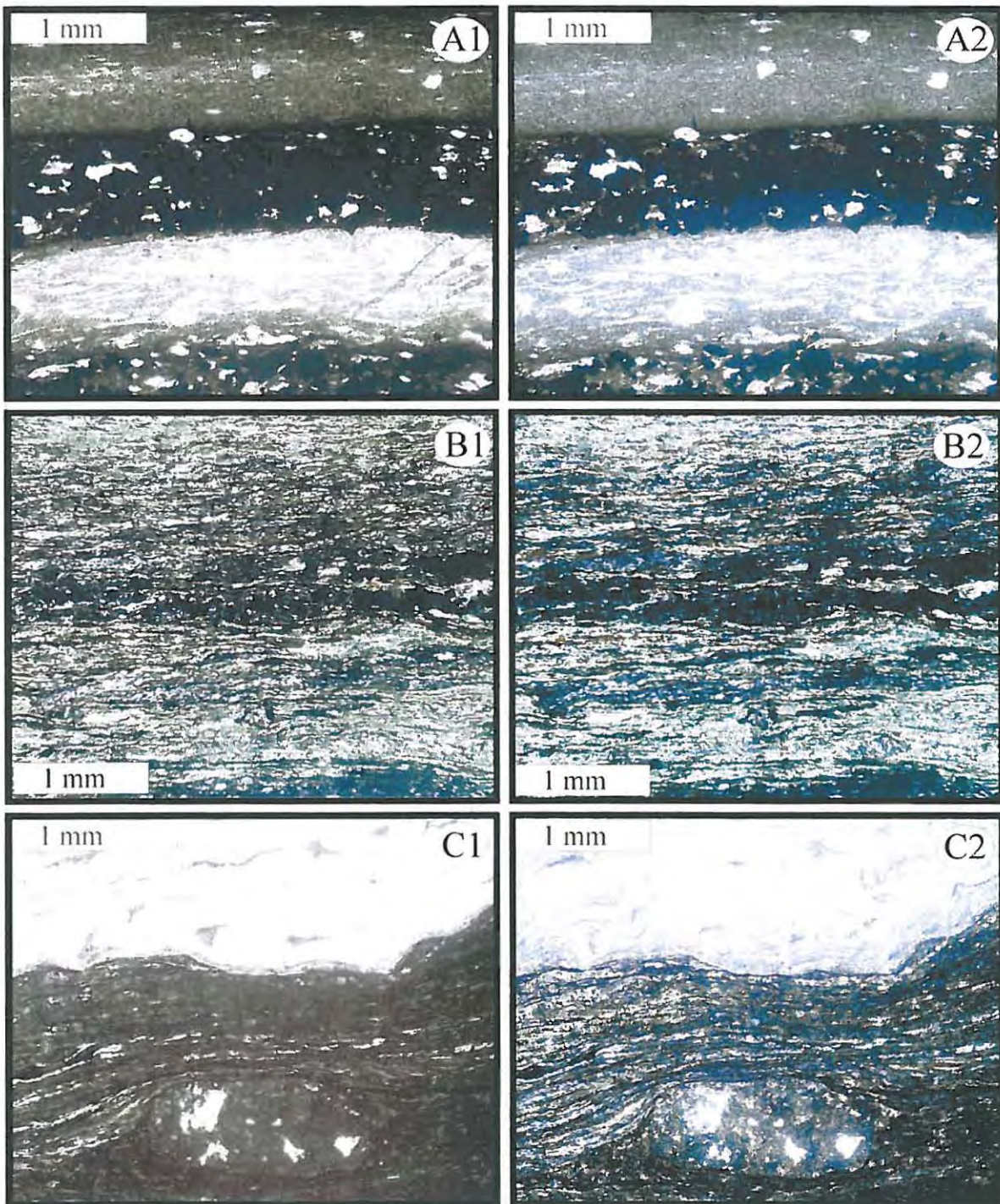
Figure III.7. A1 (plain polarized light) and **A2** (cross polarized light): greenalite-magnetite rhythmite (REX41-140.80). **B1** (plain polarized light) and **B2** (cross polarized light): greenalite-magnetite rhythmite, note greenalite flakes defining laminations (REX41-140.20). **C1** (plain polarized light) and **C2** (cross polarized light): Dropstone within greenalitic facies, note that such structure may also be due to compaction (REX41-140.80).

III.3.2. Petrography of the diamictites

III.3.2.1. Petrography of the Makganyene diamictites

As shown in table III.1, the diamictites occur both below and above the Ongeluk Formation. Diamictites are the main rock type of the Makganyene Formation. They generally consist of a heterogeneous mixture of cherty clasts with or without a sandy to shaly ferruginous matrix. Unlike observations by de Villierss and Visser (1977) and Visser (1981, 1999), no plagioclase and no microcline were observed using the standard petrographic studies and the XRD methods.

The majority of the clasts present within the diamictite consist of sub-rounded to angular chert rock fragments. Their size varies from sand-grain size up to 60 cm in diameter (Du Toit, 1954). Other more rare clast types are present, and consist of BIFs, volcanic tuffs, and even sulphides. The clast material provides information regarding the source of the diamictites.

As shown in figure III.8 (A1 and A2), the large clast present belongs to the peloidstone BIFs (shown in figure III.1). Since this peloidstone facies of BIFs is part of the unconformity surface in the Hotazel area, further north it should have been eroded away, and further south it should be present lower in the stratigraphy, thus indicating the source of the diamictite material. It is also proof that the ice-sheet was eroding the previously deposited Asbestos Hills Subgroup in the Hotazel area. The poor roundness of the clast also shows that the detrital material was transported over relatively short distance. The rest of the rock fragments in this sample are a quarter to a tenth of a millimeter in diameter and consist of sub-rounded chert (micro-crystallised quartz grains) and single quartz grains. All the fragments are set in a very fine matrix consisting of calcite, ankerite, magnetite, stilpnomelane, greenalite and quartz, corresponding to the early diagenetic to low grade metamorphic BIF mineral assemblages.

In figure III.8 (B1 and B2), the largest clast shown is a volcanic tuff fragment. It is easily identified with its chloritised quartz shards. The photomicrographs C1 and C2 in figure III.8 show a stromatolitic clast. The other clasts are sub-rounded quartz grains and chert grains. The very fine matrix contains the same minerals described as before: calcite, ankerite, stilpnomelane, greenalite, magnetite and quartz.
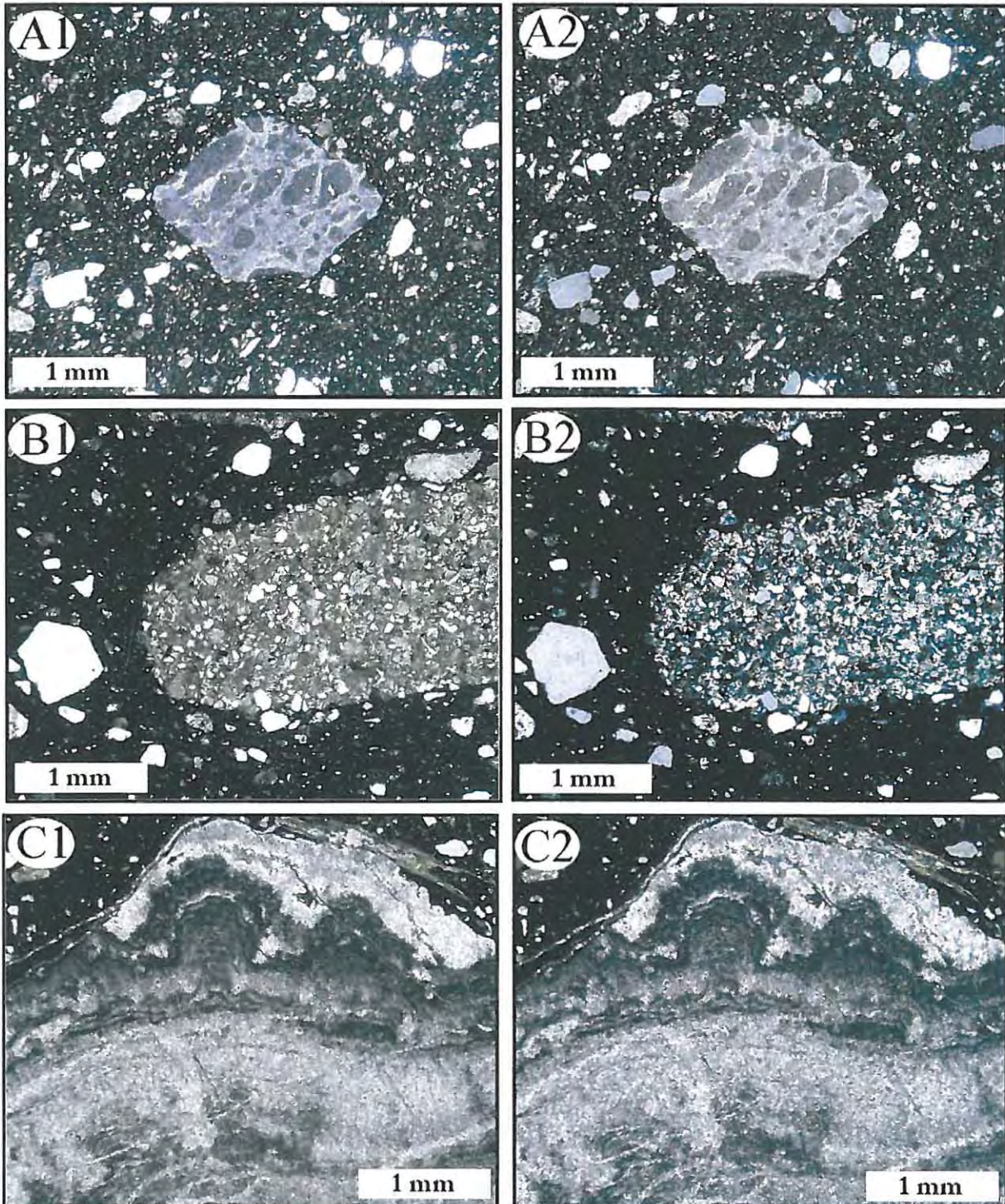
Figure III.8. A1 (plain polarized light) and **A2** (cross polarized light): peloidstone clasts (BH171/93-192.10). **B1** (plain polarized light) and **B2** (cross polarized light): volcanic tuff clast (BH171/93-192.10). **C1** (plain polarized light) and **C2** (cross polarized light): stromatolitic clast (GA107-285.50).

Figure III.9 shows the most abundant clast type (A1 and A2). The latter consists of an angular chert clast. The other clasts are angular to well rounded quartz grains. The small angular quartz grains were attributed by de Villierss and Visser (1977) to be of volcanic origin, and called "volcanic glass". Such shards occur throughout the diamictite, but are more abundant towards the top of the Makganyene Formation, near the base of the Ongeluk lava. Therefore, if these grains are indeed volcanic shards, volcanism would have been coeval with the glacial Makganyene event, but this input was minor within the diamictites.
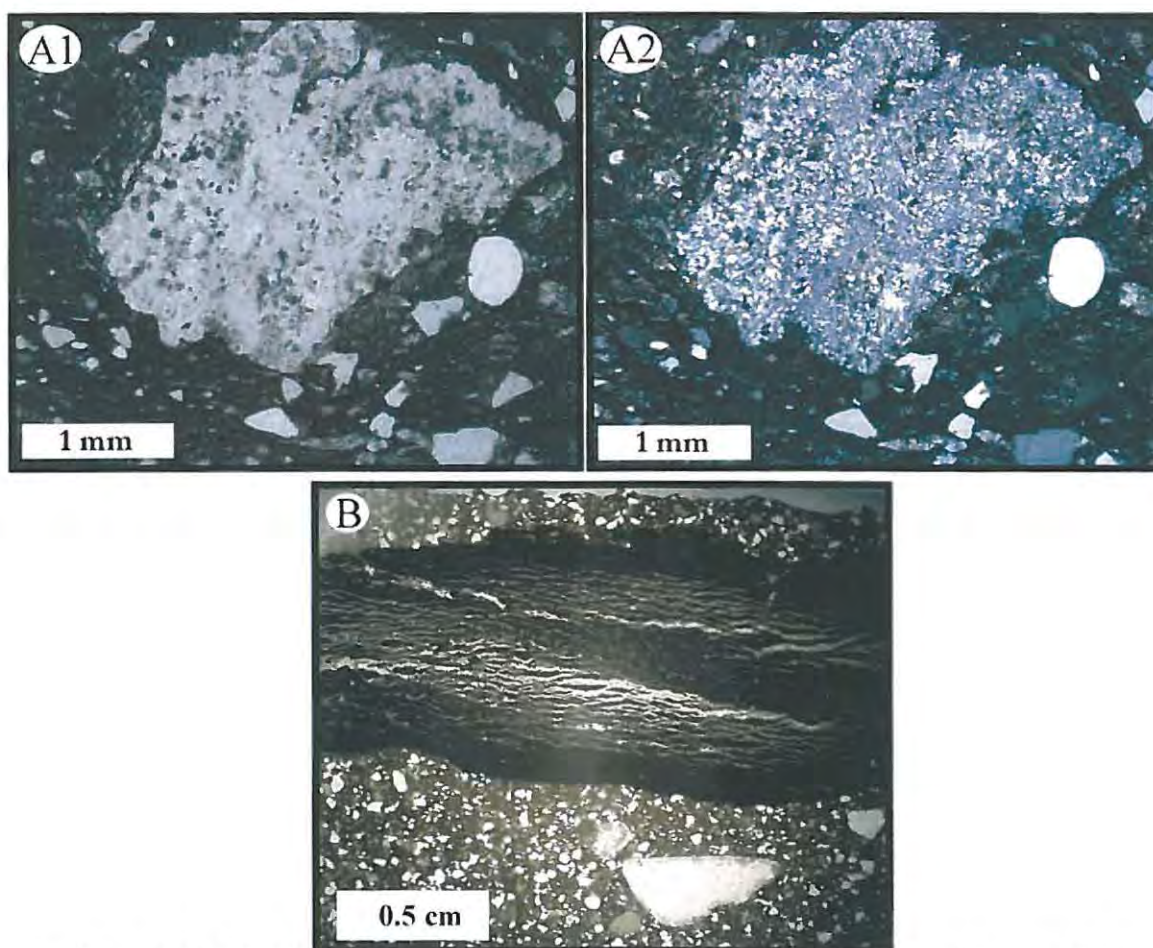
Figure III.9. A1 (plain polarized light) and **A2** (cross polarized light): angular chert clast (BH171/93-162). **B** (plain polarized light): sulphide clast (pyrite) (BH171/93-180.20).

The last lithological type of clast is the pyrite clast. Only one has been observed, and is shown in figure III.9 (B). It is a cylindrically shaped clast, about 3 centimeters diameter and 1 centimetre in length. It is set in a shaly and sandy matrix containing other clasts consisting of sub-angular chert coated by calcite (similar to the largest clast below the opaque pyrite

clast in figure III.9.B). This sulphide clast does not have a replacement, metamorphic or diagenetic origin but was simply eroded, transported, deposited and finally preserved due to the cold glacial climate of the glacial Makganyene Ocean.

All the described clasts occur in debris flows making up the diamictites of the Makganyene Formation. Other major types of clasts are striated pebbles (see figure II.11.B) and dropstones (see figure III.10.A, B, and C), which occur in a different setting and strongly favour a glacial influence for deposition of the Makganyene Formation. The dropstones consist of chert and can be rimmed by calcite (see figure III.10.C), which is associated with stilpnomelane. The dropstones shown are typically angular, with sediment laminations draped over them (Hart and Roberts, 1994). The presence of striations on clasts of the pebble class occurs north of the Griquatown Hinge Zone and represent clasts that have been released by grounded ice. Dropstones are restricted in the Matsap area, south of the Griquatown Hinge Zone, and represent clasts that have been dropped by floating ice into laminated sediments, causing disturbances in an otherwise regular banding (as shown in figure III.10.A, B, and C). The exclusive occurrences of dropstones and striated pebbles suggest that the Griquatown Hinge Zone represents a transitional zone, from grounded ice-sheet in the north to floating ice-shelf in the south.

As mentioned above, some chert clasts may be rimmed by calcite, as shown in figure III.10 (C and D) and also in the figure III.9.B (see the angular chert clast below the pyrite clast). This rim is attributed to burial diagenetic carbonate formation (Fairchild et al., 1994) and is common in glacial settings. According to Fairchild et al. (1994), carbonate crust on the clasts, if it is not a replacement feature, comes from the glacial weathering of carbonate rocks to rock flour size, which would be precipitated due to changes in environmental chemistry. The calcareous rim formed simultaneously or prior to the brown needles of stilpnomelane (see figure III.10.D for best example). This implies that the stilpnomelane is of diagenetic origin. The calcite clast shown in figure III.10.D has also been replaced by stilpnomelane along its periphery, but this particular clast also has late diagenetic growth of euhedral to sub-euhedral magnetite grains, which are getting coarser from the sides towards the centre.
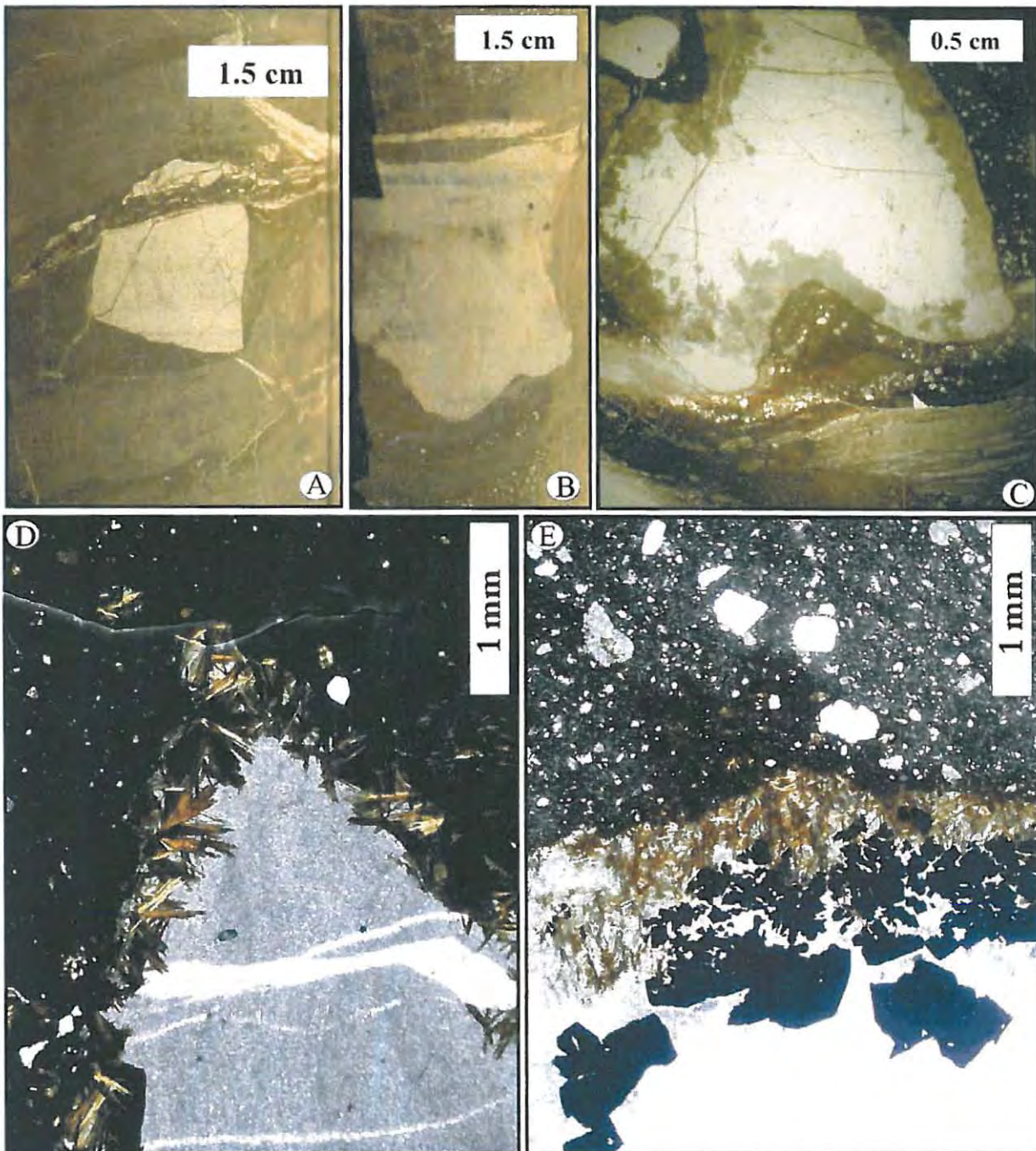
Figure III.10. A (MTP9-I3) and **B** (MTP9-I5) are dropstones in laminated sediments. **C**: dropstone with calcite rim (MTP9-I2). **D**: chert clast with calcite coating, brown needles of stilpnomelane are replacing calcite (BH171/93-217.20). **E**: calcite clast replaced by brown stilpnomelane along the sides, and opaque magnetite grains (BH171/93-205).

Other replacement features are present in the Makganyene diamictite, and these affect chert clasts as well as carbonate and magnetite clasts. These replacement features are displayed in figure III.11 (A1, A2, B1, B2, C1, and C2), and generally start from the clast margins and progress inwards. They are identical to the previously described calcite crust, with stilpnomelane replacing this carbonate rim.

The first example of replacement is shown in figure III.11 (A1 and A2). It consists of a chert clast having its rim replaced by the typically green flakes of greenalite. This is not surprising since greenalite has so far been described as being associated with chert. This type of replacement seems to occur when the sample is greenalite-rich, and the smaller chert clasts are completely replaced by greenalite (see figure III.11.A1 and A2).

The likely reactions that are responsible for the typical associations of chert/Fe-oxide/greenalite, and carbonate/stilpnomelane are:

$$3\ Fe_2O_3 + 2\ SiO_2 + 2\ H_2O + 2\ C_{org} \longrightarrow 2\ Fe_3Si_2O_5(OH)_4 + 2\ CO_2$$

3 hematite + 2 chert + 2 water + 2 carbon $\longrightarrow$ 2 greenalite + 2 gaz

$$6\ CaFeCO_3 + Fe_2O_3 + 12\ SiO_2 + 6\ C_{org} + 27\ H_2O \longrightarrow 2\ Fe_8Si_{12}(OH)_{27} + 6\ CaCO_3$$

6 ankerite + hematite + 12 chert + 6 carbon + 27 water $\longrightarrow$ 2 stilpnomelane + 6 calcite
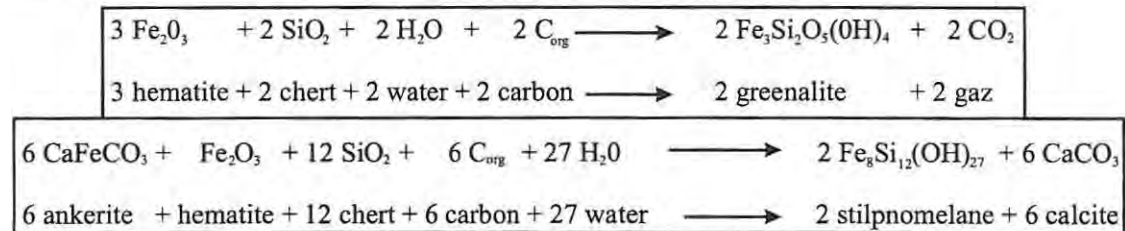
According to Tsikos (1999), the needle-shaped amphibole riebeckite is a rare mineral in the Hotazel Iron Formation. It has also been observed in the Makganyene diamictite as an alteration mineral. Riebeckite occurrences are shown in figure III.11 (B1, B2, C1 and C2). Riebeckite appears to be replacing iron-rich carbonate clasts consisting of peloidstone as shown in figure III.11 (B1 and B2). In this example, riebeckite needles grow from the edge of this clast inward. This replacement feature is very rare and therefore has not been extensively observed in other samples. The smaller clasts above have also been replaced by riebeckite. In the figure III.11 (C1 and C2), riebeckite is replacing a hematite clast in the same way that it replaces the carbonate clast of figure III.11 (B1 and B2). According to Tsikos (1999), the presence of riebeckite in the Hotazel Formation is due to dissolution processes involving Na-rich diagenetic fluids in close association with stylolites. All the samples containing riebeckite come from borehole BG5, from the Hotazel area where Na-metasomatism is known to have occurred. Therefore riebeckite is not of a diagenetic origin in the Makganyene Formation in the Hotazel area, but a product of late alteration involving sodium-rich fluids, which will be discussed further in chapter IV. Samples from the Hotazel area tend to be more sodium-rich than any other area sampled during this study.
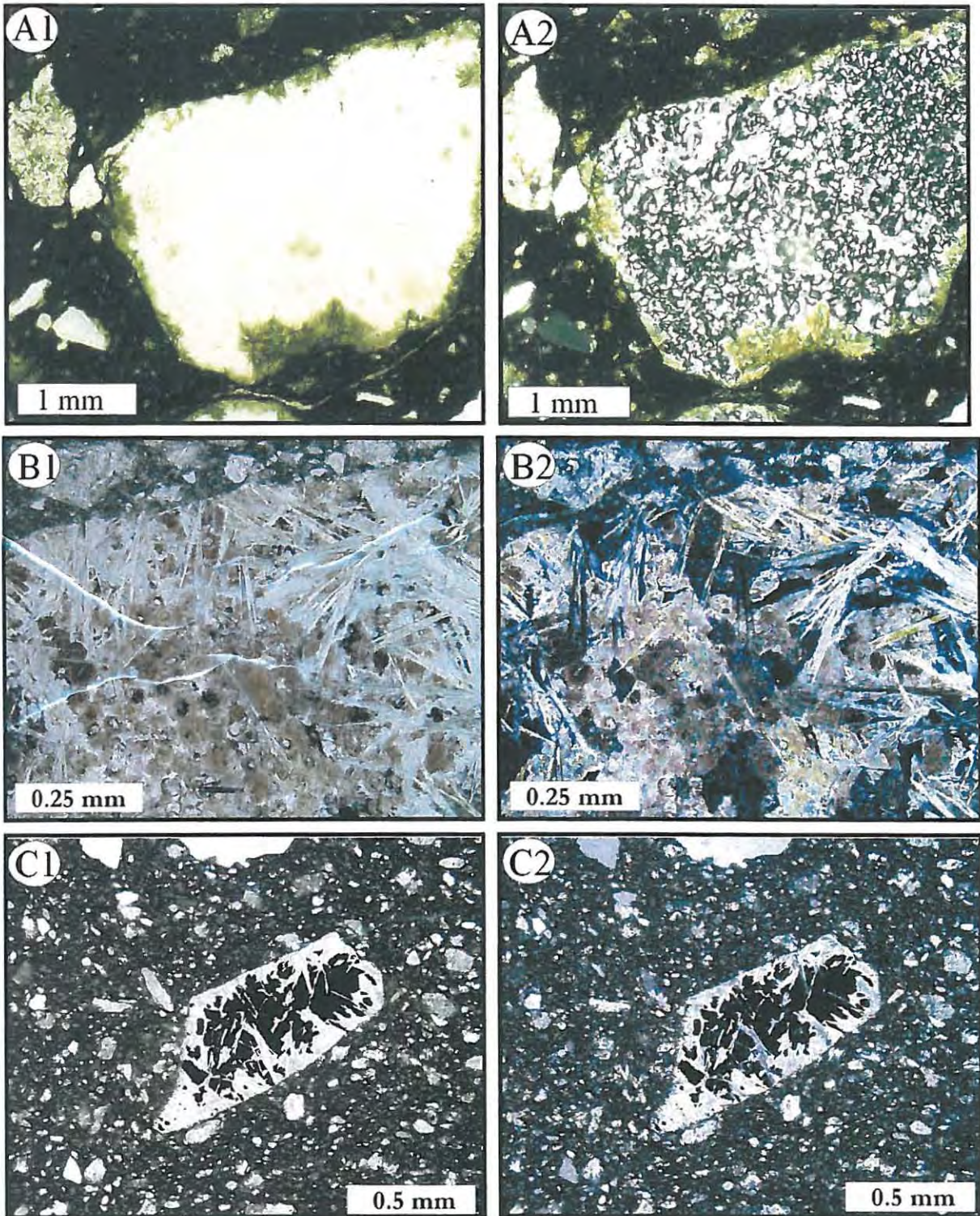
Figure III.11. A1 (plain polarized light) and **A2** (cross polarized light): greenalite replacing chert clast (MTP4-M13). **B1** (plain polarized light) and **B2** (cross polarized light): riebeckite needles replacing a carbonate clast (BG5-109.40). **C1** (plain polarized light) and **C2** (cross polarized light): riebeckite needles replacing a hematite clast (BH171/93-199).
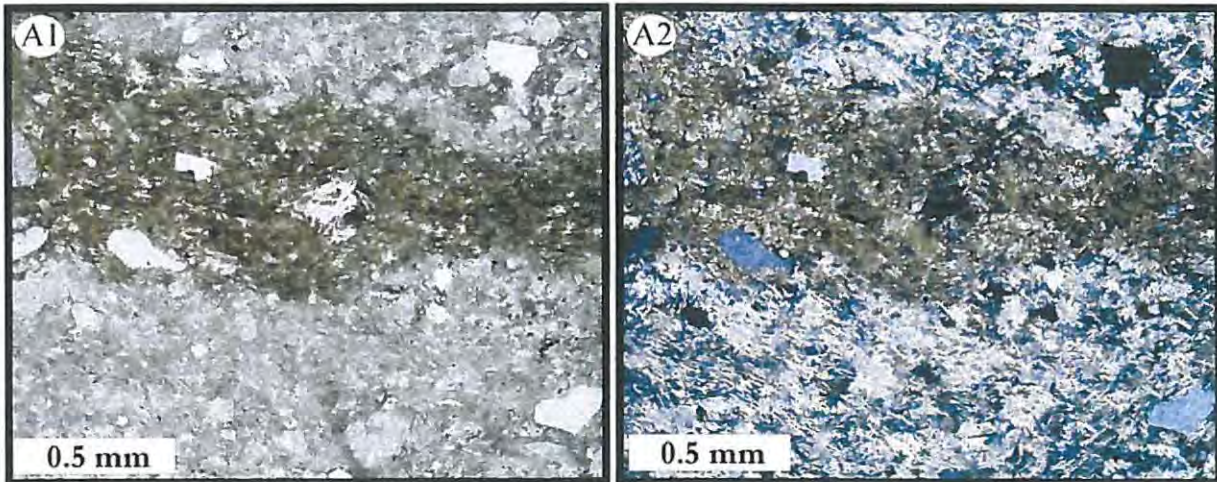
Figure III.12. A1 (plain polarized light) and **A2** (cross polarized light): riebeckite-rich diamictite matrix (BG5-108.60).

Riebeckite is also found in the matrix of the Makganyene diamictite (see figure III.12.A1 and A2). In this sample, the riebeckite needles have a parallel arrangement. Since it has previously been observed replacing carbonate and hematite minerals, the riebeckite that appears within the matrix of the diamictite is probably replacing similar minerals. Because the matrix is very fine-grained, it is not possible to conclude that riebeckite from the matrix replaced more carbonate than hematite minerals. By comparison with the other diamictite samples, it is highly likely that riebeckite replaced mostly carbonate minerals. The figure III.12 (A1 and A2) also shows a brown stilpnomelane patch which is of diagenetic origin.

III.3.2.2. Petrography of diamictites above the Ongeluk Formation

Diamictites have also been reported from above the Ongeluk Formation and are restricted to the base of the Hotazel Formation. They are intimately associated with volcanic tuffs or hyaloclastites, which will be discussed later. Kirschvink et al. (2000) described these Hotazel diamictites as glacial, containing small dropstones. As shown in table III.1, they contain the same proportions of oxide minerals as the diamictites of the Makganyene Formation, which correspond to quartz, magnetite and hematite (James, 1954). The differences between the Makganyene and Hotazel diamictites are:

  ➢ their carbonate mineralogy (Makganyene diamictite: dolomite-ankerite-siderite; Hotazel diamictite: calcite only),
  ➢ their silicate mineralogy, especially with the significant increase in stilpnomelane content, generally interpreted as altered volcanic ash (Beukes, 1983).
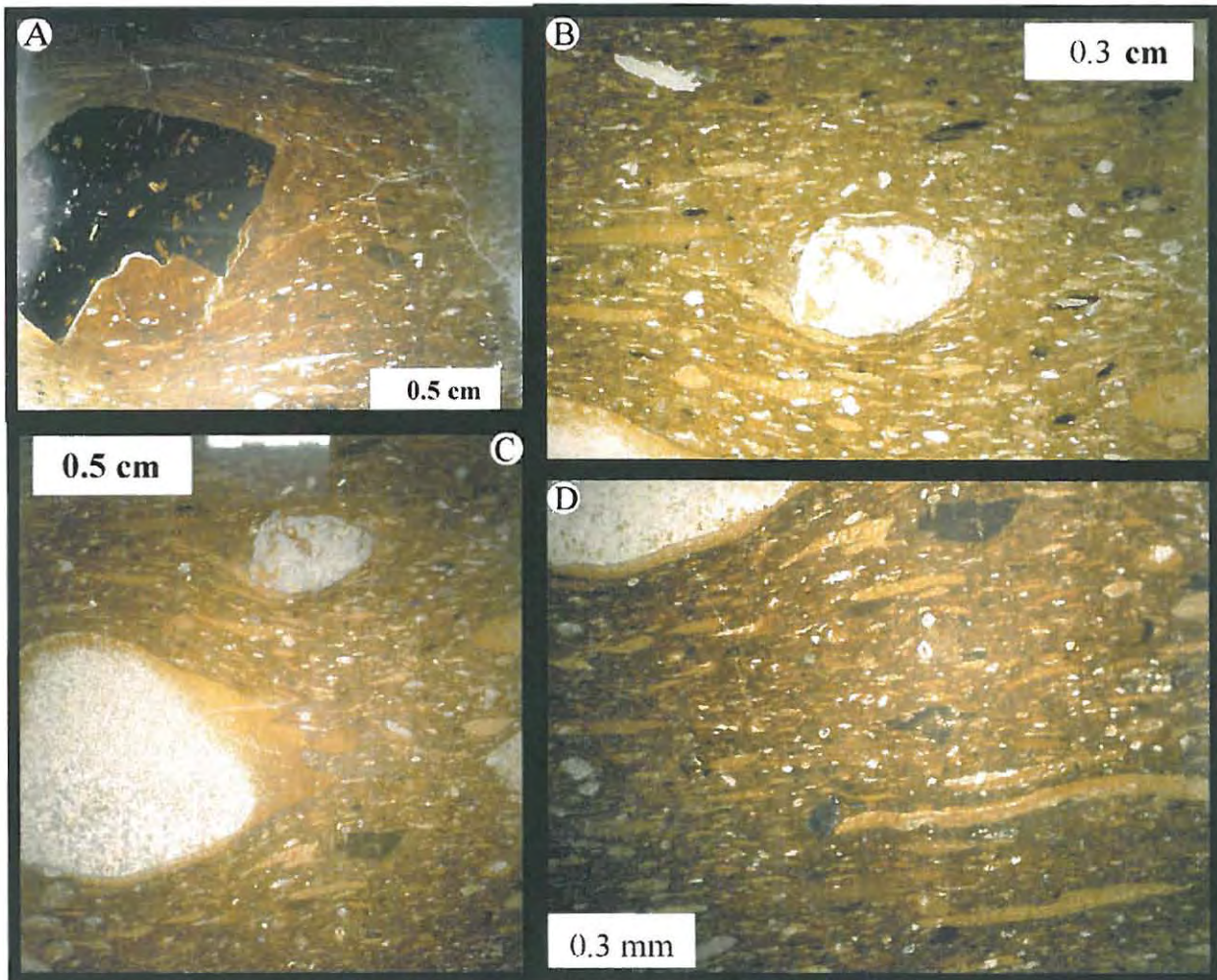
Figure III.13. **A** (REX41-132.80), **B** (REX41-133.80), **C** (REX41-133.80), **D** (REX41-133.80): photomicrographs in plain-polarised light, showing the main features of the Hotazel diamictite such as brown-colour matrix, clasts disturbing the laminations, rounded calcite and angular magnetite clasts, as well as flat and elongated carbonate-stilpnomelane features.

Because of the high proportions of stilpnomelane in the matrix (see table III.1 and figure III.13 A, B, C and D), the general colour of the diamictite matrix in fresh samples is brown. The stilpnomelane modal proportions reflect a possible volcanic influence (Beukes, 1983) and also represent the carbonate content of the matrix, which is more than 20%. It also contains clasts that are small in size (from silt grain size to 1.5 cm diameter) and some of the larger ones are shown in figure III.13. In figure III.13.A an angular magnetite clast has disturbed the laminations of the matrix. Figures III.13.B and D respectively represent the top and the base of figure III.13.C. In these photomicrographs, other smaller angular magnetite-rich clasts as well as carbonate clasts are present. The carbonate clasts are rounded and have not been replaced by stilpnomelane. Figure III.13.C contains in the centre, a large carbonate clast that has its outer rim replaced by stilpnomelane. Such large clasts commonly exhibit pressure shadows outlined by stilpnomelane (see figure III.13.C). On the other hand, other smaller rounded carbonate clasts with irregular contours do not exhibit pressure shadow textures.

Another feature of the Hotazel diamictites is the presence of elongated, flat carbonate-stilpnomelane lenss (see figure III.13, D in particular). These are not clasts and are interpreted as being precipitated under the same conditions as the carbonate-rich BIFs previously described in paragraph III.3.1.2 and shown in figure III.5 (C1 and C2). The conditions of deposition of the Hotazel diamictites are crucial for the development of a genetic model for the deposition of the Kalahari Manganese Field. Therefore, if a glacial origin is diagnosed for these diamictites by petrographic studies, it should be confirmed by geochemical studies (see chapter IV).

Another piece of evidence for dropstones is the appearance of an isolated large fragment, totally out of the size range of the enclosing sediments. Figures III.14 and III.15 show all the types of clasts which could be identified as dropstones. Figure III.14 (A1 and A2) shows a sub-rounded magnetite-chert clast disturbing the laminations. The laminations are draping over the clast, which is diagnostic for a glacial dropstone (Hart and Roberts, 1994), but were also "pierced" by the clast when it penetrated the unconsolidated sediment. The clast is vertically orientated as most of the other dropstone-like clasts. Therefore this clast could be interpreted as a glacial dropstone. The following pictures (see figure III.14 B1, B2, C1 and C2) are similar in the way that the clasts are clearly disturbing the laminations.

However, one could argue against a glacial origin for these rocks if such deformation structures are interpreted as compaction of sandy shale, with formation of pressure shadow at the tips of large clasts that probably formed during burial.
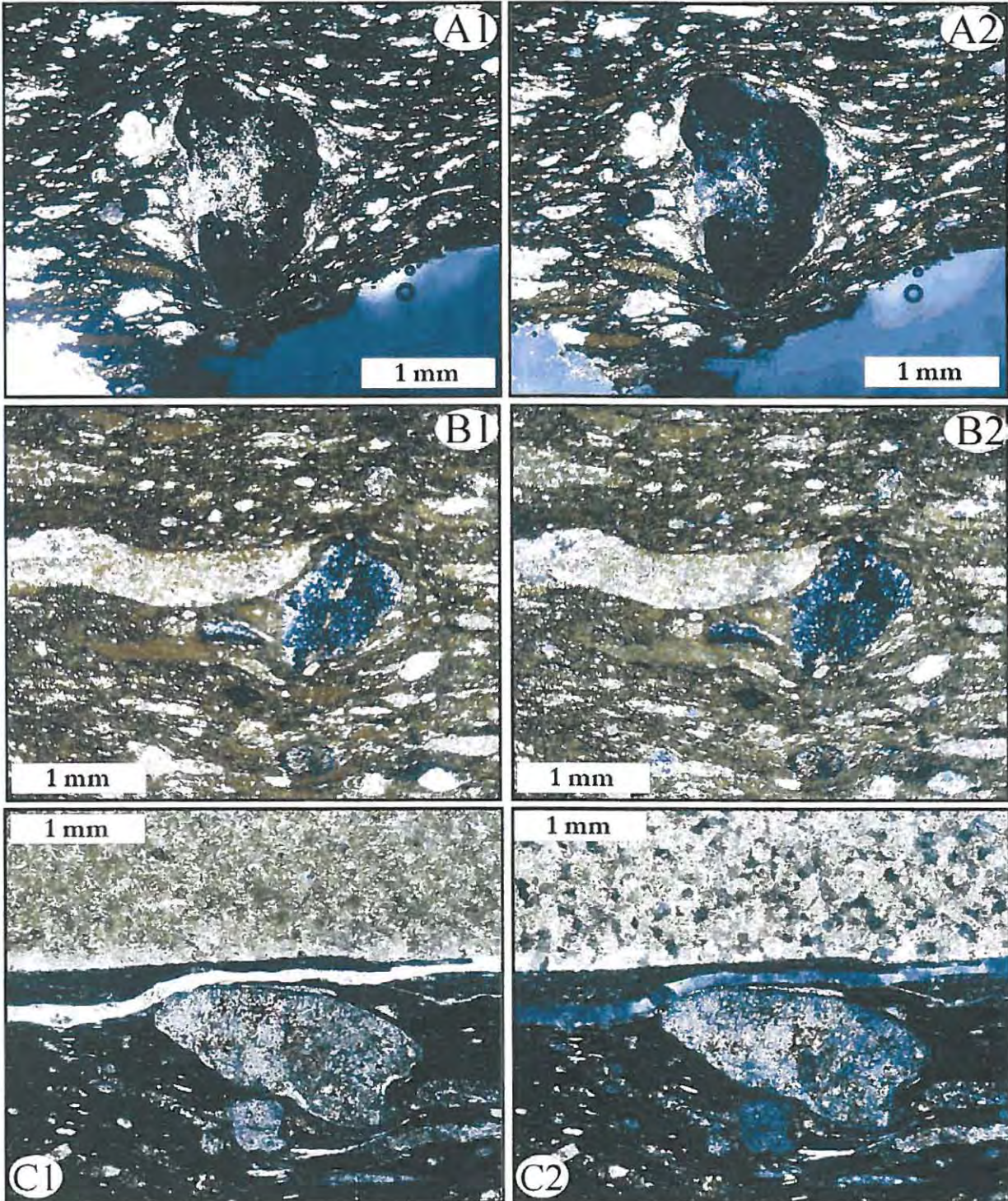
Figure III.14. A1 (plain polarized light) and **A2** (cross polarized light): vertical chert-magnetite clast interpreted as a glacial dropstone (REX41-131.20). **B1** (plain polarized light) and **B2** (cross polarized light): magnetite-chert clast interpreted as dropstone (REX41-134). **C1** (plain polarized light) and **C2** (cross polarized light): chert-magnetite clast interpreted as dropstone with calcite-stilpnomelane band from the carbonate-rich BIFs shown in figure III.5 (C1 and C2) (REX41-131.20).

Figure III.14 (C1 and C2) shows a magnetite-chert clast which could also be interpreted as a dropstone. It is overlain by a stilpnomelane-calcite band of the carbonate-rich BIFs described in paragraph III.3.1.2 and shown in figure III.5 (C1 and C2). The contact is sharp and might simply mark a sudden termination of clastic influx while carbonate precipitation continued.

Figure III.15 (A1 and A2) is a close-up photograph of a calcite clast. Calcite grains are fine along the edge of the clast, while in the centre they are significantly coarser. Few stilpnomelane flakes are located in the outer fine-grained rim of the clast. The contact between the clast and the matrix of the Hotazel diamictite is sharp. In the matrix of the diamictite, along the contact, very fine-grained stilpnomelane defines a pressure shadow. This would have most likely formed during compaction caused by burial that flattened the clast into the shape of an eye.

Microphotographs from figure III.15 (B1 and B2) represent a close-up of the flattened carbonate-stilpnomelane lenss. As stated previously, they are interpreted as continuous carbonate precipitation disrupted by clastic influx of possible ice-rafted debris (shown in figure III.14). In the carbonate-rich BIFs, the carbonate bands occur as irregular pods. In the case of the Hotazel diamictite, the carbonate pods may have been flattened during burial to their present from. Chert and magnetite form the same carbonate-rich BIFs are present in the matrix of the diamictite, between the flattened carbonate-stilpnomelane lenss, but their very fine-grained nature makes optical identification difficult, even though chert and magnetite have been detected by means of XRD.

III.3.2.3. Petrogenetic constraints

Differences between the Makganyene and Hotazel diamictites exist due to their stratigraphic positions. This difference in mineralogy does not necessarily mean that the environments of deposition were different, but may represent a shift in the source rocks. The Makganyene Formation source is mainly represented by BIFs, and to a lesser extent carbonate and other crustal rocks with a pelitic composition, and few observed angular fragments of possible volcanic origin (de Villierss and Visser, 1977). The Hotazel diamictite has a distal volcanic signature with its high stilpnomelane content (no volcanic angular glass shards have been observed) and it is intimately interbedded within hyaloclastites related to the directly underlying Ongeluk volcanics.
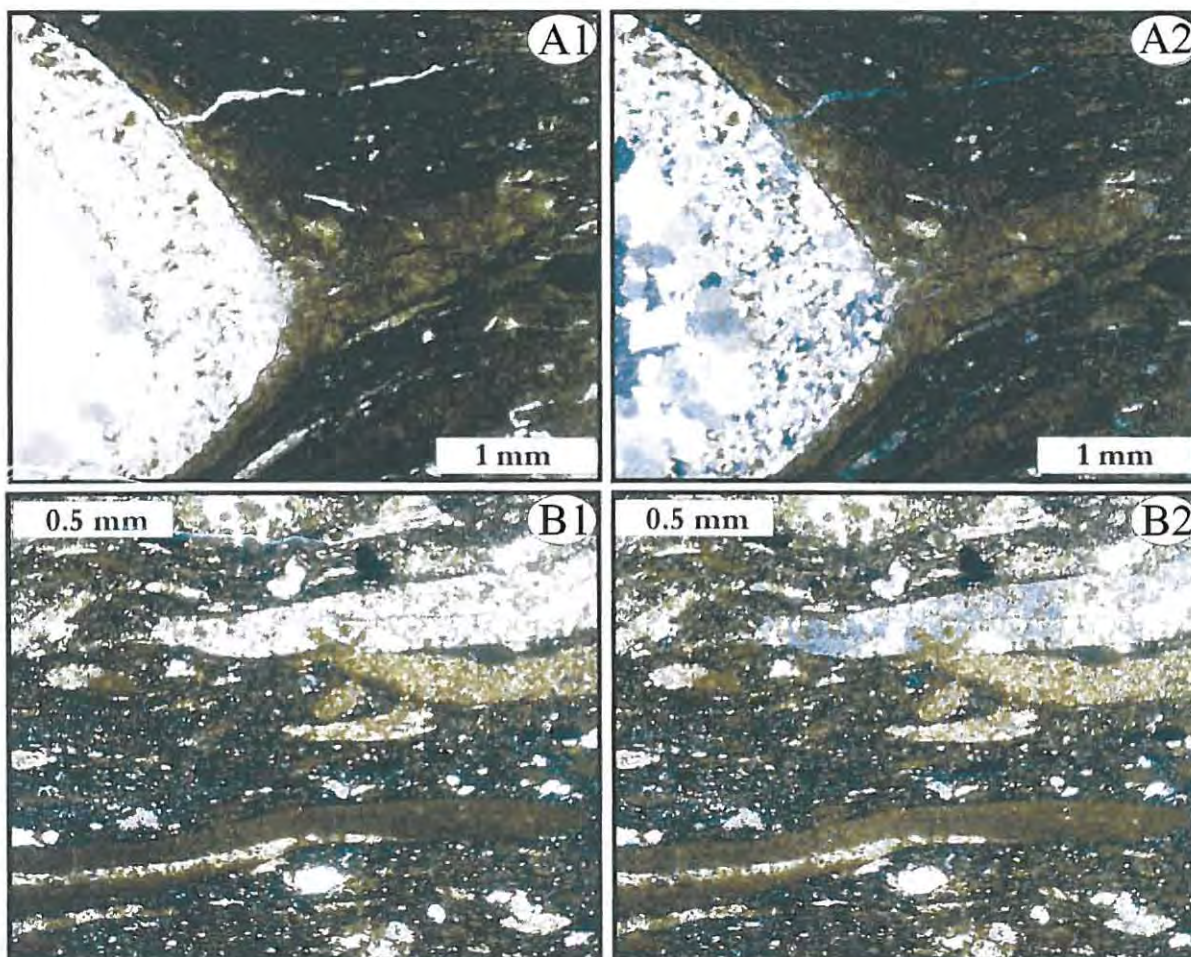
Figure III.15. A1 (plain polarized light) and **A2** (cross polarized light): calcite clast displaying pressure shadow textures (REX41-132.90). **B1** (plain polarized light) and **B2** (cross polarized light): carbonate-stilpnomelane flattened lenss in the matrix of the Hotazel diamictite (REX41-134).

The Makganyene diamictite has a definite glacial origin (presence of dropstones, striated pebbles, preserved sulphide clast) while the glacial origin for the Hotazel diamictite is less definite, mostly due to complete absence of outcrop, which makes observations restricted to boreholes. The definite identification of some clasts as glacial dropstones or as a result of compaction and soft-sedimentation deformation is difficult in the Hotazel diamictites. In this study, the author favours a glacial origin for the deposition of the Hotazel diamictite that was confirmed by geochemical studies (see chapter IV).

In the samples observed in the Makganyene Formation from Sishen, the environment was more reducing during later glacial times than at the beginning. This is evident from corresponding colour changes of the matrix, from red at the base with interbedded BIFs to grey, which reflects the oxidation state of iron.

III.3.3. Petrography of volcanic tuffs

III.3.3.1. Petrography of volcanic tuffs below the Ongeluk Formation

As shown in table III.1, the volcanic tuffs occur both below and above the Ongeluk Formation. The volcanic tuffs from the Makganyene Formation are developed as stacked graded cycles 1 to 30 (average 10) centimetres thick, located in the uppermost parts of the formation and interbedded with the diamictite and the Ongeluk lava. A single unit of stacked graded cycles may be as much as 6 meters thick, but is generally 1 meter thick. The grains are very angular, resembling volcanic shards and are set in a chloritic matrix giving them a greenish colour (see figure III.16). They are interpreted as having a volcanic origin because of the presence of volcanic glass shards, and the stratigraphic relationship with the Ongeluk Formation. Geochemistry should confirm this interpretation in the next chapter.

Figure III.16 (A1 and A2) shows a graded cycle where the basal coarse part varies from angular sand to silt grains. Figure III.16 (B1, B2, C1 and C2) shows the finest parts of a cycle that becomes laminated by very fine opaque minerals and by carbonate rhombs. All the microphotographs in figure III.16 display very sharp contacts separating each of the graded cycles.

The volcanic tuffs below the Ongeluk lava are interpreted as fall-out tuffs which were deposited after ejected particles into the atmosphere settled in the water mass. They were subsequently reworked by gravity flows probably triggered by earthquakes due to volcanism. Explosions must have been powerful, of the strombolien type, because the volcanic tuff beds are extensively present in the Griqualand West basin. Since the volcanic fall-out tuffs and the Ongeluk lava are interbedded with the Makganyene diamictites, volcanic and glacial environments were concomitant, at least towards the end of the Makganyene times.
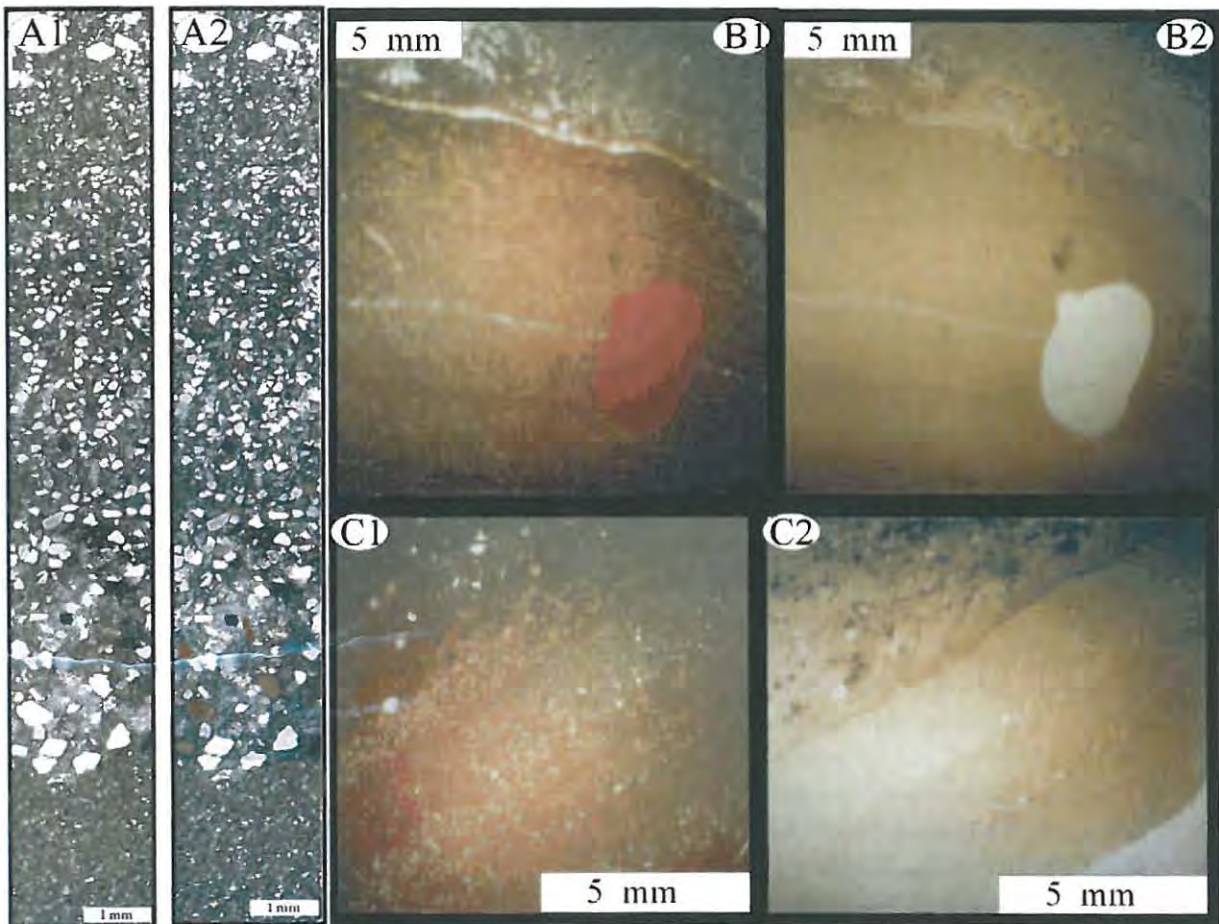
Figure III.16. A1 (plain polarized light) and **A2** (cross polarized light): coarse graded cycle, note the angular shape of the grains (sample from locality E). **B1** (plain polarized light) and **B2** (cross polarized light): very fine-grained part of a cycle showing magnetite and carbonate laminations. The "blob" is a hole in the thin section (MTP4-2H). **C1** (plain polarized light) and **C2** (cross polarized light): fine-grained part of a cycle showing magnetite and carbonate laminations, note the sharp contact between cycles (MTP4-22E). B (1&2) and C (1&2) from Polteau (2000).

III.3.3.2. Petrography of volcanic tuffs above the Ongeluk Formation

The volcanic tuffs above the Ongeluk lava are very different from those below the lava, as they do not display grading and their colour is black due to their high stilpnomelane content. They also contain coarse, very angular clasts (up to 5 cm diameter) and fine glass fragments and glass shards. They are intimately associated with the Hotazel diamictites and the contact with the latter is generally gradational. However, neither glass fragments nor glass shards of volcanic origin, were observed in the Hotazel diamictites. This indicates that the origins of the volcanic tuffs and the Hotazel diamictites are different.

Figure III.17 (A) shows an example of a tuff containing partly chloritised glass shards with a definite volcanic origin. The glass shards are set in a fine-grained matrix of brown stilpnomelane.

Figure III.17 (B) is a photomicrograph of the same horizon of tuffs. Here the background has been chloritised due to its green colour whilst greenalite is also present. Where the matrix is blue, it contains riebeckite. Stilpnomelane is also present and is associated with chlorite and greenalite in the top right corner of the photomicrograph. A pink-coloured mineral can be seen, which is a relict of plagioclase that has been replaced during devitrification. Photomicrographs III.17 (B) and III.17 (C1 and C2) are similar and both show that microspherules are present, corresponding to ovoid glass fragments. Early diagenetic carbonate rhombs can be seen and these have been replaced by magnetite. A late diagenetic generation of carbonate growth is present. Brown stilpnomelane needles are easily identified and are associated with veinlets of carbonate minerals.

Glass fragments are shown in figure III.17 (D1 and D2). They are rounded and display fibrous radial quartz and riebeckite minerals in the core, while the outer rims consist of very fine-grained quartz and stilpnomelane. Some of the spherules have been broken up, but the fragments are not dispersed. The outer rim might represent chilled margins. The matrix is fine-grained and composed of stilpnomelane, greenalite and chlorite. This rock type is identical in nature to rocks described by Grobbler and Botha (1976) who interpreted the volcanic tuffs as hyaloclastites. They originated by shattering of the water-quenched Ongeluk pillow lavas.

III.4. Conclusions

The petrography of the Transvaal Supergroup lithologies is characteristic of an early to late diagenetic crystallisation and of a low-grade metamorphism that did not exceed the very low greenschist facies.

The Griquatown BIFs consist of allochtonous graded peloidstones in the Hotazel area. This facies is typical of shallow conditions of deposition. On the other hand, the BIF facies from the Sishen and Matsap areas indicate deeper water conditions and consist of the autochthonous band-rhythmites and pillow-rhythmites. Ankerite, calcite, siderite and dolomite are all present in these rocks.
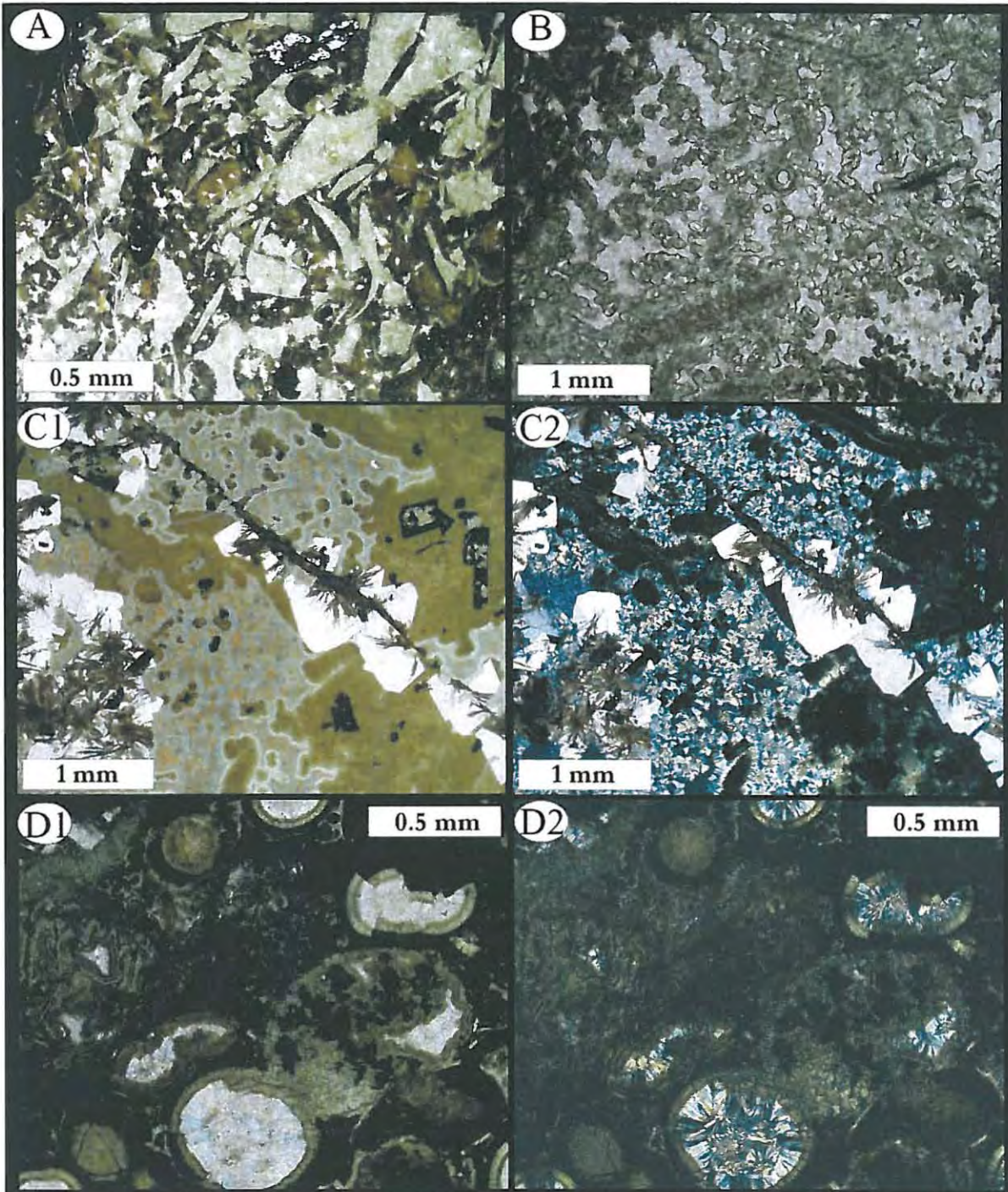
Figure III.17. A (plain polarized light): volcanic glass shards. **B** (plain polarized light): hyaloclastites with feldspar relict (REX41-136.60). **C1** (plain polarized light) and **C2** (cross polarized light): hyaloclastites (REX41-136.60). **D1** (plain polarized light) and **D2** (cross polarized light): spherules in the hyaloclastites showing chilled margins and fibrous centre of riebeckite and quartz (REX41-136.60).

The BIFs from the base of the Hotazel Formation are different and define the following cycle of deposition below the first manganese ore bed: hematite band-rhythmite – greenalite-magnetite rhythmite – calcite-magnetite rhythmite – hematite band-rhythmite. Calcite represents the only carbonate phase present. The hematite band-rhythmite was deposited in an ice-free ocean with little to no clastic input. The calcite-hematite rhythmite represents probably a shallow equivalent of the hematite band-rhythmite. The greenalite-magnetite rhythmites were deposited under an ice-sheet which was releasing clastic material by basal melting into the unconsolidated laminated fine-grained sediments.

Both the Makganyene and Hotazel diamictites contain clasts that are set in a very fine-grained matrix. The Makganyene diamictite contains clasts of volcanic tuffs, stromatolites, chert, peloidstone, sulphide and fragments of some of the Asbestos Hills rock types that could indicate transport from the shallow northeast (Hotazel area) to the southwest. The presence of a sulphide clast indicates submarine reducing and/or anaerobic glacial conditions.

In the Matsap area, the presence of dropstones implies the presence of a floating ice-sheet. However, the ice was probably grounded on the seafloor in the Hotazel area and eroded deep into the Griquatown Formation to create the unconformity surface on the Ghaap platform. The fine-grained nature of the matrix of the diamictites corresponds to normal glacial processes that crush the source rocks to form a rock-flour.

The high stilpnomelane content of the Hotazel diamictite is interpreted as representing inclusion in the glacial sediments of volcanic ash material (Beukes, 1983) as well as diagenetic origin. The Hotazel diamictite has therefore a typical brown colour. The Hotazel diamictite contains small flat stilpnomelane lenss that are outlining the bedding. The presence of small ice-rafted dropstones confers an apparent glacial origin to the Hotazel diamictite.

The Makganyene volcanic tuffs consist of stacked 2-3 cm thick fine-grained graded cycles. They are interpreted as being deposited as a result of distal volcanic sub-aerial eruptions because they appear to have covered the entire surface of the Griqualand West Basin. The Hotazel volcanic tuffs are more proximal and consist of volcanic shards and spherules set in a glassy matrix. They are interpreted as being hyaloclastites.

CHAPTER IV

Geochemistry

IV.1. Introduction

This chapter deals with the geochemistry of the lithologies immediately below and above the Ongeluk lavas. Two main lithofacies, namely a chemical facies (BIFs) and a clastic facies (diamictite and volcanic tuff), were differentiated and will be examined separately. Lithofacies from the Makganyene Formation are compared with equivalent lithofacies from the base of the Hotazel Formation on the same diagrams. The emphasis here is to assess the signature of the geochemical evolution from the BIFs below the Makganyene diamictite, through to the BIFs below the first manganese horizon from the Hotazel Formation.

Two different methods were used to perform these comparisons. The first was whole-rock geochemistry and the second was stable isotope geochemistry. The results are described and evaluated in two different sections corresponding to each method, which represent the bulk of this chapter. Interpretations are drawn in conjunction with corresponding stratigraphic position, rock type and mineralogy, and focus on the genetic processes that controlled the cyclic deposition of the Transvaal Supergroup in the Griqualand West Basin.

IV.2. Whole-rock geochemistry

IV.2.1. Introduction

Major and trace element analyses were carried out on the majority of the different rock types present within the Makganyene Formation, as well as those from the base of the Hotazel Formation.

As mentioned by Tsikos (1999), whole-rock geochemical analyses of major and trace elements on BIFs have not been the main focus in previous studies. This is due to the fact that BIFs have a bimodal chemical composition (Fe-oxides and silica which exhibit strong negative correlations). However, extensive use of other analytical methods (stable isotope and rare-earth element analyses) seems to be more useful in terms of genetic constraints. Bulk-rock geochemical data on BIFs are used, as in this study, to compare their geochemical signature on a global scale (e.g., Klein and Beukes, 1993; Horstmann and Hälbich, 1995; Tsikos, 1997, 1999), to complement petrographic studies (e.g. Klein and Beukes, 1989; Tsikos, 1997) and to provide important constraints on genesis (e.g. Tsikos, 1997, 1999).

In contrast, bulk-rock geochemical data of clastic sediments are widely used for provenance studies (e.g. Wronkiewicz and Condie, 1987; Roser and Korsh, 1988; Feng and

Kerrich, 1990; McLennan et al., 1995; Fedo et al., 1996; Nesbitt et al., 1996; Polteau, 2000), for craton evolution studies (e.g. McLennan, 1983; Condie and Wronkiewicz, 1990; McLennan and Taylor, 1991), for tectonic setting studies (e.g. Bhatia and Crook, 1986; Condie, 1986; Manikyamba et al., 1997) and for paleoclimatic studies (e.g. Wronkiewicz and Condie, 1987; Nesbitt et al., 1996; Fedo et al., 1996, 1997; Polteau, 2000).

Provenance studies on the Makganyene Formation were presented by Polteau (2000). His main finding was that the Makganyene Formation has a similar whole-rock geochemical signature to its main source rocks, which are the underlying BIFs of the Asbestos Hills Subgroup, with minor input from carbonates (Campbellrand Subgroup) and negligible siliclastic contribution.

The CIA (Chemical Index of Alteration) is usually used as a paleoclimatic tool on clastic rocks deriving from an igneous source (from granite to gabbros) to assess the most important weathering effects of the source (i.e. mechanical weathering or chemical leaching) by measuring the ratio of insoluble oxides or oxihydroxides (Al_2O_3) to other soluble cations (CaO, Na_2O, K_2O) as expressed in the following formula (Nesbitt and Young, 1982, Andrews et al., 1996):

$$CIA = \frac{Al_2O_3}{Al_2O_3 + CaO + Na_2O + K_2O} \times 100 \quad \boxed{\begin{array}{l} CaO^* \text{ included in} \\ \text{silicate minerals} \end{array}}$$

The CIA has values around 100% when chemical weathering dominated (hot and humid climate), whereas low CIA values around 50 to 75% suggest that the principal weathering process was mechanical (cold climate). According to Polteau (2000), the use of the Chemical Index of Alteration is of no use for the Makganyene diamictite because of its unusual source rock (mainly BIFs).

IV.2.2. Sample selection and method

A total of 75 fresh borehole samples were selected for bulk-rock geochemistry. The samples comprise different lithologies, from chemically precipitated BIFs and carbonates to clastic diamictites and volcanic tuffs. The samples belong to two different stratigraphic positions (i.e. the Makganyene Formation and the base of the Hotazel Formation). The boreholes were drilled in the Sishen area (GA107), as well as the Hotazel area (BG5, BH171/91, and REX41). These two localities represent the northern part of the Griqualand West Basin. Data from Polteau (2000) from the Matsap area (central part of the basin) as

well as from the Sishen area were incorporated, in order to assess geochemical variations in conjunction with geographic position.

Because mining companies own the sample material, and since they drill intensively for planning of mining activities, they reduce core sample storage costs by discarding old cores if they are located in the mined out portion of the open-pit (e.g. Sishen). Therefore sample selection was restricted by availability of cores that exhibited the following characteristics:

> presence of the top and bottom contacts of the Makganyene Formation,
> minimum of thrusting affecting the Makganyene Formation and underlying formations,
> absence of dolerite dykes.

Individual samples (all lithologies) from borehole cores were selected according to the following characteristics:

> absence of secondary veining,
> representative of the section,
> sufficient quartered core lengths (30 cm minimum) for homogeneity,
> rarity of clasts (for the diamictite and volcanic tuffs),
> all facies of BIFs have been sampled.

The main limiting factor in the geochemical study is that borehole material intersecting the Makganyene Formation is geographically restricted, and all boreholes come from mining activities, which are concentrated along the Blackridge Thrust Fault (Stowe, 1986; Beukes and Smit, 1987). Therefore fresh borehole samples from the southern parts of the basin (from the Matsap area, south to Prieska) are seriously lacking. Boreholes intersecting the Makganyene Formation associated with the Koegas Subgroup exist in the Matsap and Sishen areas.

Each selected sample has had its large clasts removed (>3 centimetres), crushed in two stages (swing mill and automatic agate pestle and mortar) and analysed for 10 major elements and fifteen trace elements using the standard X-Ray Fluorescence (XRF) method of Norrish and Hutton (1969). Major elements (except Na) were determined on fused duplicate lithium tetraborate glass discs, while trace elements and Na were determined on pressed powder pellets (Norrish and Hutton, 1969). The analyses were carried out on a Philips PW 1480 X-Ray spectrometer in the Geology Department at Rhodes University. All analytical runs were

calibrated using a variety of international and in-house standards. Corrections for dead time, background, spectral line interference, instrumental drift and mass absorption were made in all determinations.

The forthcoming sections are divided in two parts. The first part (section IV.2.3) presents the raw data, using bivariate plots displaying the variations of selected major and trace elements through the stratigraphic succession, thus permitting discrimination of different rock types and assessing any stratigraphically controlled geochemical trends. The second part (section IV.2.4) presents the inter-elemental relationships for each rock type compared with their respective geographical sampling site and stratigraphic positions, using a range of bivariate and triangular plots. Because of the two main sedimentary rock types (i.e. chemical and clastic), further subdivisions were required for clarity.

IV.2.3. Presentation of the data

This section presents all the raw data obtained during this study for whole-rock geochemistry. It is divided in two parts, the first of which (section IV.2.3.1) displays the data from analyses carried out on the Makganyene Formation, and the next part (section IV.2.3.2) displays the data from the base of the Hotazel Formation. All sample names correspond to their respective depth in meters, whilst the rock types are also briefly described. Variation plots for selected major and trace elements are presented with the associated borehole data. Data acquired by Polteau (2000) in the Sishen and Matsap areas are not presented, but are included in the diagrams of subsequent sections.

IV.2.3.1. Data from the Makganyene Formation and associated rock types

The bulk-rock geochemical data of borehole GA107 from the Sishen area are presented in table IV.1 and accompanying figure IV.1. Stable isotopes of carbon and oxygen are also included in figure IV.1 and are discussed in section IV.3.

GA107	105 25	241 4	245 3	248 4	252	273	277	281	284 2	288	290	297 8
Lithology	S	T	GD	GD	GD	GD	GD	GD	GD	GD	GD	GD
wt%												
SiO$_2$	50.99	54.65	62.28	57.63	30.25	53.21	60.72	47.32	52.83	52.12	57.89	51.46
TiO$_2$	0.57	1.20	0.21	0.21	0.12	0.27	0.31	0.17	0.18	0.24	0.23	0.20
Al$_2$O$_3$	8.98	11.75	4.70	3.92	2.23	5.17	6.75	3.11	4.14	4.92	5.22	4.65
*Fe$_2$O$_3$	25.76	16.92	15.72	17.51	8.00	18.94	19.65	16.22	17.63	20.03	20.13	21.87
MnO	0.09	0.11	0.43	0.84	0.33	0.67	0.20	0.71	0.54	0.46	0.53	0.43
MgO	4.00	8.48	5.17	6.65	2.99	7.59	4.93	5.85	4.69	4.68	5.41	4.04
CaO	1.26	0.50	9.97	11.75	6.22	11.76	3.11	9.98	7.50	6.41	7.60	5.85
Na$_2$O	1.43	lld	lld	0.01	lld	0.02	lld	0.10	0.04	0.07	0.03	0.11
K$_2$O	1.32	0.48	0.01	0.08	0.03	0.10	0.05	0.23	0.14	0.23	0.12	0.35
P$_2$O$_5$	0.07	0.15	0.08	0.08	0.04	0.09	0.10	0.06	0.07	0.11	0.08	0.06
LOI	2.47	5.57	0.93	0.93	49.10	0.62	3.25	15.25	11.94	5.41	2.49	11.61
H$_2$O	2.06	0.37	0.48	0.25	0.42	0.61	0.99	0.23	0.46	8.20	0.51	2.60
TOTAL	99.00	100.17	99.98	99.85	99.72	99.04	100.05	99.21	100.15	100.89	100.22	100.03
ppm												
Sc	28	38	6	5	5	6	9	4	6	6	7	6
V	173	343	29	27	31	36	52	25	28	34	35	28
Cr	581	8	45	56	57	69	103	59	48	55	61	44
Co	37	42	12	6	9	6	13	7	8	9	10	7
Ni	155	35	41	28	32	33	43	28	29	28	33	28
Cu	77	49	25	12	14	28	42	14	14	13	27	18
Zn	140	84	20	29	33	36	38	27	22	22	24	20
Rb	29	28	lld	3	2	7	4	18	10	16	7	24
Sr	63	7	9	23	22	29	10	37	26	28	21	29
Y	18	30	11	9	11	12	13	10	13	13	14	14
Zr	68	129	63	50	57	63	85	48	62	69	69	78
Nb	3	6	4	4	5	6	6	3	5	5	5	4
Ba	137	15	lld	82	65	18	63	83	52	104	176	257
Pb	107	3	3	3	5	5	3	4	4	6	8	3
Th	7	5	4	4	4	5	6	4	5	6	6	6

Totals calculated by the sum of major element concentrations only
All volatiles as LOI (Loss Of Ignition)
lld = less than lower limit detection
bold sample name not included
* total Fe as Fe$_2$O$_3$

S: sulphide in Ongeluk Lava
GD: Diamictite with Grey matrix
T: Volcanic tuff

Table IV.1. Whole rock chemical analysis for 36 samples from the Makganyene Formation, Sishen area (GA107).

GA107	302.2	304.2	308.6	312	316.9	320.5	324	328.5	332	336.4D	336.4B	336.9
Lithology	GD	GD	GD	GD	GD	GD	GD	GD	GD	RD	BIFd	RD

wt%												
SiO₂	62.15	53.52	55.10	57.9	55.62	52.74	58.23	60.57	24.65	63.05	52.62	57.75
TiO₂	0.17	0.19	0.19	0.21	0.17	0.18	0.20	0.20	0.10	0.19	0.05	0.11
Al₂O₃	4.20	4.23	4.50	4.85	4.26	4.36	4.52	4.43	2.14	4.76	1.64	3.55
*Fe₂O₃	19.31	18.14	23.67	23.21	21.17	21.10	21.83	20.97	11.69	20.07	34.66	22.21
MnO	0.43	0.44	0.51	0.45	0.53	0.41	0.59	0.45	0.29	0.24	0.27	0.46
MgO	3.97	4.69	5.33	4.81	4.99	4.66	5.61	4.54	2.95	4.27	2.39	4.56
CaO	6.13	6.81	7.70	5.66	7.75	5.35	7.14	5.50	3.91	4.12	4.97	6.83
Na₂O	0.05	0.05	0.06	0.08	0.07	0.09	0.03	0.01	0.02	lld	lld	lld
K₂O	0.17	0.16	0.21	0.25	0.22	2.72	0.12	0.08	0.01	0.01	0.01	0.01
P₂O₅	0.07	0.07	0.08	0.07	0.07	0.07	0.08	0.08	0.03	0.08	0.04	0.06
LOI	2.952	10.86	1.61	1.45	4.36	9.42	0.97	1.72	53.11	2.34	2.34	4.05
H₂O	0.82	1.01	0.49	0.91	0.52	1.25	0.66	0.96	0.89	0.85	0.85	0.54
TOTAL	100.43	100.15	99.44	99.84	99.72	102.34	99.96	99.52	99.78	100.00	99.87	100.12

ppm												
Sc	5	5	5	6	5	6	6	6	6	6	4	6
V	26	31	27	30	26	29	27	28	35	29	5	13
Cr	40	48	41	45	39	42	43	41	73	47	17	23
Co	6	7	6	8	6	8	7	6	7	8	lld	4
Ni	22	27	28	29	27	27	25	26	31	28	21	23
Cu	14	21	18	23	15	16	41	46	18	86	14	23
Zn	21	21	21	24	25	25	21	22	22	22	9	17
Rb	12	12	17	17	14	18	7	46	lld	lld	lld	lld
Sr	22	24	32	25	30	24	18	14	141	12	9	26
Y	13	13	14	13	12	12	12	13	14	13	10	17
Zr	61	61	67	71	58	63	61	61	58	80	19	63
Nb	3	4	4	5	4	5	5	3	5	3	2	3
Ba	141	77	157	261	214	150	194	128	16	7	5	4
Pb	3	4	4	6	3	4	lld	4	5	4	lld	2
Th	5	5	4	5	5	5	4	5	3	7	lld	4

Totals calculated by the sum of major element concentrations only
All volatiles as LOI (Loss Of Ignition)
nd = not determined
lld = less than lower limit detection
bold sample name not included
* total Fe as Fe₂O₃

GD = Diamictite with grey matrix
RD = Diamictite with red matrix
BIFd = BIF disturbed

Table IV.1. Whole rock chemical analysis for 36 samples from the Makganyene Formation, Sishen area (GA107, continued).

86

GA107	336.7	337.2B	337.2D	338.3	339	339.2	339.4	340.3	340.9	341.2	**341.7**	342.4
Lithology	RD	BIF	GD	RD	GD	BIFd	BIFd	RD	RD	BIF	BIFd	BIFd
wt%												
SiO$_2$	52.92	55.06	65.82	47.33	58.17	55.93	59.73	49.59	51.75	55.93	19.34	57.19
TiO$_2$	0.17	0.04	0.18	0.15	0.18	0.04	0.03	0.15	0.17	0.03	0.08	0.04
Al$_2$O$_3$	3.93	0.92	4.40	3.44	4.04	0.65	0.42	3.78	3.69	0.39	0.35	0.66
*Fe$_2$O$_3$	22.92	36.59	17.45	23.97	23.57	34.21	29.66	23.30	25.49	23.79	14.29	31.84
MnO	0.30	0.14	0.26	0.52	0.55	0.44	0.43	0.42	0.38	0.26	0.08	0.34
MgO	4.45	1.21	4.15	4.77	5.18	2.44	2.53	4.51	4.05	2.40	0.93	2.37
CaO	4.86	2.54	4.54	5.31	5.70	5.02	5.45	4.99	3.46	7.05	2.36	5.00
Na$_2$O	lld	lld	lld	lld	lld	lld	lld	lld	lld	lld	lld	lld
K$_2$O	0.01	0.01	0.01	0.01	0.01	0.01	0.01	0.01	0.01	0.01	lld	0.01
P$_2$O$_5$	0.08	0.03	0.08	0.06	0.07	0.03	0.03	0.07	0.07	0.04	0.01	0.02
LOI	10.01	1.74	1.74	11.91	1.44	1.53	1.55	12.74	10.37	9.99	62.09	1.70
H$_2$O	0.48	1.34	1.34	2.07	0.75	0.08	0.07	0.62	0.47	0.37	0.55	0.95
TOTAL	100.12	99.61	99.95	99.53	99.66	100.37	99.89	100.19	99.91	100.23	100.02	100.10
ppm												
Sc	5	2	nd	5	6	3	3	6	5	2	3	3
V	28	5	nd	28	28	6	lld	27	29	4	11	6
Cr	50	25	nd	39	44	19	16	40	46	15	20	20
Co	9	lld	nd	7	lld	lld	lld	9	10	lld	lld	lld
Ni	30	27	nd	31	30	23	22	28	31	16	26	24
Cu	60	25	nd	17	40	16	18	18	21	21	20	25
Zn	25	10	nd	21	20	10	9	17	24	7	7	11
Rb	lld	lld	nd	1.93	lld	lld	lld	lld	lld	lld	lld	lld
Sr	16	13	nd	16	13	10	15	14	11	28	306	16
Y	12	6	nd	12	13	11	8	16	13	11	8	7
Zr	69	13	nd	52	56	8	8	59	60	7	14	11
Nb	5	lld	nd	4	5	lld	lld	3	5	lld	lld	lld
Ba	7	8	nd	9	5	10	11	8	10	5	5	8
Pb	5	lld	nd	5	6	lld	lld	3	5	lld	lld	lld
Th	4	lld	nd	4	6	lld	lld	5	4	lld	lld	lld

Totals calculated by the sum of major element concentrations only
All volatiles as LOI (Loss Of Ignition)
nd - not determined
lld - less than lower limit detection
bold sample name not included
*Total Fe as Fe$_2$O$_3$

BIF - BIF
BIFd - disturbed BIF
RD - Diamictite with red matrix
GD - Diamictite with grey matrix

Table IV.1. Whole rock chemical analysis for 36 samples from the Makganyene Formation, Sishen area (GA107, continued).
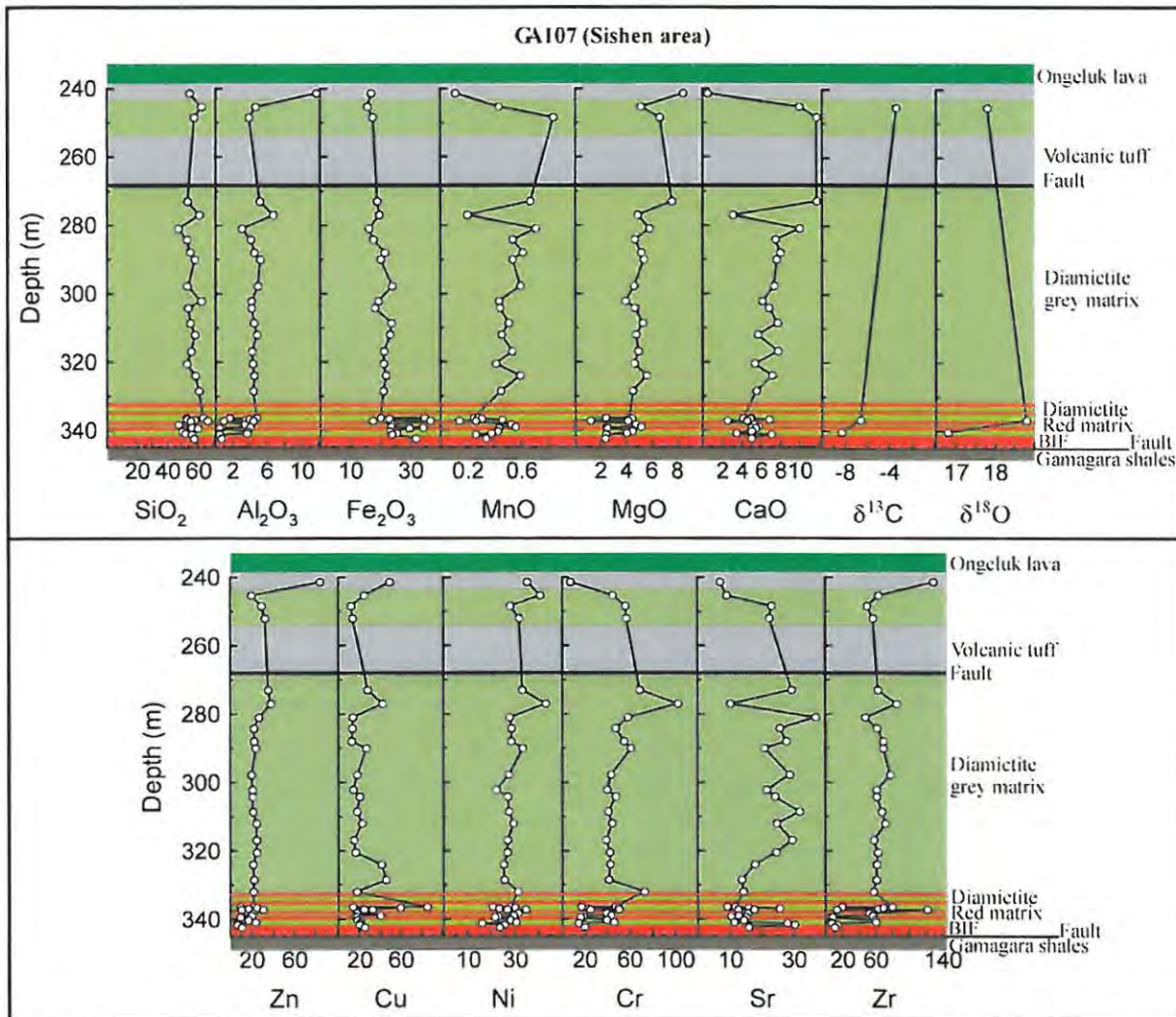
Figure IV.1. Variation plots of selected major and trace elements, as well as carbon and oxygen stable isotopes, for a representative stratigraphic profile of the different rock types present in borehole GA107 in the Makganyene Formation in the Sishen area. Note the transitional nature of the basal contact with the underlying Rooinekke Formation which does not display an extensive thickness due to the presence of a fault.

The base of the profiles shown in figure IV.1 consists of the Rooinekke Formation. It contains high concentrations of SiO_2 (55wt%), about 30wt% of Fe_2O_3, low concentrations of CaO, MgO (5wt % and 2wt %, respectively) and very low concentrations of MnO, Al_2O_3, TiO_2, K_2O and Na_2O (0.5wt%, 0.2wt%, 0.5wt%, 0.1wt%, to below detection limit respectively). The bulk composition reflects the mineralogy of the Rooinekke BIFs, which consist mainly of chert, hematite-magnetite and minor ankerite-siderite. Regarding trace elements, they are all in the concentration range of a few tens of ppm. No geochemical trend can be observed since sampling included only the BIFs at the contact due to the presence of a

fault. The BIFs are easily discriminated from the Makganyene diamictites which have a higher concentration in Al_2O_3 (2-7wt%), TiO_2 (0.1-0.5wt%), MgO (4-8wt%) and CaO (4-12wt%), lower concentrations in Fe_2O_3 (11-24wt%) and similar concentrations in SiO_2, MnO, K_2O and Na_2O. The diamictites interbedded with the BIFs have a red matrix (hematite-rich) and therefore contain significantly higher concentrations of Fe_2O_3 (>22wt%, up to 25wt%) than the rest of the overlying Makganyene diamictites.

As shown in table IV.1 and figure IV.1, the concentrations of SiO_2 and Al_2O_3 have constant concentrations throughout the entire thickness of the Makganyene diamictite. On the other hand, MnO, MgO and CaO concentrations have steadily increasing values (MnO: from 0.3 to 0.8wt%; MgO from 2 to 7wt%; and CaO from 5 to 12wt%), whereas Fe_2O_3 concentrations synchronously decrease (from 20 to 15wt%). The decrease of iron throughout the stratigraphy of the diamictite is thought to reflect a change in the source for the sediments, from BIFs of the Asbestos Hills Subgroup to carbonates of the Campbellrand Subgroup. The whole-rock geochemical data of the Makganyene diamictite therefore reflect the Ghaap Group stratigraphy in reverse order. An alternative explanation would be that the MgO/CaO increase could reflect an increase in the chemical component of the diamictites, which is explained by the presence of carbonate units (stromatolitic bioherms) that have been described in the upper part of the Makganyene Formation further south. The remaining major elements (Na_2O, K_2O and TiO_2) have very constant and low concentrations (~0.1wt%). The trace elements also have fairly constant concentrations, in the order of few tens ppm throughout the stratigraphy.

The tuffs present at the top of the Makganyene diamictite, consisting of stacked graded cycles, are significantly different to both BIFs and diamictites. The volcanic tuffs contain higher concentrations of Al_2O_3 (12wt%), and much lower concentrations of MnO and CaO (0.1wt% and 0.5wt%, respectively) than the diamictites. The difference in composition is also marked by the trace elements: the volcanic tuffs have higher concentrations in Zn (85 ppm), Cu (50 ppm) and Zr (130 ppm) than the diamictites, but lower concentrations in Cr (7.5 ppm) and Sr (7 ppm). This indicates that the graded beds are indeed volcanic in origin, and not just reworked diamictite material.

Two other boreholes, from the Hotazel area, were sampled for bulk-rock geochemical analysis (BG5 and BH171/93, see figure II.19 for borehole locations). Their geochemical compositions are shown in tables IV.2 and IV.3 respectively, while their concentrations plotted against depth are displayed in figures IV.2 and IV.3 respectively.

BG5	107 8	108	108 6	109 4	123 75	125 4	131 4	145 3	160 6	169 6
Lithology	D	D	D	D	D	BIFd	BIF	BIFd	BIFd	Disc
wt%										
SiO$_2$	58 57	55 00	52 27	53 34	45 17	40 1	26 38	28 02	43 96	58 67
TiO$_2$	0 23	0 22	0 22	0 21	0.09	0 05	0 05	0 05	0 18	0 11
Al$_2$O$_3$	5.22	5 00	4 86	4 65	1 03	0 47	0 69	0 20	2 94	1 15
*Fe$_2$O$_3$	19 69	19 93	22 34	20 37	35 75	53 09	42 38	31 40	39 42	18 86
MnO	0 28	0 28	0 36	0 24	1 22	0 31	1 89	1 95	0 75	0 41
MgO	2 33	2 28	2 40	2 24	2 65	1 12	4 29	5 56	6 24	2 97
CaO	11 88	11 92	14.08	8 86	9 76	2 22	5.01	8 63	3 26	4 62
Na$_2$O	0 13	0 14	0 23	0 21	0 10	0 06	0 08	0.01	0 29	0 18
K$_2$O	0 37	0 44	0 70	0 55	0 26	0 12	0 27	0 05	1 24	0 50
P$_2$O$_5$	0.09	0 08	0 09	0.08	0.06	0.09	0.05	0 03	0 06	0 04
LOI	1 04	3 32	2 13	9.27	3 58	1 16	18 6	27 14	1 44	14 18
H$_2$O	0 42	1 46	0 28	0 39	0 31	0.36	0 30	0 20	0 34	0 00
Total	100 24	100 08	99 95	100.40	99.98	99.17	100	100.09	100.12	99 79
ppm										
Sc	6	5	5	6	3	2	2	1	5	3
V	31	31	28	31	13	8	5	lld	26	11
Cr	46	47	44	47	26	32	19	13	47	26
Co	6	8	6	4	lld	lld	lld	lld	6	3
Ni	29	28	30	32	30	52	37	29	40	17
Cu	40	26	27	31	24	31	29	18	22	14
Zn	22	21	25	21	17	13	15	20	26	16
Rb	24	29	43	39	12	7	13	2	64	26
Sr	23	23	25	22	13	7	11	18	17	24
Y	12	12	13	12	6	5	8	15	8	5
Zr	66	67	66	68	10	6	7	3	27	11
Nb	4	4	4	5	lld	lld	lld	lld	lld	lld
Ba	69	81	112	103	23	19	19	lld	48	39
Pb	5	5	4	4	4	lld	lld	4	lld	lld
Th	6	6	5	6	lld	lld	lld	lld	lld	lld

Totals calculated by the sum of major element concentrations only
All volatiles as LOI (Loss Of Ignition)
nd   not determined
lld   less than lower limit detection
bold sample name not included
*Total Fe as Fe$_2$O$_3$

D: Diamictite
BIF BIF (allochemical)
BIFd disturbed BIF
Disc Diselutite

Table IV.2. Whole rock chemical analysis for 10 samples from the Makganyene Formation and the Griquatown Iron-Formation, Hotazel area (BG5).
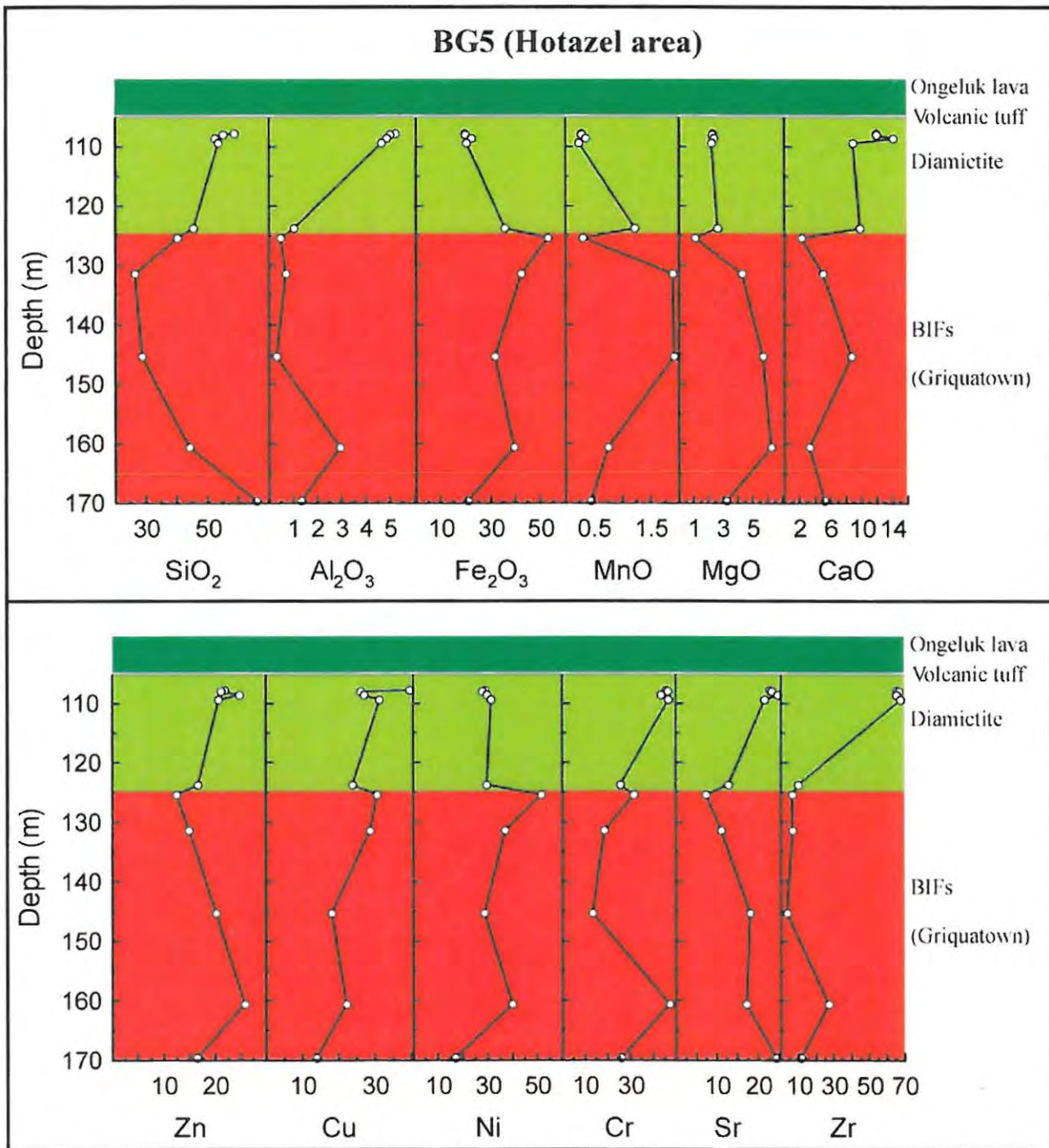
Figure IV.2. Variation plots of selected major and trace elements for a representative stratigraphic profile of the different rock types present in borehole BG5 in the Griquatown Iron-Formation and the Makganyene Formation in the Hotazel area. Note the sharp nature of the basal contact with the underlying Griquatown Iron-Formation.

Figure IV.3. Variation plots of selected major and trace elements for a representative stratigraphic profile of the different rock types present in borehole BH171/93 in the Makganyene Formation in the Hotazel area. Note the sharp nature of the basal contact with the underlying Griquatown Iron-Formation.

Sampling of Griquatown BIFs from borehole BH171/93 was not carried out due to the presence of a fault (figure II.19, and IV.3) that brecciated and silicified the thin BIF horizon available. Borehole BG5 (see table IV.2 and figure IV.2) was sampled to assess the

geochemical composition of the Griquatown BIFs underlying the Makganyene diamictite. As described in the previous chapter, the Griquatown BIFs of the Hotazel area are allochemical and consist of peloidstones-grainstones. Therefore their Al_2O_3 (0.3-3wt %) content is higher than the Sishen BIFs, with the highest value of 3wt % corresponding to disc-lutite. SiO_2 decreases from 60 to 30wt % in the younging direction while Fe_2O_3 and MnO concentrations increase (15 to 50wt% and 0.5 to 2wt%, respectively). MgO and CaO do not show significant variations across the stratigraphy, but appear to decrease slightly stratigraphically upwards. The latter is more apparent with respect to Sr concentrations. The remaining major elements, TiO_2, K_2O and Na_2O, exhibit very low concentrations, invariably below 1wt %. Regarding trace elements, Zn, Cr, Sr and Zr have concentrations decreasing by a few ppm upward in the stratigraphy, while Cu and Ni concentrations increase slightly.

When considering the diamictites from the Hotazel area, the data from borehole BG5 are included with data from borehole BH171/93. Sampling of the diamictites was more continuous in borehole BH171/93, which contains a substantially higher thickness of Makganyene diamictite (60m) than that of borehole BG5 (20m). SiO_2 and Al_2O_3 values are more variable than in the Sishen area, and increase from 50 to 60wt% and 4 to 6wt%, respectively. A decrease of Fe_2O_3 concentrations, tied with an increase of CaO contents, reflects the same geochemical trend as in the Sishen area. MgO values are constant, at about 4wt%. Concentrations of the remaining major elements of the diamictite, TiO_2, K_2O and Na_2O, are invariably low and remain below 1wt %. With regard to the trace elements, Zr is the only element having a constant concentration throughout the diamictite stratigraphy (50 ppm), while the other elements are more variable, but the transitional metals such as Ni, Cu and Cr show an upward increase of a few tens of ppm.

The volcanic tuff immediately beneath the Ongeluk Formation has a similar geochemical signature to the tuff described in the Sishen area, and therefore further discussion is not necessary.

In summary, similarities and differences can be noted between the diamictites from the Sishen and Hotazel areas. The similarities are the upward increase in concentrations of CaO and Sr tied to a decrease in Fe_2O_3 content, and a similar increase in concentrations of transition metals (Ni, Cu and Cr) and Zr at both localities. Al_2O_3 and SiO_2 values are essentially constant in the Sishen area, while they are more variable and exhibit upward increases in the Hotazel area. The behaviours of MgO and MnO are also different: while their concentrations increase upward in the Sishen area, they decrease slightly in the Hotazel area.

IV.2.3.2. Data from the base of the Hotazel Formation and associated rocks types

The succession of rock types from the base of the Hotazel Formation is more diverse, ranging from BIFs (hematite-rich, greenalite-rich and carbonate-rich) to diamictites and hyaloclastites. The bulk compositional data are presented in table IV.4 and geochemical variations of selected major and trace elements across the stratigraphy are presented in figure IV.4.

REX41	126	128.9	129.9	130.6	131	131.2	131.5	132.8	133.2	134.3	139.7	140.2	140.8	141.7	144.9
Lithology	HBIF	T	CBIF	CBIF	D	D	D	D	D	GBIF	GBIF	GBIF	GBIF	T	HBIF
wt%															
SiO_2	31.73	35.11	49.38	18.00	41.74	33.74	42.87	30.53	32.91	39.61	51.68	66.39	70.69	45.40	39.05
TiO_2	0.03	0.71	0.07	0.12	0.03	0.17	0.23	0.24	0.28	0.05	0.02	0.02	0.03	0.95	0.05
Al_2O_3	0.24	7.16	0.49	0.74	0.51	1.61	2.25	2.46	2.50	0.10	0.17	0.38	0.06	8.70	0.10
$*Fe_2O_3$	45.66	36.84	10.31	76.14	45.04	29.34	36.38	51.88	39.78	37.46	41.92	27.09	8.33	29.39	41.29
MnO	10.15	0.56	1.05	0.24	0.31	0.77	0.83	0.69	0.82	0.49	0.44	0.25	0.50	0.40	0.36
MgO	3.28	7.65	0.65	0.84	0.34	1.92	2.56	2.72	3.00	0.29	1.11	0.66	0.46	9.41	0.23
CaO	1.07	1.85	20.46	1.80	7.34	15.01	12.46	4.76	8.58	12.55	2.56	2.89	10.84	4.95	9.78
Na_2O	0.01	0.09	0.04	0.10	0.03	0.19	0.25	0.36	0.37	0.02	0.00	0.01	0.00	0.03	0.00
K_2O	0.02	0.44	0.08	0.22	0.08	0.54	0.79	0.88	0.97	0.04	0.01	0.03	0.01	0.10	0.03
P_2O_5	0.09	0.22	0.11	0.08	0.09	0.18	0.20	0.16	0.17	0.10	0.19	0.35	0.00	0.11	0.13
LOI	5.26	9.40	18.34	0.06	1.86	13.76	0.51	2.52	14.84	12.82	1.55	1.68	9.86	0.25	11.97
H_2O	0.29	0.23	0.30	0.38	0.22	1.09	0.46	0.62	0.30	0.30	0.47	0.45	0.20	0.47	0.40
TOTAL	97.82	100.26	100.23	98.71	97.57	98.31	99.79	97.81	100.53	100.06	100.10	100.21	100.14	100.16	99.26
ppm															
Sc	2	21	lld	4	3	3	7	9	9	1	2	nd	2	17	1
V	lld	189	8	44	lld	31	47	81	66	lld	lld	nd	lld	189	lld
Cr	14	76	11	30	14	21	25	38	31	11	14	nd	9	77	15
Co	6	18	lld	6	lld	7	8	13	11	lld	lld	nd	lld	28	lld
Ni	45	57	13	83	37	30	36	55	49	32	36	nd	9	60	35
Cu	27	45	18	76	26	22	32	63	34	26	22	nd	12	65	25
Zn	43	97	20	68	17	49	54	68	66	20	36	nd	13	105	23
Rb	lld	33	7	17	8	50	63	73	77	lld	lld	nd	lld	9	lld
Sr	7	10	165	9	44	56	34	16	29	95	11	nd	44	21	64
Y	11	22	10	6	6	15	16	14	14	9	10	nd	3	18	11
Zr	5	71	5	12	6	20	26	33	31	3	4	nd	2	101	4
Nb	lld	5	lld	lld	lld	3	lld	lld	lld	lld	lld	nd	lld	8	lld
Ba	70	722	77	82	36	119	139	156	166	13	8	nd	lld	212	28
Pb	lld	5	lld	lld	lld	4	4	5	lld	lld	lld	nd	lld	5	lld
Th	lld	4	lld	lld	lld	lld	lld	lld	lld	lld	lld	nd	lld	4	lld

Totals calculated by the sum of major element concentrations only   HBIF: Hematitic BIF (red)
All volatiles as LOI (Loss Of Ignition)   CBIF: Calcareous BIF
nd not determined   GBIF: Greenalitic BIF
lld less than lower limit detection   T: Hyaloclastite
bold sample name not included   D: Diamictite
* Total Fe as Fe_2O_3

Table IV.4. Whole rock chemical analysis for 15 samples from the base of the Hotazel Formation, Hotazel area (REX41).
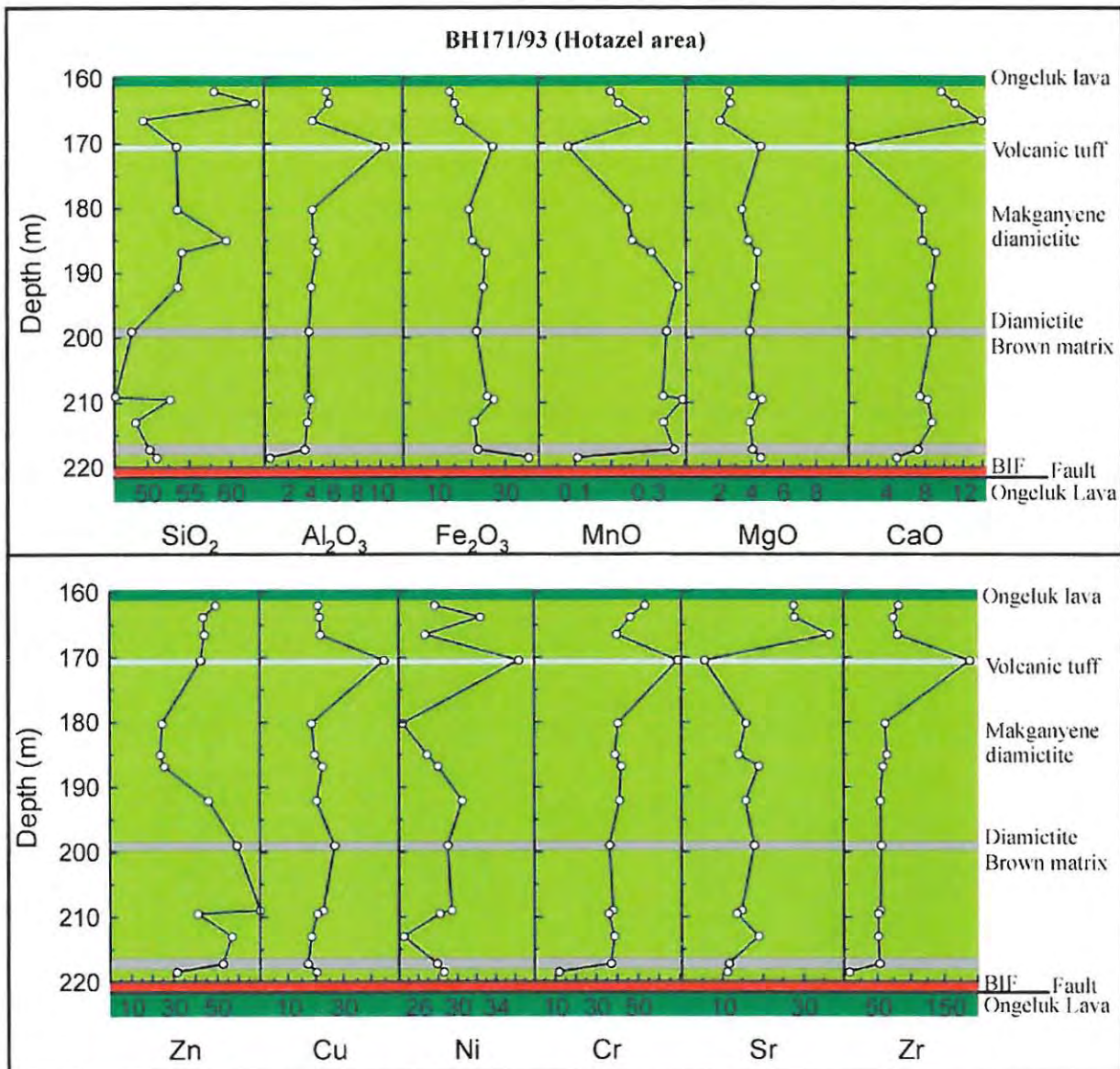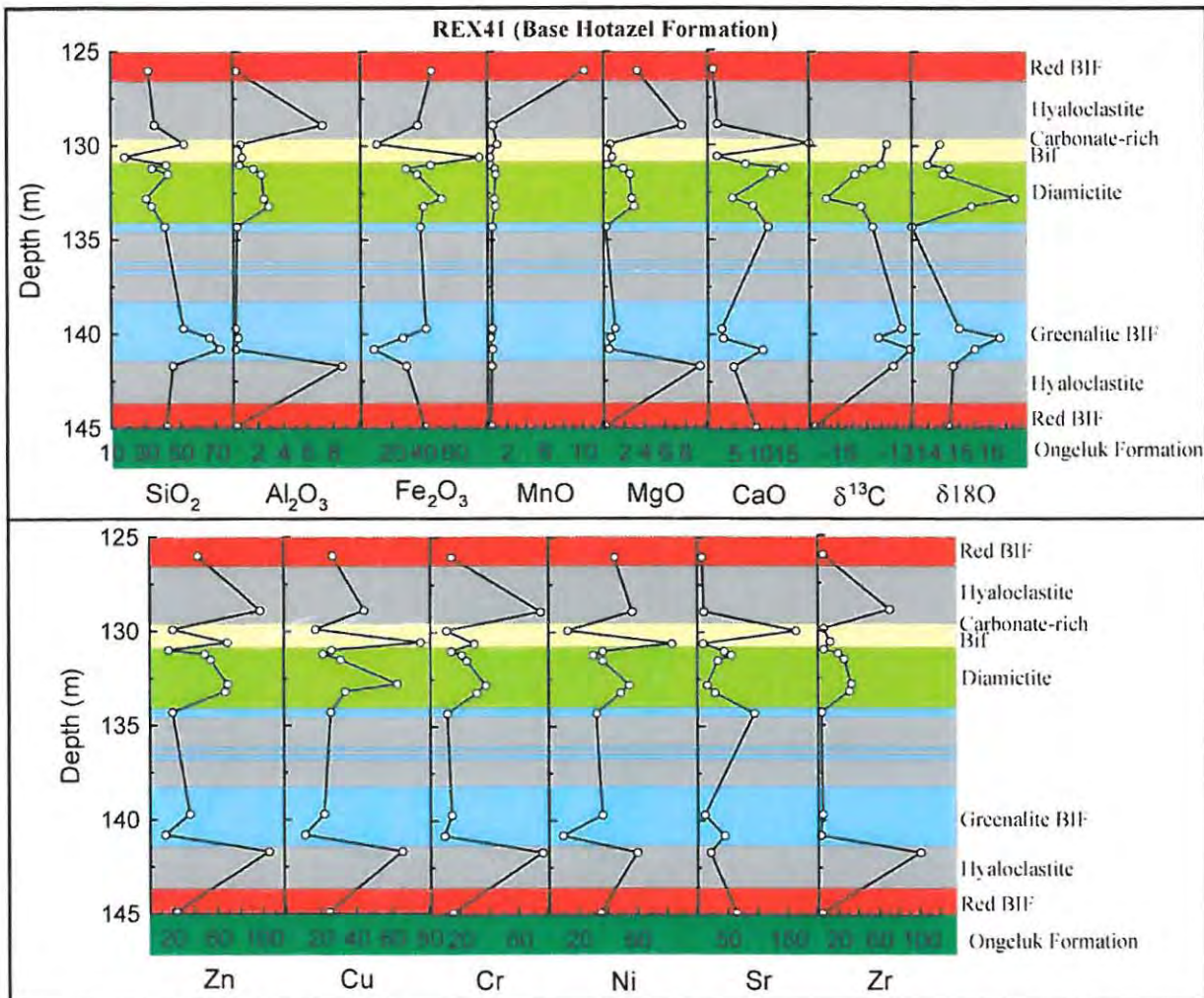
Figure IV.4. Variation plots of selected major and trace elements for a representative stratigraphic profile of the different rock types present in borehole REX41 at the base of the Hotazel Formation in the Hotazel area.

Below the stratigraphic depth of 145 metres, hematite-rich BIFs directly overlie the 900m thick Ongeluk Formation (see figure IV.4). As shown in table IV.4 and figure IV.4, the elemental concentrations are variable throughout the base of the Hotazel Formation, but each rock type has a unique geochemical signature. For example, the hematite-rich BIFs at the base and top of the profile have identical geochemical compositions, except for the MnO contents, which increased from 0.3wt% at the base to 10wt% at the top, and CaO, which decreases from 10 to 1wt%, together with a decrease of Sr content (65 ppm to 7.5 ppm). The remaining major and trace elements exhibit similar concentrations.

The greenalite-rich BIFs display decreasing SiO_2 concentrations coupled with increases in Fe_2O_3 upward in the stratigraphy (70 to 40%wt and 10 to 30wt%, respectively). Their Al_2O_3, MgO, MnO, K_2O and Na_2O concentrations are constant and very low (below 1wt%) while CaO concentrations are variable, ranging from 2.5 to 12wt%. The trace elements, Zn, Cu, Ni and Cr behave in the same manner, and all have concentrations of approximately 20 ppm (see table IV.4 and figure IV.4). Zr concentrations are constant and very low (less than 10 ppm), whilst Sr behaves in the same way as CaO.

Only two samples of the carbonate-rich BIFs were analysed for whole-rock composition. As shown in table IV.4 and figure IV.4, the proportions of SiO_2, Fe_2O_3 and CaO vary significantly, with SiO_2 and CaO increasing upward simultaneously (from 15 to 50wt% and from 2.5 to 20wt%, respectively), while Fe_2O_3 decreases (from 65 to 10wt%). These changes reflect a decline in Fe-oxide content (hematite-magnetite), and corresponding upward increase in relative proportions of chert and calcite. The other elements exhibit concentrations similar to the other BIFs (hematite- and greenalite-rich), except for Al_2O_3 that has slightly higher concentrations (0.65wt% to 0.75wt%). Zn, Cu, Cr and Ni values behave in a similar way and decrease upwards by a few tens of ppm. Only Sr increases upward in its concentration, in similar fashion to CaO.

A thin layer of diamictite is present in borehole REX41, containing dropstone material (see chapter III). SiO_2, Fe_2O_3 and MnO concentrations occur in the same proportions as the BIFs from the same profile. Al_2O_3 and MgO concentrations vary in a similar manner, from 4 to 1wt% at the top (MgO concentrations are approximately half those of Al_2O_3). CaO concentrations vary (ranging from 5 to 15wt%) and behave similarly to Fe_2O_3. Zn, Zr, Cu, Ni and Cr have the same trend as Al_2O_3 and MgO, while Sr behaves in a similar fashion to the CaO trend.

Figure IV.5 represents spidergrams allowing direct comparisons between both the major and trace element concentrations of volcanic tuffs, BIFs and diamictites. This diagram has been constructed employing the following steps:

> Calculation of averages of each rock type from each locality and stratigraphic position (see table IV.5 for values and variances),

> Each average is normalised to the average of volcanic tuffs,

> Leaving REX41 BIFs and REX41 diamictites as individual curves to compare them directly with the Griquatown/Rooinekke BIFs and Makganyene Diamictites respectively.

Normalising each rock type of similar stratigraphic position against a very different rock type, the volcanic tuffs, provides one of the best ways of assessing the stratigraphic differences in compositions and confirming or not their potential volcanic origin. The compositional field of the BIFs from the Griquatown and Rooinekke Formations is compared with the BIFs from the base of the Hotazel Formation (see figure IV.5.A and D). The compositional field of the Makganyene diamictite is compared with the Hotazel diamictite (see figure IV.5.B and E).

Figure IV.5 (A and D) compares the BIFs from above and below the Ongeluk Formation. It is evident that the geochemical trends of both BIFs are similar, regarding major (figure IV.5.A) and trace elements concentrations (figure IV.5.D). Both BIFs exhibit enrichment (except Na_2O) or depletion (except P_2O_5) of the same elements compared to the volcanic tuffs. The Hotazel BIFs are slightly depleted in Al_2O_3, MgO and K_2O, while they are enriched in MnO (one sample has 10wt% MnO which heightens the average), CaO (due to the presence of carbonate-rich BIFs containing only calcite) and P_2O_5. The compositional fields for the trace elements are almost identical (see figure IV.5.D) and therefore any depletion or enrichment is negligible, except for the net enrichment of Sr (related to the increase in carbonates) and depletion in Zr (related to the decrease in detrital major elements) in the Hotazel BIFs.

Figure IV.5 (B and E) compares the diamictites from the Makganyene and Hotazel Formations. The stratigraphically different diamictites are identical in geochemical composition and display similar concentration curves. The Hotazel and Makganyene diamictite curves show the same elemental enrichments (except Fe_2O_3, MnO and P_2O_5) and depletions (except Pb) compared to the volcanic tuff.

The Makganyene diamictite compositional field is very restricted, and the Hotazel diamictite broadly follows the general trend. The Hotazel diamictite is relatively enriched in Fe_2O_3, MnO, CaO, Na_2O, K_2O, P_2O_5, Rb and Sr (related to the increase in modal proportions of calcite and stilpnomelane) and depleted in SiO_2, TiO_2, Al_2O_3, MgO, Zr and Nb (corresponding to the decrease in detrital components as well as the complete disappearance of dolomite/ankerite).

Diagram C from figure IV.5 represents a combination of diagrams A and B, while diagram F is a combination of diagrams D and E. These spidergrams demonstrate important genetic implications for the Makganyene and Hotazel diamictites: both of them exhibit a dominant BIF component within the diamictites.

	MkMdiam n 7	MkSdiam n 28	MkHdiam n 19	Mkdiam n 54	RBIFs n 15	GBIFs n 5	RGBIF n 20	REX41 diam n 5	REX41 BIFs n 8	tuffs n 4
wt% n										
SiO₂	59.64 (12.30)	56.82 (5.06)	53.2 (4.40)	55.91 (7.15)	51.94 (10.05)	41.00 (15.72)	49.21 (12.25)	36.47 (5.48)	46.87 (17.72)	51.33 (14.88)
TiO₂	0.25 (0.09)	0.23 (0.11)	0.21 (0.13)	0.22 (0.11)	0.04 (0.02)	0.08 (0.06)	0.05 (0.04)	0.19 (0.10)	0.04 (0.03)	0.77 (0.42)
Al₂O₃	6.58 (2.48)	4.77 (1.52)	4.34 (1.97)	4.85 (1.86)	0.71 (0.48)	0.90 (1.16)	0.75 (0.68)	1.93 (0.91)	0.36 (0.21)	8.46 (2.42)
Fe₂O₃	17.05 (7.19)	20.24 (3.34)	22.61 (5.91)	20.66 (4.43)	28.57 (9.23)	37.5 (12.05)	30.8 (10.44)	40.61 (8.54)	36.17 (21.57)	24.65 (10.26)
MnO	1.29 (1.05)	0.45 (0.17)	0.33 (0.23)	0.52 (0.57)	0.34 (0.25)	1.06 (0.78)	0.52 (0.53)	0.68 (0.21)	1.67 (3.44)	0.51 (0.36)
MgO	2.29 (0.72)	4.78 (1.00)	3.69 (1.56)	4.07 (1.38)	2.06 (0.74)	4.12 (2.05)	2.58 (1.46)	2.10 (1.05)	0.92 (1.00)	6.81 (3.47)
CaO	0.88 (1.61)	6.40 (2.49)	8.53 (3.69)	6.43 (3.22)	5.49 (2.34)	4.88 (2.47)	5.33 (2.32)	9.67 (4.08)	7.50 (6.60)	1.84 (2.20)
Na₂O	0.09 (0.10)	0.06 (0.05)	0.20 (0.16)	0.12 (0.06)	0.03 (0.02)	0.12 (0.11)	0.04 (0.07)	0.24 (0.13)	0.03 (0.03)	0.04 (0.04)
K₂O	0.76 (0.84)	0.40 (0.83)	0.36 (0.26)	0.43 (0.83)	0.06 (0.06)	0.45 (0.49)	0.15 (0.29)	0.64 (0.35)	0.05 (0.07)	0.34 (0.17)
P₂O₅	0.03 (0.02)	0.08 (0.02)	0.08 (0.03)	0.07 (0.03)	0.04 (0.02)	0.06 (0.02)	0.05 (0.02)	0.16 (0.04)	0.14 (0.10)	0.12 (0.09)
ppm										
Sc	7 (2)	6 (1)	6 (2)	6 (2)	3 (0)	3 (2)	3 (1)	6 (3)	2 (1)	20 (14)
V	46 (15)	32 (11)	29 (13)	33 (13)	9 (4)	13 (9)	9 (6)	56 (22)	26 (25)	188 (128)
Cr	71 (22)	51 (18)	41 (11)	50 (20)	20 (3)	27 (13)	22 (7)	26 (9)	15 (7)	53 (32)
Co	16 (7)	8 (2)	7 (2)	9 (5)	5 (2)	4 (2)	1 (2)	10 (3)	6 (0)	26 (11)
Ni	45 (18)	31 (6)	29 (3)	32 (11)	22 (7)	35 (13)	26 (10)	41 (10)	36 (24)	46 (14)
Cu	68 (94)	27 (17)	24 (7)	31 (46)	23 (12)	23 (7)	23 (11)	35 (16)	29 (21)	43 (22)
Zn	45 (15)	25 (8)	38 (16)	32 (13)	12 (4)	18 (5)	14 (5)	51 (21)	32 (19)	84 (24)
Rb	30 (25)	20 (23)	32 (21)	26 (22)	2 (5)	22 (25)	7 (21)	54 (28)	12 (7)	20 (13)
Sr	16 (9)	20 (8)	19 (7)	19 (8)	21 (12)	16 (7)	20 (11)	35 (15)	57 (58)	12 (6)
Y	16 (3)	13 (2)	14 (4)	14 (3)	11 (5)	8 (4)	11 (5)	13 (4)	8 (3)	22 (6)
Zr	98 (28)	68 (18)	64 (36)	70 (23)	10 (5)	11 (9)	10 (6)	23 (11)	5 (3)	105 (26)
Nb	6 (2)	5 (2)	5 (4)	5 (2)	lld	lld	lld	lld	lld	6 (1)
Ba	89 (104)	97 (88)	39 (33)	76 (90)	10 (7)	31 (14)	12 (13)	123 (52)	46 (34)	241 (334)
Pb	25 (51)	5 (2)	7 (5)	8 (22)	6 (5)	lld	2 (5)	4 (1)	lld	4 (1)
Th	18 (25)	5 (2)	6 (3)	7 (12)	3 (2)	lld	1 (2)	lld	lld	6 (2)

lld: less than Lower Limit of Detection
n number of samples
59.64 (12.30) mean (standard deviation)

MkMdiam Makganyene Matsap diamictite
MkSdiam Makganyene Sishen diamictite
MkHdiam Makganyene Hotazel diamictite
Mkdiam average Makganyene diamictite

RBIF Rooinekke BIFs
GBIF Griquatown BIFs
RGBIF average BIFs below Ongeluk

REX41 diam REX41 diamictite
REX41 BIFs REX41 BIFs
tuffs volcanic tuffs

Table IV.5. Summary of analytical data of samples according to their geographic and stratigraphic locations. Note that Mkdiam is the average of Makganyene diamictite samples independently of their geographic location. RGBIF represents the average of BIFs present below the Ongeluk Formation.
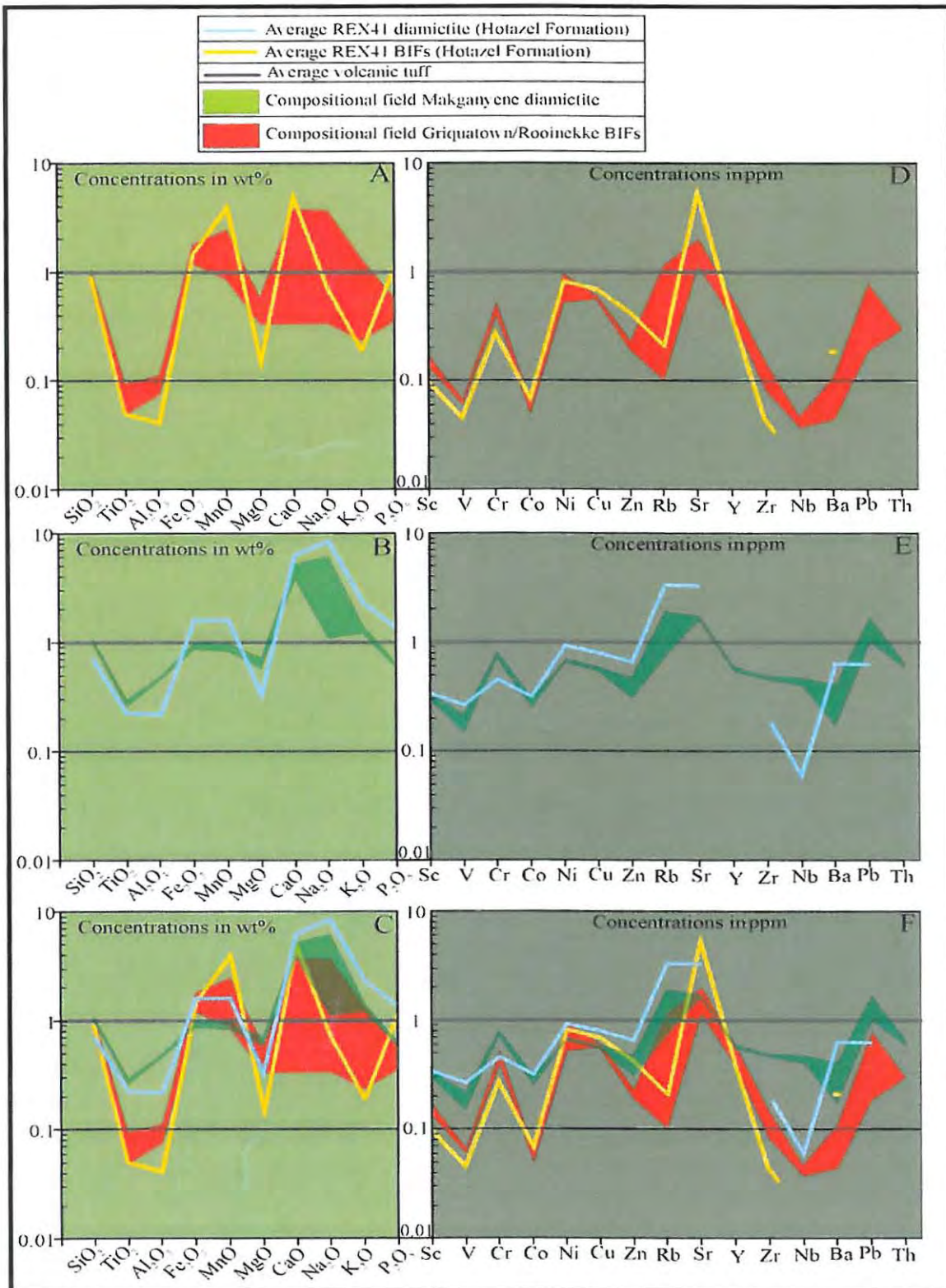
Figure IV.5. Compositional fields for major (A, B, C) and trace elements (D, E, F) of BIFs, and diamictites from below and above the Ongeluk lava, normalised to the average of volcanic tuffs regardless of their stratigraphic position.

IV.2.4. Inter-elemental relationships

This section is divided in two parts. The first presents inter-elemental relationships between the different BIFs analysed during this study (section IV.2.4.1), while the second deals with the clastic rocks (section IV.3.4.2). The inter-elemental relationships will be established using bivariate and triangular diagrams.

IV.2.4.1. Inter-elemental relationships for BIFs

After examining the geochemical variations across the stratigraphy intersected by the sampled boreholes, and comparing the concentrations of different elements as a function of their lithologies, further plotting on bivariate diagrams is required to provide a more detailed assessment of the geochemistry of BIFs. Selected elements are plotted against Fe_2O_3, CaO and Al_2O_3, the latter representing respectively the Fe-oxide, carbonate, and silicate mineral phases present in BIFs (James, 1954). BIFs from below and above the Ongeluk lava are plotted on the same diagrams for the purpose of comparing elemental concentrations across the stratigraphy.

Elements that show positive correlation to Fe_2O_3, CaO or Al_2O_3 are interpreted as occurring mostly in the Fe-oxide group (magnetite and hematite), the carbonate group (calcite, dolomite-ankerite, siderite) or the silicate group (greenalite, stilpnomelane, riebeckite), respectively, while no obvious correlation trend would mean that the two elements compared are not influencing each other.

Figure IV.6 illustrates the behaviour of selected elements against Fe_2O_3. Diagrams A and B show that the Fe-oxide group has strong negative correlation to SiO_2 (A) and CaO (B). Diagram C shows that MnO behaves the same way as SiO_2 and CaO, but with a lesser negative correlation trend. Meanwhile Zn (diagram D) and Cr (diagram E) occur within the Fe-oxide minerals, as indicated by positive correlations with Fe_2O_3. However Zn occurs also in the aluminous phase (figure IV.8.I) that is represented by detrital and stilpnomelane minerals.

Figure IV.6. Whole-rock Fe-oxide geochemical signature of selected samples from Sishen, Hotazel, and REX41 BIFs displayed in bivariate plots.

Figure IV.7 displays the behaviours of SiO_2, MnO, Sr and MgO in relationship to the carbonate mineral phase, and hence were plotted against CaO. No obvious relationsip between CaO and SiO_2 can be deduced from diagram A. By showing positive correlations, diagrams B and C illustrate that MnO and Sr are occurring in, or associated with, the carbonate mineral phase regardless of their stratigraphic and geographic positions. The different behaviour of MgO from the Sishen/Hotazel and REX41 BIFs is illustrated in diagram D. MgO occurs in the carbonate phase (dolomite-ankerite series) in the BIFs below the lava. On the other hand, MgO from the REX41 BIFs is not present in the carbonate phase, and this is expressed by a slightly negative correlation shown in diagram D. Indeed, the REX41 BIFs contain only calcite, and hence MgO occurs in another mineral phase which is stilpnomelane.
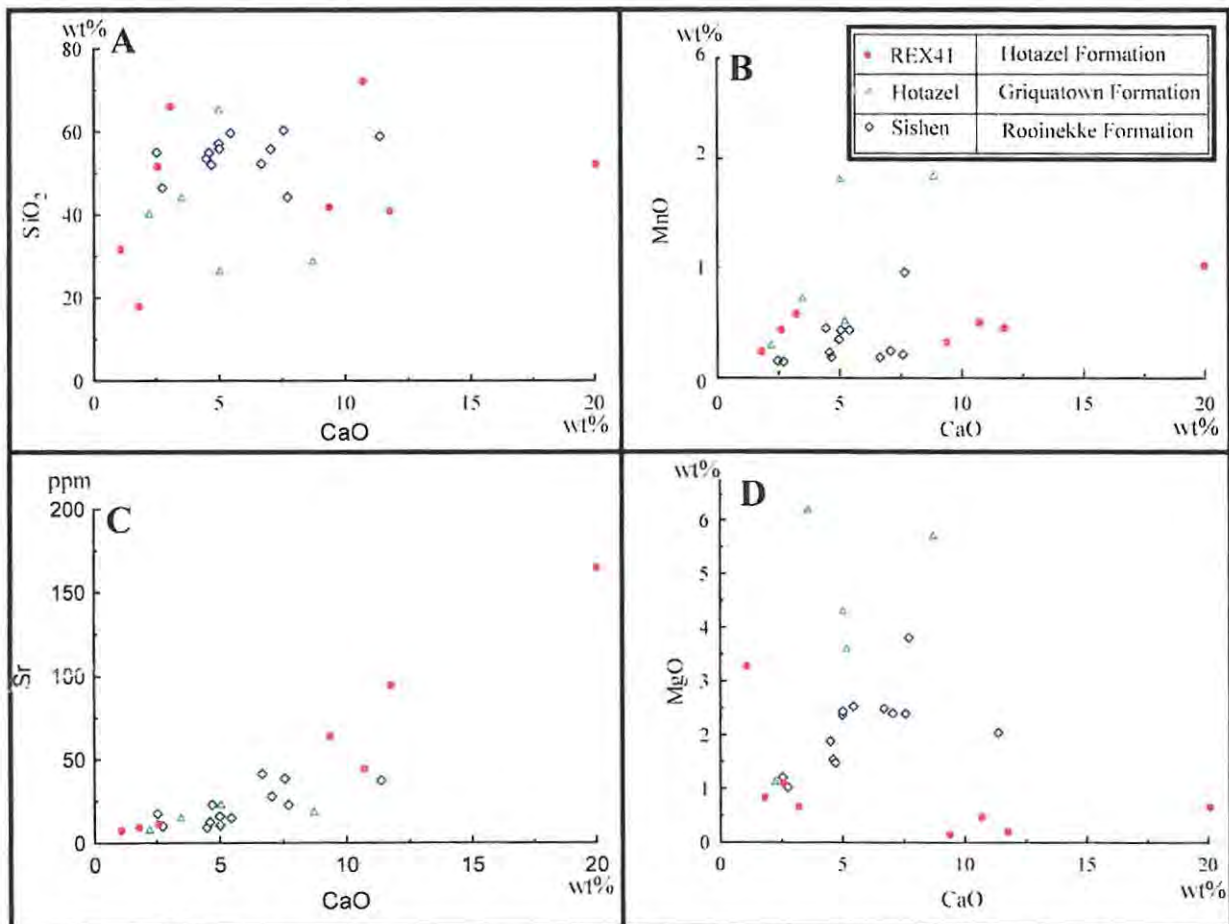
Figure IV.7. Whole-rock carbonate geochemical signature of selected samples from Sishen, Hotazel, and REX41 BIFs displayed in bivariate plots.

The final set of bivariate plots, shown in figure IV.8, displays the relations between selected elements and Al_2O_3 to assess the geochemical signature of the silicate phase present in the BIFs analysed for this study. There is a lot of scatter in these diagrams and the trends are mostly poor. This is due to comparing Al (~1wt%) to CaO and Fe_2O_3 (5 to 50wt%).

Diagram A displays an antithetic correlation between Fe_2O_3 and Al_2O_3, indicating that Fe does not reside in the alumino-silicate phase in these rocks. Diagrams B, D and H show that carbonate elements do not correlate with silicate minerals, except for the REX41 BIFs, due to the presence of large amounts of stilpnomelane.
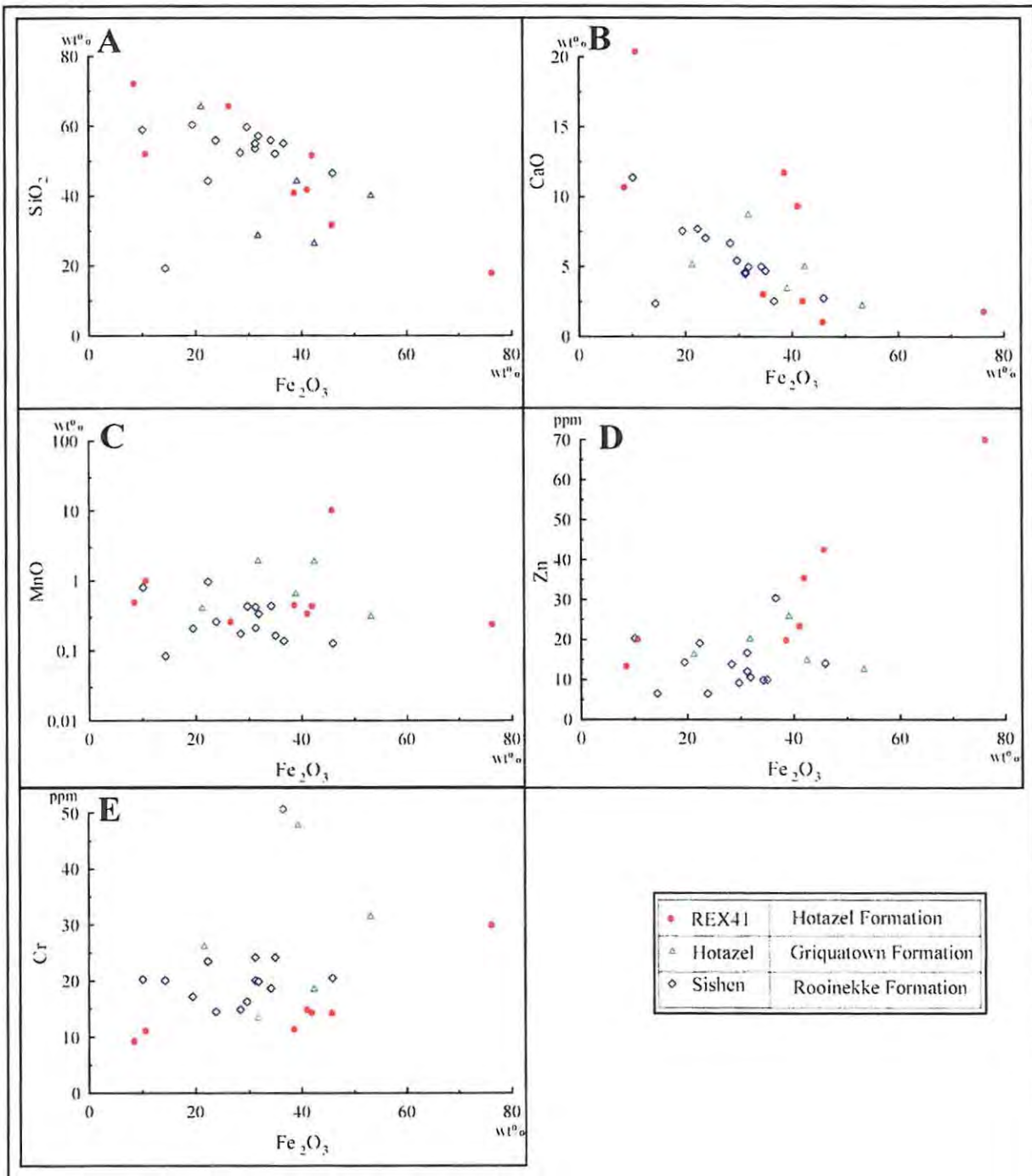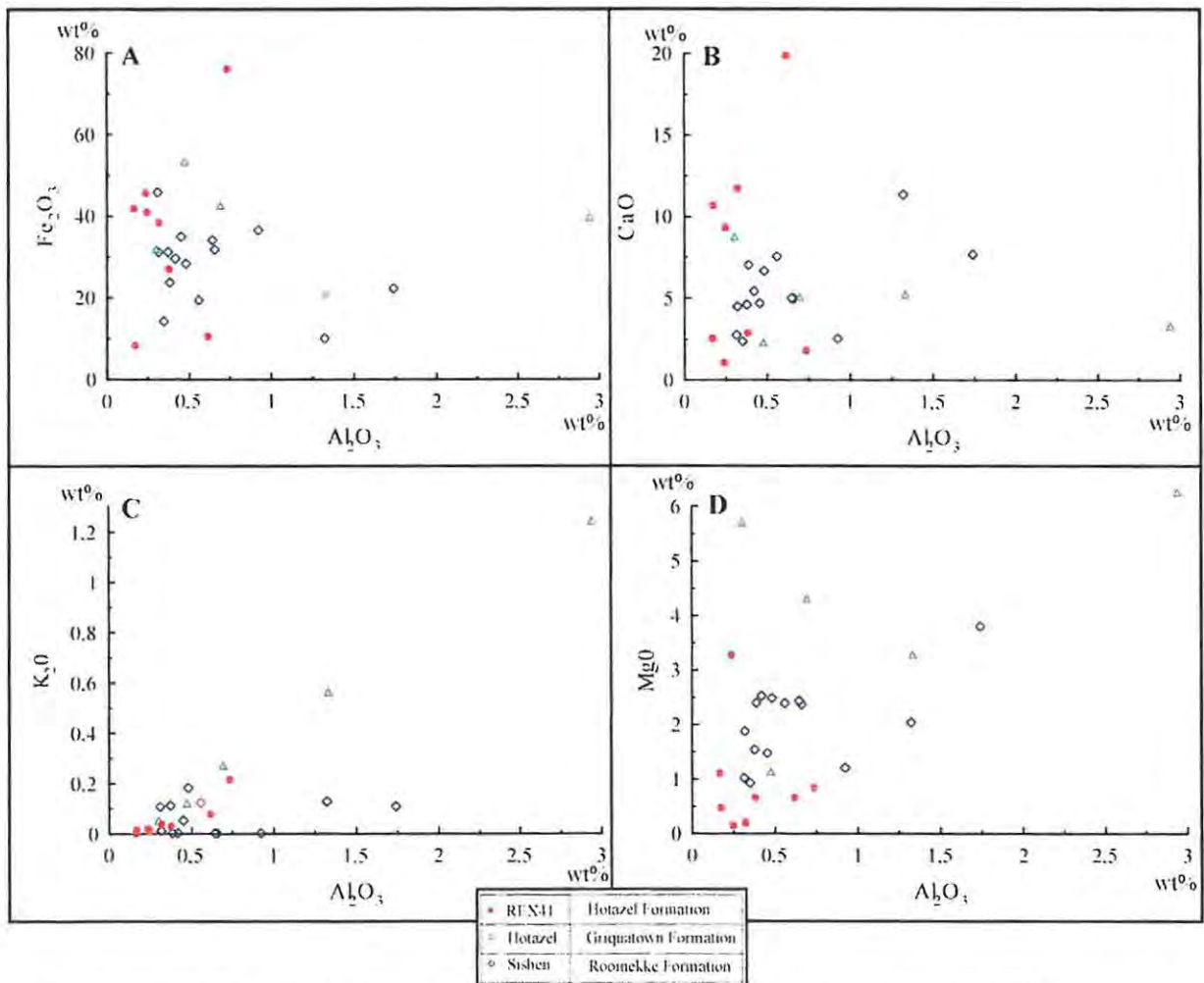

Figure IV.8. Whole-rock silicate geochemical signature of selected samples from Sishen, Hotazel, and REX41 BIFs displayed in bivariate plots.
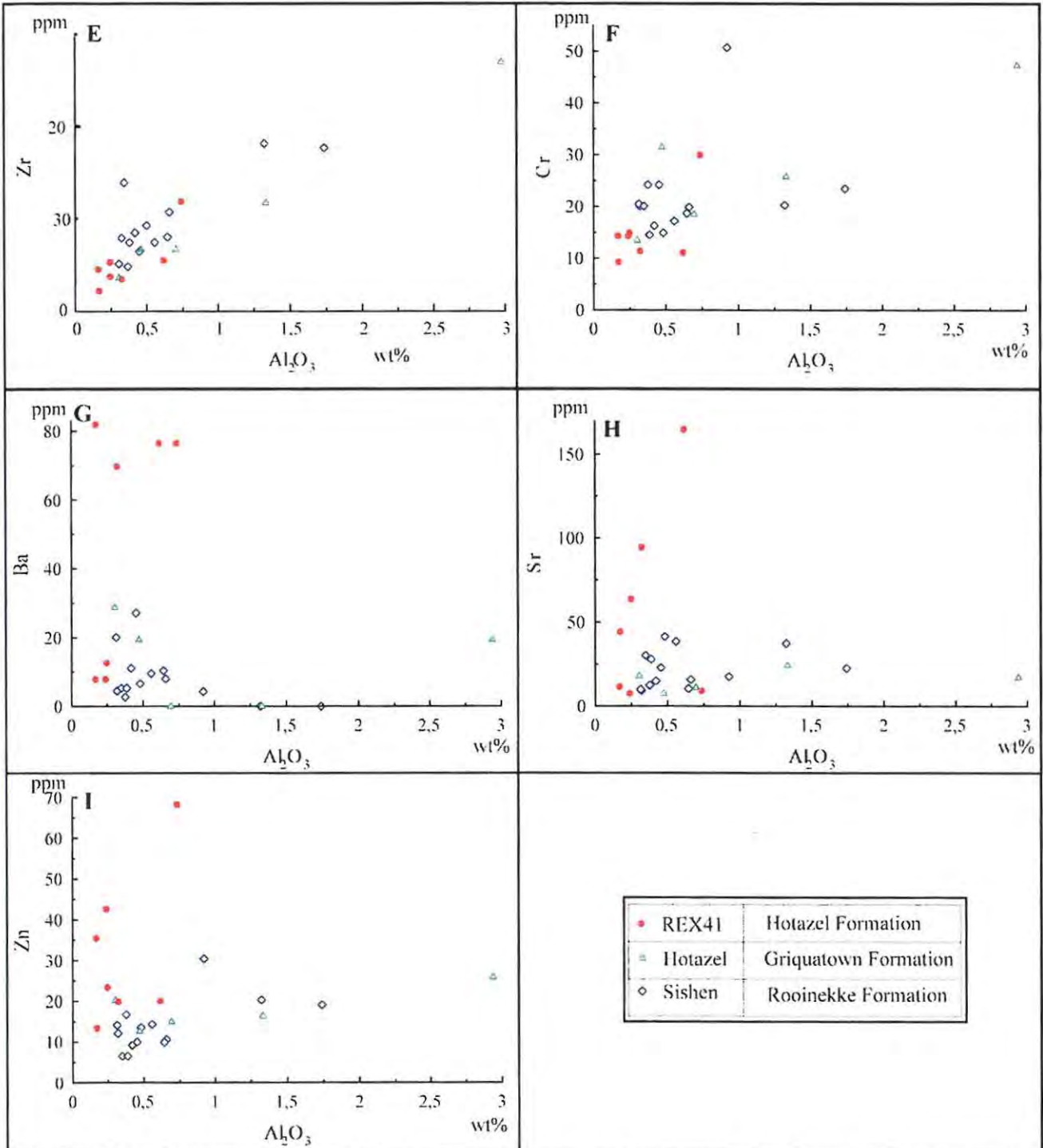
Figure IV.8. Whole-rock silicate geochemical signature of selected samples from Sishen, Hotazel, and REX41 BIFs displayed in bivariate plots (continued).

The rest of the diagrams of figure IV.8 (i.e. C, E, F, G and I) display positive correlations. The corresponding elements (K_2O, MgO, Zr and Cr) are included in the silicate phase. The strong correlation of Zr with Al_2O_3 indicates that the silicate phase has a definite detrital origin. Ba and Zn, which have similar correlation trends to that of CaO, MgO and Sr, can be assigned to the carbonate mineral phase.

IV.2.4.2. Inter-elemental relationships for the diamictites

This section is subdivided in two parts. The first deals with inter-elemental relationships of the diamictites on bivariate plots. The second part consists of provenance studies where bivariate plots and triangular diagrams are used to assess differences in compositions for the Makganyene diamictites according to their geographic positions. The diamictite samples from the Matsap area have been included (Polteau, 2000).

Because it is postulated that the BIFs are the main source rock for the Makganyene diamictites, any deviations in the geochemical composition of the diamictite compared to that of the BIFs would indicate that another rock type also acted as a source for the diamictites. Also, the compositional differences between the Makganyene and Hotazel diamictites will be evaluated.

IV.2.4.2.1. Bivariate and ternary diagrams

As in the case with the BIFs, bivariate plots applied to the Makganyene Formation are used to evaluate the elemental association with one of the three mineral groups (i.e. Fe-oxide, carbonate and silicate). Figure IV.9 illustrates the relationships of selected elements against Fe_2O_3. The values are more scattered than for the BIFs. Diagram A shows that CaO correlates antithetically with Fe_2O_3 for both Makganyene and Hotazel diamictites. Diagram B displays a clear negative correlation between SiO_2 and Fe_2O_3 for the Makganyene diamictite, while a slight negative correlation is observed for the Hotazel diamictite.
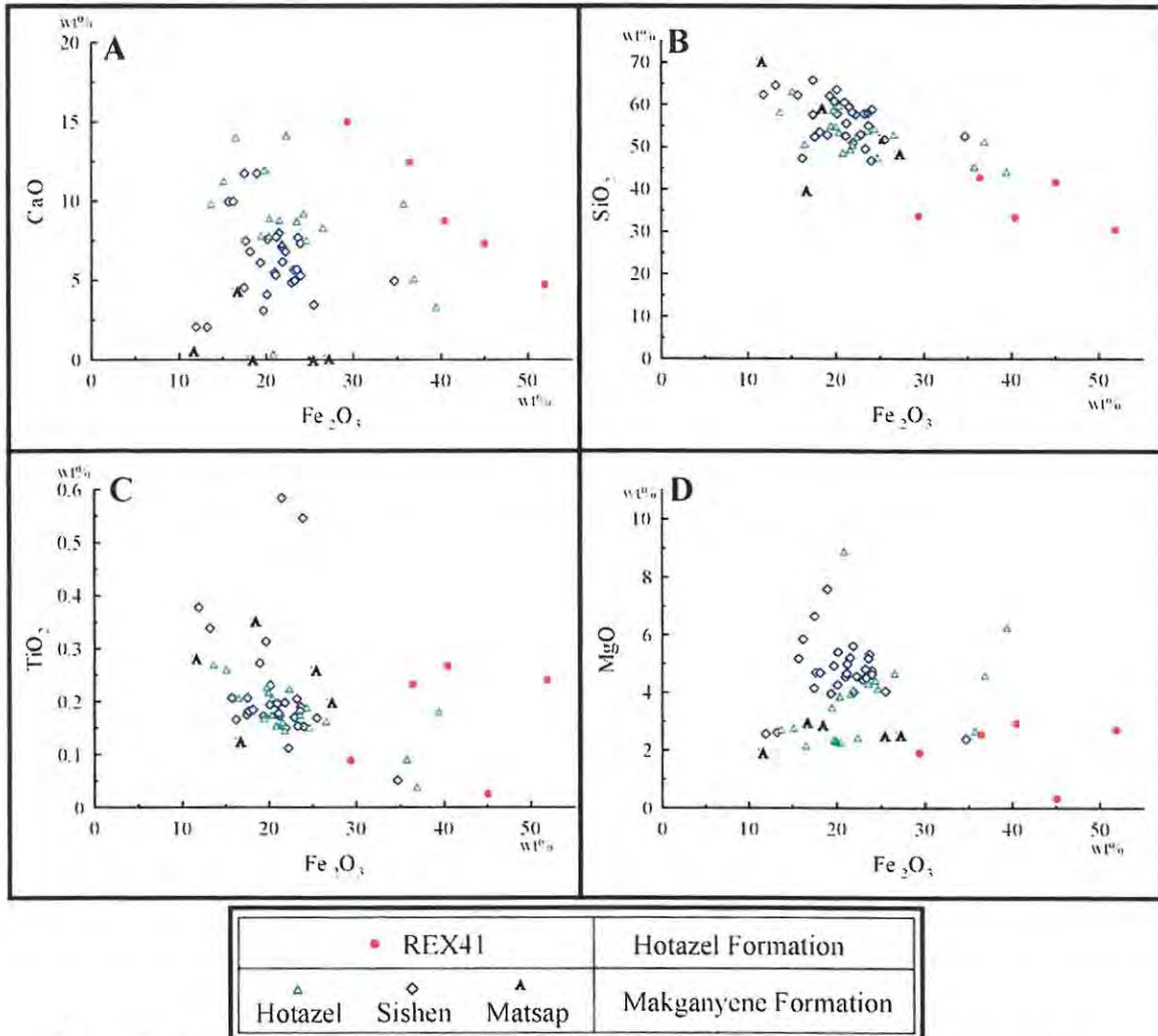
Figure IV.9. Whole-rock Fe-oxide geochemical signature of diamictites of selected samples from the Makganyene and Hotazel diamictites.

Diagram C shows a negative correlation between TiO_2 and Fe_2O_3 for the Makganyene diamictite while the Hotazel diamictite does not display any specific correlation trend. In diagram D, the Makganyene and the Hotazel diamictites do not show any particular correlation trend between MgO and Fe_2O_3. It appears evident that distinct differences are present between Makganyene diamictites from different geographic locations. The carbonate elements (CaO, MgO) increase in concentration northward, from the lowest values in the southern samples from the Matsap area, to higher concentrations from Sishen, and finally the highest in the northernmost sampled location in the Hotazel area.

Figure IV.10. Whole-rock Fe-oxide geochemical signature of selected samples from the Makganyene and Hotazel diamictites displayed in bivariate plots.
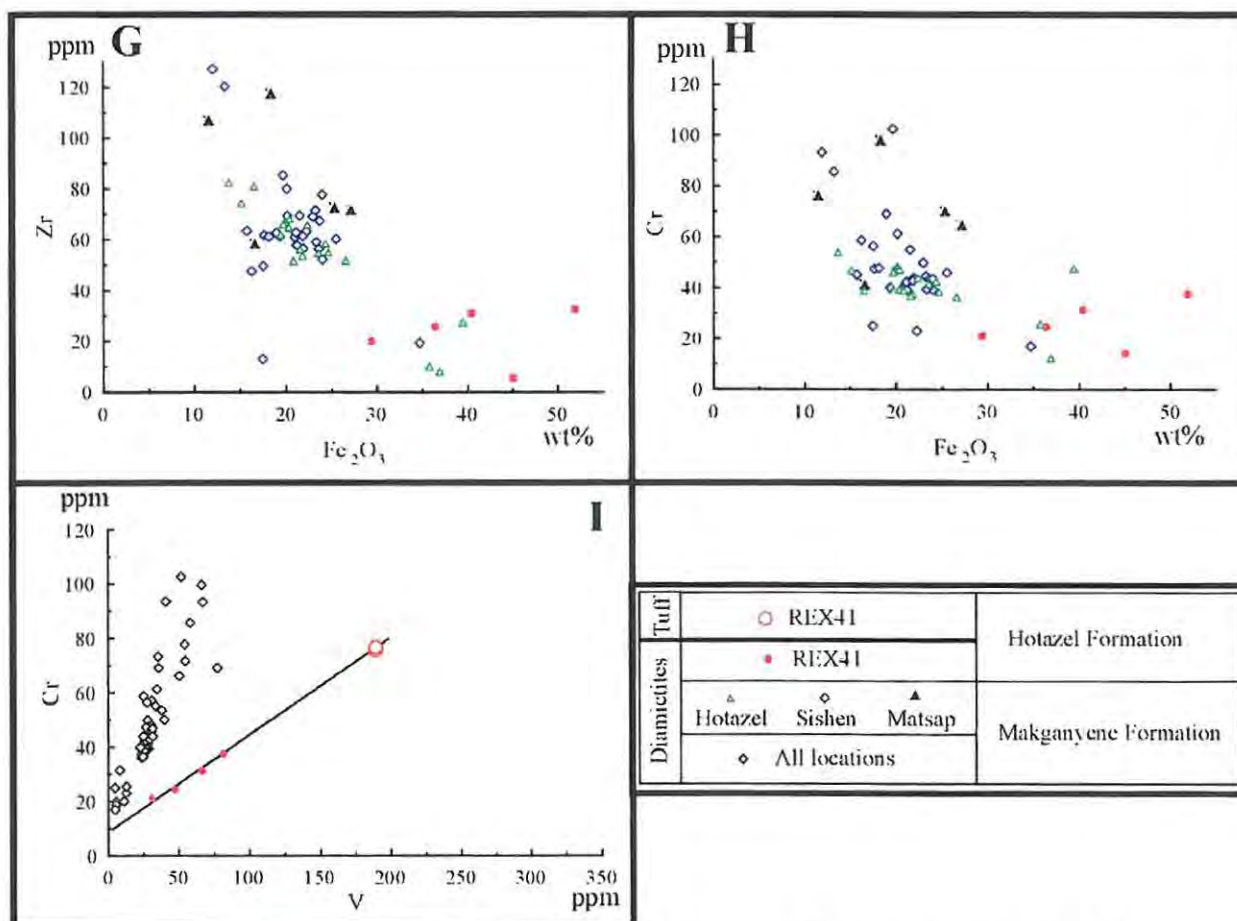
Figure IV.10. Whole-rock Fe-oxide geochemical signature of selected samples from the Makganyene and Hotazel diamictites displayed in bivariate plots (continued).

Diagram A from figure IV.10 shows that the Hotazel diamictite is significantly enriched in Sr and Fe_2O_3 compared to the Makganyene diamictites. Both diamictites show a negative correlation trend between Fe_2O_3 and Sr. The remaining diagrams (from plot B to H) show that the transition elements (V, Sc, Co, Zn, Ni, Zr and Cr) display marked antithetic correlations with Fe_2O_3 for the Makganyene diamictites, but have positive correlations in the Hotazel diamictites. This shows that the transition elements and Fe reside in the (alumino-) silicate phase (i.e. stilpnomelane) in the Hotazel diamictites, while they are related to the Fe-oxide phase in the Makganyene diamictites. This clearly indicates that both BIFs and another rock type acted as the main source rocks. This other source for the Hotazel diamictite, besides BIFs, was probably the volcanic tuffs (figure IV.10.I) as they exhibit the same trend with the Hotazel diamictite. In all the diagrams from figure IV.10, the Makganyene diamictite plots within a relatively narrow compositional field, which hinders the assessment of compositional

differences between the different sampling locations. However, the Hotazel diamictite is generally enriched in the transitional elements relative to the Makganyene diamictite.

Figure IV.11 illustrates the behaviour of selected major elements when plotted against CaO. Diagram A does not show any relative change in SiO_2 concentration with changes in concentration of CaO, for either the Hotazel or the Makganyene diamictites. The Hotazel diamictites contain lower amounts of SiO_2 compared to the Makganyene diamictite. Diagram B illustrates that MgO is incorporated in the carbonate minerals in the Makganyene diamictite in the form of dolomite-ankerite. A negative correlation trend is observed in the Hotazel diamictite (as in the BIFs) and reflects the difference in carbonate mineralogy between the Makganyene diamictite (dolomite-ankerite series) and the Hotazel diamictite (calcite). The remaining diagrams (C and D) display positive correlations for CaO with Sr and MnO, indicating that these two components occur in the carbonate phase regardless of their stratigraphic positions. MnO concentrations are the highest (3wt%) in the Matsap samples.

The behaviour of transitional elements (V, Sc, Co, Zn, Ni, Zr and Cr) in the Hotazel diamictite, plotted against CaO, is similar to the behaviour of these trace elements plotted against Fe_2O_3 for the same diamictite. The Makganyene diamictite does not show any correlation with V, Sc, Co, Zn, Ni, Zr and Cr.

Figure IV.12 displays the behaviours of selected elements from the Makganyene and Hotazel diamictites plotted against Al_2O_3. Diagrams A and C both display positive correlations, indicating that Al_2O_3 is associated with TiO_2 and SiO_2. Diagram B shows negative correlation between Al_2O_3 and Fe_2O_3 implying that the Fe-oxide mineral phase is not detrital. Diagram D shows again the different behaviour of MgO above and below the lava due to differences in carbonate mineralogy. As in the Hotazel BIFs, MgO, K_2O and TiO_2 occur in the (alumino)-silicate mineral group (stilpnomelane) in the Hotazel diamictites.

Figure IV.13 displays the behaviour of selected trace elements of the Makganyene and Hotazel diamictite plotted against Al_2O_3. All elements correlate positively with the aluminous fraction of the diamictites.

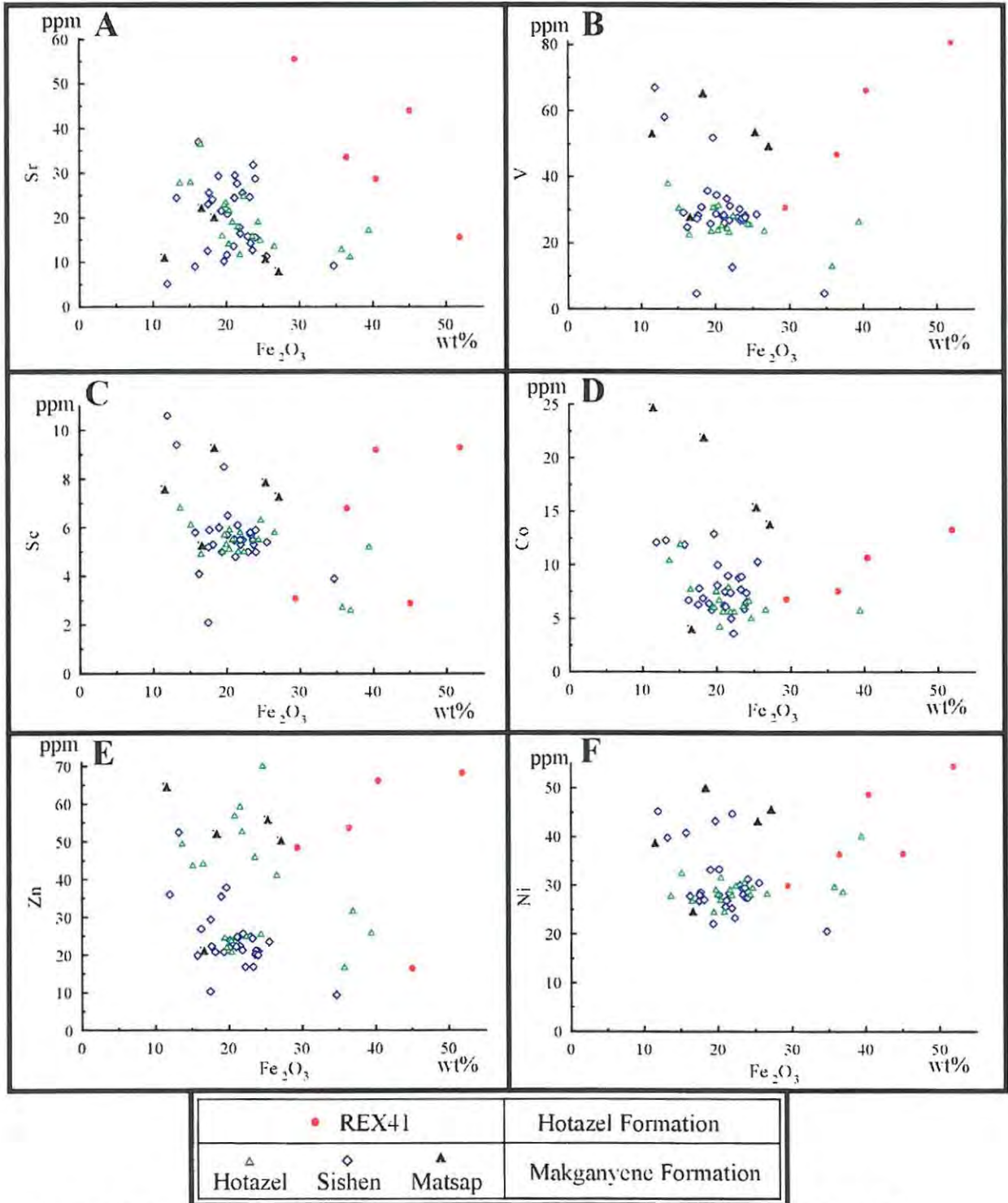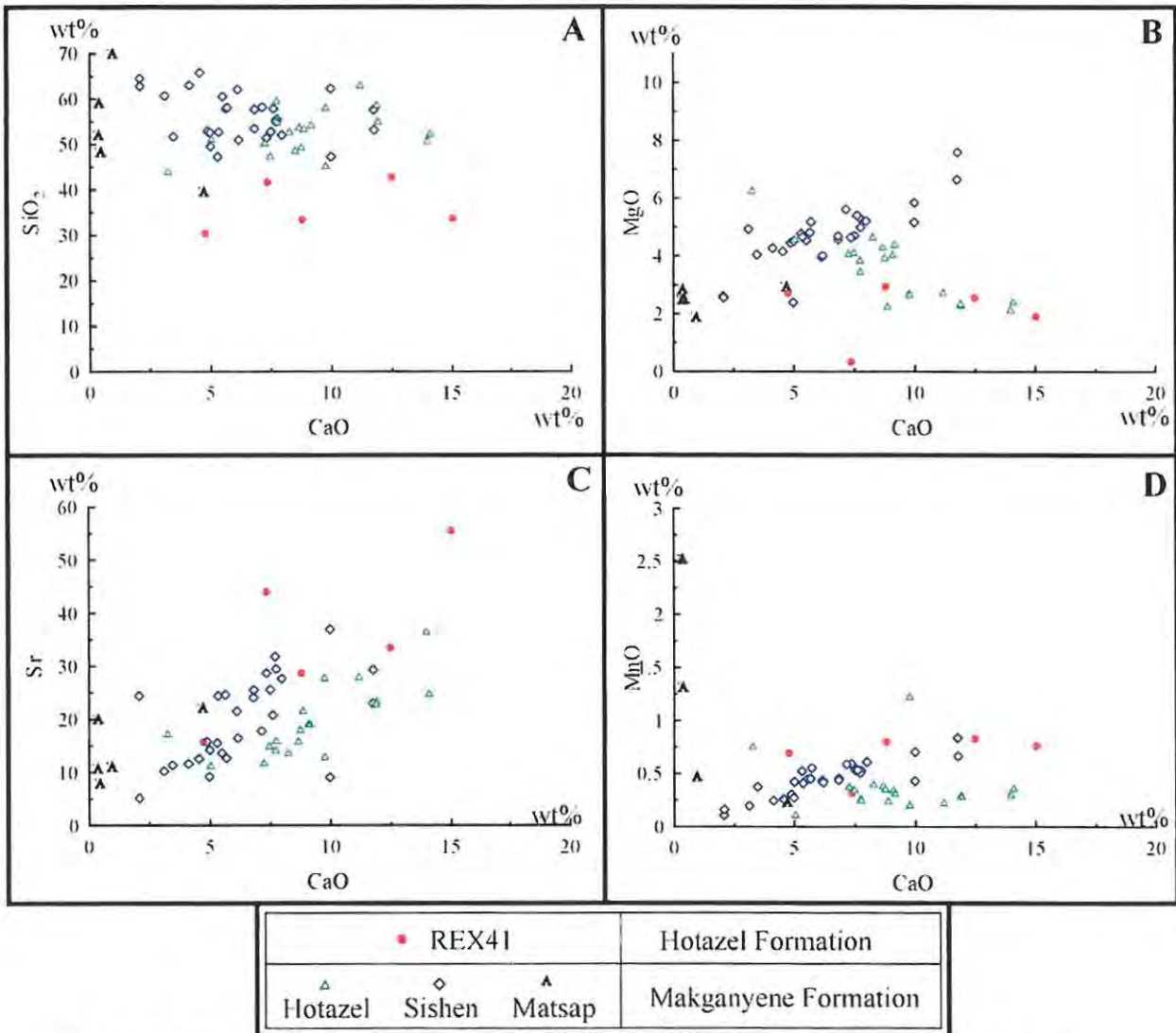**Figure IV.11.** Whole-rock carbonate geochemical signature of the Makganyene and Hotazel diamictites displayed in bivariate plots.

Diagram A from figure IV.13 displays a very strong correlation trend for Zr, which represents the detrital fraction in both diamictites. Plot E (Cr) also displays a strong positive correlation similar to diagram A. Plot B exhibits clearly two different positive correlation trends for V in the Makganyene and Hotazel diamictites. This difference is interpreted as reflecting a basic volcanic input added onto the pre-existing BIF source for the Hotazel diamictite. The remaining plots (C, D and F corresponding to Ni, Sc and Y, respectively) show broad positive correlations with Al_2O_3. In these diagrams, the Hotazel diamictite illustrates different behaviours compared to the Makganyene diamictite.
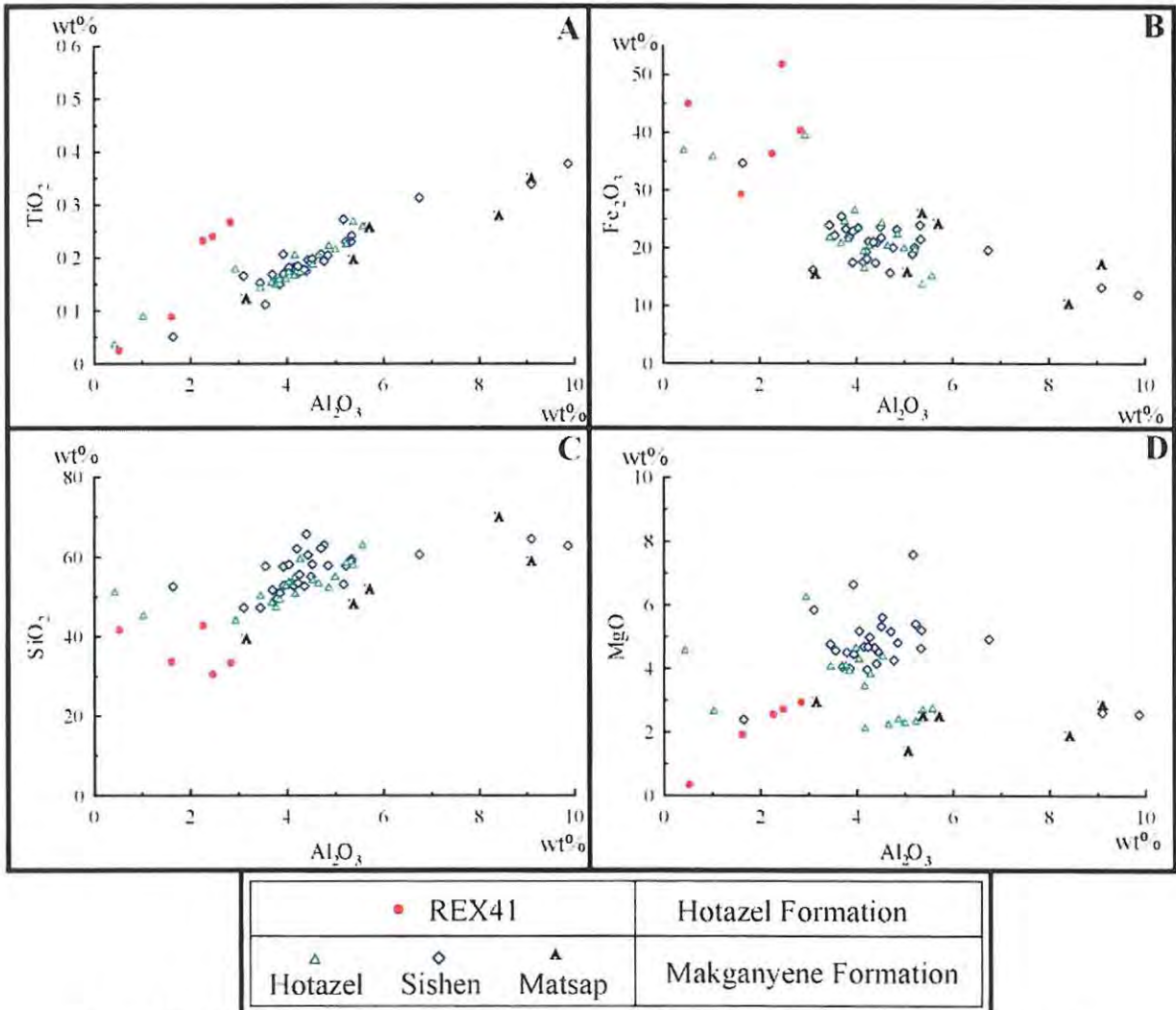
Figure IV.12. Whole-rock detrital silicate signature of selected Makganyene and Hotazel diamictites displayed in bivariate plots.
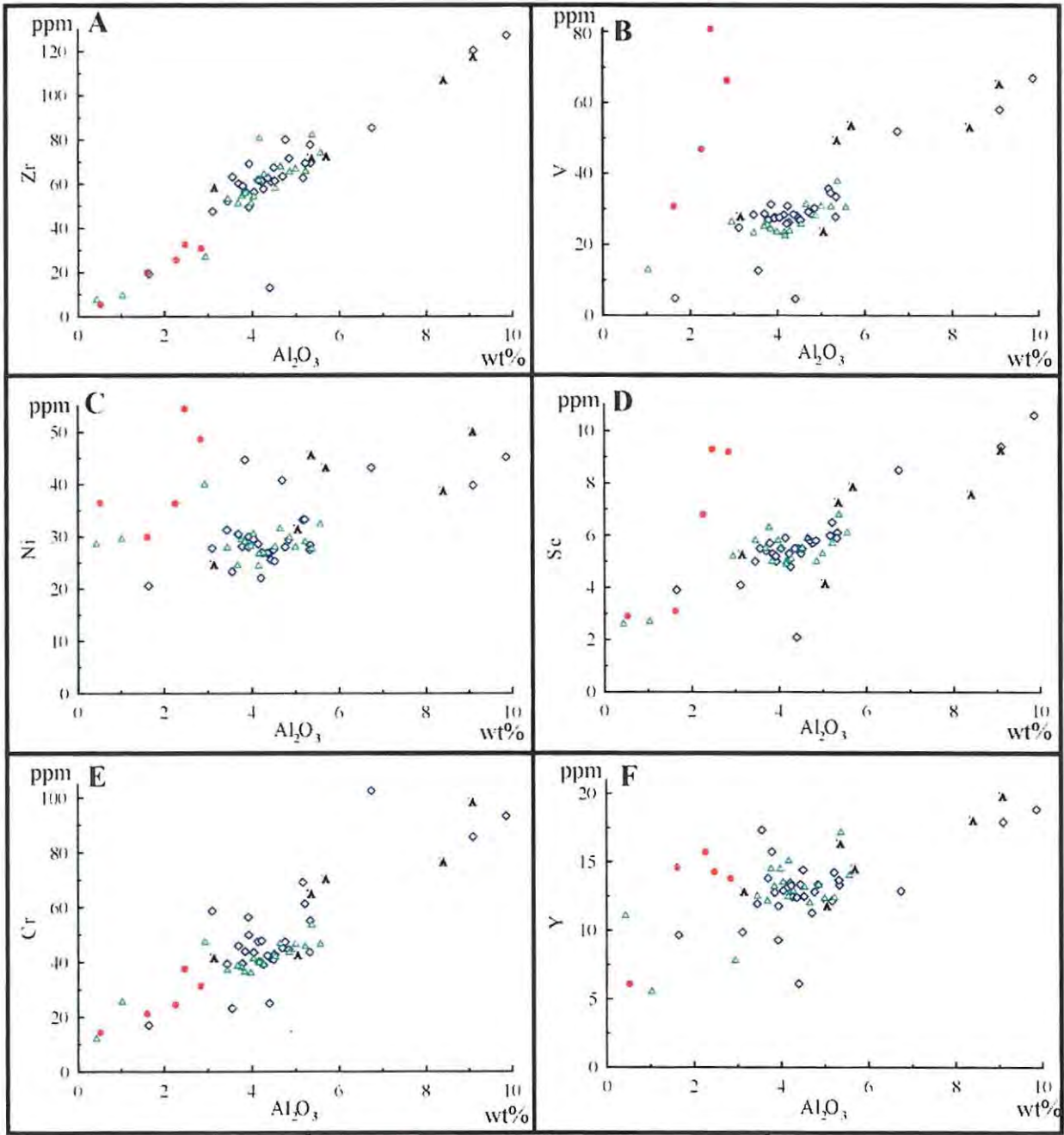
Figure IV.13. Whole-rock detrital silicate signature of selected Makganyene and Hotazel diamictites displayed in bivariate plots.

The Makganyene diamictites from the three different geographic locations (Matsap, Sishen and Hotazel areas) are compared to each other using triangular diagrams. The apices of the triangular diagrams represent a distinct geographical region. The Matsap area represents the southernmost sampled area, situated between Griquatown and Postmasburg (see figure II.1). The Sishen area is located in the central part of the Griqualand West Basin, and the Hotazel area represents the northern most sampled area.
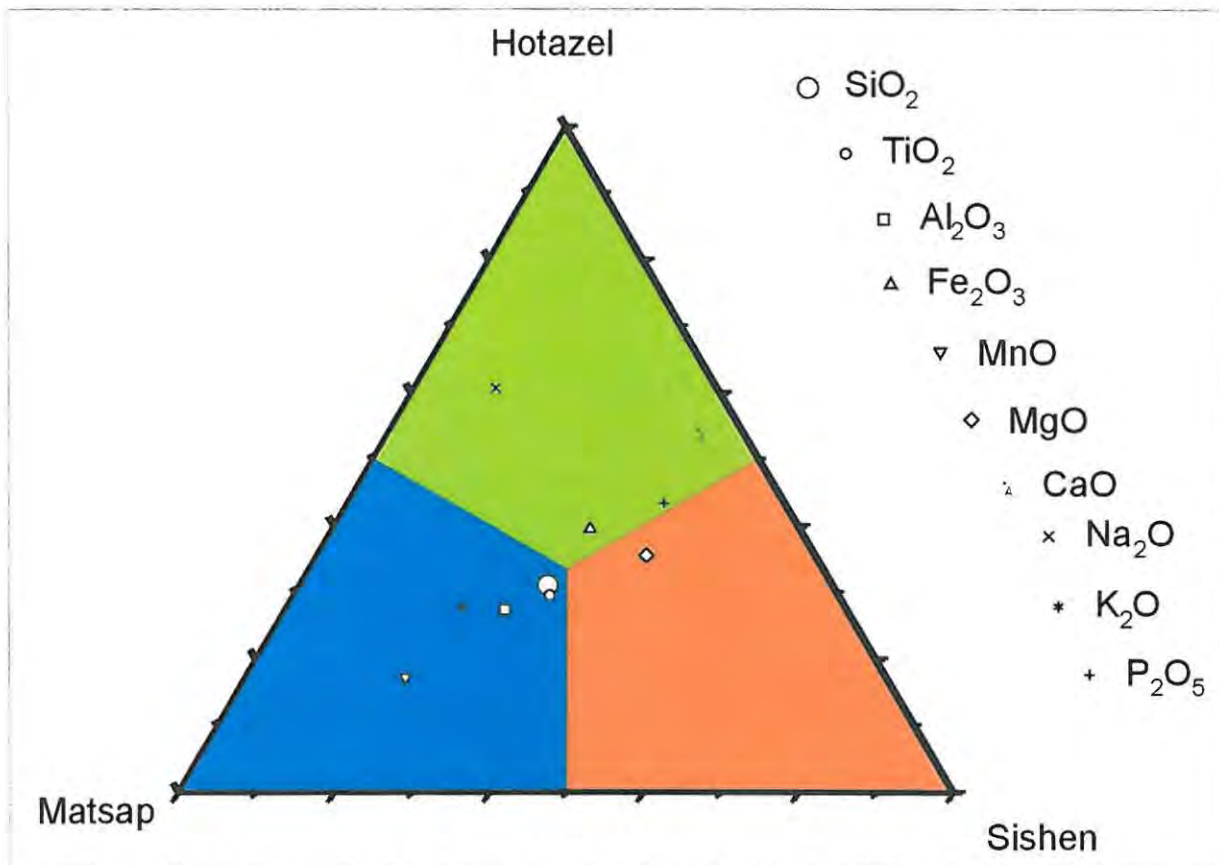
Figure IV.14. Geographical variations in major element concentrations for the Makganyene diamictite sampled in the Matsap, Sishen, and Hotazel areas. Values used to construct this diagram are presented in table IV.5.

Figure IV.14 illustrates how major element concentrations of the Makganyene diamictite vary according to their geographic position. The Sishen and Hotazel areas have minor differences in their major element composition, which is expressed by the trend following a line joining the Matsap pole with the tie-line between the Sishen and Hotazel quadrants. The Matsap area contains the highest proportions in Al_2O_3, TiO_2, K_2O and SiO_2,

representing the fine clay component of the Makganyene diamictite. MnO has the highest concentrations in the Matsap area. This is not surprising since manganese was being deposited off the shelf in deeper waters where it was stored. Fe_2O_3, MgO, P_2O_5, Na_2O and CaO are most abundant in the Sishen and Hotazel area, and these elements represent the detrital BIFs and carbonate fraction of the Makganyene diamictites. Na_2O concentrations are the highest in the Hotazel area, which may reflect late Na-metasomatism (Tsikos, 1999). This diagram is useful in separating sedimentary domains, from platform to slope facies. The Ghaap platform contains the highest concentrations in heavy minerals and the deeper Prieska basin/slope displays the highest detrital element contents in the fine clay fraction of the Makganyene Formation.
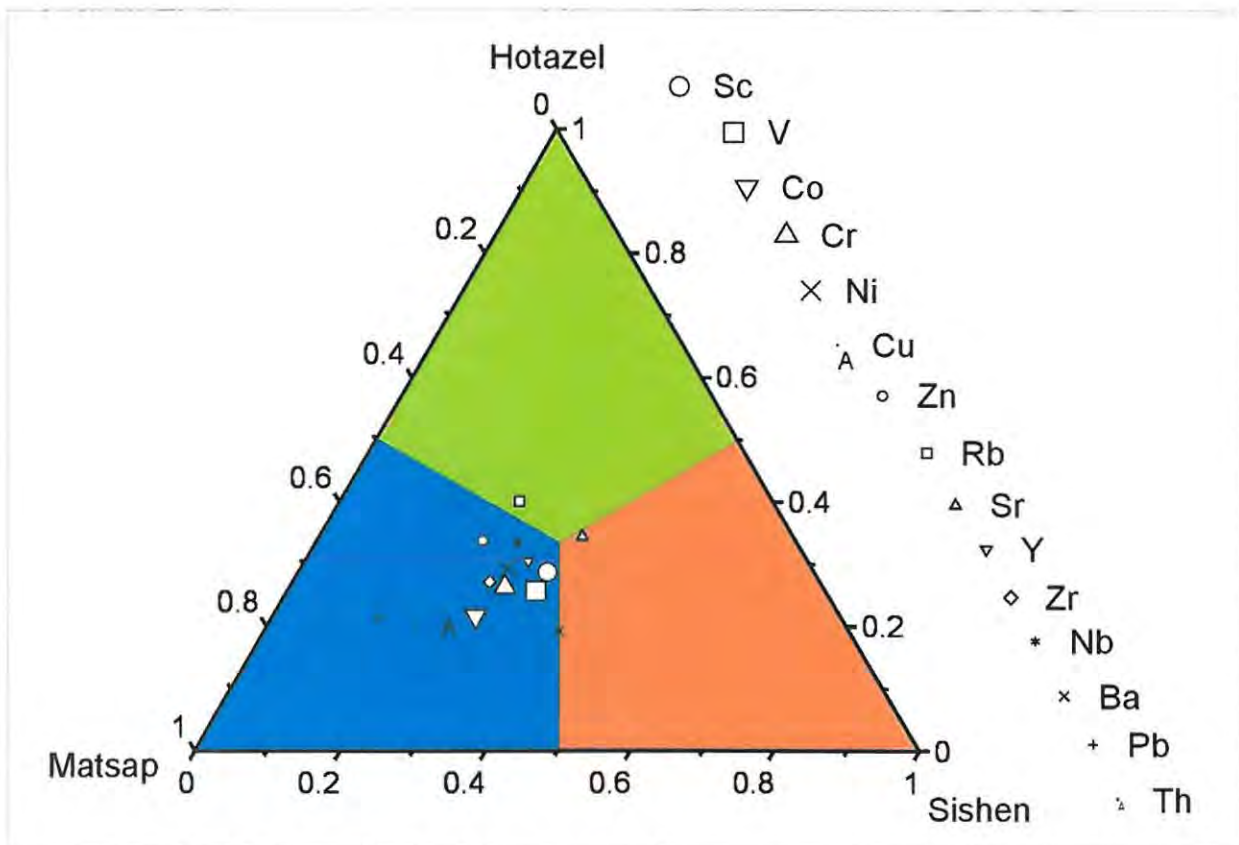
Figure IV.15. Geographical variations in trace element concentrations for the Makganyene diamictite sampled in the Matsap, Sishen, and Hotazel areas. Values used to construct this diagram are presented in table IV.5.

Figure IV.15 shows that most of the trace elements have highest concentrations in the Matsap area. This is explained by the bivariate plots shown in figure IV.13, where the detrital fraction of the diamictite, occurring as fine clay, is positively correlated with most of the trace elements. Only Sr and Rb have higher concentrations in the Sishen and Hotazel area. Sr is associated with Ca in the carbonate fraction, and therefore its high concentration in the Sishen and Hotazel area is not surprising.

On the other hand, Rb correlates with K_2O and therefore should belong to the silicate phase of the Makganyene diamictite. Its location in the Hotazel area was therefore not anticipated and somewhat unusual. Rb is associated with stilpnomelane, which modal proportions correlate positively with the carbonate contents.

IV.2.4.2.2. Provenance studies

The compositions of the Makganyene and Hotazel diamictites from the different geographical areas shown in figure IV.5 are plotted with the compositions of the BIFs from the Griquatown, Makganyene and Hotazel Formations. The Makganyene composition is very similar to that of BIFs. BIFs therefore are the main source material for the Makganyene diamictites. A useful triangular diagram for assessing the importance of other possible sources has one apex representing the BIF source ($SiO_2+MnO+Fe_2O_3$), a second apex representing the carbonate source ($CaO+MgO$) and the third apex representing an igneous or clastic source ($Al_2O_3+Na_2O+K_2O$) (Polteau, 2000). These three types of source rock are the most probable since they occur as major lithologies in the Transvaal and underlying Ventersdorp Supergroups. One problem with this diagram is that the BIF apex includes SiO_2, which overemphasizes the BIF signature in the Makganyene diamictites. A similar diagram, shown in figure IV.16, was plotted, excluding SiO_2. Diamictite from all areas plot near the BIF apex. Differences for the three areas noted by Polteau (2000) can be seen, and correspond to an increase in carbonate concentrations in the Sishen-Hotazel area while the Matsap area plots closer to the igneous apex. The REX41, or Hotazel diamictite plots also near the BIF apex, along the carbonate-BIF tie line.

The igneous/clastic apex does not differentiate between mafic, felsic or clastic origin. Bivariate plots were used to find out if the main igneous source was either felsic or mafic. These are shown in figure IV.17, where trace elements such as Sc, Co, Ni and Cr, are plotted against Zr. These particular trace elements were selected as they show different trends for felsic and mafic rocks. The mafic and felsic trends were constructed using data from Taylor

and McLennan (1985), and represent averages of Archaean mafic and felsic end-member compositions.
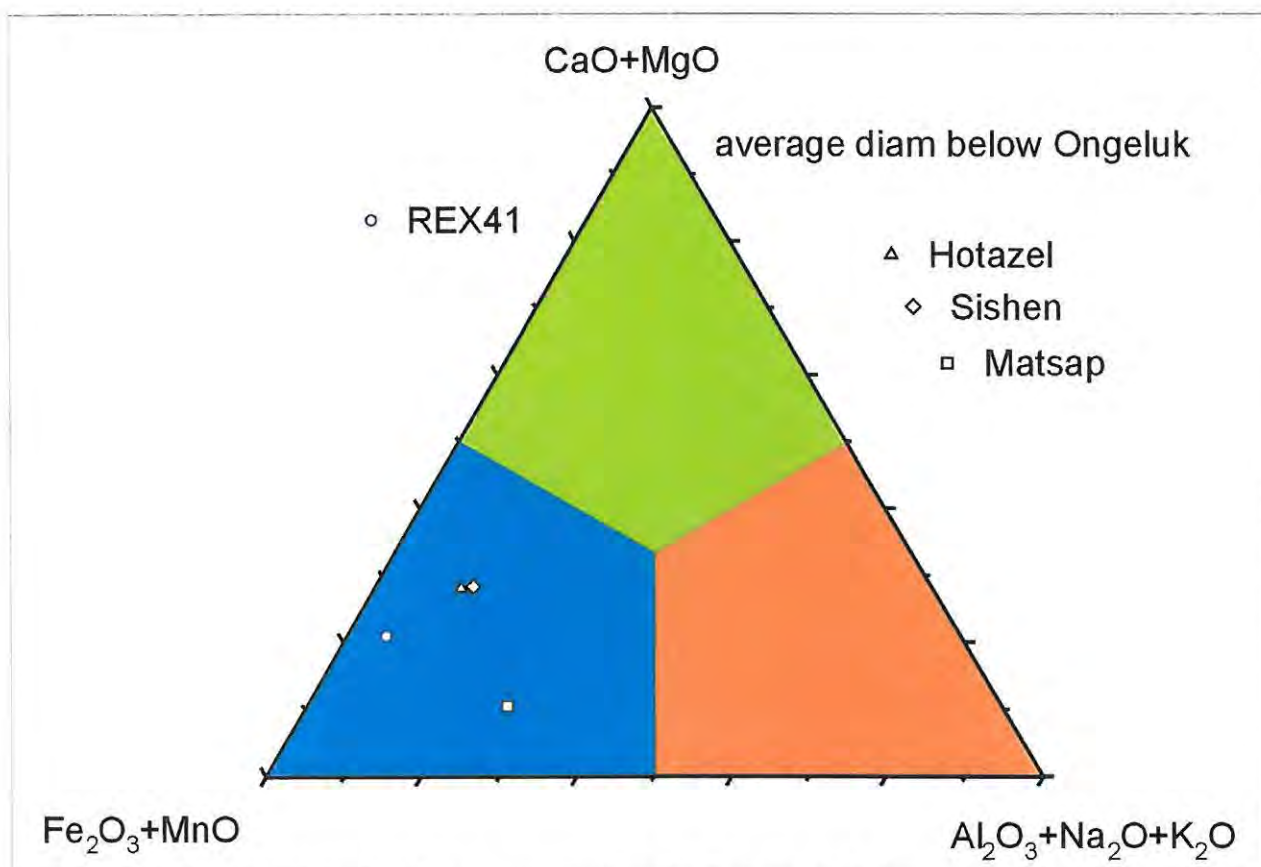
Figure IV.16. Triangular diagram representing the three most likely source rocks for the Makganyene and Hotazel diamictites.

All the diagrams from figure IV.17 clearly show that the Makganyene diamictite has an intermediate trend between felsic and mafic end-members (i.e. dacitic to andesitic or granodioritic to dioritic). This could be indicative of a source from the Ventersdorp Supergroup.

On the other hand, the Hotazel diamictites show a greater shift towards a mafic signature in their composition. This is reasonable since it is immediately underlain by the andesitic Ongeluk lava and interbedded with hyaloclastites. The ice sheet would have eroded newly extruded and deposited mafic volcanic material, and incorporated this material in the Hotazel diamictite matrix, giving the diamictite a more mafic trend.
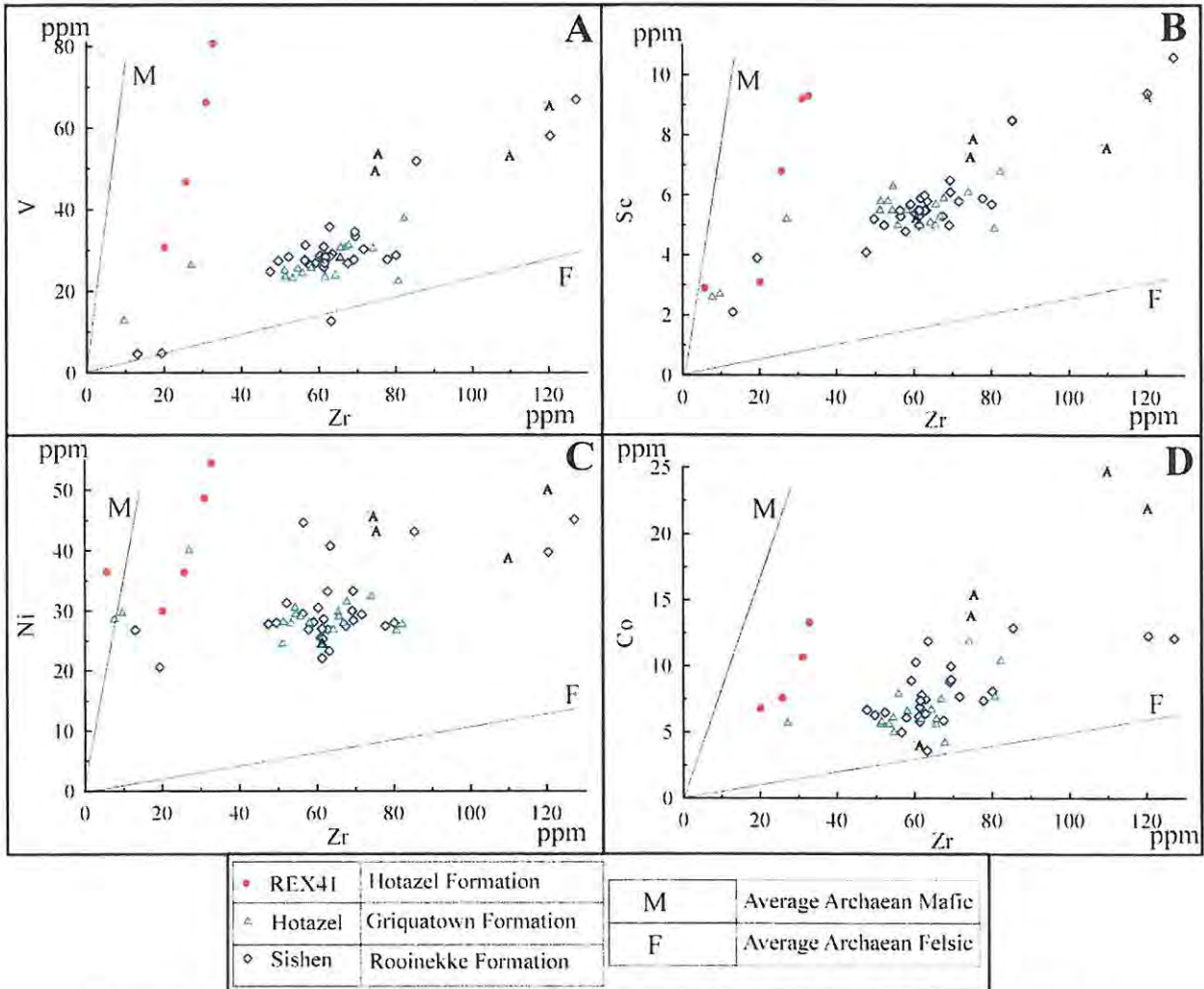
Figure IV.17. Whole-rock igneous signatures of selected samples from the Makganyene and Hotazel diamictites, displayed in bivariate plots.

The glacial origin of the Hotazel diamictite may still be in doubt. The main counter-argument would be that the Hotazel diamictites plot along the trend of the volcanic tuffs (figure IV.10.I). The Hotazel diamictites have therefore been directly compared to the analysed interbedded hyaloclastites. This is shown in figure IV.18, where the volcanic tuffs from the base of the Hotazel Formation have been averaged (see table IV.5) and normalised to the average composition of the Hotazel diamictites.

Figure IV.18 clearly shows that the hyaloclastites from the base of the Hotazel Formation are enriched in volcanic components (such as TiO_2, Al_2O_3, MgO, Sc, V, Cr, Co, Ni, Cu, Zn, Y, Zr and Nb) and depleted in elements commonly in BIFs (such as Fe_2O_3, MnO,

CaO and Sr) and clay minerals (such as Na$_2$O, K$_2$O and Rb). This demonstrates that the Hotazel diamictite is compositionally very different from the hyaloclastites, as already described by petrographic means (see chapter III), and shows that they also incorporate BIF material, including dropstones.
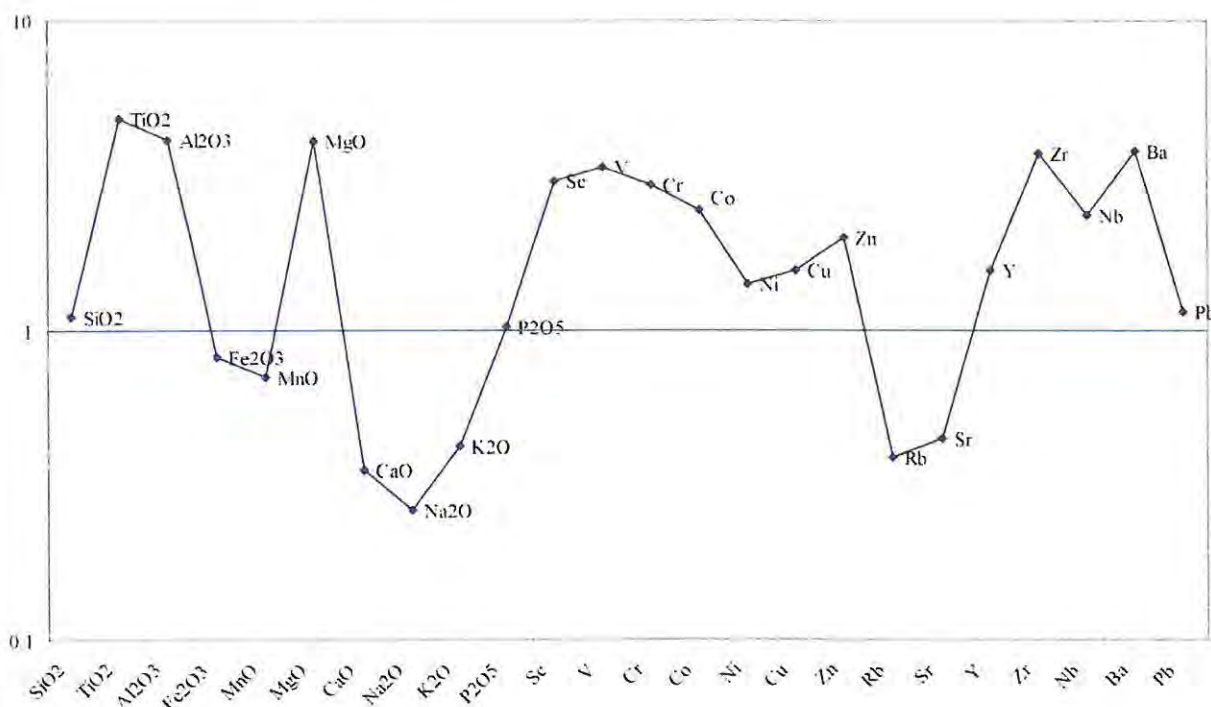
gure IV.18. Average volcanic tuffs from the base of the Hotazel Formation normalised to the average composition of the Hotazel diamictite (values from table IV.5).

Taylor and McLennan (1985) state that the Cr/Th and Sc/Th ratios reflect the composition of the continental crust, and that they are insensitive to weathering, alteration and metamorphism. According to Condie and Wronkiewicz (1990), these ratios vary due to changes in the source rock. The Cr/Th ratio applied to the Makganyene diamictites and the clastic Pretoria Group have similar very low values (figure IV.19, diagrams A and B). One of the main controversies in the regional stratigraphy of the Transvaal Supergroup in the Griqualand West Basin is the correlation of the Postmasburg Group with the Pretoria Group (Polteau, 2000; Moore et al., 2001). The Wits and Lower Transvaal have ratios that suggest a mafic source, while the Pretoria and Makganyene ratios suggest a granitic source similar to other pelitic rocks on the Kaapvaal Craton (Condie and Wronkiewicz, 1990). The Th, Cr and

Sc are very minor components of the Makganyene diamictites. Therefore these ratios cannot be used to correlate the Postmasburg with the Pretoria Group.
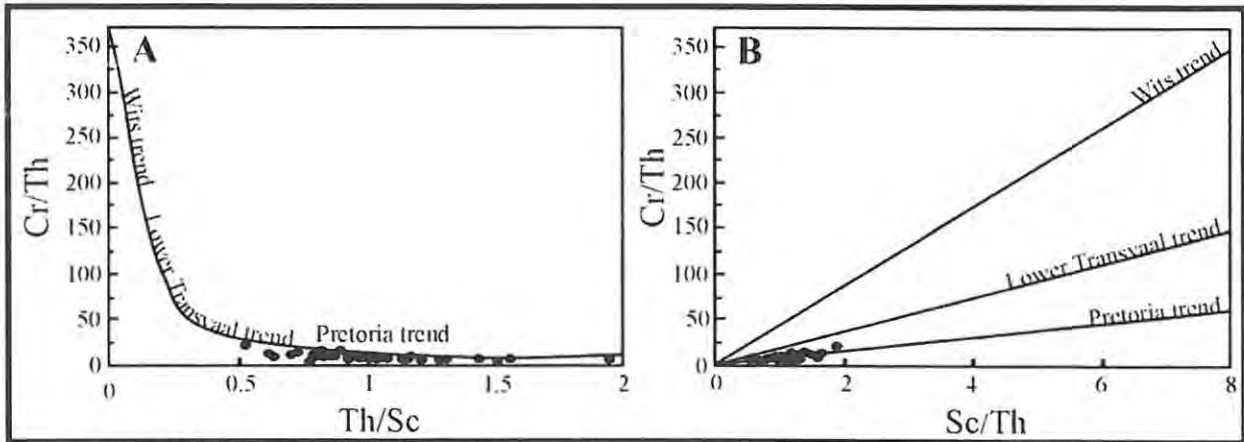
Figure IV.19. Cr/Th and Sc/Th ratios as indicative of crustal evolution. The Makganyene diamictites share the same trend as the Pretoria Group (after Condie and Wronkiewicz, 1990).

To briefly summarise the geochemical affiliations, the Makganyene diamictite and the Griquatown/Makganyene BIFs share similar bulk compositions. This is reflected by the occurrence of an Fe-oxide phase with affinity to transitional metals such as Ni, Cr and V, while the carbonate mineral group includes MgO and Sr, and by a similar geochemical affinity of the silicate mineral phase with most of the trace elements analysed (Co, Sc, Ni, V, Rb, Zr and Cr). The Makganyene diamictite displays a felsic (or crustal) signature.

On the other hand, the Hotazel diamictite has a mafic component attributed to the contamination of the original Makganyene composition by the andesitic Ongeluk lava, but is significantly different from the composition of the volcanic tuffs in that it also contains a significant BIF signature. The geochemical affiliations are also similar, with the exception of MgO, which is included in the silicate phase (stilpnomelane).

The main source rocks for both diamictites were mostly BIFs, with minor influences from igneous/pelitic and carbonate rocks. The Makganyene diamictite sampled in the Sishen-Hotazel area contains a greater carbonate component than in the Matsap area. The latter area contains more fine clay components, reflecting different sedimentary environments (from platform to slope facies).

Finally Cr/Th and Th/Sc ratios do not reflect ages of the sediments, but rather the nature of source rocks. The Makganyene diamictites have ratios implying a dominantly

granitic source similar to other pelitic rocks on the Kaapvaal Craton (Condie and Wronkiewicz, 1990).

IV.3. Carbon and oxygen isotope geochemistry

IV.3.1. Introduction

This section covers the application of stable isotope geochemistry to the carbonate minerals present in the different rock types encountered in the borehole sections from Sishen and Hotazel. The minerals of the carbonate phase present within BIFs, diamictites and volcanic tuffs are calcite, dolomite/ankerite and siderite (see chapter III). The variation in isotopic composition of the elements C and O in these carbonate minerals has been applied by previous workers to assess primary and diagenetic control over isotopic compositions (Kaufman et al., 1990) and to assess the chemical composition of the depositional waters (Beukes et al., 1990; Klein and Beukes, 1993). They have also been applied towards deciphering secular variations in isotopic compositions and thus major geochemical events in Earth's history that were potencially linked to paleoclimate changes, tectonic evolution, etc (Knoll et al., 1986; Schidlowski, 1988; Des Marais et al., 1992; Derry et al., 1992; Des Marais, 1994; Karhu and Holland, 1996; Condie et al., 2001).

The carbon and oxygen isotopic compositions of geological material are conventionally expressed as $\delta^{13}C$ and $\delta^{18}O$ values according to the following equations.

$$\delta^{13}C = \left[\frac{(^{13}C/^{12}C)_{sample}}{(^{13}C/^{12}C)_{standard}} - 1\right] \times 1000 \ (\text{‰PDB}) \qquad \delta^{18}O = \left[\frac{(^{18}O/^{16}O)_{sample}}{(^{18}O/^{16}O)_{standard}} - 1\right] \times 1000 \ (\text{‰SMOW})$$

The standard PDB is a modified acronym of the Pee Dee Belemnite, which is a belemnite sample (*Belemnitella americana*) from the Cretaceous Peedee Formation and corresponds to the $^{13}C/^{12}C$ ratio of this specific carbonate fossil (Schidlowski, 1988). The standard SMOW is the acronym for Standard Mean Ocean Water and represents the approximated $^{18}O/^{16}O$ ratio of modern seawater.

A positive value of $\delta^{13}C$ indicates a higher $^{13}C/^{12}C$ ratio in the sample relative to the standard, and hence corresponds to a ^{13}C "enrichment" or "heavy" $\delta^{13}C$. A negative value implies a lower $^{13}C/^{12}C$ ratio in the sample relative to the standard, and hence corresponds to a ^{13}C "depletion" or "light" $\delta^{13}C$. The same nomenclature applies to $\delta^{18}O$.

IV.3.2. Sample selection and methods

A total of 15 samples were selected, corresponding to different rock types, as well as different stratigraphic positions. Three samples come from borehole GA107 from Sishen. Twelve samples come from a single borehole (REX41) intersecting the base of the Hotazel Formation in the Hotazel area. Analyses undertaken by the author during his M.Sc. thesis (Polteau, 2000) were also included, and correspond to five more samples from the Makganyene Formation from the Sishen area: three samples from borehole GA171 and two samples from borehole GA129.

Only a few analyses were undertaken from the Makganyene Formation because few facies variations are present. Essentially two rock types are present in the Makganyene Formation: BIFs and diamictites. Also previous analyses, completed by the author (Polteau, 2000), essentially characterise the base of the Makganyene Formation where BIFs and diamictites are intimately interbedded. Sample selection for borehole REX41 intersecting the base of the Hotazel Formation was more continuous because the succession is more complete, and consists of BIFs (Fe and carbonate facies), diamictites and hyaloclastites.

The isotopic compositions were obtained using a Finnigan MAT 252 mass spectrometer in the Department of Geological Sciences, University of Cape Town. Carbon dioxide was evolved from bulk-rock powder samples by placing between 30 to 110 mg (depending on the amount of carbonate minerals determined by XRD methods) in 100% H_3PO_4 at 25°C for 4 hours (calcite) or 50°C for 8 hours (for ankerite and dolomite). The results are presented in table IV.6, while the profiles are shown in figures IV.1 and IV.4.

IV.3.3. Results

The carbon and oxygen isotopic compositions of the selected samples are presented in table IV.6. The negative $\delta^{13}C$ values are characteristic of light carbon enrichment. The $\delta^{13}C$ values of the diamictites from the Hotazel Formation fall within the narrow range of −15.4‰ to −13.5‰, while the diamictites from the Makganyene Formation are marked by less depleted $\delta^{13}C$ values (−8.3‰ and −3.4‰). The $\delta^{13}C$ values for the BIFs from the Hotazel Formation have slightly less depleted values compared to the $\delta^{13}C$ of the Hotazel diamictites, and range between −12.5‰ and −13.8‰. The $\delta^{13}C$ of the hyaloclastite is also low (-15.8‰).

The $\delta^{18}O$ compositions of the diamictites from the Hotazel Formation display values between 14‰ and 16.8‰, while the Makganyene diamictites exhibit even more enriched values between 16.8‰ and 18.8‰. For the BIFs of the Hotazel Formation, the $\delta^{18}O$ values

are similar to the values of the Hotazel diamictites, and fall within the range of 13.5‰ and 16.3‰. The hyaloclastite of the Hotazel Formation has a $\delta^{18}O$ value of 14.7‰.

Sample name	Rock type	$\delta^{13}C$ ‰(PDB)	$\delta^{18}O$ ‰(SMOW)
REX41 131	Diamictite	-13.5	14.0
REX41 131.2	Diamictite	-14.1	14.7
REX41 131.5	Diamictite, brown matrix	-14.4	14.5
REX41 132.8	Diamictite	-15.4	16.8
REX41 133.2	Diamictite	-14.2	15.4
REX41 144.9	Red BIF like Hotazel BIF	-13.8	13.5
REX41 134.3	Greenalite BIF with magnetite bands	-12.8	15.0
REX41 139.7	Greenalite BIF with magnetite bands	-13.6	16.3
REX41 140.2	Greenalite BIF with magnetite bands	-12.5	15.5
REX41 140.8	Greenalite BIF with magnetite bands	-13.1	14.8
REX41 129.9	Carbonate BIF	-13.3	14.4
REX41 141.7	Hyaloclastite	-15.8	14.7
GA107 245.3	Diamictite, grey matrix	-3.4	17.8
GA107 336.7	Diamictite, red matrix	-6.6	18.8
GA107 340.3	Diamictite, red matrix	-8.3	16.8

Table IV.6. Isotopic compositions of the 15 samples selected.

The data in table IV.6 are summarised in the $\delta^{18}O$-$\delta^{13}C$ plot for all samples selected for isotopic analyses (figure IV.20). Samples from the Makganyene diamictite and BIFs analysed by Polteau (2000) are also included in this diagram. Clearly two clusters are present within figure IV.20, and these are defined by similar $\delta^{18}O$ (-13 to -17‰) and different $\delta^{13}C$ (between –4 and -10‰ for the Makganyene Formation, and between –12 and -16‰ for the Hotazel Formation). The first isotopic compositional group is that of the base of the Hotazel Formation, and includes all lithologies. This group is characterised by a strong depletion in $\delta^{13}C$ compared to the Makganyene group. The $\delta^{13}C$ values show a stratigraphically controlled variation by displaying one cluster with heavy values for the Hotazel Formation and a second cluster with lighter values.
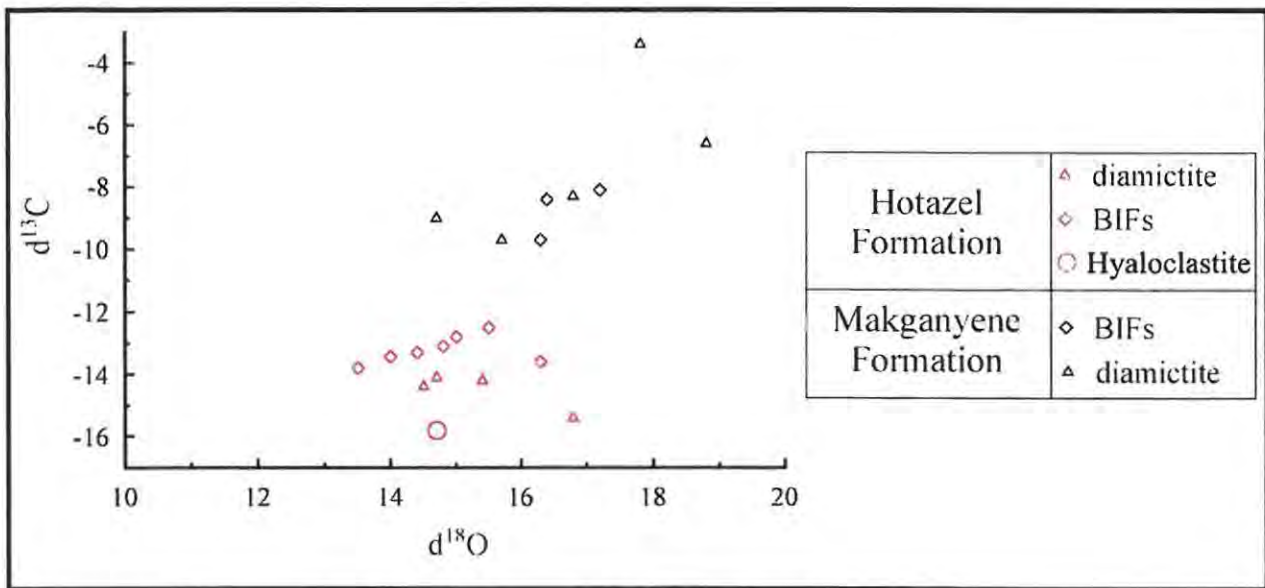
Figure IV.20. Bivariate plot of $\delta^{18}O$ versus $\delta^{13}C$ (values are in ‰).

Figure IV.21 displays diagrams where $\delta^{13}C$ has been plotted against selected major elements such as Al_2O_3 (A), Fe_2O_3 (B) and CaO (C). Two diamictite samples from Polteau (2000) have been omitted because they do not have major elemental compositions associated with their isotopic composition. Diagram A separates the diamictites from the BIFs, but also discriminates these lithologies stratigraphically. Therefore four clusters are present, corresponding to each lithology from each stratigraphic position. Diagram B illustrates distinct $\delta^{13}C$ values for the Makganyene and Hotazel BIFs and diamictites that are not influenced by Fe_2O_3 contents. Diagram C shows that the concentrations of carbonate minerals do not influence the $\delta^{13}C$ for all the lithologies of the Hotazel and Makganyene Formations.
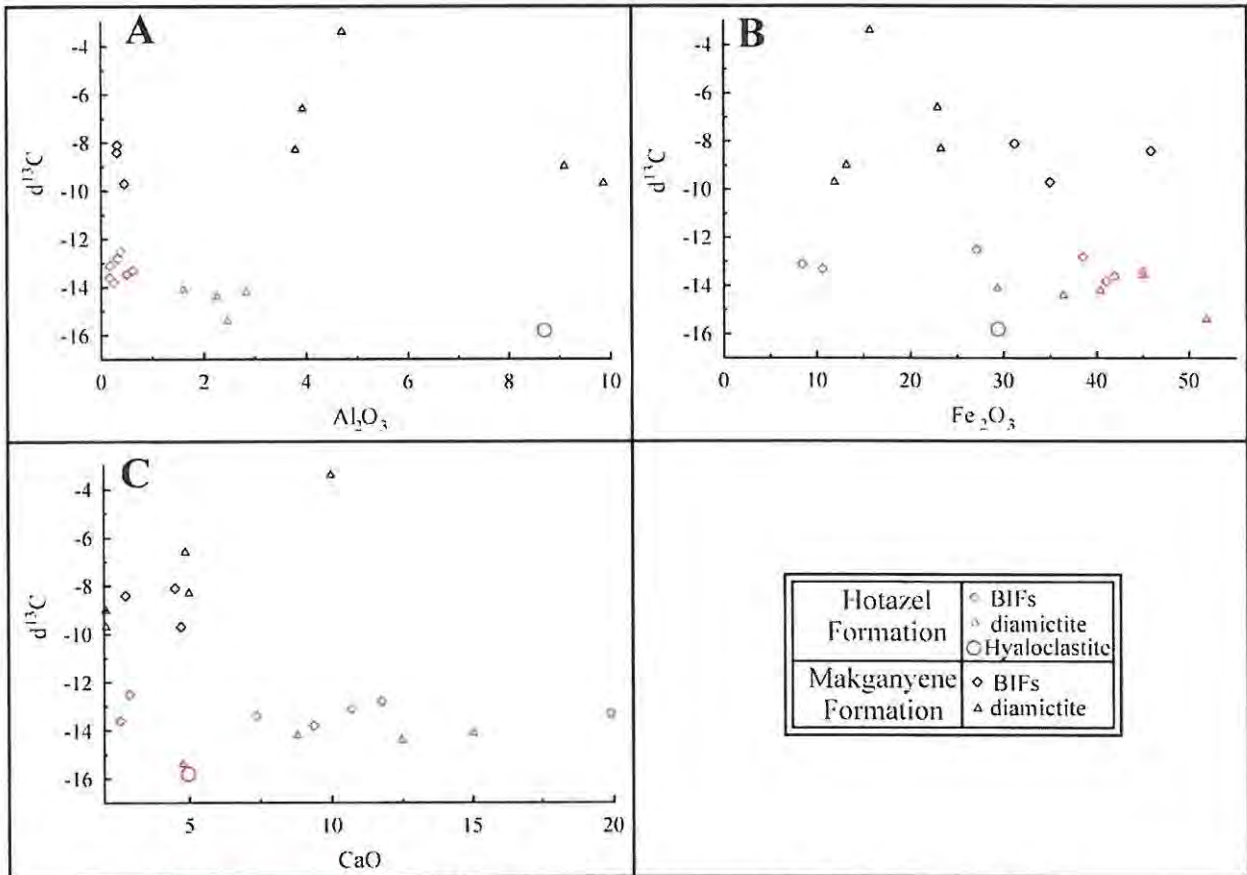
Figure IV.21. Bivariate plots of $\delta^{13}C$ against Al_2O_3 (diagram A), Fe_2O_3 (diagram B), and CaO (diagram C).

A vertical isotopic stratigraphic profile throughout the upper Transvaal Supergroup can be drawn if data from Tsikos (1999) and Polteau (2000), as well as the present data, were to be combined. This is illustrated in figure IV.22 and represents the carbon and oxygen isotopic variations across the stratigraphy of the Postmasburg Group. The Ongeluk volcanics are not included in this sedimentary profile.

The $\delta^{13}C$ curve for the Hotazel Formation exhibits cyclicity as well as general enrichment (see figure IV.22), which relates to the cyclicity between BIFs, Mn ore and carbonates. The $\delta^{18}O$ trend is also one of general enrichment with cyclic peaks in the Mn horizons, related to oxidation of manganese and reduction of carbon (Tsikos, 1999).

These changes in isotopic composition can be seen as marking the depositional environments from glacial/clastic sedimentation in the Makganyene Formation, to iron precipitation in the BIFs of the Hotazel Formation, to manganese/carbonate precipitation at the top of the Hotazel/Mooidraai Formations.
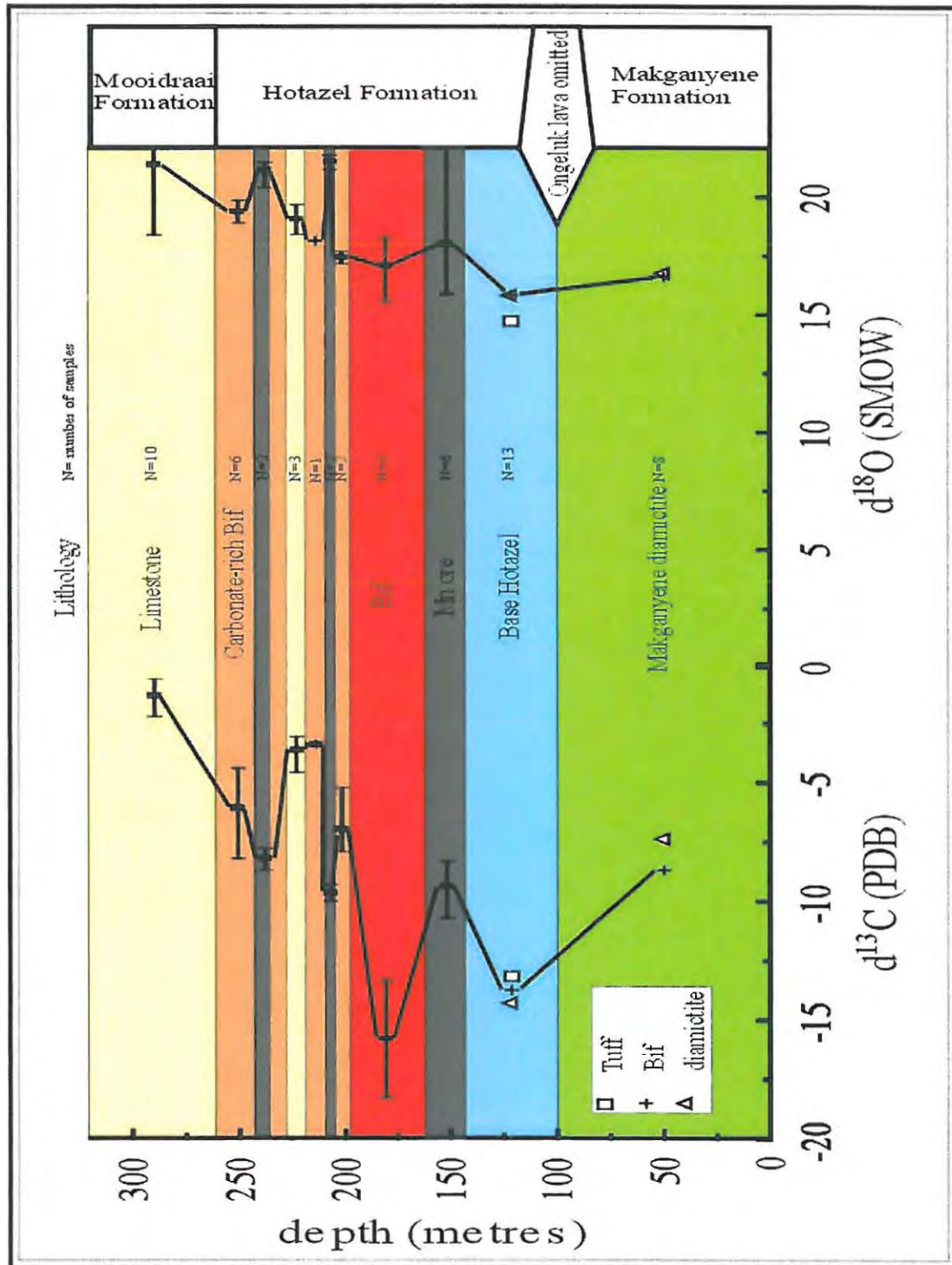
Figure IV.22. Carbon and oxygen isotopic variations across the Postmasburg Group. Lithologies are indicated, and the curve joins BIF values. Values are in ‰ and from Tsikos (1999), Polteau (2000), and the present study. Note that the Ongeluk Formation is excluded; the base of the Hotazel Formation corresponds to the thickness of this formation studied during this project, horizontal lines represent the range of values of Tsikos (1999).

Figure IV.23 (after Polteau, 2000) displays the $\delta^{13}C$ and $\delta^{18}O$ variations across the entire stratigraphy of the Transvaal Supergroup. The $\delta^{18}O$ curve has heavy values (22.0‰) in the Campbellrand dolomites. Then the $\delta^{18}O$ values go steadily lighter in the Kuruman and Griquatown Formations of the Asbestos Hills Subgroup (19.8, 21.0 and 21.1‰). The $\delta^{18}O$ values are lightest in the Makganyene (16.1‰) and Hotazel diamictites (15.2‰). Heavier values systematically re-appear in the Hotazel BIFs and the Mooidraai carbonates (19.2 and 20.4‰, respectively).

The $\delta^{13}C$ curve displays the same smooth trend. Both curves emphasise the symmetrical sedimentary succession of rock types in the Transvaal Supergroup of the Griqualand West Basin (carbonate – BIFs – diamictite – BIFs – carbonate) placing the diamictites at the centre of the symmetry. The Ongeluk Formation is omitted because it is a volcanic event that is considered to have had little influence on the Transvaal Supergroup sedimentary package (Tsikos and Moore, 1997; Tsikos, 1999; Polteau, 2000; Polteau and Moore, 2002). This symmetrical lithological cycle is also observed in the symmetrical variations of both $\delta^{13}C$ and $\delta^{18}O$ curves, and again the diamictites are in the centre of this cycle. This emphasises the pivotal role played by the Makganyene glacial event.
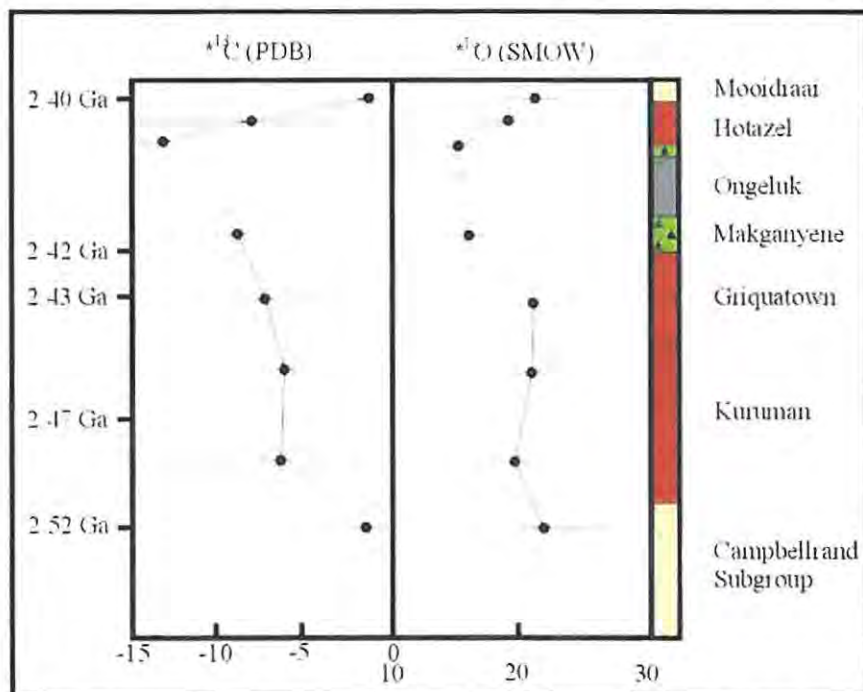
Figure IV.23. Stratigraphy of the Transvaal Supergroup in the Griqualand West Basin, with corresponding ages and $\delta^{13}C$ and $\delta^{12}O$ curves (averages, and horizontal lines represent the range of values, modified after Polteau, 2000).

IV.3.4. Genetic implications

It could be argued that the isotopic composition of carbonate minerals from the matrix of the Makganyene diamictite has the signature of its sources. However, the Makganyene values are more depleted than the sources, the underlying Campbellrand and Asbestos Hills Subgroup (shown in figure IV.23). According to Crossing and Gostin (1994), the isotopic composition of carbonate minerals from the matrix of the Appila Tillite represents the re-equilibration of the calcareous rock flour by isotopically light pore-water fluids during early diagenesis. Moreover, Fairchild et al. (1994) show that calcareous rock flour could undergo dissolution and isotopic re-equilibration with ambient seawater during deposition. So, as chemically precipitated carbonates, the isotopic composition of the carbonate minerals present in the matrix of the Makganyene diamictite represents the isotopic environment of deposition, along with its subsequent diagenetic alteration.

In the Early Proterozoic, carbon isotopic compositions of carbonate minerals from BIFs are characterised by depleted $\delta^{13}C$ values, and this statement is valid for the BIFs of the Postmasburg Group, but also for the diamictites of the Makganyene Formation. According to most authors, two key processes were responsible for such marked depletion (Becker and Clayton, 1972; Kaufman et al., 1990; Beukes et al., 1990; Carrigan and Cameron, 1991; Karhu and Holland, 1996; Tsikos, 1999). The first explanation is that carbonate minerals precipitated from a stratified water column with the bottom part being enriched in light ^{12}C supplied by hydrothermal activity, and the second explanation is coupled organic carbon oxidation - iron reduction (from Fe^{3+} to Fe^{2+}) during diagenesis/metamorphism.

According to Kaufman et al. (1990) and Beukes et al. (1990), a stratified ocean has deep water enriched in light ^{12}C supplied by submarine hydrothermal vents. The model of Klein and Beukes (1989) and Beukes et al. (1990) is based on major and trace element compositions, rare earth element patterns and kerogen contents of various lithofacies. Their results suggest that the near-shore environment was dominated by high organic activity and minor siliciclastic input in an iron-depleted shallow water mass where limestones and shales were deposited with $\delta^{13}C \approx -1‰$. On the other hand, the BIFs were deposited in an iron-enriched deeper water mass, removed from high organic productivity and any terrigeneous detritus (Klein and Beukes, 1989; Beukes et al., 1990) and was ^{12}C-enriched, hence the carbon isotopic signature of the BIFs at around $-5‰$. These two different water masses were separated by the chemocline (see figure V.5 from Klein and Beukes, 1989).

The conversion of inorganic carbon as CO_2 to living matter by biochemical pathways entails fractionation of ^{12}C and ^{13}C (Schidlowski, 1988). Biogenic substances produced by the action of living organisms display a marked preference for light carbon, leaving ^{13}C mostly as dissolved bicarbonate in seawater (Schidlowski, 1988). This has been the case for the last 3.8 Ga (Knoll et al., 1896; Schidlowski, 1988; Des Marais et al., 1992). This ^{13}C depleted organic carbon is buried, but can still react during early diagenesis with the oxidant that yields the most free energy per mole of organic carbon oxidised (Tsikos, 1999). The organic carbon will react until depletion of the most efficient oxidants, or depletion of the organic carbon. In the modern environment, the high valence Fe^{3+} and Mn^{4+} are commonly oxidising agents of the organic matter. The series of reactions involved will produce secondary magnetite and isotopically light secondary carbonate minerals. Therefore the early diagenetic oxidation of light organic carbon, which released light ^{12}C that is reprecipitated as isotopically light carbonate minerals, was not the only process to cause carbon isotopic depletion during the glacial Makganyene event.

The other depleting mechanisms can be described briefly in three main points: onset of glaciation, established glaciation and deglaciation. The onset of glaciation marks the destabilisation of a stratified ocean (Condie et al., 2001) and upwelling of deep anoxic, isotopically light organic carbon onto the shelf, lowering the value of $\delta^{13}C$ (Crossing and Gostin, 1994). Stabilisation of the system by reduction of the temperature gradient between warm and cold areas will ultimately cause the establishment of a stratified and stagnant glacial ocean. The $\delta^{13}C$ is lowered by the oxidation of light organic carbon by iron according to the stratified ocean model, but also by the constant supply of fresh meltwater caused by the thawing of the ice shelf. The deglaciation will supply even more fresh water, and causes a transgression of deep anoxic and iron-rich waters onto the organic-rich shelf. This can be simplified by saying that a glacial event is marked by a net $\delta^{13}C$ depletion, which could be seen in figure IV.23.

According to Kaufman et al. (1990) and Beukes et al. (1990), the stratified ocean model would be responsible for primary $\delta^{13}C = -5$‰. The secondary shift is caused by the oxidation of organic carbon by ferric iron. Kaufman et al., (1990) and Beukes et al (1990) argued that the secondary shift is of the order of 3‰. This order of shift is in good agreement for the diamictites of the Makganyene Formation (average value around -8‰, including values from Polteau, 2000). The other processes attributed to glaciation-deglaciation events could account for the depletion of single samples up to $\delta^{13}C = -9.7$‰. The Hotazel

diamictites display shifts up to 13‰. This can be explained due to the respective stratigraphic positions. The base of the Hotazel Formation is characterised by a deglaciation event (see chapter II) and this time period would correspond to an increase in fresh water supply (coming from melted ice), significantly lowering the $\delta^{13}C$ (Crossing and Gostin, 1994).

Another unlikely process that may have contributed to lower $\delta^{13}C$ was the oxidation of the atmosphere which occurred at about 2.4-2.2 Ga (Kirschvink, 2002). During any rise in oxygen production, assumed to be principally biogenic, oxidised methane (not stable in presence of free oxygen) and its very light carbon ($\delta^{13}C \approx -60‰$) will return to the ocean and atmosphere as CO_2 to cause an extreme $\delta^{13}C$ depletion in carbonate minerals (Kennedy et al., 2001). Such dramatic depletion has not been observed in the analysed samples, which make the methane oxidation process unlikely.

Finally, metamorphism was not the cause of depletion in $\delta^{13}C$ for the Hotazel Formation (Tsikos, 1999) because the mineral assemblage is characteristic of very low-grade metamorphism, and because no homogenisation of the isotopic values is observed (Kaufman, 1990; Crossing and Gostin, 1994). It is also rejected in this study for the same reasons.

IV.4. Conclusions

Geochemistry is a useful tool that has been applied to the Makganyene Formation. Whole-rock compositions allowed direct comparisons between all the different lithologies from different localities and different stratigraphic levels. It also reveals the elemental affiliation with specific minerals and mineral phases.

All the BIFs from the Transvaal Supergroup in the Griqualand West Basin share similar mineralogy and chemistry with typical Superior-type BIFs (Tsikos, 1999), and thus essentially bear no resemblance to rocks that are common hosts of volcanogenic deposits, such as Algoma-type iron-formations (figure IV.24).

Whole-rock compositions of the Makganyene diamictite are similar to the BIFs, which acted as the main source rock for the diamictite. Other sources include carbonates coming probably from the Campbellrand Subgroup and a minor pelitic/granitic component. The Ventersdorp Supergroup most probably represents the small crustal component present within the Makganyene diamictite.

Sorting processes and paleoenvironmental conditions are interpreted to have generated the observed geochemical variations noted at the different localities investigated. The elements Ca, Fe, P and Mg are characteristic of the chemical carbonate of the Ghaap platform (Hotazel and Sishen area). The latter area appears to have undergone late Na-metasomatism,

which resulted in high Na values. On the other hand, Al, Ti, K and most of the trace elements correspond to the detrital fraction that is concentrated in the slope facies (Matsap area).
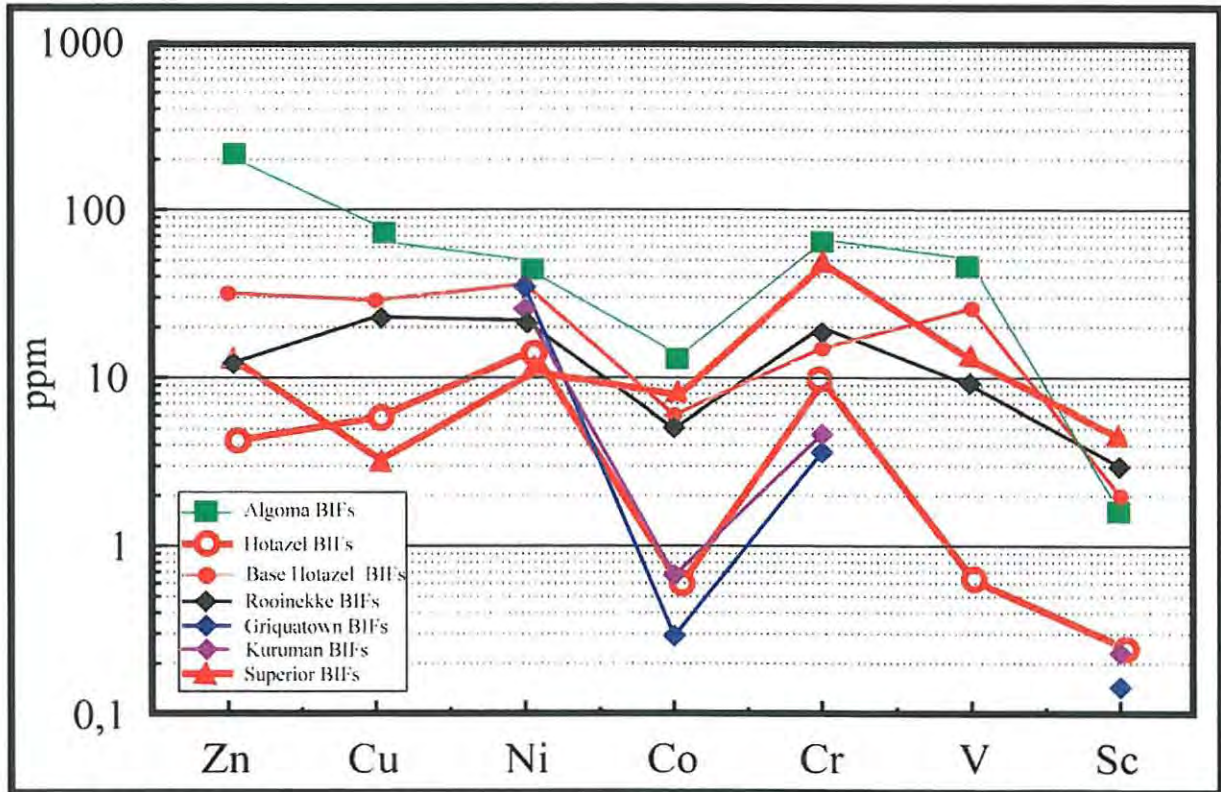
Figure IV.24. Plot of average transition metals values of Pristine Hotazel BIFs (Tsikos, 1999), Algoma- and Superior-types BIFs of Canada (Gross and McLeod, 1980), Kuruman and Griquatown BIFs (Klein and Beukes, 1989), Rooinekke, and base of the Hotazel BIFs (this study). Note the depleted transition-metal character of the BIFs of the Transvaal Supergroup, relative to volcanogenic Algoma-type BIFs.

The iron content in the Makganyene diamictite decreases upward in the stratigraphy, while the calcium content increases upward. This could be interpreted as representing increasing carbonate chemical sedimentation that was included in the diamictites. Such carbonate precipitation was observed as stromatolite bioherms in the topmost part of the Makganyene Formation in the southern portion of the Griqualand West Basin, south of the Griquatown Hinge Zone.

The Hotazel diamictite is only recorded in the Hotazel area, which corresponds to the shallow platform facies of the Postmasburg Group. The extrusion of the basaltic andesitic lava of the Ongeluk Formation between the Makganyene and Hotazel Formations is responsible

for the compositional differences. The Hotazel diamictites have included in their groundmass some Ongeluk material and therefore display a basic volcanic component.

The carbon and oxygen stable isotope curves of the entire Transvaal Supergroup succession in the Griqualand West Basin display a symmetrical negative incursion centred on the Makganyene/Hotazel glacial diamictites. Such smooth curves are interpreted as representing the gradual shift from warm climatic conditions of the Campbellrand Subgroup, to progressively colder Asbestos Hills Subgroup, to glacial Makganyene/Hotazel diamictites, and finally back to warmer Voëlwater Subgroup paleoclimatic conditions in the Hotazel BIFs and Mooidraai carbonates. The $\delta^{13}C$ curve across the Hotazel Formation shows cyclicity as well as a general enrichment, which relates to the cyclicity between BIFs, Manganese ore and carbonates. In addition, the $\delta^{13}C$ depletion in the Makganyene Formation can be interpreted as a combination of processes such as the oxidation of organic carbon by iron as well as precipitation of carbonate minerals in a stratified and reduced glacial ocean.

CHAPTER V

Synthesis

V.1. Sequence stratigraphy

V.1.1. Introduction

The sequence stratigraphy approach represents the best method for basin analysis and correlation for Proterozoic rocks (Cheney, 1996) for different reasons:

➤ the absence of fossil remains,

➤ the application of seismic stratigraphy to Proterozoic sequences (Tinker et al., 2002) is still in its very early stages,

➤ the poor age constraints on the different formations.

Sequence stratigraphy models have been drawn up for the Early Proterozoic Transvaal Basin (Catuneanu and Eriksson, 1999), for the Lower Transvaal Supergroup in the Griqualand West Basin (Altermann and Nelson, 1998), for the McGrath Trough in Western Australia (Martin et al., 2000) and for the northern Fennoscandinavian Shield (Strand and Laajoki, 1999). This concept has been used to establish interbasinal correlations (Polteau, 2000; Moore et al., 2001) and intercratonic basin correlations (Winter, 1989; Cheney et al., 1990; Cheney and Winter, 1995; Cheney, 1996). The sequence stratigraphy concept deals with the genetic interpretation of vertical and lateral facies changes of a basin-fill that is determined by the balance between sediment supply and relative sea level changes (Catuneanu and Eriksson, 1999). The processes controlling the geometry of the stacked sequences need to be addressed before exploring the various models from Catuneanu and Eriksson (1999) and Nichols (1999).

The accumulation of sediments in a basin depends on the accommodation space, which is the space available for sediments to be deposited and preserved in a sedimentary basin. Accommodation space is created either by sea-level rise or subsidence of the seabed. The balance between the creation of accommodation space and sediment supply controls the stacking geometry of sequences and system tracks. Three types of stacking patterns exist: aggradation, progradation and retrogradation.

Aggradation corresponds to a perfect balance between sediment supply and creation of accommodation space, and is expressed by the vertical stacking of the facies belts (see figure V.1.A). This situation is usually short-lived (Nichols, 1999) because of changing rates of sea level rise and fall. Progradation refers to a greater sediment supply compared to the creation of accommodation space, and corresponds to a vertical and seaward migration of the facies

belts (see figure V.1.C). This is referred to as a regression. If the accommodation space is reduced due to a relative sea level fall (absolute sea level fall, or tectonic uplift of the sea bed), it is referred to as a forced regression characterised by erosion in the shallower environment causing typical downstepping geometry of the deposits (see figure V.1.D). Retrogradation reflects the creation of accommodation space that is greater than the supply of sediments, and is translated by a vertical and landward facies shift (see figure V.1.B).
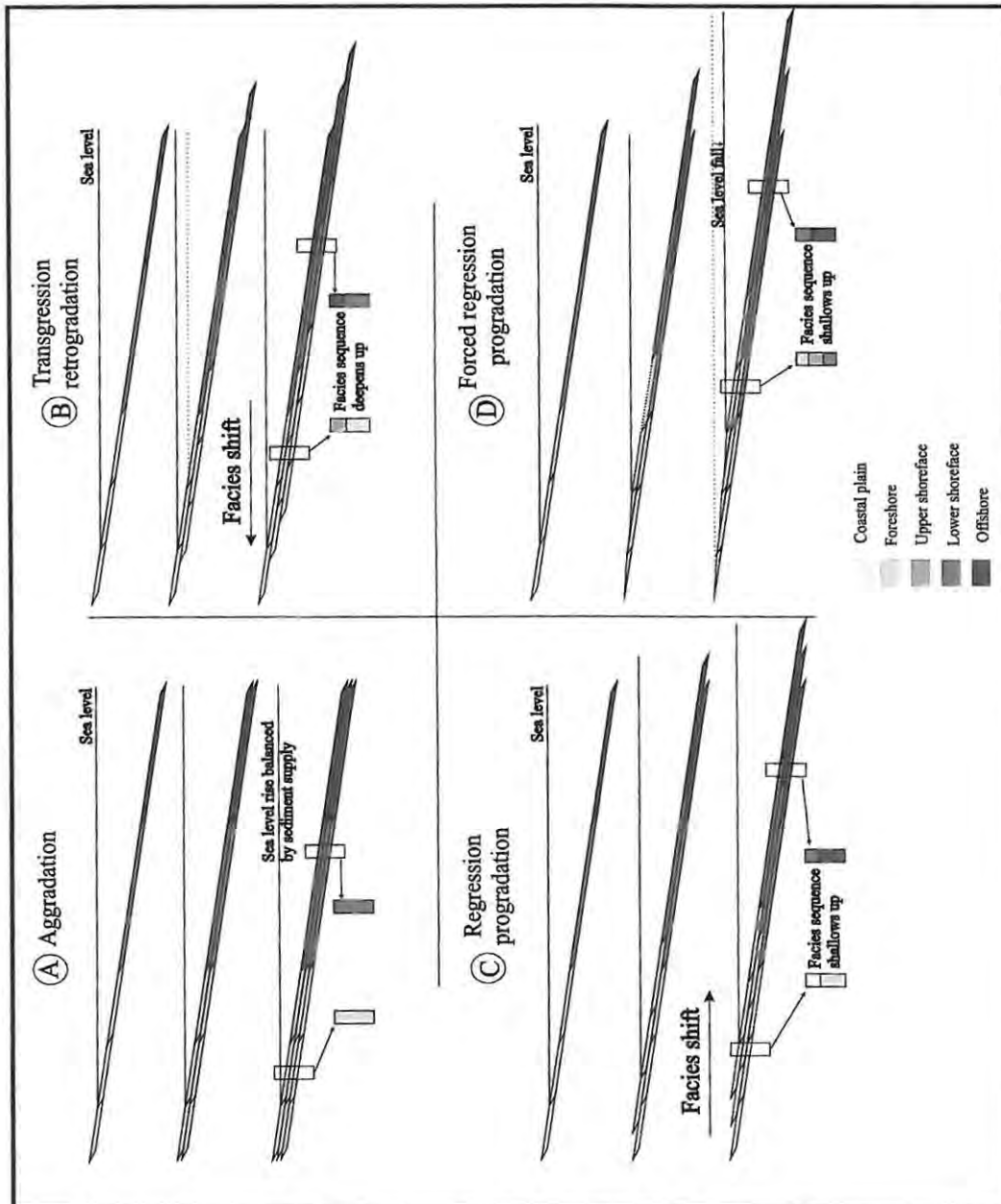
Figure V.1. A: aggradation, B: transgression or retrogradation, C: regression or progradation, D: forced regression or progradation (from Nichols, 1999).

Sediments normally accumulate during periods of relative sea level rise, but in response to sea level changes, they will display aggradation, progradation and retrogradation stacking patterns that characterise systems tracts. On the other hand, periods of relative sea level fall will create bounding surfaces separating systems tracts, and unconformities separating depositional sequences of systems tracts. The key in the sequence stratigraphy approach is in correctly identifying the bounding surfaces between the systems tracts. Different bounding surfaces have the acronyms SU, BSFR, RS, CTS and MFS.

➤ The SU or Subaerial Unconformity is an erosional surface created during relative sea level fall when the shelf was exposed to subaerial weathering. It has a marine correlative conformity (cc).

➤ The BSFR or Basal Surface of Forced Regression is an erosional surface created by wave action in the shallow portion of the basin, or a scour surface generated by gravity flows in the deeper portion of the basin.

➤ The RS or Ravinement Surface is an erosional surface created by wave-cut action during transgression.

➤ The CTS or Conformable Transgressive Surface is a conformable surface characteristic of a relative sea level rise exceeding sediment supply.

➤ The MFS or Maximum Flooding Surface is a conformable surface that is generated when sediment supply exceeds the rate of relative sea level rise.

These bounding surfaces, characteristic of relative sea level changes, delimit different types of systems tracts. The systems tracts that are commonly used in sequence stratigraphy have the acronyms HST, FSST, LST and TST.

➤ The HST or Highstand Systems tract is bound by a Maximum Flooding Surface at the base and by a Subaerial Unconformity and Basal Surface of Forced Regression at the top. It generally shows aggradation and progradation, characteristic of relative high sea level and reduction of accommodation space. A vertical profile through the Highstand Systems tract would show shallowing upward in the environment of deposition.

➤ The FSST or Falling Stage Systems tract is bound by a Maximum Flooding Surface at the base and by a Subaerial Unconformity and its marine correlative conformity (cc) at the top. The Falling Stage Systems tract develops during a relative sea-level fall that exposes the shelf to erosion, thus creating the Subaerial Unconformity. The sediments accumulate mostly on the slope and basin beyond the edge of the shelf, and consist of

a progradational succession of shallow marine deposits which are filling the available accommodation space. The Falling Stage Systems tract represents a forced regression.

> The LST or Lowstand Systems tract is bound by a Subaerial Unconformity and its correlative marine conformity at the base, and by a Conformable Transgressive Surface at the top. It forms during the early stages of relative sea-level fall when the sediment supply is exceeding the creation of accommodation space. The Lowstand Systems tract represents a normal regression, and contains the coarsest portion of both marine and nonmarine successions. A nonmarine Lowstand Systems tract forms the base of a fining-upward section, while a marine Lowstand Systems tract ends a coarsening-upward section.

> The TST or Transgressive Systems tract is bound by a marine Conformable Transgressive Surface and its nonmarine correlative at the base, and by a Maximum Flooding Surface at the top. The Transgressive Systems tract forms when the creation rate of accommodation space exceeds sediment supply, which is typical of a marine transgression or relative sea level rise. The sediments are retrograding and fining upward, representing a deepening of the depositional environment.

Different stratigraphic sequences are currently identified depending on the bounding surfaces chosen to delimit them. The depositional sequence is bound by an SU and its marine cc that are generated by relative sea-level changes. The depositional sequence is therefore composed of LST-TST-HST-FSST. On the other hand, the genetic stratigraphic sequence is bound by an MFS, which is controlled by the interaction between sediment supply and the creation of accommodation space, or transgression-regression curves. The genetic stratigraphic sequence consists of the stacking of HST-FSST-LST-TST. In the marine Transvaal Supergroup of the Griqualand West Basin, unconformities are a contentious issue, and therefore the SU-bound genetic sequence is not the model to use. However, MFSs are easily identified within the different rock types characteristic of relative sea-level changes along the western edge of the Kaapvaal Craton. The Transvaal Supergroup in the Griqualand West Basin is assumed to have been deposited along a rimmed shelf or carbonate platform, because a 950-metres deep escarpment separated the platform from the deep marine environment during accumulation of the Ghaap Group (Altermann, 1997). Such morphology was preserved at least up to the base of the Postmasburg Group (Altermann, 1997).
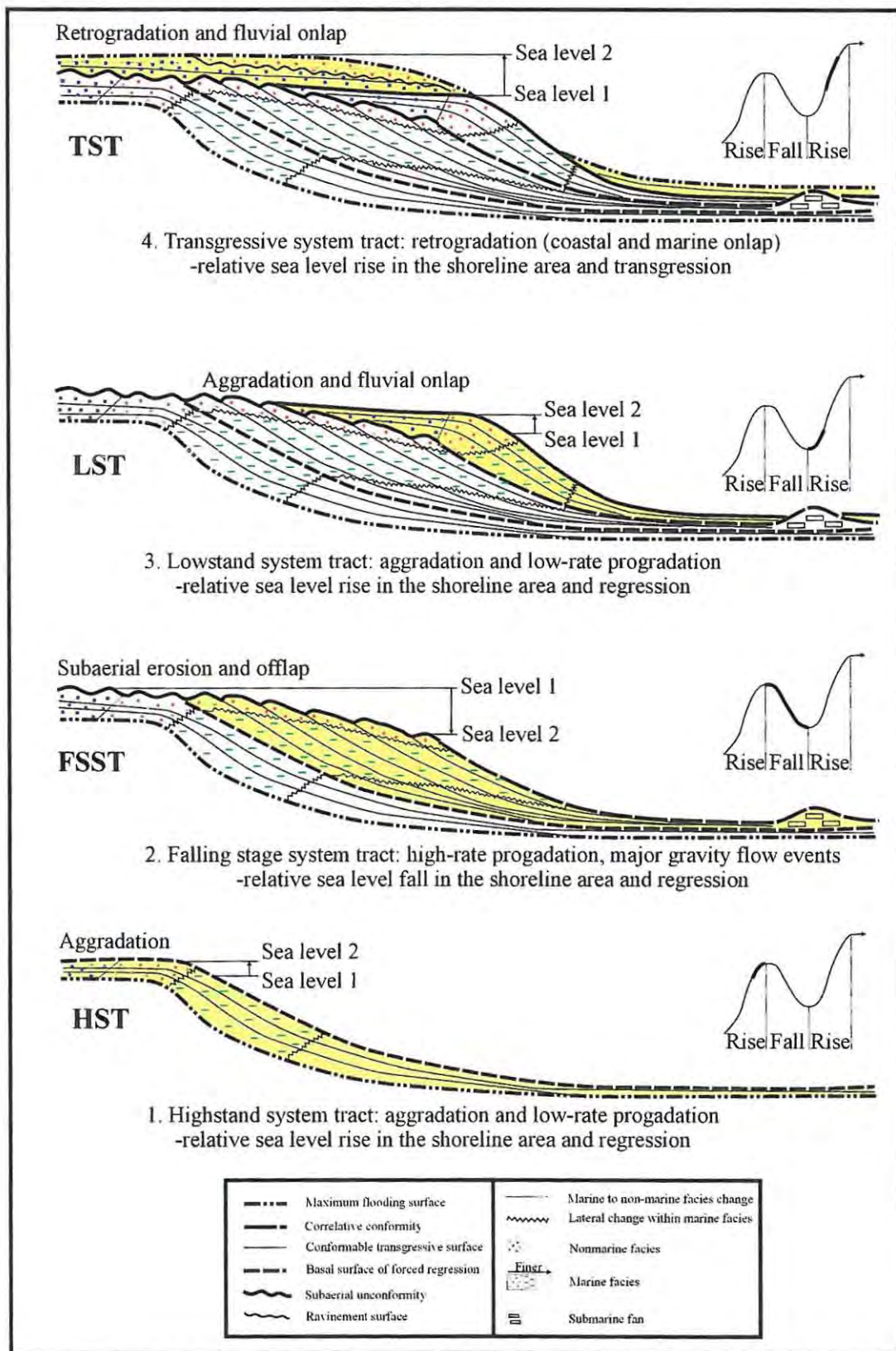
Figure V.2. Diagnostic stacking patterns for the HST, FSST, LST, and TST. The sinusoidal curves illustrate relative sea level changes, and the timing of each systems tracts relative to sea level curves. From Catuneanu and Eriksson (1999).

V.1.2. Identification of bound sequences

First-order sequences correspond with events that had a duration of ~50 Ma (Altermann and Nelson, 1998). The Ventersdorp Supergroup, the Ghaap Group (including the Koegas Subgroup) and the Postmasburg Group are considered by Altermann and Nelson (1998) to be first-order sequences. They can be subdivided into second-order sequences that correspond to events of the order of tens of millions of years in duration. The Schmidtsdrif Subgroup, the Campbellrand Subgroup, the Asbestos Hills Subgroup, the Koegas Subgroup, the Makganyene Formation and the Voëlwater Subgroup are second-order sequences.

The correlation of the Ghaap and Chuniespoort Group is widely accepted (Beukes, 1983; Clendenin et al., 1988; Cheney and Winter, 1995; Cheney, 1996; Altermann and Nelson, 1998; Martin et al., 1998; Eriksson et al., 1999; Nelson et al., 1999; Catuneanu and Eriksson, 1999; Eriksson et al., 2001; Moore et al., 2001; Tinker et al., 2002) and it is therefore assumed that both the Transvaal and Griqualand West Basins were contiguous during the development of the Ghaap and Chuniespoort carbonate platform. To establish a direct parallel between these two sub-basins, the stratigraphic names are grouped with their correlatives according to the rule Griqualand West/Transvaal basin (i.e. Vryburg/Black Reef) only when there is no contention.

Similar relative sea level changes should be recorded synchronously in the different portions of the Ghaap/Chuniespoort sedimentary pile if the sea bottom is horizontal. However, the western edge of the Kaapvaal Craton is rimmed, implying that a relative sea-level rise will be recorded first in the deep Prieska basin due to subsidence in the basin, and it will finally reach the shallow Ghaap platform when transgression progresses. This implies that the stratigraphic record would be more complete in the Prieska area than in the Ghaap and Transvaal areas.

The Schmidtsdrif Subgroup/Black Reef Formation is bound by two second-order SUs (Catuneanu and Eriksson, 1999; Eriksson et al., 2001). The upper SU implies that the Black Reef sea underwent total retreat and exposed the Kaapvaal Craton to erosion.

The onset of widespread carbonate accumulation is diachronous across the Kaapvaal Craton (Altermann, 1996, 1997; Altermann and Nelson, 1998). Supported by radiometric ages on volcanic tuff layers, Altermann (1996, 1997) and Altermann and Nelson (1998) deduced that drowning started in the Prieska area that was separated from the Ghaap platform by a 950-metres high escarpment resulting from active faulting in the Griquatown Fault Zone. As relative sea level was rising, the Naute shales were being deposited in the deep Prieska basin while carbonate precipitation started on the Ghaap platform and in the Transvaal Basin

(Altermann, 1997). According to Catuneanu and Eriksson (1999) and Eriksson et al. (2001), the base of the Chuniespoort Group in the Transvaal basin consists of a condensed section of black shales corresponding to a preserved TST with the MFS located at the base of the calcareous succession.

The second-order relative sea level curves for the rest of the Ghaap Group in the Prieska and Ghaap platform areas (Altermann and Nelson, 1998) match up with the interpreted second-order sequence stratigraphy of the Chuniespoort Group in the Transvaal Basin of Catuneanu and Eriksson (1999). The thick Ghaap/Chuniespoort carbonate deposition requires continuous creation of accommodation space, drowning of clastic sources and tectonic stability. All these characteristics are typical of an HST (Catuneanu and Eriksson, 1999; Eriksson et al., 2001). It is commonly believed that the overlying Asbestos Hills/Penge Iron Formations are deep-water deposits (Beukes and Klein, 1990; Altermann and Nelson, 1998), implying that a relative sea-level rise, which was probably induced by tectonic subsidence, occurred at the end of carbonate accumulation. The BIFs display a normal regression because they commonly shallow upward (Beukes, 1983). However, Catuneanu and Eriksson (1999) argue that if BIFs are deep-water deposits, the drowned carbonate platform should have developed a drowning unconformity onlapped by clastic facies. However, both the drowning unconformity and the clastic facies have not been observed, and the contact between the carbonates and the BIFs is transitional (Beukes and Klein, 1990; Beukes et al., 1990; Hälbich et al., 1992). This led Catuneanu and Eriksson (1999) to propose that the Asbestos Hill/Penge Iron Formations represent the final regressive stage of the HST (Highstand Systems tract), a point of view that is also supported by the shallowing-upward model of Klein and Beukes (1990). A small relative sea level rise is preferred for the deposition of the Asbestos Hills/Penge BIFs in this study because the easiest way of protecting the BIFs from detrital contamination is to drown the clastic source. Nevertheless, the grouping of the carbonate and BIF successions of Catuneanu and Eriksson (1999) as an HST is conserved because the BIFs shallow upward.

From the end of the Asbestos Hills/Penge Iron Formation deposition, interbasinal correlations are contested (Polteau, 2000; Moore et al., 2001) and therefore only the Griqualand West Basin sequence stratigraphy is considered. The different morphological characteristics of the Griqualand West Basin are shown in figure V.3. A relative sea level drop is inferred for the deposition of the Koegas Subgroup (Beukes, 1983). Lacustrine deposition occurred in depressions on the Ghaap platform at the transition Griquatown BIFs-Koegas Subgroup (Beukes, 1983), which was exposed to subaerial erosion and developed an

SU (Subaerial Unconformity). South of the Griquatown Hinge Zone, the Koegas Subgroup lies conformably on the Asbestos Hills BIFs, making this contact the BSFR (Basal Surface of Forced Regression). The Koegas Subgroup consists mainly of slope deposits with the Naragas representing a large submarine fan accumulation, and the Rooinekke Formation representing the clastic-contaminated equivalent of the Asbestos Hills BIFs. The Koegas Subgroup is characteristic of a FSST (Falling Stage Systems tract) that is bound at its top by the marine correlative conformity (cc) of the SU (Subaerial Unconformity). The whole Koegas Subgroup deposition represents the time gap between the end of the Asbestos Hills BIFs deposition and the Makganyene glacial accumulation.
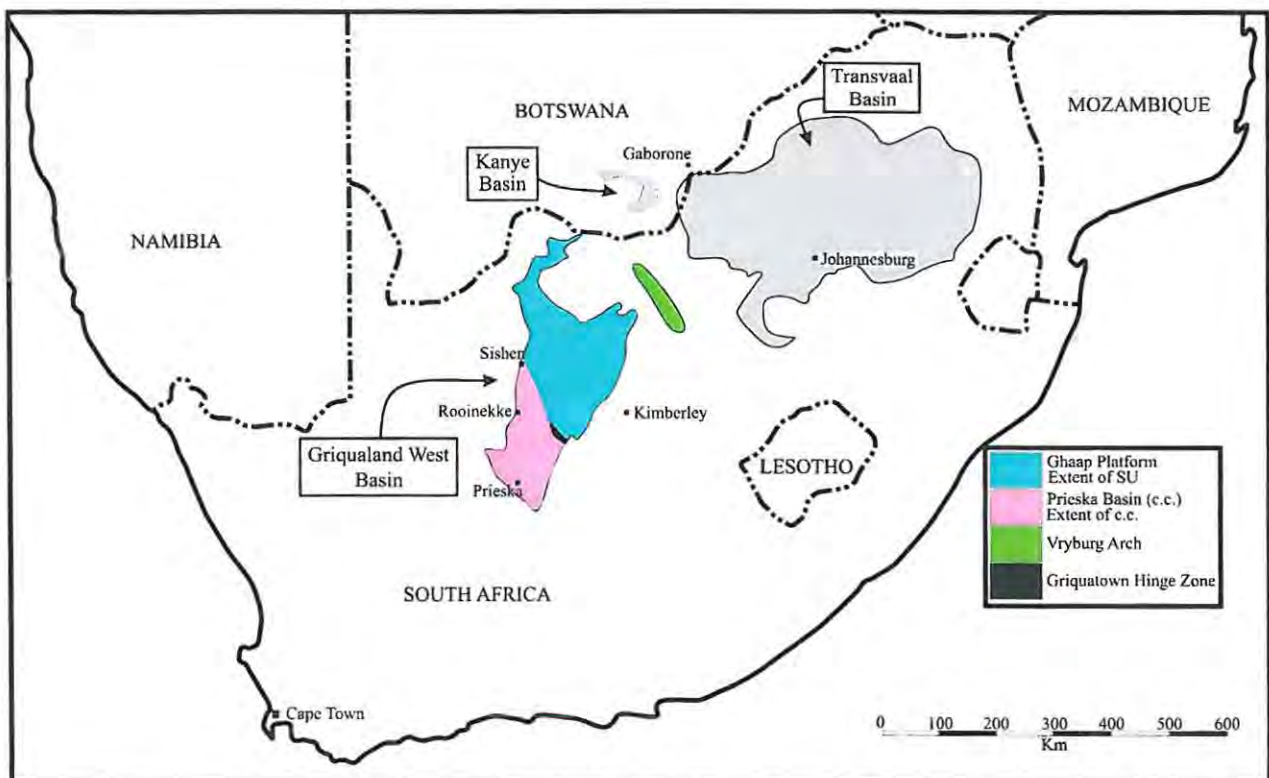
Figure V.3. Extent of SU and cc developed during the Koegas Subgroup deposition, and morphological features of the Griquatown West Basin (modified after Moore et al., 2001).

It is generally understood that any glacial event triggers a major eustatic sea-level drop that causes regional unconformities. In chapter II, the occurrence of a diamictite lens below the base of the Naragas Formation has been described, implying that the Makganyene glacial event was initiated at the start of the Koegas times, but apparently extensive ice sheets did not develop. The Makganyene Formation represents the coarsest part of the Transvaal Supergroup

depositional sequence. North of the Griquatown Hinge Zone, the Makganyene Formation rests on the Asbestos Hills BIFs along an SU that was created during the Koegas Subgroup deposition. At the Hinge Zone, the pinch-out area of the Koegas Subgroup, the Makganyene diamictites lie also on top of the Rooinekke Formation along the cc (correlative conformity) of the SU. As shown in figure V.3, the marine cc extends deeper in the basin, that is south of the Griquatown Hinge Zone. The Makganyene Formation corresponds to a typical LST that has a CTS (Conformable Transgressive Surface) as its top contact.

The Ongeluk andesitic lava conformably overlies the Makganyene Formation. This eruptive volcanic formation is assumed to have been a short-lived and accidental event that had very little influence on the sedimentary patterns of the younger Voëlwater Subgroup (Tsikos and Moore, 1997; Tsikos, 1999; Polteau, 2000; Moore et al., 2001). However, the Ongeluk Formation has obscured the stratigraphic relationship between the Makganyene Formation and the Voëlwater Subgroup. The Voëlwater bottom contact should be represented by a CTS, which is not seen, as it would correspond to a time line within the Ongeluk lava. The Voëlwater Subgroup consists of BIFs of the Hotazel Formation overlain conformably by the Mooidraai carbonates. This succession is the mirror image of the HST of the lower Transvaal Supergroup mentioned above. The Voëlwater Subgroup marks a relative sea level rise or transgression that drowned the clastic source of the Makganyene Formation. The Hotazel Formation contains three manganese beds that were deposited in the shallow portion of the Griqualand West Basin (Tsikos, 1999). The overlying Mooidraai carbonates reflect an upward-shallowing sequence (Tsikos, 1999). The Voëlwater Subgroup has the characteristics of a TST that preferentially accumulates on the platform and in the deep basin, with no noticeable accumulation on the slope. Its top contact, the MFS (Maximum Flooding Surface), has been removed by post-Transvaal erosional events.

As already suggested by Tsikos (1997, 1999), Polteau (2000) and Moore et al. (2001), the combination of field-work observations and detailed sequence stratigraphy analysis shows that the Transvaal Supergroup in the Griqualand West Basin corresponds to a single depositional event that corresponds to a genetic stratigraphic sequence bound by MFSs. Such a depositional cycle, illustrated in figure V.2, is incorporated in the depositional model of the Transvaal Supergroup in figure V.6 (section V.3.2):

-1- HST corresponds to the Ghaap/Chuniespoort and Asbestos Hills/Penge Subgroups.

-2- FSST represents the deposition of the Koegas Subgroup.

-3- LST is characteristic of the Makganyene Formation.

-4- TST is typical of the Voëlwater Subgroup.

V.1.3. Correlations

V.1.3.1. Introduction

Rock type inter-relationships and lithostratigraphy provide essential information on the relative timing of events that occurred during the Earth's history. The process of correlating rock formations relies on a combination of information from a number of different sources and techniques (Nichols, 1999).

The lithological attributes of rock units are used to assess similarities and differences between geographically separated exposures and to determine whether or not they belong to the same formation. The remarkably similar lithological associations between the Archean to mid-Proterozoic stratigraphic record of the Griqualand West, Kanye and Transvaal basins of the Kaapvaal Craton and the Hamersley Basin of the Pilbara Craton in Australia have led many workers to propose the contiguity of the different basins within a supercontinent (Winter, 1989; Cheney et al., 1990; Cheney and Winter, 1995; Cheney, 1996). However, because rock units are defined according to their lithological characteristics, lithostratigraphic correlations may be diachronous (Nichols, 1999).

Sequence stratigraphic concepts can be used to establish a chronostratigraphy because the different bounding surfaces always separate older underlying from younger overlying strata (Nichols, 1999). Sequence boundaries are caused by relative sea-level changes that can be correlated across adjacent basins (Winter, 1989; Cheney et al., 1990; Cheney and Winter, 1995; Cheney, 1996). It has been proposed that sequence boundaries in a succession can be related to global sea level curves (Nichols, 1999). This is true, of course, if there are no other causes of relative sea-level changes.

Radiometric dating provides a more absolute way of correlating sequences. Rb/Sr and Pb/Pb whole-rock, and U/Pb zircon techniques are the three radiochronologic methods that have been used in the Transvaal Supergroup (Eriksson et al., 1993, 1995; Cornell et al., 1996; Sumner and Bowring, 1996; Romer and Bau, 1998; Martin et al., 1998; Moore et al., 2001; Pickard, 2003). However, correlations principally based on Rb/Sr and Pb/Pb whole rock analyses, such as on the Ongeluk and Hekpoort Formations (Cornell et al., 1996; Romer and Bau, 1998), are contested because subsequent metamorphic/metasomatic processes have possibly significantly affected both ages (Moore et al., 2001). Tinker et al. (2002) compiled geochronological data for the Griqualand West and Transvaal Basins, which is included in table V.2 (after Polteau, 2000; Moore et al., 2001). Nelson et al. (1999) discredited the Pilbara and Kaapvaal connection because the Kaapvaal Craton does not contain similar volcanic formations to the Pilbara Craton. Based on the SHRIMP U-Pb zircon dating technique,

Pickard (2003) showed that both cratons have synchronous volcanic events, suggesting contiguity of the Transvaal/Griqualand West and Hamersley basins or global magmatic events during the deposition of the Kuruman BIFs.

Paleomagnetism has also been used as a correlative tool. By measuring the paleomagnetic inclination of sediments, one can determine the inclination of the sample magnetism that is translated into paleolatitude positioning. Such studies have been used to assess the contiguity of cratons. For example, Wingate (1998) used the paleomagnetic method to discredit any possible connection between the Pilbara and Kaapvaal Cratons at 2.78 Ga.

One last correlation method used in Proterozoic successions is chemostratigraphy. Elemental and/or isotopic compositions are compared with their possible correlatives. Elemental compositions of clastic rocks may vary across a basin, and depend on the composition of the detrital source. However, carbon and oxygen isotopic compositions are thought to represent specific chemical conditions that were present at a particular time in the depositional environments. The isotopic values can vary across the basin, but globally they show similar secular variation patterns, and these variations can be correlated across the same basin, or different basins (Nichols, 1999).

In conclusion, valid correlations between equivalent sequences use a combination of the above-described methods. The aim is to isolate global events that can be identified in different basins across the world. Such worldwide events are eustatic sea-level changes that generate bounding surfaces, volcanism, glaciation, and extraterrestrial impacts producing widespread spherule layers. Different models have been proposed to correlate the Griqualand West Basin with the Transvaal Basin (Eriksson et al., 1993, 1995; Eriksson et Reczko, 1995; Cheney and Winter, 1995; Cheney, 1996; Martin et al., 1998) and so far none have been widely accepted (Polteau, 2000; Moore et al., 2001; Tinker et al., 2002). Therefore, intercratonic correlations are even more controversial.

V.1.3.2. Correlations within the Transvaal Supergroup

Correlations of the lower Transvaal Supergroup across the Kaapvaal Craton are widely recognised (Winter, 1989; Cheney et al., 1990; Cheney and Winter, 1995; Cheney, 1996; Altermann and Nelson, 1998; Eriksson et al., 2001; Moore et al., 2001; Tinker et al., 2002). The correlation of the Schmidtsdrif Subgroup with the Black Reef Formation (table V.1) is based on a similar unconformable basal contact with all underlying proto-basinal lithologies and Archean basement (Cheney and Winter, 1995; Eriksson et al., 1995; Cheney, 1996), and similar unconformable upper contact with the overlying Campbellrand/Malmani carbonates

(Catuneanu and Eriksson, 1999; Eriksson et al., 2001). Both consist of transgressive feldspathic quartz arenites (Beukes, 1986). The correlation of the Schmidtsdrif Subgroup and the Black Reef Formation is stratigraphically and lithologically well constrained.

The Campbellrand Subgroup in the Griqualand West Basin and its correlative, the Malmani Subgroup in the Transvaal Basin, comprise dolomites and subordinate limestones, and represent a carbonate ramp model incorporating supratidal, intertidal, subtidal and shallow basinal facies (Beukes, 1983, 1986; Eriksson et al., 1995). The Campbellrand Subgroup has ages that range between 2555 ± 19 Ma at the base (SHRIMP U-Pb zircon, Altermann and Nelson, 1998) and 2521 ± 3 Ma at the top (U-Pb zircon, Sumner and Bowring, 1996). The Malmani Subgroup has similar ages bracketed between 2550 ± 3 Ma at the base (zircon Pb-evaporation, Walvaren and   Martini, 1995) and 2583 ± 5 Ma at the top (SHRIMP U-Pb zircon, Martin et al., 1998). Therefore the correlation of the Campbellrand Subgroup with the Malmani Subgroup is stratigraphically, lithologically and geochronologically well constrained (see table V.1).

The Campbellrand/Malmani Subgroups grade upward into BIFs of the Asbestos Hills Subgroup/Penge Iron Formation (Beukes and Klein, 1990; Eriksson et al., 1995). Both the Asbestos Hills Subgroup and Penge Iron Formation contain chemically precipitated BIFs overlain by clastic BIFs (Beukes, 1983; Cheney and Winter, 1995; Cheney, 1996). Furthermore, some Penge Iron Formation macrocycles (10-20 m thick) can be correlated with similar sections of the Kuruman Iron Formation of the Asbestos Hills Subgroup (Cheney and Winter, 1995; Cheney, 1996). The base of the Asbestos Hills Subgroup has an age of 2465 ± 5 Ma (SHRIMP U-Pb zircon, Pickard, 2003) and 2489 ± 33 Ma (SHRIMP U-Pb zircon, Trendall, unpublished and referenced in Nelson et al., 1999). One SHRIMP U-Pb zircon age of 2480 ± 6 Ma is available for the Penge Iron Formation (Trendall, unpublished reference in Nelson et al., 1999). The correlation of the Asbestos Hills Subgroup with the Penge Iron Formation is also stratigraphically, lithologically and geochronologically well constrained (see table V.1).

In the Transvaal Basin, the Penge Iron Formation is separated from the younger overlying Pretoria Group sediments by a prominent chert breccia and chert-dominated conglomerates developed on a paleokarst surface (Eriksson et al., 1993). The Penge Iron Formation is only preserved in the northern parts of the Transvaal Basin (Eriksson and Reczko, 1995). The Pretoria Group is elsewhere resting directly on the Malmani carbonates with an irregular karstic contact (Eriksson et al., 1993). The unconformity progressively

transgresses across the Chuniespoort Group from north (Potgietersrust) to south (Carolina) where, in places, the entire lower sequence has been eroded, a thickness of up to 3 km (Eriksson and Reczko, 1995; Moore et al., 2001).

In the Griqualand West Basin, two conflicting interpretations have been proposed (see table V.1). The first interpretation predominantly rests on similarities of two thick basaltic andesitic volcanic units occurring in both Pretoria and Postmasburg Groups. The eastern Hekpoort Formation of the Pretoria Group (2184 Ma, Rb-Sr isochron age, Cornell et al., 1996) and the western Ongeluk Formation of the Postmasburg Group (2222 Ma, Pb-Pb isochron age, Cornell et al., 1996) have similar ages. Beukes (1983) and many others consider the Hekpoort and the Ongeluk Formations as correlative.

The analogous unconformity in the Griqualand West Basin is characterised by the overlying glacial Makganyene Formation that rests on the BIFs of the Asbestos Hills and Koegas Subgroups (Beukes, 1983, 1986; Beukes and Smit, 1987). According to Beukes (1983), the unconformity progressively transgresses across the Ghaap Group from south (Prieska) to north (Griquatown and northwards) where the entire Koegas has been eroded, a thickness of up to 600 m.

The interpretation of the Makganyene Formation basal unconformity, together with the correlation of the Hekpoort/Ongeluk Formations, implies that the Pretoria and Postmasburg Groups are equivalents (Beukes, 1983). However such correlations are controversial due to alternative interpretations of the Ghaap-Postmasburg Group contact in the Griqualand West Basin, and differences in lithology and geochronology between the Postmasburg and Pretoria Groups (Polteau, 2000; Moore et al., 2001; Polteau and Moore, 2002).

In this study, it has been demonstrated that the unconformity at the base of the Makganyene Formation developed north of the Griquatown Hinge Zone during the Koegas Subgroup deposition. The Makganyene Formation rests on the Koegas Subgroup along a conformable contact. The disappearance of the Koegas Subgroup at the Griquatown Hinge Zone corresponds to a pinch-out related to basin-floor morphology. The unconformity in the Griqualand West Basin does not exhibit a prominent chert-breccia and is significantly different to the unconformity in the Transvaal Basin.

With its alternating shallow-marine and fluvial sediments and subordinate periglacial deposits, the Pretoria Group represents an intermediate stage between intracratonic rift and sag basin settings (Catuneanu and Eriksson, 1999) where lithological and thickness variations

are common. The stratigraphy is truncated by several disconformities, some underlain by paleosols (Button, 1986). On the other hand, the sheetlike Postmasburg Group, consisting of a basal glacial diamictite overlain by basaltic andesitic lavas, BIFs and manganese ore from the Hotazel Formation, and finally Fe-, Ca- and Mg-carbonates, is more comparable to the chemical Ghaap Group than the clastic Pretoria Group (Tsikos and Moore, 1997; Polteau, 2000; Moore et al., 2001). None of the fourteen volcano-clastic formations of the Pretoria Group can be directly correlated to any of the four clastic-volcanic-chemical formations of the Postmasburg Group.

The correlation of the Ongeluk Formation with the Hekpoort Formation is also questionable. The Ongeluk Formation in the Griqualand West Basin contains pillow lavas and hyaloclastites, indicative of subaquaeous conditions, and shows extensive alteration that has been ascribed to sea-floor processes (Cornell et al., 1996). The Hekpoort Formation in the Transvaal Basin consists of subaerial coarse and fine graded volcaniclastics and associated amygdaloidal lavas, also showing intense alteration/metamorphism, probably related to the Bushveld Complex intrusion (Oberholzer and Eriksson, 2000). In addition, Myers et al. (1987) have shown that 13 different basaltic andesite units that have erupted onto the Kaapvaal Craton between 3.0 and 2.1 Ga have a fundamentally uniform trace element pattern. These eruptions are associated with repeated melting of homogeneously metasomatised subcontinental lithosphere (Myers et al., 1987). This, together with significant degrees of subsequent alteration, makes identification of individual basaltic volcanic units in the Transvaal Supergroup difficult on geochemical grounds alone.

The ages obtained for both Ongeluk (2222 Ma, Pb-Pb isochron age, Cornell et al., 1996) and Hekpoort Formations (2184 Ma, Rb-Sr isochron age, Cornell et al., 1996) are thought to have been significantly influenced by later metamorphism/metasomatic processes (Cheney, 1996) that also affected lavas of the older Ventersdorp Supergroup (Moore et al., 2001). The latter have yielded 2150 Ma Rb-Sr whole rock, 2370 Ma Pb-Pb whole-rock and 2693 Ma U-Pb zircon ages (see Armstrong et al., 1991) (table V.2). Subsequent single-zircon dating of the Ventersdorp basaltic andesite indicated a 2714 Ma crystallisation age, with a significant population of authigenic zircons giving ages between 2370 and 1765 Ma (Armstrong et al., 1991). The recent age of 2.394 Ga for the Mooidraai carbonates (Pb/Pb whole-rock isochron from Bau et al., 1999) confirmed that the Ongeluk Formation should be closer to 2.4 Ga (Cheney, 1996). Therefore the Hekpoort and Ongeluk Formations cannot be correlated on the basis of available whole-rock model ages.
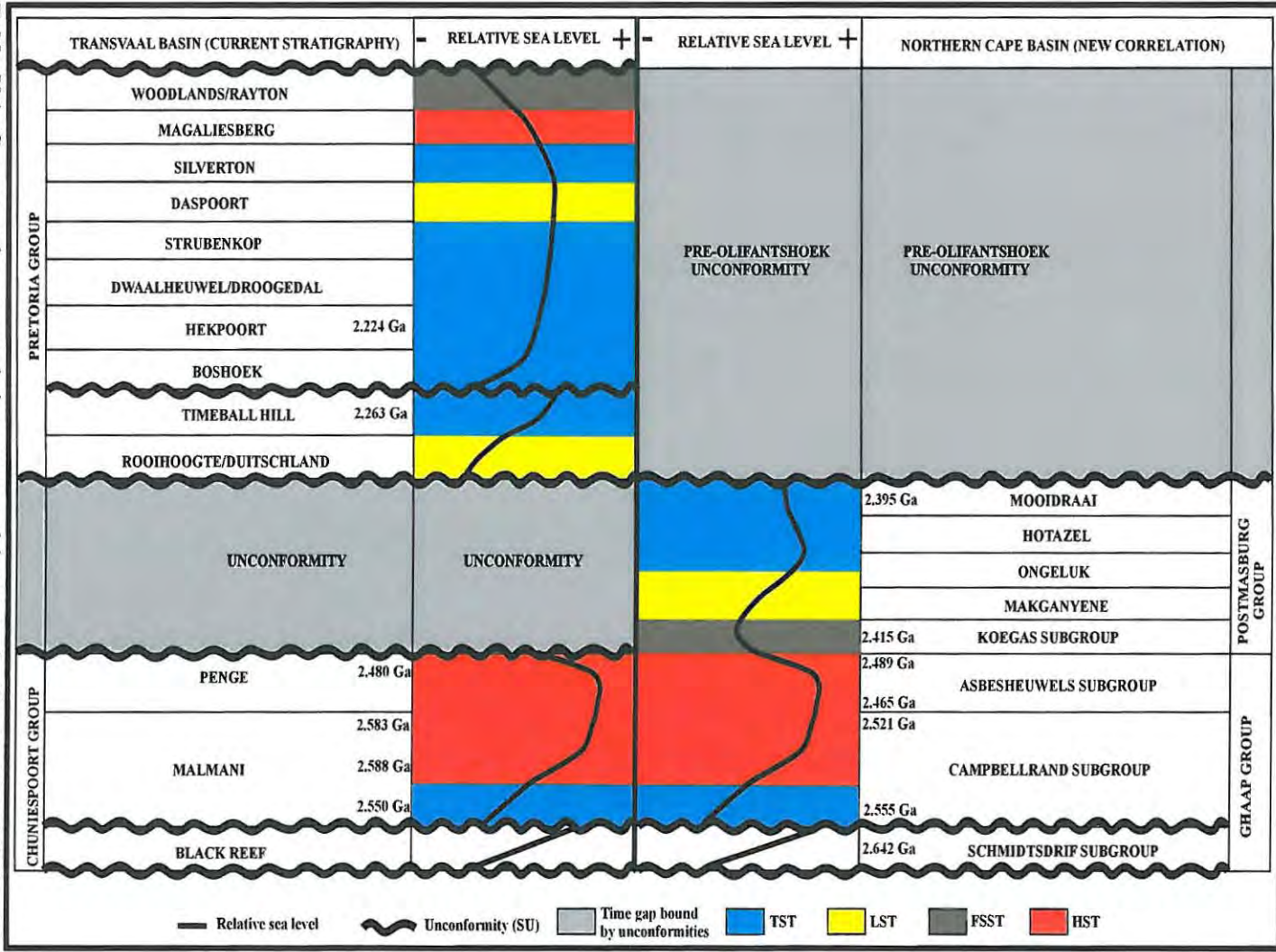
Table V.1. Current and new correlations proposed between the Transvaal and Griqualand West Basins (ages all cited in Tinker et al., 2002; and Kirschvink et al., 2000). The sea level curves from the Transvaal basin (Catuneanu and Eriksson, 1999) are different from the sea level curve from the Griqualand West Basin (Altermann and Nelson, 1998; and Catuneanu and Eriksson, 1999 for the Ghaap/Chuniespoort Group, the rest of the curve is from this study).

TRANSVAAL BASIN (CURRENT STRATIGRAPHY)	– RELATIVE SEA LEVEL +	– RELATIVE SEA LEVEL +	NORTHERN CAPE BASIN (NEW CORRELATION)
WOODLANDS/RAYTON			
MAGALIESBERG			
SILVERTON			
DASPOORT		PRE-OLIFANTSHOEK UNCONFORMITY	PRE-OLIFANTSHOEK UNCONFORMITY
STRUBENKOP			
DWAALHEUWEL/DROOGEDAL			
HEKPOORT 2.224 Ga			
BOSHOEK			
TIMEBALL HILL 2.263 Ga			
ROOIHOOGTE/DUITSCHLAND			
		2.395 Ga MOOIDRAAI	
		HOTAZEL	
UNCONFORMITY	UNCONFORMITY	ONGELUK	POSTMASBURG GROUP
		MAKGANYENE	
		2.415 Ga KOEGAS SUBGROUP	
PENGE 2.480 Ga		2.489 Ga ASBESHEUWELS SUBGROUP 2.465 Ga	
MALMANI 2.583 Ga 2.588 Ga 2.550 Ga		2.521 Ga CAMPBELLRAND SUBGROUP	GHAAP GROUP
BLACK REEF		2.555 Ga 2.642 Ga SCHMIDTSDRIF SUBGROUP	

Legend: — Relative sea level   ∿ Unconformity (SU)   ▨ Time gap bound by unconformities   🟦 TST   🟨 LST   ⬛ FSST   🟥 HST

PRETORIA GROUP — CHUNIESPOORT GROUP

	Rb/Sr (whole-rock)	Pb/Pb (whole-rock)	U-PB (zircon)
Hekpoort Formation	2224 ± 21		
	2184 ± 76	?	?
Ongeluk Formation	2023 ± 217	2236 ± 60	
		2222 ± 13	?
Ventersdorp Supergroup	c. 2150	2370 ± 70	2693 ± 60

Table V.2. Radiometric ages (Ma) for the Hekpoort and Ongeluk Formations and Ventersdorp Supergroup (from Moore et al., 2001; data from Armstrong et al., 1991; Cornell et al., 1996; and references therein).

Based on the Ongeluk-Hekpoort correlation, the lithological differences between the Pretoria and Postmasburg Groups have been attributed to the broad facies model of Button (1986) with a proximal north-eastern coarse-clastic environment (Pretoria Group) to a distal chemical setting in the south-west (Postmasburg Group). However, no change in the subaerial volcaniclastic nature of the Hekpoort volcanics or in the immediately overlying coarse clastic nature of sediments of the Pretoria Group have been observed in the extensions of the Transvaal Supergroup into southern Botswana (Key, 1983; Moore et al., 2001). Possible extensions of the Postmasburg Group into southern Botswana are obscured by younger Kalahari cover, whereas undoubted Pretoria Group sediments occur in the Kanye and Molopo areas (Crockett, 1972), preserved as an erosional remnant surrounding the syn-Bushveld Molopo Farm igneous complex (Gould et al., 1987). This continuity of the Pretoria Group clastic sediments into the Kanye Basin, places it in close juxtaposition with, if not superposition on, the Postmasburg Group (Moore et al., 2001), contradicting the proposed broad facies model (Winter, 1989; Cheney et al., 1990; Cheney and Winter, 1995; Cheney, 1996).

Relative sea level changes, as displayed in table V.1 are similar for the Ghaap and Chuniespoort Groups. If the Pretoria and Postmasburg Groups were synchronously deposited in the closely spaced Transvaal and Griqualand West Basins, relative sea level changes must be similar. As shown in table V.1, these curves are different, and therefore negate any Pretoria-Postmasburg correlation.

The basal contact of the Makganyene Formation is broadly conformable with the underlying Koegas Subgroup in the central and southern parts of the Griqualand West Basin. North of the Griquatown Hinge Zone, this basal contact becomes an unconformity created during the deposition of the Koegas Subgroup, and separating the Postmasburg Group from the Asbestos Hills Subgroup. No time gap is present between the deposition of the Ghaap/Chuniespoort and the Postmasburg Groups in these parts of the basin. The entire

Postmasburg Group correlates to the major unconformity that cuts the Penge Iron Formation in the Transvaal Basin. The Ghaap, Chuniespoort and Postmasburg Group should be included in a single Supergroup with an approximate age range 2.65-2.40 Ga. Therefore the Pretoria Group does not correlate to any formation of the Transvaal Supergroup in the Griqualand West Basin (Polteau, 2000; Moore et al., 2001) and should be considered for exclusion from the Transvaal Supergroup.

As pointed out by Polteau (2000) and Moore et al. (2001), the one-kilometer-thick Duitschland Formation (Martini, 1979; Taussig and Maiden, 1986) may be a lateral equivalent of the Postmasburg Group. Both share a similar succession, from basal diamictite overlain by basaltic andesites and post-glacial cap-carbonates on top (Bekker et al., 2001). This correlation may well be valid because the Duitschland Formation rests on the Penge BIFs upon an unconformity that may well be related to the subaerial unconformity (SU) and its correlative conformity (cc), the basal Makganyene contact. However there is still a debate as to whether the Duitschland Formation occurs within the Chuniespoort Group (Button, 1986; Eriksson et al., 1993) or the Pretoria Group (Martini, 1979). The general absence of Postmasburg Group equivalents in the Transvaal Basin may simply be related to the extensive pre-Pretoria erosion cycle (Moore et al., 2001).

The eastern Pretoria Group has recently been correlated with the Gamagara/Mapedi Formation of the Olifantshoek Supergroup in the Griqualand West Basin by using paleomagnetic techniques on paleosols (Evans et al., 2002). In this model, the Gamagara/Mapedi Formations and Drakenstein-Wolhaarkop paleosols are younger than 2.220 Ga (Evans et al., 2002). This is supported by strongly ^{13}C-enriched carbonates within the conformably overlying Lucknow Formation that probably correlates with a globally recognised period of such enrichment between 2.20 and 2.06 Ga (Karhu and Holland, 1996).

This study confirms that the correlation of the Pretoria Group with the Postmasburg Group is not valid, as already suggested by Polteau and Moore (1999, 2002), Polteau (2000) and Moore et al. (2001). The Postmasburg Group does not have any lateral equivalent in the Transvaal Basin (except maybe the Duitschland Formation), and the Pretoria Group may correlate with the post-Transvaal Supergroup Gamagara/Mapedi Formation of the Olifantshoek Supergroup in the Griqualand West Basin (Evans et al., 2002). Erosional processes removed the Postmasburg Group prior to the deposition of the Pretoria Group in the Transvaal Basin. These new correlations are presented in table V.1 that also displays relative sea level changes for comparisons.

V.1.3.3. Intercontinental correlations

The difficulty in determining stratigraphic equivalents of basins within the same craton makes intercontinental correlations especially challenging. The most commonly proposed intercontinental correlation at around 2.4 Ga is between the Hamersley Supergroup of the Pilbara Craton and the Transvaal Supergroup of the Kaapvaal Craton (Winter, 1989; Cheney et al., 1990; Cheney and Winter, 1995; Cheney, 1996) and between the Yilgarn and Superior Cratons of Western Australia and Canada, respectively (Nelson et al., 1999). Only correlations between the Kaapvaal and the Pilbara Cratons are considered here (table V.3).

Both cratons may have formed part of the Vaalbara Supercontinent (Winter, 1989; Cheney et al., 1990; Cheney and Winter, 1995; Cheney, 1996). The Kaapvaal and Pilbara Cratons display similar lithological associations, which consist of basal sandstones, overlain by carbonates, followed by BIFs and finally clastic rocks.

The base of the Transvaal Supergroup is characterised by the Schmidtsdrif Subgroup/Black Reef Formation/Vryburg Formation that are correlated with the Jeerinah Formation, upper part of the Fortescue Group on the Pilbara Craton, because they share similar lithology (arkosic sandstone and basaltic andesite), similar ages of <2687 ± 2 Ma, they rest unconformably on the pre-basinal basement, and they form the same unconformity-bounded sequence (Cheney, 1996).

Correlation of the Wittenoom Formation of the Hamersley Basin with the Campbellrand/Malmani Subgroups is based on lithological and geochronological similarities (Cheney, 1996). A carbonate platform is well developed on both Griqualand West and Hamersley Basins, and consists of intertidal and supratidal cherty and stromatolitic dolomite and deeper carbonaceous, pyritic, clastic carbonate with ankeritic BIFs (Beukes, 1983; Cheney, 1996). Pb-Pb whole-rock ages of 2561 ± 8 Ma have been directly measured on Wittenoom Formation carbonates (Trendall et al., 1998), and Pb-Pb whole-rock ages of 2551 ± 13 Ma and 2541 ± 18 Ma (Woodhead et al., 1998) were measured on microtectites in the upper part of the Wittenoom Formation. A Pb-Pb whole-rock age for the Campbellrand Subgroup of 2557 ± 49 Ma (Jahn et al., 1990) appears to be due to post-depositional alteration (Sumner and Bowring, 1996; see table V.2). SHRIMP U-Pb dates from the Campbellrand Subgroup of 2588 ± 6 Ma and 2549 ± 7 Ma for the middle and the upper part of the Nauga Formation, and 2516 ± 4 Ma for the upper Gamohaan Formation and 2555 ± 19 Ma for the upper Monteville Formation (Altermann and Nelson, 1998) may confirm the lithological correlation of the Campbellrand/Malmani carbonate platform of the Transvaal Supergroup with the Wittenoom Formation of the Hamersley Group.

Correlation of the Brockman Iron Formation in Australia with the Kuruman Iron Formation in South Africa is stratigraphically (Cheney, 1996) and geochronologically well constrained (Pickard, 2003). Trendall and Blockley (1970) described 17 macrocycles consisting of BIFs units alternating with shaly, stilpnomelane- and siderite-bearing units in the Brockman Iron Formation of the Hamersley Group. Beukes (1983) has recognised these 17 macrocycles in the Kuruman Iron Formation of the Asbestos Hills Subgroup. The interbedded stilpnomelane-rich tuffaceous mudrocks within the Kuruman and Brockman Formations show a similar mafic to felsic volcanic trend, similar ages (both about 2460 Ma, SHRIMP U-Pb zircon) and similar zircon-age spectra and Pb-loss history (Pickard, 2003).

The Turee Creek Group of Western Australia constitutes a clastic wedge derived from the south that was deposited in an east-southeast-trending foreland basin (Martin et al., 2000). The Turee Creek Group rests conformably on underlying BIFs, and contains the glacially derived Meteorite Bore Member (Trendall, 1976). The Meteorite Bore Member overlies marine siltstone and sandstone of the Kungarra Formation (Martin et al., 2000) in the same way that the glacial rocks of the Makganyene diamictite conformably, or rather transitionally overlie the Koegas Subgroup.

It should be emphasised that diamictites are present at the base of the Koegas Subgroup in its southern outcrops at Klooffontein, and this particular diamictite lens may have been derived from the south, because no continuation of such a lens has been observed further north towards the Ghaap plateau. According to Altermann (1996, 1997), a volcanic arc existed south of Prieska and supplied pelitic sediments south of the Griquatown Hinge Zone. As displayed in Nelson et al. (1999), the relative sea-level changes for the Pilbara and Kaapvaal Cratons are very similar from the carbonate through to the clastic (Koegas/Turee Creek) successions. Nelson et al. (1999) attributed these similarities to global events and not as evidence for contiguity of both cratons. The views of Nelson et al. (1999) are debatable, because the similar lithologies and timing of relative sea-level changes suggest that both cratons were close to each other in both space and time. Wingate (1998) suggested, on the basis of paleomagnetic data, that the Kaapvaal and Pilbara Cratons were not joined at 2.78 Ga. However, he did not reject the possibility that both formed part of a Vaalbara Supercontinent after that time (i.e. between 2.78 Ga and 2.3 Ga). Furthermore, Martin et al. (1998) proposed that flexural reactivation was responsible for the Turee Creek and Koegas Subgroup clastic style of deposition. The implication is not that both cratons were contiguous, but that they may have lain along the same ocean margin (Martin et al., 1998).

One way to test for contiguity would be to carry out provenance studies on the Turee Creek and Koegas rocks and compare their respective source rocks. If they shared identical origins, then the Kaapvaal and Pilbara Cratons were next to each other. Eriksson et al. (1999) suggested that a southern supercontinent, consisting of cratonic blocks from present-day Australia, Africa, India, South America and Antarctica, would explain these similarities. Alternatively, global mantle overturn triggered a superplume event, and as a result, sea level was globally controlled by mid-ocean ridge activity (Nelson, 1998). This would result in similar sea-level patterns on unrelated continental masses.

PILBARA CRATON, WESTERN AUSTRALIA		KAAPVAAL CRATON, SOUTH AFRICA		
KAZPUT FORMATION		2 395 Ga	MOOIDRAAI	POSTMASBURG GROUP
			HOTAZEL	
			ONGELUK	
METEORITE BORE MEMBER			MAKGANYENE	
KUNGARRA FORMATION		2 415 Ga	KOEGAS SUBGROUP	GHAAP GROUP
BROCKMAN IRON FORMATION	2 470 Ga	2 489 Ga	ASBESHEUWELS SUBGROUP /	
		2 465 Ga	PENGE FORMATION	
WITTENOOM FORMATION	2 541 Ga	2 521 Ga	CAMPBELLRAND SUBGROUP /	
	2 561 Ga	2 550 Ga	MALMANI SUBGROUP	
JEERINAH FORMATION	2 682 Ga	2 642 Ga	SCHMIDTSDRIF SUBGROUP	

FC FORTESCUE GROUP   Unconformity

Table V.3. Possible correlations of the Pilbara Craton with the Kaapvaal Craton. Correlation of the Kazput Formation with the Voëlwater Subgroup is uncertain. Ages from Eriksson et al. (1999), Martin et al. (2000), Cornell et al. (1996).

V.2. The Paleoproterozoic Earth

V.2.1. Introduction

Classic sedimentary models are almost entirely based on Phanerozoic occurrences and modern-day processes and products (Eriksson et al., 1998). Application of such models (e.g. sequence stratigraphy, see paragraph V.2.) to Precambrian and increasingly older clastic sequences may be inaccurate due to significantly different environmental conditions. To propose a convincing depositional model for the Makganyene Formation, as well as the Transvaal Supergroup, a review of the different sedimentary environments of the

Paleoproterozoic Earth and of the controlling factors of the Precambrian atmosphere, oceans, plate tectonics and climate will be presented using geological evidence. This will assist in creating an awareness of the unique features of Proterozoic (bio)chemical and clastic rocks, but also demonstrating the variety of interdependent processes that controlled Precambrian basin evolution. A depositional model for the Makganyene Formation together with the Transvaal Supergroup follows this review.

V.2.2. Paleoproterozoic atmosphere

The composition of the Proterozoic atmosphere can be deduced from theoretical constraints and from geological evidence. The main theoretical constraint is the 'faint young Sun paradox'. Almost all models predict, as we go back in time, a decrease in solar luminosity in the order of 25% of the value of today (Newman and Rood, 1977; Kasting, 1987), with a value of 18% for 2.5 Ga (Kasting, 1987). If the composition of the atmosphere has not changed significantly over time, this decrease in solar luminosity would create an entirely frozen Earth, which would require higher luminosity values than present to thaw the ice (Newman and Rood, 1977; Kasting, 1987). However, the presence of liquid water on the surface of the Earth has been deduced from occurrences of sedimentary deposits dating as far back as 3.8 Ga. The solar luminosity values for the Precambrian are believed to be accurate estimates, leading to a conflict with the temperature history of the Earth. A solution is to consider an atmosphere with a different composition than today, where greenhouse gas concentrations would be sufficient to maintain the Earth's temperatures above freezing.

The main greenhouse gases were CO_2, with required concentration of at least a 100 times present concentration (360 ppm) or P_{CO_2} of $10^{-3.44}$ atm (Kasting, 1987; Rye et al., 1995) for cloud-free cover, and CH_4 (Kennedy et al., 2001; Cowen, 2002). Rye et al. (1995) suggest that due to radiative feedback processes, only 5 times the present value of CO_2 is needed with added cloud cover to increase the temperature by 6°C. Methane is a very potent greenhouse gas that is sixty times more powerful than CO_2, mole per mole (Cairns, 2001). CH_4 would be a better candidate, because it is not affected by ultraviolet radiation in an O_2-free atmosphere (Rye et al., 1995), and would have contributed with CO_2 to maintaining the surface temperatures of the early Earth above freezing. Formation of methane was the main cause in the sink of atmospheric oxygen (Kirschvink, 2002). Cloud cover introduced another greenhouse gas, i.e. water in the vapour state. NH_3 is another greenhouse gas that might have had an influence on surface temperatures. However, NH_3 was not significant because it is

sensitive to ultraviolet radiation, and maintaining a constant partial pressure is difficult (Rye et al., 1995).

According to Eriksson et al. (1998), chemical weathering was greater in the Archean, supporting arguments for higher concentrations of CO_2 in the atmosphere. Such aggressive weathering of the emerged continental mass led to a decrease in CO_2 in the atmosphere, and transport of CO_2 and other dissolved nutrients to coastal waters. Another sink mechanism for atmospheric CO_2 was microbial photosynthetic activity, which caused the accumulation of extensive platform carbonates, such as the Chuniespoort/Ghaap Group from the Transvaal Supergroup (South Africa) and the Hamersley Group in Australia (Des Marais, 1994; Holland, 2002). The CO_2 content of the atmosphere was dependant on a supply from volcanic degassing and subduction (Eriksson et al., 1998; Holland, 2002). This balance between atmospheric CO_2 supply and removal could have controlled climatic conditions (Eriksson et al., 1998).

The rate of burial of organic carbon controlled the O_2 content of the atmosphere (Des Marais et al., 1992; Derry et al., 1992; Karhu and Holland, 1996; Holland 2002; Lasaga and Ohmoto, 2002). During photosynthetic reaction, one mole of organic carbon buried represents one mole of O_2 that still exists or has reacted with some oxidisable substance. However, Holland (2002) demonstrated that the atmospheric oxigen rise was due to a gradual increase in of oxidation state of volcanic gases and hydrothermal inputs. According to Kasting (1991), the growth of the atmospheric oxygen occurred in three stages (figure V.4):

1) a reducing stage where no free oxygen was present in the atmosphere or in the ocean,

2) an oxidising stage where free oxygen was located in the atmosphere and at the surface of the ocean,

3) an aerobic stage where free oxygen was also present in the deep ocean.

During the reducing stage, photosynthetic micro-organisms were producing organic carbon and oxygen. The main sink of O_2 was Fe^{2+}, and this is expressed as the accumulation of BIFs in the Archean greenstone-belt successions. The second oxidising stage is characterised by the deposition of major Early Proterozoic BIFs, and increased amounts of clastic red beds. The last stage is characterised essentially by the cessation of BIF deposition.

The transition between the oxidising and aerobic stages has an approximate age of 1.7 Ga. Kasting's model does not explain the occurrence of Neoproterozoic BIFs as due to a rise in atmospheric O_2, but as related to global glacial events.

This model is therefore still debated and some authors favour the existence of an oxidising atmosphere since the Archean (Clemmey and Badham, 1982). The timing of these

three stages is also debated (Holland, 2002; Lasaga and Ohmoto, 2002). The transition between the reducing and oxidising stage is characterised by a significant decrease of detrital uraninite and pyrite, and by an increase in occurrence of red beds (Kasting, 1987). It has an approximate age of 2.4 Ga, but could be as young as 2 Ga (Kasting, 1991). However Des Marais et al. (1992), Derry et al. (1992) and Des Marais (1994) argue that the atmospheric oxygen level increased in a stepwise fashion, with peaks at approximately 2.0 and 0.6 Ga, corresponding to peaks in organic carbon burial. Coincidentally, these two peaks correspond to major worldwide deposition of BIFs, as well as extensive sedimentary glacial deposition and the break-up of supercontinents.
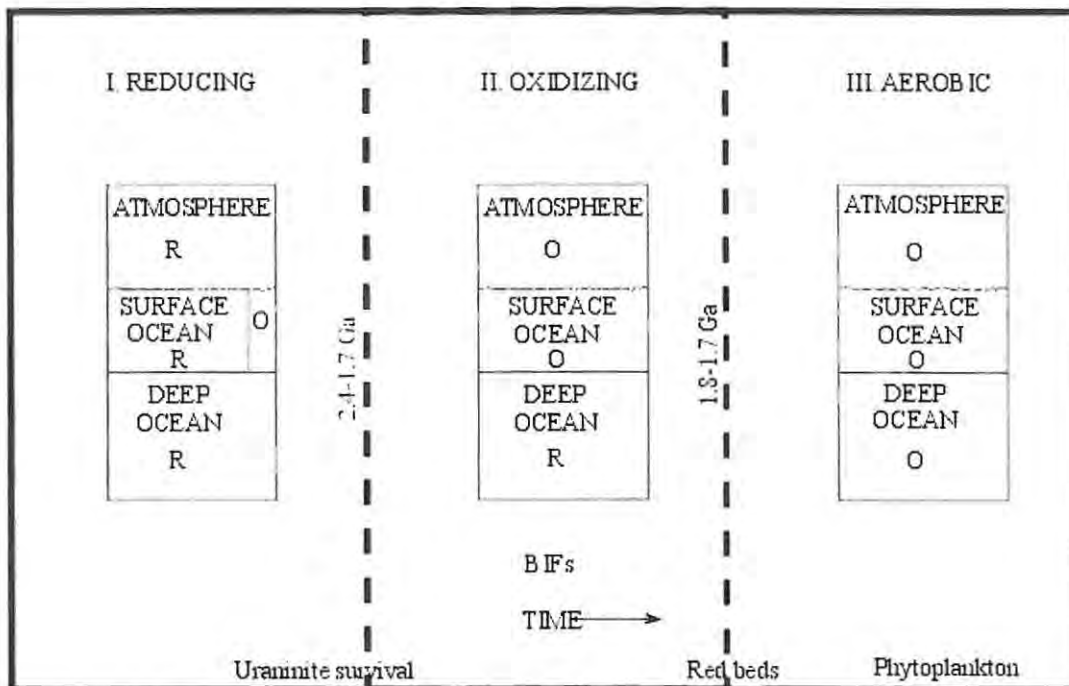
Figure V.4. Three-stage box model for the evolution of atmospheric oxygen. O indicates the presence of free oxygen; R indicates reducing conditions. The O in Stage I represents a localised "oxygen oasis" in an otherwise anoxic surface ocean. The ages between the stages are indicated along the boundaries, and at the bottom are shown the rock types defining each stage (Modified from Kasting, 1987, 1991).

Regarding the Early Proterozoic period, most authors argue for a significant rise in atmospheric O_2 between 2.2 and 2.0 Ga (Knoll et al., 1986; Holland et al., 1986; Kasting, 1987, 1991; Kasting et al., 1992; Des Marais et al., 1992; Derry et al., 1992; Des Marais, 1994; Karhu and Holland, 1996; Eriksson et al., 1998; Bau et al., 1999; Beaumont and Robert, 1999). However, there is mounting geochronological evidence which suggests that such a rise

occurred at about 2.4 Ga, specifically for the North China and Kaapvaal cratons (Yanjing and Yongchao, 1997; Bau et al., 1999; Holland, 2002).

V.2.3. Paleoproterozoic ocean

The atmosphere and ocean represent the most important chemical reservoirs during the Proterozoic, and therefore the evolution of one is linked to the evolution of the other. A widely accepted theory on the formation of the ocean is that it originated from the condensation of atmospheric water early in the Earth's history (Eriksson et al., 1998). This early ocean might have been more acidic due to higher partial pressures of CO_2 and other acidic components such as H_2S and HCl, resulting in a pH < 7 (Eriksson et al., 1998). This situation, however, was probably short-lived because large amounts of Na, Ca and Fe would have been introduced into the system by recycling through ocean ridges. The pH of the oceans during Makganyene times was probably similar to the modern value of 8.1 (Grotzinger and Kasting, 1993). Although a few early workers maintain that the chemistry of ocean water has been highly conservative over time (Holland, 1972), differences still exist between present day and Proterozoic chemical deposits (more precisely those around 2.4 to 2 Ga).

The Proterozoic hydrothermal supply of iron to the ocean was greater than the modern values (4.0-12.1 x 10^6 t.a^{-1}) (Bühn and Stanistreet, 1997), and evidence exists to support a hydrothermal source for iron in BIFs (Young, 1976; Klein and Beukes, 1989, 1993; Kimberley, 1989; Bühn and Stanistreet, 1997; Glasby, 1997), although Holland (1984) opposes this idea because he estimates that this source would have been too small. Beukes and Klein (1990) and others have provided detailed studies on BIFs that have REE patterns characteristic of a hydrothermal origin that could be far removed from the deposition site. REE patterns of the Hotazel BIFs, however, have a similar pattern to modern sea-water, indicating that the REE (and potentially Fe and Si) from the Hotazel BIFs were intrinsic constituents of the ambient water (Tsikos and Moore, 1997). According to Glasby (1997), thermodynamic calculations also suggest that the solution responsible for the deposition of the Precambrian BIFs must have been much richer in iron than was likely for Proterozoic seawater and a hydrothermal source would satisfy this requirement. The silica concentration in the Proterozoic ocean was not limited by biological uptake as at present, and could have had two origins: hydrothermal or intense Proterozoic chemical weathering of silicate rocks (Glasby, 1997).

According to Kasting (1987, 1991) and Kasting et al. (1992), the oceans followed the trend of Proterozoic atmospheric oxidation, but with a slight delay. Only the shallow surface

zone of the ocean was initially oxidising once the atmosphere became oxidised, while the deep ocean remained anaerobic. The progressive (Kasting, 1987, 1991; Kasting et al., 1992; Holland, 2002) or stepwise oxidation (Des Marais et al., 1992) of the atmosphere induced similar oxidation processes in the oceans. According to Walker and Brimblecombe (1985), Proterozoic deep anaerobic ocean water was rich in iron supplied by hydrothermal vents (Young, 1976; Klein and Beukes, 1989, 1993; Kimberley, 1989; Bühn and Stanistreet, 1997; Glasby, 1997) because of the deficiency in oxygen (Knoll et al., 1986; Holland et al., 1986; Kasting, 1987, 1991; Kasting et al., 1992; Des Marais et al., 1992; Derry et al., 1992; Des Marais, 1994; Karhu and Holland, 1996; Eriksson et al., 1998; Bau et al., 1999; Beaumont and Robert, 1999) and sulphides in the ocean (Cameron, 1982; Walker and Brimblecombe, 1985; Klein and Beukes, 1989; Grotzinger and Kasting, 1993; Holland, 2002). From such water, insoluble iron oxides and iron sulphides precipitated prior to about 2 Ga.
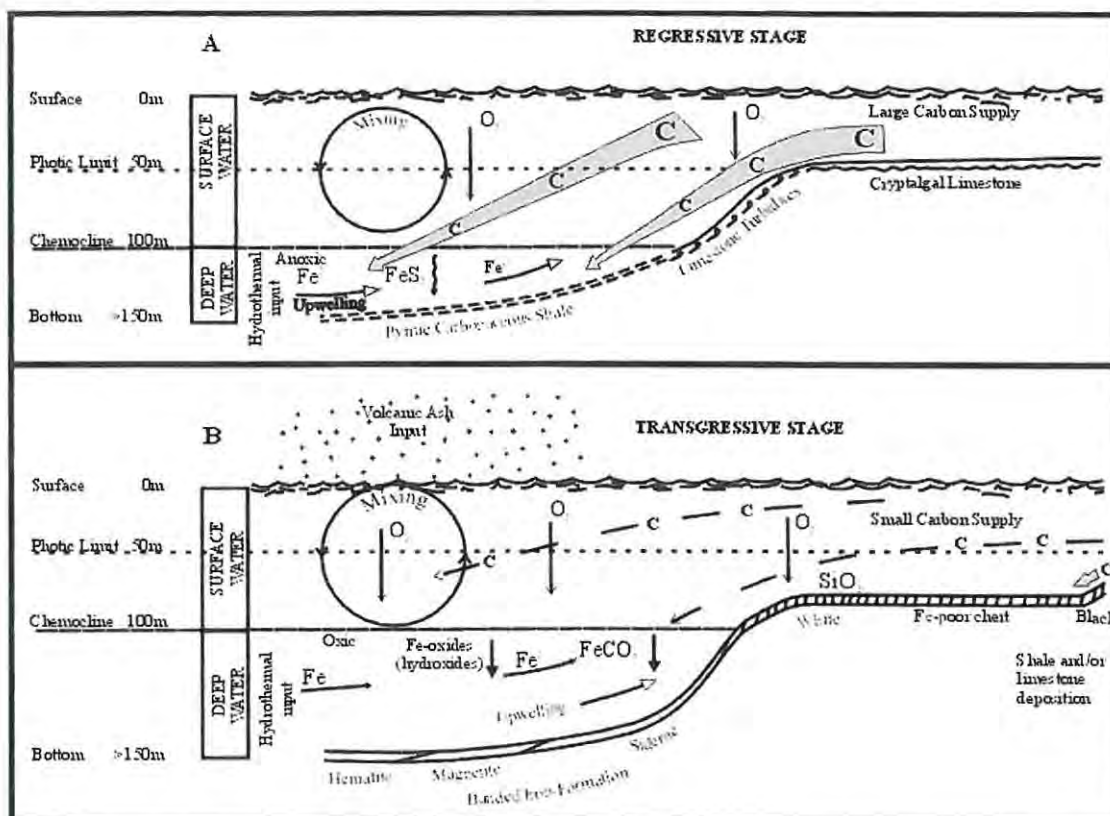
Figure V.5. Schematic depositional environment for BIFs and associated lithofacies in a marine system with a stratified water column in (**A**) regressive stage and (**B**) transgressive stage. The thick arrows labelled C (carbon) in (A) represent high carbon productivity and supply, and the narrow arrows in (B) represent much less carbon productivity and supply (from Klein and Beukes, 1989).

The oxidising surface water and deeper anaerobic water defined a stratified water mass separated by a chemocline (figure V.5). This oceanic chemical stratification is the main argument for the deposition of BIFs (Beukes 1980, 1983, 1984, 1986; Beukes and Klein, 1990; Beukes et al., 1990; Klein and Beukes, 1989, 1992, 1993) that took place when deep iron-rich anaerobic water was upwelled into the oxidising shallow-platform environment.

In a stratified ocean model (Klein and Beukes, 1989), sea-level controls the association of facies. During a regressive stage (figure V.5.A), the photic zone reaches the floor of the deep shelf where cryptalgal laminated limestones accumulate. In deeper parts of the basin, pyritic carbonaceous shale deposition is favoured by a large supply of organic carbon. During a transgressive stage (figure V.5.B), the photic zone is considerably above the floor of the deep shelf where various BIFs facies and chert accumulate.

Another difference in the composition of Proterozoic ocean water is related to the order of precipitation of minerals in marine evaporite sequences (Grotzinger and Kasting, 1993). During the evaporation of modern-day seawater, the precipitation of small amounts of carbonate with/without dolomite is followed by the precipitation of large quantities of anhydrite with/without gypsum, and the halite starts to precipitate when about 90% of the initial amount of water has evaporated (Holland et al., 1986). By contrast, in the Proterozoic, halite is present in evaporite successions whereas gypsum is absent, such as in the Late Archean of the Fortescue Basin, Western Australia (2.7 Ga), the Rocknest Formation (1.9 Ga) of Western Canada and the Perthei Group (1.88 Ga) in the East Great Slave Lake, Canada (Grotzinger and Kasting, 1993). This difference between modern-day and Proterozoic occurrences of gypsum might be explained by a very low concentration of sulphur in the ocean (Cameron, 1982; Walker and Brimblecombe, 1985; Klein and Beukes, 1989; Grotzinger and Kasting, 1993). Another possibility for the absence of gypsum in Early Proterozoic evaporitic sequences would be that calcium was exhausted before the gypsum field was reached during evaporation, due to a sufficiently high ratio of bicarbonate/sodium (Grotzinger and Kasting, 1993).

An additional difference is the unusual occurrence of primary aragonite precipitates, for example in the Rocknest Formation of Western Canada (Grotzinger and Reed, 1993). Archean carbonate sedimentation featured prolific precipitation of primary aragonite that occurred as giant botryoids up to 1 metre in radius and extended laterally over 100 km (Grotzinger and Kasting, 1993). The Paleo-, Meso- and Neoproterozoic were marked by progressively less spectacular occurrences of massively precipitated aragonite and calcite

cement (Burdett et al., 1990; Grotzinger and Kasting, 1993). Today, the precipitation of massive calcareous cement on the seafloor is unknown, despite the oversaturation of modern surface seawater with respect to calcium carbonate (Grotzinger and Kasting, 1993).

Cerium anomalies are used as indicators of redox reactions that occur in the environment of deposition. For example, modern sea-water has a pronounced negative Ce-anomaly, while ferromanganese nodules and crusts display a significant positive Ce-anomaly. Both are the result of the oxidation of Ce^{3+} to Ce^{4+} and subsequent decoupling of Ce from the other REEs due to the formation of insoluble Ce^{4+} (Tsikos, 1999). Negative Ce-anomalies have been described for the Kuruman and Griquatown BIFs (Klein and Beukes, 1989) and for the BIFs and carbonates of the Voëlwater Subgroup (Tsikos, 1999). Such negative Ce-anomalies may represent an oxidation of iron during BIF deposition at some depth below the zone of mixing rather than at the surface (Towe, 1991). However, interpreting the behaviour of Ce in marine precipitates is complicated by the anomalous abundance of La (Bau and Dulski, 1996) in the Asbestos Hills Subgroup (Klein and Beukes, 1989) and in the Voëlwater Subgroup (Tsikos, 1999).

V.2.4. Paleoproterozoic plate tectonics

The Earth has undergone spectacular changes in size, relative position and geographic distribution of its continents, all of which have a major impact on atmosphere, ocean, climates, and thus on the global stratigraphic record (Aspler and Chiarenzelli, 1998). According to Gurnis (1988), Abbott and Menke (1990), Gaál (1992), De Wit et al. (1992) and Eriksson et al. (1998, 1999, 2001), the first evidence of plate tectonics dates as far back as the earliest geologic record (4.0-3.5 Ga) and is represented by greenstones, anorogenic granites, mafic dyke swarms and accretionary orogens. Greenstones are considered to have originated from plume-generated plateaux that were subsequently accreted to continental nuclei (Eriksson et al., 1998, 1999, 2001). Other workers such as Nelson et al. (1999) and Condie et al. (2001) consider that layered mantle convection gave way to whole mantle convection during short-lived global and catastrophic magmatic periods in the Archean (Eriksson et al., 2001), termed superplume events, that could be associated with the formation of a supercontinent (Condie et al., 2001).

The period of cratonic formation lasted from 3.7 Ga to its stabilisation at 2.7 Ga (De Wit et al., 1992). The early development of the granite-greenstone crusts of the Kaapvaal and Pilbara Cratons was characterised by a continuous and long-lived magmatic episode. This was followed by thick Archean volcanic sequences characteristic of superplume events of 60-200

Ma duration affecting the style of crustal growth, intensity of volcanism, subaerial erosion and eustasy (Nelson et al., 1999; Eriksson et al., 2001). A particularly well defined global magmatic event at 2.7 Ga (2.76-2.68 Ga) has been recognised in the Pilbara (Australia), Amazon (South America), São Francisco (South America), Kaapvaal (South Africa) and Karnataka (India) Cratons (Nelson et al., 1999; Eriksson et al., 2001). The end of the formation and stabilisation of the cratons corresponds to this Late Archean 2.7 Ga superplume event that was immediately followed by the deposition of chemical (BIFs and banded chert) and clastic sediments (turbidites and coarse grained units) (Nelson et al., 1999).

The Late Archean Earth was probably undergoing supercontinent formation (Gaál, 1992; De Wit et al., 1992; Eriksson et al., 1998, 1999, 2001). It is currently postulated that there were two supercontinents, a northern supercontinent called Kenorland and a southern supercontinent named Zimvaalbara (Aspler and Chiarenzelli, 2001) or Vaalbara (Cheney, 1996). The North American Archean provinces as well as the Baltic and Siberian Shields made up Kenorland (Aspler and Chiarenzelli, 2001). Zimvaalbara consisted of the assembly of the Zimbabwe, Kaapvaal, Pilbara, Antarctica and the São Francisco Cratons and the Indian blocks (Eriksson et al., 1999; Aspler and Chiarenzelli, 2001). Although evidence has been presented that the Pilbara and Kaapvaal Cratons were not contiguous because of latitudinal separation by 30° of the two cratons (Wingate, 1998) and that some magmatic events were not present on both cratons at the same time (Nelson et al., 1999), the two cratons could have been located along the same ocean-margin (Martin et al., 1998). According to Gaál (1992), Mertanen et al. (1999), Eriksson et al. (1999) and Aspler and Chiarenzelli (2001), at 2.5-2.4 Ga and earlier for the southern Zimvaalbara (2.65 Ga), both supercontinents were subjected to attenuation and initiation of supercontinent break-up, consistent with a superplume event characterised by the presence on all cratons of mafic intrusions (dyke swarms, layered mafic intrusions) as well as continental volcanic extrusion, accompanied by major transgressions. The ca. 2.4 Ga global glacial event is present on most cratons and also appears to be related to a superplume event (Eriksson et al., 1999) that caused rifting (Worsley et al., 1984; Young and Nesbitt, 1985; Gaál, 1990, 1992; De Wit et al., 1992; Dalziel, 1995, 1997; Bühn and Stanistreet, 1997; Aspler and Chiarenzelli 1997; Condie et al., 2001; Eriksson et al., 2001). Finally, Kenorland and Zimvaalbara broke up and dispersed at around 2.2-2.0 Ga (Gaál, 1990, 1992; Bühn and Stanistreet, 1997; Aspler and Chiarenzelli 1997; Condie et al., 2001; Eriksson et al., 2001). Morel and Irving (1978), Bond et al. (1984), Hartnady (1991), Park (1994), Young (1995), Li et al. (1995), Bühn and Stanistreet (1997), Dalziel (1995, 1997), Dehler et

al. (2001) and many others have ascribed the origin of Late Proterozoic BIFs and glaciogenic deposits (~700 Ma and 600 Ma) to the break-up of another younger supercontinent, Pangea.

The post-accretionary tectonic evolution of the Kaapvaal Craton displayed by Paleoproterozoic cover sequences shows all the characteristics of supercontinental break-up, commencing with continental rifting and followed by ocean opening that would correspond to supercontinent fragmentation. Mid-ocean ridge activity and thermal uplift related to superplume events controlled eustasy during most of the time of the Transvaal Supergroup accumulation, even if periods of tectonic relaxation and thermal subsidence allowed for the deposition of a thick sequence of carbonates and BIFs. The glacial events at the base of both the Postmasburg and Pretoria Groups are associated with rifting periods and thermal doming during the Ongeluk (Postmasburg Group) and Hekpoort volcanism (Pretoria Group). From the end of the Ongeluk Formation, the rest of the Postmasburg Group results from decreased tectonic activity and low mid-ocean ridge activity, which translate to a regressive cycle displayed by the chemical precipitates of the Voëlwater Subgroup. The Pretoria Group does not express this tectonic quiescence seen in the Griqualand West Basin, but is rather the result of successive periods of rifting. These two radically different tectonic settings pose a problem for correlating the Postmasburg and Pretoria Groups as time equivalents. This problem has already been discussed in section V.1.3.

V.2.5. Paleoproterozoic climate

Global climatic conditions are ruled by many different factors such as the concentration of CO_2 in the atmosphere (Genthon et al., 1987; Barnola et al., 1987; Marshall et al., 1988; Raymo, 1991; Levin, 1994) and by factors such as greenhouse/icehouse conditions, the solar luminosity (Kuhn et al., 1989), the position of the continents (Kuhn et al., 1989; Crowley and Baum, 1993) and/or the Earth's obliquity (Genthon et al., 1987). In the Precambrian, the climates may also have been controlled by different spinning rates of the Earth (Hunt, 1979; Kuhn et al., 1989). Despite this, Precambrian paleoclimatic indicators are uncommon. According to Eriksson et al. (1998), the presence of Early Archean evaporites and stromatolitic carbonates generally favour rather warm climates. However, as pointed out by Walter and Bauld (1983), cold-water evaporites and stromatolitic carbonates form today in Antarctica. The precipitation of evaporitic sequences therefore results from removal of water by either evaporation or freezing. Cold-water stromatolitic carbonates have been found to be precipitated below an ice cover in a lake where geothermal brines were active (Walter and Bauld, 1983).

Red beds are considered to have formed due to the rise of atmospheric oxygen in an arid climate (Eriksson et al., 1998). An arid climate involves low annual precipitation, regardless of the temperature. Lateritic and bauxitic weathering, usually diagnostic of humid and warm climates, can form slowly in wet and cool-to-cold conditions (Taylor et al., 1992). Such paleoclimatic and/or paleolatitudinal indicators are not infallible and should be treated cautiously especially when climate is at the heart of the problem. It is, however, generally accepted that Archean and Proterozoic climates were warmer than at present (Eriksson et al., 1998), even if the solar luminosity was 25% less than the present value in the Archean (Newman and Rood, 1977; Kasting, 1987) and 18% less in the Early Proterozoic (Kasting, 1987).

As discussed in paragraph V.1.2, the faint young Sun paradox requires higher concentrations in atmospheric greenhouse gases (Newman and Rood, 1977; Kasting, 1987). Atmospheric CO_2, together with gas hydrates (methane-H_2O solids in shallow marine sediments that are released into the atmosphere when the continental shelf is exposed after marine regression), could have been important in the Proterozoic (Kiehl and Dickinson, 1987; Kennedy et al., 2001; Condie et al., 2001) and would have contributed to the greenhouse effect, preventing the surface temperatures of the Earth from freezing conditions. Greenhouse gases are believed to control global climatic conditions of the current Earth (Barnola et al., 1987; Genthon et al., 1987) and changes in their atmospheric concentrations could lead to glaciation (Marshall et al., 1988; Raymo, 1991). It has also been suggested that an increase in the thickness and amount of cloudiness would reduce the amount of greenhouse gases needed to counteract the faint young Sun paradox (Kiehl and Dickinson, 1987).

Silicate and carbonate weathering is a common process that extracts and removes the atmospheric CO_2, and influences global climate. Carbon enters the ocean-atmosphere system by weathering, volcanism and metamorphism (Condie et al., 2001). Part of this carbon is in a reduced state because it includes organic carbon remobilised during destruction of older sediments (Condie et al., 2001). In the surface environment, carbon is rapidly cycled through the biosphere by biosynthesis. The amount of organic carbon and carbonate buried depends on global rates of erosion and sedimentation, and upon recycling processes on the sea floor (Derry et al., 1992; Condie et al., 2001). A supercontinent undergoing intense silicate and/or carbonate weathering would remove proportionally more atmospheric CO_2. The amalgamation of continents would trigger a major regression that would cause an augmentation in the albedo due to an increasing land/ocean ratio (Walker, 1982). Weathering together with increased albedo would favour cold climates (Condie et al., 2001).

Studies of tidal rhythmites not only indicate that the rotation rate of the Earth during the Proterozoic was faster than at present (Hunt, 1979), with 17.1 to 18.9 hours per day at 2.5 Ga (Williams, 1998), with 18 to 21.9 hours at 0.9 Ga (Sonnet et al., 1996; Williams, 1997) and 21.9 hours at 650 Ma (Williams, 1990, 1998), but also indicate the lunar retreat rate (Williams, 1989, 1993, 1997, 1998; Chan et al., 1994). A shorter day length increases the coldness of the poles, and also the equator-to-pole temperature difference because less energy is transported poleward (Hunt, 1979; Kuhn et al., 1989). A closer Moon will have the effects of reducing the length of the Milankovitch orbital cycles (105, 17, and 13 kilo-years; Walker and Zahnle, 1986) that force the climate by modulating ice ages and increasing the tidal friction (Williams, 1998). However, Williams (2000) has suggested that a dramatic approach of the Moon has never occurred during Earth's history.

Even if the chemical conditions in the Proterozoic were different from those of today, the occurrence of glacial deposits in the rock record is diagnostic for cold climate if such deposits are convincingly identified (see paragraph V.1.6), because they form almost exclusively by mechanical processes rather than chemical ones. Glacial deposits have been recorded as far back as 3.0 Ga in the Pongola Supergroup of Southern Africa (Von Brunn and Gold, 1993), but these deposits are isolated and may be related to local conditions. Three main glacial periods have been reported worldwide during the Proterozoic: the Huronian Glaciation in the Early Proterozoic (2.4-2.2 Ga, named after the occurrence of glacial rocks in the Huronian Supergroup in Canada), and the Sturtian-Rapitan (750-700 Ma) and Marinoan-Varangian-Ice Brook (610-590 Ma) Neoproterozoic glaciations (Kennedy et al., 1998).

The apparent absence of glacial (and BIF) accumulations between the Early and Late Proterozoic is puzzling (Young, 1991; Eriksson et al., 1998), because glaciations should have developed on the Mesoproterozoic supercontinents such as "Atlantica" and "Nena" (Eriksson et al., 1998). Young (1991, 1995) proposed that widespread anorogenic magmatism during the Mesoproterozoic provided the atmosphere with sufficient CO_2 to balance CO_2 drawdown by weathering. Another explanation would be that possible glaciations in the Mesoproterozoic were continental, and therefore would have had a very low preservation potential. Glaciomarine deposits are generally better preserved than continental glacial deposits.

The Proterozoic climatic paradox arose as a result of paleomagnetic studies on Proterozoic glacial deposits that were found to have accumulated at low latitudes (Harland and Bidwood, 1959; Harland et al., 1966; Harland, 1983; Chumakov and Elston, 1989; Evans et al., 2000; Pisarevsky et al., 2001). Recent paleomagnetic studies (Park, 1997; Evans et al.,

1997; Williams and Schmidt, 1997; Schmidt and Williams, 1999; Sohl et al., 1999; Kirschvink et al., 2000) confirm that both Early and Late Proterozoic glacial events took place within 30° from the equator at sea level (Williams et al., 1995). The association of these low-latitude glacial deposits with warm climatic indicators (evaporites, carbonates and other postulated arid-climate deposits, but see also paragraph V.1.6 that questions the validity of such indicators) challenges the modern climatic models and defines the Proterozoic Climatic Paradox.

Several hypotheses have been proposed in an effort to explain this paradox (Chumakov and Elston, 1989; Hoffman et al., 1998; Sohl et al., 1999): (1) the diamictites have a non-glacial origin, (2) the entire solid shell (crust and mantle) rotated 90° relative to the inertial-interchange true polar wander (Hoffman et al., 1998), (3) the paleomagnetic data are incorrect (Meert and van der Voo, 1994, 1995; Moore et al., 2001), (4) an atmospheric ice ring similar to the one of Saturn shed a shadow over the equator (Ives, 1940 in Schwarzbach, 1963), (5) the glaciation was global and covered the Earth from pole to pole ("Snowball Earth" hypothesis; Kirschvink, 1992), (6) the Slushball Earth model (Cowen, 2002), (7) an increased inclination of the Earth's obliquity that favoured glacial conditions at low latitudes (Williams, 1975; Oglesby and Ogg, 1998).

The first hypothesis is rejected because most of the concerned diamictites have been identified as having a glacial origin (Young, 1976; Trendall, 1976; Harland, 1983; Marmo and Ojakangas, 1984; Miall, 1985; Young and Nesbitt, 1985; Mustard and Donaldson, 1987; Strand and Laajoki, 1993; Klein and Beukes, 1993). The second is difficult to support on paleomagnetic grounds since there is no record of a high-latitude position of cratons for their postulated excursion into polar regions (Chumakov and Elston, 1989), and it does not explain the low paleomagnetic inclinations for the glacial deposits themselves (Hoffman et al., 1998). The third hypothesis is also rejected because of the consistency over the past 40 years of paleomagnetic studies (from Harland and Bidwood, 1959; to Sohl et al., 1999). The fourth hypothesis can also be rejected because an ice ring cannot exist so close to the Sun and because the insolation at the equator is not reverted (Williams, 1993).

This leaves the three most controversial hypotheses: the Snowball Earth, Slushball Earth and high Earth obliquity. Some authors find in the Snowball Earth many answers to enigmatic Proterozoic features and reject any alternative models (Kirschvink, 1992; Evans et al., 1997; Hoffman and Maalof, 1999; Hoffman, 1999; Hoffman et al., 1998; Hyde et al., 2000; Runnegar, 2000; Hoffman and Schrag, 2000; Kirschvink et al., 2000; Kirschvink, 2002; Hoffman and Schrag, 2002), while some others are not convinced (Embleton and Williams,

1986; Meert and van der Voo, 1994; Meert and van der Voo, 1995; Schmidt and Williams, 1995; Williams et al., 1995; Williams and Schmidt, 1997; Jenkins and Scotese, 1998; Williams et al., 1998; Kennedy et al., 1998, 2001, 2002; Williams, 2000; Schmidt and Williams, 1999; Polteau, 2000; Kerr, 2000; Shapiro, 2002; Moore et al., 2001). Biologists mainly favour an alternative to the Snowball Earth, that is the Slushball or Softball Earth (Cairns, 2001; Cowen, 2002). The Williams theory of the large value of the Earth's obliquity has also some support (Williams, 1975, 1979, 1989, 1993, 1994, 1997, 1998, 2000; Embleton and Williams, 1986; Schmidt and Williams, 1995; Williams et al., 1995, 1998, 2000). It is necessary to review briefly each hypothesis, by describing the theoretical processes involved in the formation of the peculiar Proterozoic features that are still enigmatic.

It was Kirschvink (1992) who first proposed the Snowball Earth hypothesis. The prerequisite is that continents were located at low latitudes, either as isolated masses or as supercontinents (Kirschvink, 2002). The Earth was left with very large oceans covering middle to high latitudes. Recent studies predict that complete freezing of the planet was easily accomplished with large oceans (Jenkins and Scotese, 1998; Kimura et al., 2002) when the polar seas become isolated from warm tropical waters by the pattern of surface currents (Hoffman et al., 2002; Cowen, 2002). Silicate/carbonate weathering was the main drawdown mechanism for atmospheric CO_2 that helped in the lowering of global surface temperatures (Derry et al., 1992; Kirschvink, 1992; Des Marais, 1994; Condie et al., 2001; Hoffman and Schrag, 2002).

These combined effects led to a colder planet with the growth of large floating ice caps along the coastal areas (Kirschvink, 1992; Hoffman and Schrag, 2002). As these ice sheets spread, they reflected more and more solar radiation back into space in a runaway albedo cooling reaction that only stopped once the oceans were completely sealed off from the atmosphere by a continuous carapace of ice (Hyde et al., 2000; Hoffman and Schrag, 2002; Kirschvink, 2002). Very little atmospheric CO_2 remained, locking the Earth into the Snowball stage (Kirschvink, 2002; Hoffman et al., 1998, 2002). General circulation models have successfully created such a Snowball Earth (Hyde et al., 2000; Donnadieu et al., 2003) although other models did not attain this state (Crowley and Baum, 1993; Jenkins and Scotese, 1998; Poulsen et al., 2002). In such catastrophic conditions, primitive life forms were maintained only around sea floor hydrothermal vents and on top of the ice, in tropical areas where the ice was thin enough (10 metres or less) to let sunlight penetrate and preserve photosynthetic life (McKay, 2000). Reduced metals of hydrothermal origin, such as iron and

manganese, are soluble in an anoxic ocean sealed off from the atmosphere and can reach high concentrations.

The only escape mechanism (suggested by Kirschvink, 1992, 2002; Hoffman et al., 1998; Hoffman, 1999; Hoffman and Schrag, 2002) would be the gradual increase of atmospheric CO_2 coming from volcanic degassing, undisturbed by the Snowball Earth event. The required levels of atmospheric CO_2 are in the order of 120,000 ppm, that is 330 times the present value of 366 ppm, before triggering rapid deglaciation and melting of the ice (Kennedy et al., 2001). The excess of atmospheric CO_2 would place the Earth into an extreme greenhouse period. The thawing of the sea ice established gas exchanges between the surface ocean and the CO_2-rich atmosphere and triggered rapid carbonate precipitation (cap-carbonate) characterised by a negative $\delta^{13}C$ incursion. The oceans would precipitate the iron in solution as BIFs by upwelling of the deep iron-rich waters in shallow oxic passive margin settings (Kirschvink, 1992; Klein and Beukes, 1993; Hoffman and Schrag, 2002). Hoffman et al. (1998), Hoffman and Schrag (2002) and Kirschvink (2002) attributed the $\delta^{13}C$ depletion of cap-carbonates to the volcanic origin of the CO_2 atmospheric build-up prior to rapid deglaciation.

The Snowball Earth hypothesis explains some of the enigmatic features of both Neoproterozoic and Paleoproterozoic glacial deposits (Williams, 1998; Hoffman and Schrag, 2002) such as:

> the widespread low-latitude glacial deposition;

> the main Proterozoic glacial events started and ended abruptly;

> the restriction of the BIFs and manganese deposits to both Paleo- and Neo-Proterozoic periods;

> the worldwide occurrence of cap-carbonate immediately covering the Neoproterozoic glacial deposits;

> the existence of highly positive and negative $\delta^{13}C$ anomalies bracketing glacial events.

> the survival of primitive photosynthetic organisms.

However, the Snowball Earth hypothesis cannot account for other peculiarities observed in the Paleoproterozoic and Neoproterozoic glacial accumulations. Indeed the Snowball Earth theory of Kirschvink (1992, 2002) describes such an event as our mind can conceive it, and this could be a caricature of a real Snowball Earth event (Hoffman and Schrag, 2002).

The creation of a frozen Earth implies a rapid major global regression that should be observed on all continents. As seen in chapter II, the unconformable contact of the Makganyene Formation on the Ghaap platform is consistent with a major regression/low

freeboard. The problem with a Snowball Earth is that the unconformable contact grades rapidly into a southward conformity from the Griquatown Hinge Zone and has a transitional nature in the Sishen area, indicating that the forced eustatic regression was not as dramatic as Hoffman and Schrag (2002) and Kirschvink (2002) predicted.

The same gradational change, from the Boolgeeda BIFs to the Kungarra siliciclastics to the Meteorite Bore glacial deposition, is observed in the Hamersley Basin in Australia (Martin et al., 2000). The Early Proterozoic glacial deposits of the Honkala Formation in Scandinavia (Strand and Laajoki, 1993), and the Gowganda Formation in Canada (Miall, 1985; Young and Nesbitt, 1985) also show that even if unconformities are present at the base of the diamictites, conformable and erosional relationships do occur in restricted parts of the concerned basins. The global eustatic sea-level fall is not as dramatic and rapid as predicted by the Snowball Earth Hypothesis.

The Snowball Earth theory implies that all glacial deposits have been deposited synchronously. Regarding the Early Proterozoic, it appears that age constraints are poor and inconsistent (Moore et al., 2001). As shown in table V.4, only the Makganyene Formation has a well bracketed age, close to 2.4 Ga. On the other hand, all other Early Proterozoic glaciogenic formations' ages are poorly constrained, but could also have formed at 2.4 Ga. Further accurate dating studies would reveal either the simultaneous nature of the glacial event at 2.4 Ga, or a diachronous glacial event.

	Makganyene (South Africa)	Honkala (Scandinavia)	Meteorite Bore Member (Australia)	Gowganda (Canada)	Dhanjori (India)
Min. age	2.394 Ga (Mooidraai)	2.2-2.1 Ga (diabase dykes)	2.209 Ga (Wyloo Group)	2.1 Ga (diabase dykes)	2.1 Ga (Kolhan Group)
Max. age	2.415 Ga (Koegas)	2.6-2.7 Ga (Archean basement)	2.45 Ga (Woongarra Rhyolite)	2.5-2.6 Ga (Archean basement)	2.55 Ga (Younger Iron Ore Group)

Table V.4. Age constraints on Early Proterozoic glaciogenic deposits present in South Africa (Bau et al., 1999; Kirschvink et al., 2000), Scandinavia (Strand and Laajoki, 1993), Australia (Martin et al., 2000), Canada (Young and Nesbitt, 1985), and India (Eriksson et al., 1999).

The Snowball Earth theory implies that such a dramatic event occurred once in the Early Proterozoic and twice in the Late Proterozoic. In the Kaapvaal Craton, the Makganyene and the Duitschland/Timeball Hill Formations may represent one or even two distinct glacial events, and further geochronological work should determine this. In the Pilbara, Scandinavian and Indian cratons, only one event has been recorded, while in Canada, three glacial events

have been noted (Polteau, 2000). This strongly suggests that the Snowball Earth model cannot account for multiple glaciations observed in the Early Proterozoic.

The genetic relationship between a Snowball Earth event and massive deposition of iron as BIFs is not as clear as Hoffman and Schrag (2002) make it seem. BIFs would precipitate only after a Snowball Earth event, once the gas exchange between the atmosphere and ocean are re-established. Young (2002) demonstrated that Early Proterozoic BIFs are not necessarily directly associated with glacial deposits. As described in the Early Proterozoic of Canada and Australia (Young, 2002), no direct evidence of BIFs and associated diamictite can be observed. The glacial deposits are either situated remotely above the occurrence of BIFs (Australia), or below a 300 Ma unconformity separating the BIFs (Canada). However, the Transvaal Supergroup in the Griqualand West Basin displays a gradual change from carbonate to BIFs to diamictites, and from diamictites to BIFs back to carbonates, making climate the driving force that controlled the deposition of the Transvaal Supergroup.

Cap-carbonates represent the corner-stone of the Snowball Earth hypothesis because they provide a mechanism for terminating the frozen Earth scenario: the gradual increase of atmospheric CO_2. The 120,000 ppm of CO_2 required to trigger melting of the ice is however unrealistic (Kennedy et al., 2001). Kennedy et al. (2001) proposed that massive destabilisation of ice-like methane gas hydrate coincided with Neoproterozoic postglacial warming. According to Cowen (2002), methane is trapped under winter ice in the Sea of Okhotsk in Siberia. In addition, there are huge deposits of methane gel (clathrate) in the sediments in the Sea of Okhotsk. Methane is released through cracks in the ice during summer, and seeps through mineralised chimneys suggesting that methane seep sites are not ephemeral (Cowen, 2002). Since methane is a greenhouse gas sixty times more potent than CO_2 mole per mole (Cairns, 2001), and has a $\delta^{13}C \approx -60‰$ (Kennedy et al., 2001), it has a greater influence on climate than CO_2. The negative carbon isotopic excursion in the cap-carbonate ($\delta^{13}C = -5‰$) reflects the input of light ^{13}C from methane (Kennedy et al., 2001). The presence of methane is ascribed to the photosynthetic processes by Cowen (2002), a phenomenon that is supposed to be virtually non existent in a Snowball Earth, except under thin ice or on the surface (McKay, 2000). On a Snowball Earth, life would be barely surviving and not producing massive methane reservoirs. For Early Proterozoic glaciations, such as the Makganyene glacial event, no such cap-carbonate has been observed, and therefore a convincing mechanism that triggers greenhouse conditions still requires formulation, especially since solar luminosity was 18% less than at present, and as a result the atmospheric CO_2 levels required would have been too high.

The last main obstacle the Snowball Earth hypothesis has to overcome is to demonstrate that similar processes of transport and deposition of rafted debris were active in Proterozoic glacial deposits as well as their contemporaneous high latitude equivalents (Miall, 1985; Young and Nesbitt, 1985; Strand and Laajoki, 1993; Eriksson et al., 1999). On a Snowball Earth, the hydrological cycle would be shut down because low temperatures would inhibit sublimation and precipitation (Schmidt and Williams, 1995), and would therefore stop glacial advance and sediment delivery to the basin. The counter argument of Hoffman and Schrag (2002) and Donnadieu et al. (2003) is that glacial deposits formed on a Snowball Earth when sufficient greenhouse gases were present to change dry-based glaciers to wet-based glaciers, possibly in ice streams and ice surges. This statement implies a still stand in deposition for the duration of a Snowball Earth event except during the establishment of wet-based glaciers and/or vice-versa. Ice-rafted debris such as dropstones and striated pebbles are present in the Makganyene Formation (Polteau, 2000; and this study), indicating that the Makganyene glacial environment was active with transport and deposition of sediments, arguing against still stand conditions of a Snowball Earth event.

An alternative model to the Snowball Earth is the Slushball Earth corresponding to a partial Snowball Earth with an equatorial belt of open water that nurtured the early evolution of life (Cowen, 2002). Poulsen et al. (2002) and Hyde et al. (2000) provide computerised general circulation models that easily attain the Slushball Earth state. This model pleases the geobiologists who are concerned that the Snowball Earth would have killed off many of the animal phyla which had supposedly formed according to molecular clock analyses up to several hundred million years before the glacial events reverted life to an Archean biology of anaerobic bacteria and archaea (Cairns, 2001; Kirschvink, 2002; Cowen, 2002). The hydrological cycle would not have been shut down, and would have provided enough precipitation to favour glacial advance and transport of débris. Intense Slushball upwelling, caused by the restricted open-water area, would have supplied nutrients to evolving primitive life forms (Cowen, 2002) and may have contributed to the deposition of BIFs. The end of a Slushball Earth would need a less dramatic rise in greenhouse gases, required by the Snowball Earth (Cowen, 2002). Kirschvink (2002) and Cowen (2002) argued that the first glacial event was triggered by a rise of atmospheric oxygen that consumed the most powerful greenhouse gas, methane. With combined lower solar luminosity of 18% at 2.5 Ga (Kasting, 1987), Snowball or Slushball Earth would have been easily created (Poulsen et al., 2002; Hyde et al., 2000).

The counterarguments for the Slushball Earth are the following (Cairns, 2001):

➤ the long-term stability of a Slushball Earth has not been demonstrated;

➤ the greenhouse build-up would cause the ice to rapidly recede, and therefore the occurrence of BIFs and cap-carbonates is not explained;

➤ the photosynthetic organisms would grow (not develop as suggested by Cowen (2002) but rather survive in such conditions) even if no open water were present (McKay, 2000).

The high-obliquity hypothesis also explains the occurrence of glacial deposits forming at low-latitudes at sea level by invoking a substantial increase in the Earth's obliquity relative to the plane of the ecliptic (Williams, 1993). According to Williams (1975, 1993, 1997, 1998, 2000), Embleton and Williams (1986), Schmidt and Williams (1995) and Williams et al. (1995, 1998), when the obliquity of the Earth exceeds 54°, low latitudes would receive less solar luminosity annually and hence would be preferentially glaciated. The climatic zonation reverses at an obliquity of 54° (Williams, 1975, 1993, 1998). At an obliquity below the critical 54°, glaciation would preferentially occur at high-latitudes (Williams, 1993).

Williams (1993, 1997, 1998, 2000) suggests that the original Earth's obliquity value of 70° was induced by a collision with a single giant impactor that was responsible for the formation of the Moon 4.5 Ga ago. This value constantly decreased to acquire a value of 60° just before the Cambrian lower boundary. At the Proterozoic-Phanerozoic boundary, the Earth's obliquity value dropped rapidly to a value in the order of the present value of 23° (Williams, 1993). The shift of climatic zone, from reversed to normal, is presumed to have been triggered by unique conditions at the core-mantle boundary that caused a significant increase in dissipative core-mantle torques together with the climate friction phenomenon or obliquity-oblateness feedback (Williams, 1993). Williams (1975, 1993) and Williams et al. (1998) suggested that a delayed response to the redistribution of ice/water mass may have introduced variation in obliquity.

Should the Earth have had an obliquity angle of over 54°, glaciation would be caused by a decrease in greenhouse gases in the atmosphere (Williams, 1993). Williams (1993) explained that such an Earth would have intensified seasonality and the climatic zonation would be diminished because the area between latitudes 30-60° would be both within the tropics and polar circle (Williams, 1993). Certain structures such as ice and sand wedges that are common in permafrost soils and are normally attributed to large seasonal temperature fluctuations, have been identified in glaciogenic accumulations in the Neoproterozoic of Australia (Williams, 1975, 1993, 1998; Williams et al., 1995, 1998) and would fit the high

obliquity model. The direction of zonal winds such as the tropical and mid-latitude westerlies would be reversed, resulting in westerly zonal surface winds at low-latitudes, evidence of this having also been observed in the Neoproterozoic of Australia (Williams, 1993). Microorganisms would have survived in this stressful environment.

The high-obliquity hypothesis explains the following enigmatic characteristics of the same Neoproterozoic and Paleoproterozoic glacial deposits (Williams, 2000):

➤ the widespread low-latitude glacial deposition;

➤ the present inclination of the lunar orbit with respect to the ecliptic (5°);

➤ the intimate association of "warm" climatic indicators and glaciogenic rocks;

➤ the zonal winds;

➤ the survival of primitive photosynthetic organisms.

There are, however some problems with this model. According to Pais et al. (1999), Levrard and Laskar (2000) and Levrard (2003) the mechanism of climate friction or obliquity-oblateness feedback suggested by Williams (1993) cannot reduce the high obliquity (over 54°) to normal values (23°). The extreme seasonality described by Williams (1993) would make glacier growth extremely difficult (Cairns, 2001). This model does not explain the occurrence of BIFs, and finally ice/sand wedges can form without extreme seasonality (Cairns, 2001; Hoffman and Schrag, 2002).

Table V.5 (modified after Kirschvink, 2002) summarises the various geological observations mentioned above and compares them with modern glacial environments. Any single model does not cover all the problems. Therefore compromises are necessary and adaptation of the Snowball/Slushball Earth hypothesis is imperative.

	Snowball Earth	Slushball Earth	High Obliquity	Modern Glacial Environment
Low latitude glacial deposition	Yes	Yes	Yes	No
Association with BIFs and Manganese	Yes	Yes	No	No
Presence of cap-carbonate	Yes	No	No	No
Negative δ13C excursions in cap-carbonates	Yes	No	No	No
Glacial rain-out intervals	No	Yes	Yes	Yes

Table V.5. Summary of the various geological observations of the different models proposed (modified after Kirschvink, 2002).

This study of the Makganyene Formation sheds some light on the Paleoproterozoic global glacial event, because none of the proposed models can account for all the characteristics of the Makganyene Formation. An alternative solution will be proposed in the next section dealing with the depositional model for the Makganyene Formation.

V.3. A depositional model for the Makganyene Formation

V.3.1. Introduction

This section presents a depositional model for the Transvaal Supergroup in the Griqualand West Basin, with particular emphasis on the Koegas Subgroup and the Makganyene Formation. The sequence stratigraphy model presented earlier has influenced the depositional model.

V.3.2. The Makganyene depositional model

The Makganyene depositional model is influenced by the rest of the Transvaal succession of the Griqualand West Basin. This is necessary because the Early Proterozoic Transvaal Supergroup represents a single depositional sequence that is marked by a period of transition, from an anaerobic to an aerobic atmosphere that was recorded by the deposition of BIFs and massive manganese beds. Therefore the evolution of paleoenvironmental conditions specific to the Early Proterozoic Earth is included in the extended version of the sequence stratigraphy model described in figure V.2 (after Catuneanu and Eriksson, 1999). The depositional model for the Transvaal Supergroup is presented in figure V.6 and comprises five stages corresponding to the Ghaap Group (stage A, HST), the Koegas Subgroup (stage B, FSST), the Makganyene Formation (stage C, LST), the Ongeluk Formation (stage D, an intermediate stage between the LST and TST) and the Voëlwater Subgroup (stage E, TST).

However, in order to place the depositional model into perspective, it is necessary to briefly introduce the tectonic events that affected the Kaapvaal Craton from its stabilisation to the beginning of the Transvaal Supergroup deposition (i.e. the interval ca. 3.0-2.6-2.7 Ga). The initiation of the depositional basins on the Kaapvaal Craton started in the Archean, Clendenin et al. (1988) and Clendenin (1989) proposed a three-stage rift model that consists of a succession of pre-graben, graben and post-graben thermal-subsidence basins, and that was initiated by the oblique collision of the Zimbabwe Craton with the Kaapvaal Craton along the southwesterly curving Limpopo orogenic belt (Clendenin et al., 1988; Clendenin, 1989; De Wit et al., 1992). Each basin was influenced by existing zones of crustal weaknesses, horizontal and vertical crustal movements and high heat flow in a thinned or thinning lithosphere, all of which are characteristics of divergent zones (Clendenin et al., 1988; Clendenin, 1989). The base of the Transvaal Supergroup, the Black Reef Quartzite/Schmidtsdrif Subgroup (2.64 Ga), marks the start of the post-graben system which corresponds to the commencement of thermal subsidence that led to the opening of a shallow

epeiric sea on the Kaapvaal Craton (Clendenin et al., 1988; Clendenin, 1989). Such change in tectonic style is responsible for the major unconformity present at the base of the Transvaal Supergroup (Catuneanu and Eriksson, 1999).

The Transvaal Supergroup commences with the deposition of the Schmidtsdrif Subgroup in the Griqualand West Basin (SACS, 1980). However the Schmidtsdrif Subgroup is bound by two second-order Subaerial Unconformities (SU) (Catuneanu and Eriksson, 1999; Eriksson et al., 2001) that isolate it from the rest of the Transvaal succession. The Schmidtsdrif Subgroup is therefore not included in the depositional model of figure V.6.

The initiation of the Ghaap Group (stage A of figure V.6) deposition is marked by a marine transgression, creating low continental freeboard/high sea level (Eriksson, 1999; Eriksson et al., 1999) that started a long-lived period of epeiric sea conditions. The development of the thick succession of carbonates and BIFs of the Ghaap Group necessarily implies tectonic stability and drowning of clastic sources (Eriksson et al., 2001). Thermal subsidence was therefore the main process that was active to accommodate this chemical sedimentary accumulation (Clendenin et al., 1988; Clendenin, 1989; Eriksson et al., 1993; 2001). Excessive flexure on pre-existing faults should have renewed faulting (Clendenin et al., 1988; Clendenin, 1989) such as the Griquatown Fault Zone that defined a 950 metres high scarp separating the Ghaap platform facies from the Prieska deep-water facies (Altermann, 1997).

The Ghaap Group forms a Highstand Systems tract (HST) (Catuneanu and Eriksson, 1999; Eriksson et al., 2001). The Campbellrand Subgroup consists of stromatolitic bioherms characteristic of a shallow carbonate platform on the Ghaap platform, and of deep turbidites in the Prieska deep basin (Beukes, 1983). The overlying Asbestos Hills Subgroup BIFs are deeper-water deposits (Beukes and Klein, 1990; Altermann and Nelson, 1998), indicating that a relative sea-level rise put an end to the carbonate accumulation. This relative sea-level rise was slow and of small amplitude because no drowning unconformity separates the carbonates from the BIFs (Catuneanu and Eriksson, 1999) and the nature of this contact is transitional (Beukes and Klein, 1990; Beukes et al., 1990; Hälbich et al., 1992). The Asbestos Hills BIFs represent the final regressive stage of the HST (Catuneanu and Eriksson, 1999).

Upwelling of deep anoxic waters onto shallow continental shelves supplied nutrients to primitive photosynthetic organisms that participated in the creation of O_2 in the surface waters of the oceans that, in turn, oxidised iron (Klein and Beukes, 1990; see figure V.6).
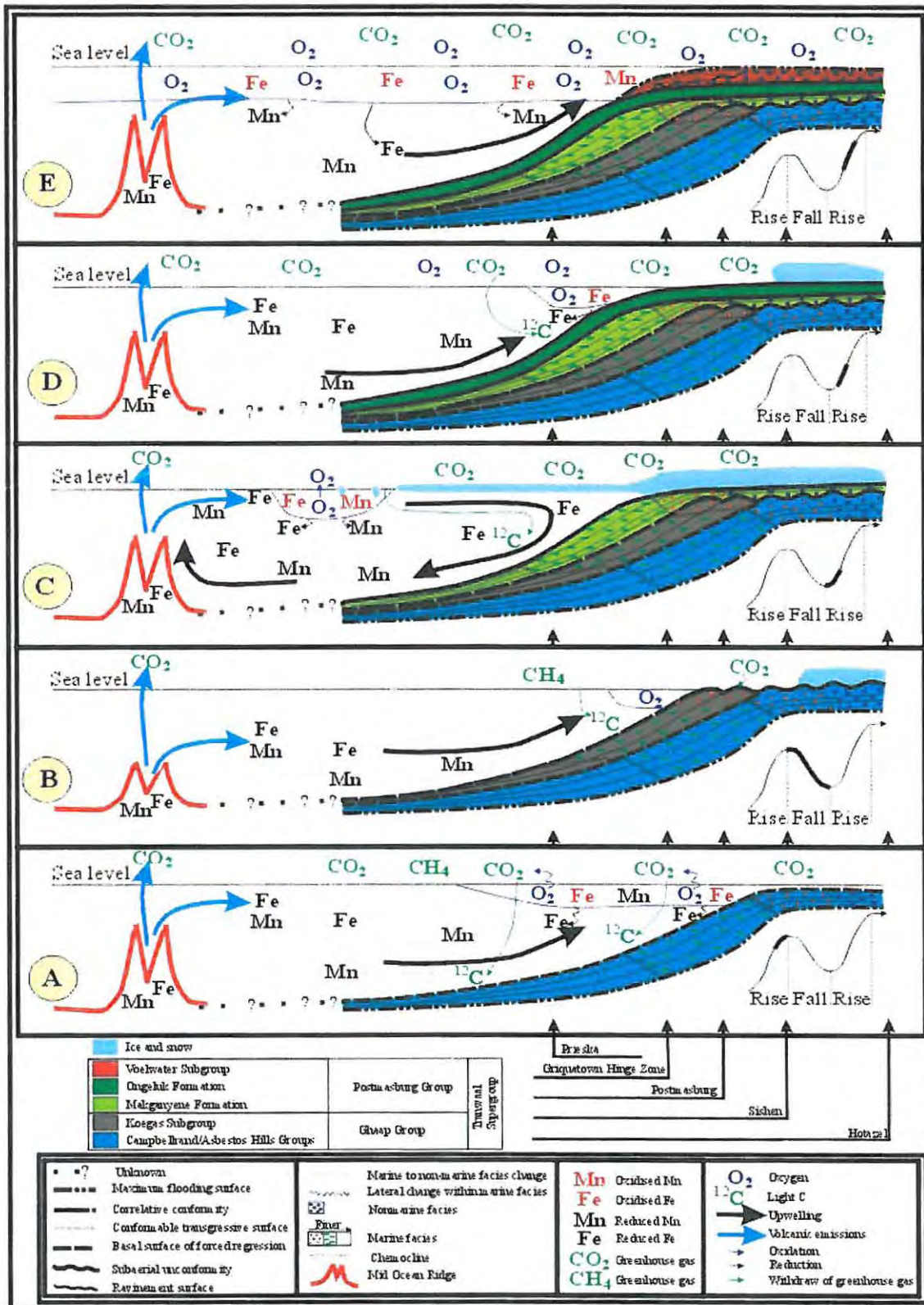
Figure V.6. Depositional model for the Transvaal Supergroup. Stages from A from E correspond to A: Ghaap Group, B: Koegas Subgroup, C: Makganyene Formation, D: Ongeluk Formation, E: Voëlwater Subgroup

Worldwide deposition of BIFs represents a rise in oxygen production, which was consumed by oxidation of iron. Glasby (1997) noted that manganese was also oxidised, and that its concentration rises throughout the Transvaal Supergroup. He proposed that the increase in manganese content reflects a rise in oxygen. The massive deposition of carbonates and carbonate BIFs of the Ghaap/Chuniespoort Group contributed directly to cooling by removal of atmospheric CO_2.

The Koegas Subgroup (stage B of figure V.6) represents the Falling Stage Systems tract (FFST) that was triggered either by the attenuation of the mid-ocean ridge activity, or by thermal doming, and caused the formation of a Subaerial Unconformity (SU) on the Ghaap plateau (see figure V.6) where Beukes (1983) described lacustrine deposits of Koegas age. Subaerial weathering withdrew atmospheric CO_2, which helped towards cooling. At that time, the Griquatown Fault Zone was inactive, and can be considered now as the Griquatown Hinge Zone. South of the hinge separating the plateau from the basinal facies, the marine Koegas, at least in its lower half, is well developed and represents submarine fan deposits that rest on the correlative conformity (cc) of the SU. BIF deposition was overprinted by clastic influx from exposed clastic sources, while biogenic oxygen production was reduced. The presence of a diamictite lens near the base of the Koegas Subgroup implies the onset of continental glaciation during Koegas times. However, the end of the Koegas Subgroup is characterised by the deposition of the Rooinekke Formation (see chapter II) consisting of turbidites and stromatolites.

The glacial Makganyene Formation (stage C of figure V.6) is located at the base of the Postmasburg Group and is related to lithospheric extension, as are the Early/Late Proterozoic glacial accumulations (Bühn and Stanistreet, 1997), and thermal doming. Thermal uplift, centred on the Vryburg Dome (Visser, 1971; De Villierss and Visser, 1977) and subsequently expressed by extrusion of the Ongeluk volcanics, was responsible for exposing the clastic source for the Makganyene Formation and for the increased Kaapvaal continental freeboard. The latter counteracted the sea-level rise caused by increased mid-ocean ridge activity. In other words, relative sea level was kept low, but high enough to deposit the Makganyene Formation conformably on top of the Koegas Subgroup south of the Griquatown Hinge Zone (Polteau and Moore, 1999; Polteau, 2000; Moore et al, 2001, and this study in chapter II). But north of this zone, the Makganyene Formation rests directly on BIFs of the Asbestos Hills

Subgroup on a low angle unconformity that is the Subaerial Unconformity (SU) formed during the forced regression at the beginning of Koegas times (see figure V.6).

North of the Griquatown Hinge Zone, along this particular contact, neither striated glacial pavements nor glacial valleys were observed at any of the visited field localities, suggesting that the ice did not scrape the pavement. The Makganyene diamictite was therefore proximal, and may have resulted from sedimentation directly below an ice-shelf that dumped its load by basal melting (rainout diamictite). The ice-rafted material included rock flour and abundant faceted and striated clasts. However, coarse and immature sandstone lenss, which are characteristic of such a dynamic glacial environment, reflect underflow deposition. The Griquatown Hinge Zone represents the southern occurrence of this facies association. This suggests that basal melting dumped most of the ice-shelf material on the Ghaap plateau. In support of this is the thickness of the Makganyene Formation which decreases generally southward.

South of the Griquatown Hinge Zone and also in the Sishen area, the contact between the Makganyene Formation and the underlying strata is gradational and therefore conformable on the Koegas Subgroup. Immediately south of the Griquatown Hinge Zone, the base of the Makganyene Formation consists of bedded (debris-flow) to massive rainout diamictites that contain striated clasts and dropstones, and of sandstone lenss that are up to 100 wide and 5 metres thick and correspond to smaller channel lenss observed on the Ghaap platform. The sandstone lenss decrease and disappear southward where the Makganyene Formation consists only of bedded diamictite.

South of the Griquatown Hinge Zone, the top of the Makganyene Formation consists of diamictite set in a calcareous matrix that also contains stromatolitic clasts. This calcareous level forms a continuous layer. Destabilisation of the calcareous layer by episodic diamictite debris flows reworked and transported these peculiar calcareous deposits deeper into the basin. Further south, towards Prieska, the calcareous bodies form stromatolitic bioherms with or without clasts. Immediately overlying this is a similar facies to the Neoproterozoic cap-carbonates described by Kennedy et al. (1998), namely highly deformed black manganese-rich carbonate. The topmost part of the Makganyene Formation consists of diamictites interbedded with volcanic tuffs. The Ongeluk extrusive event (stage D of figure V.6) started before the end of the Makganyene glacial episode.

Four different glacial depositional styles are thus preserved in the deep Prieska Basin. The first one corresponds to the Koegas Subgroup, which represents the development of continental glaciers expressed by their associated distal submarine fan sedimentation (Naragas

Formation) and distal turbidite accumulation (Rooinekke Formation). The second style corresponds to the base of the Makganyene Formation with its typical ice-shelf deposits that commonly thin out offshore. The third style represents an ice retreat and decrease in clastic influx, which is characterised by offshore carbonate deposition and reworking, and early interglacial manganese deposition. The fourth depositional style corresponds with the mixed glacial/volcanic event that marked the end of the Makganyene Formation.

Floating ice shelves extended to the edge of the Ghaap platform. Deposition of BIFs was inhibited because ice shelves occupied their depositional sites. Primitive photosynthetic organisms were located where nutrients were available, off the shelf. Ferric iron was reduced to its previous ferrous state because the chemocline did not reach the sea floor (see figure V.6, stage C).

One immediate result of a glaciation is to change the overall oceanic circulation patterns. As shown in figure V.6, surface water is cooled at the ice contact, may freeze, become dense and sink to cause downwelling. The salinity would then increase because of the removal of water by freezing. Manganese is more soluble in such a solution and has a longer residence time (Mangini et al., 1994). Manganese would be able to migrate long distances from hydrothermal vents and its terrestrial sources (from weathering of carbonates) to the reducing glacial ocean where it concentrates (Mangini et al., 1994).

It is proposed in this study that glaciation was initiated due to a decrease in the amount of greenhouse gases such as CO_2 and CH_4 in the atmosphere. CO_2 was removed from the atmosphere by carbonate deposition (Campbellrand Subgroup) and also by subaerial weathering, and was supplied to the atmosphere by continuous volcanic outgassing.

Stage D of figure V.6 represents the extrusion of the andesitic basalts of the Ongeluk Formation that blanketed the entire basin. The Ongeluk volcanic episode certainly contributed to the replenishment of CO_2 back to the atmosphere to pre-Makganyene levels, which caused the end of the Makganyene glacial episode and the re-establishment of Ghaap Group depositional conditions.

Stage E of figure V.6 corresponds to the Voëlwater Subgroup. The end of the Makganyene glacial event implies melting of the ice that increased the volume of the oceans and initiated a transgression. However, both volcanic and glacial environments did not completely stop because hyaloclastites and diamictites are interbedded at the base of the Voëlwater Subgroup. The presence of dissolved manganese in the reducing glacial ocean

favoured its postglacial episodic deposition that was caused by sea level changes (Tsikos, 1999), by the rise in free oxygen in the surface water of the ocean and in the atmosphere. The chemical nature of the Voëlwater Subgroup implies similar stable tectonic conditions to those of the Ghaap Group.

V.3.3. The Snowball Earth hypothesis reconsidered

The present study of the Makganyene Formation sheds some light on the environmental conditions that were controlling the active processes during the Early Proterozoic. The most controversial hypothesis regarding this period is the Snowball Earth. Combining field observations, sequence stratigraphy, the depositional model, theorical paleoenvironmental conditions and geochemistry, new constraints are drawn for the Early Proterozoic Snowball Earth hypothesis and an alternative model will be proposed.

It appears that all the recorded Early Proterozoic glacial events are confined to the interval 2.4-2.2 Ga. This particular time marks the significant rise in free atmospheric oxygen (Bau et al., 1999) that was released into the atmosphere by primitive photosynthetic organisms living in shallow epeiric seas where nutrients were brought by upwelling (figure V.5) (Klein and Beukes, 1992, 1993). The Asbestos Hills BIFs were laid down on the drowned Ghaap platform by oxidation of Fe^{2+} in the surface waters. Oxygen in surface waters that did not react with iron was released into the atmosphere. Global temperatures would have gradually decreased with the consumption by photosynthetic organisms of atmospheric CO_2 that was massively deposited as carbonates on the Ghaap platform. The isotopic signature of carbonate minerals in the BIFs displays carbon isotopic values progressively more depleted in ^{13}C indicating gradual cooling. This is illustrated in figure IV.23. Gradual cooling contradicts sudden freezing inferred by the Snowball Earth hypothesis. Global circulation models (Jenkins and Frakes, 1998; Runnegar, 2000; Hyde et al., 2000; Poulsen et al., 2002) predict that Slushball Earth conditions are easily achieved, and it would take some time before the ice reached low latitudes because the ocean's thermal inertia initially resists the ice advance (Poulsen et al., 2002; Hoffman and Schrag, 2002). Life forms colonising shallow waters would have been drastically reduced. Cooling would have been enhanced by a superplume event (Nelson, 1998; Eriksson et al., 1999) that kept sea level high enough to prevent erosion and the formation of subaerial unconformities at least on the Ghaap platform of the Kaapvaal Craton.

In such a scenario, valley glaciers would form on exposed land and start their descent to the sea. Valley glaciers became grounded ice-sheets, and as they progressed into the ocean,

became floating ice-shelves that could have extended to the slope. The Snowball Earth does not allow long-lived wet-based glaciers. The continental shelf would no longer be the site of deposition of BIFs because the chemocline would not reach the ocean floor, and therefore any oxidised iron and manganese would be re-dissolved and their concentrations would steadily increase in the anoxic and stratified glacial ocean. Polynyas, localised upwellings of warm water commonly melting the ice shelf, were restricted sites nurturing early photosynthetic organisms that continuously produced oxygen. Meanwhile, CO_2 was accumulating in the atmosphere by volcanic degassing (Kirschvink, 1992; 2002; Hoffman and Schrag, 2002).

The atmospheric build-up of CO_2, aided by the Ongeluk volcanic episode, finally reached levels that triggered warming and progressive ice retreat. The accumulation on the ice-shelves of heat-absorbing black ash, which originated from the Ongeluk volcanic eruptions (volcanic tuffs observed below and above the basaltic andesites), promoted melting of the ice. The ice-retreat marks the onset of an explosion of primitive photosynthetic organisms.

Pre-glacial sea levels and ocean circulation patterns, with associated upwellings, were re-established. Salinity decreased, which diminished transport and solubility of manganese (Mangini, 1994; Bühn and Stanistreet, 1997). Upwelling brought iron and manganese onto the continental margin of the Kaapvaal Craton. Precipitation of iron or manganese occurred depending on specific redox conditions that have been widely investigated (Braterman et al., 1983; Frakes and Bolton, 1984; Ingri and Pontér, 1986; Roy, 1988; Frakes and Bolton, 1992; Bühn et al., 1992; Anbar and Holland, 1992; Urban et al., 1992; Schissel and Aro, 1992; Morris, 1993; Simonson and Assler, 1996; Barley et al., 1997; Tsikos and Moore, 1998; Tsikos, 1999).

The main theorical constraints of iron and manganese deposition depend on the relative sea level that controlled the Eh-pH conditions of seawater, on the paleoclimatic variations and on the paleoenvironmental setting. Redox processes fractionated manganese from iron in shallow basinal environments during transgressive-regressive sequences (Bühn and Stanistreet, 1997; Glasby, 1997). Tsikos (1999) concluded that manganese deposition in the Kalahari Manganese Field occurred during regressive stages, while iron precipitation took place during transgressive events, thus explaining the intimate association of BIFs and manganese ore. The inferred rapid sea-level changes (Tsikos and Moore, 1998; Tsikos, 1999) are attributed to changes in mid-ocean ridge activity related to drifting after supercontinental break-up (Gurnis, 1988; Gaál, 1990, 1992; Schissel and Aro, 1992; Bühn and Stanistreet,

1997; Aspler and Chiarenzelli 1997; Condie et al., 2001; Eriksson et al., 2001) prior to another aggregation.
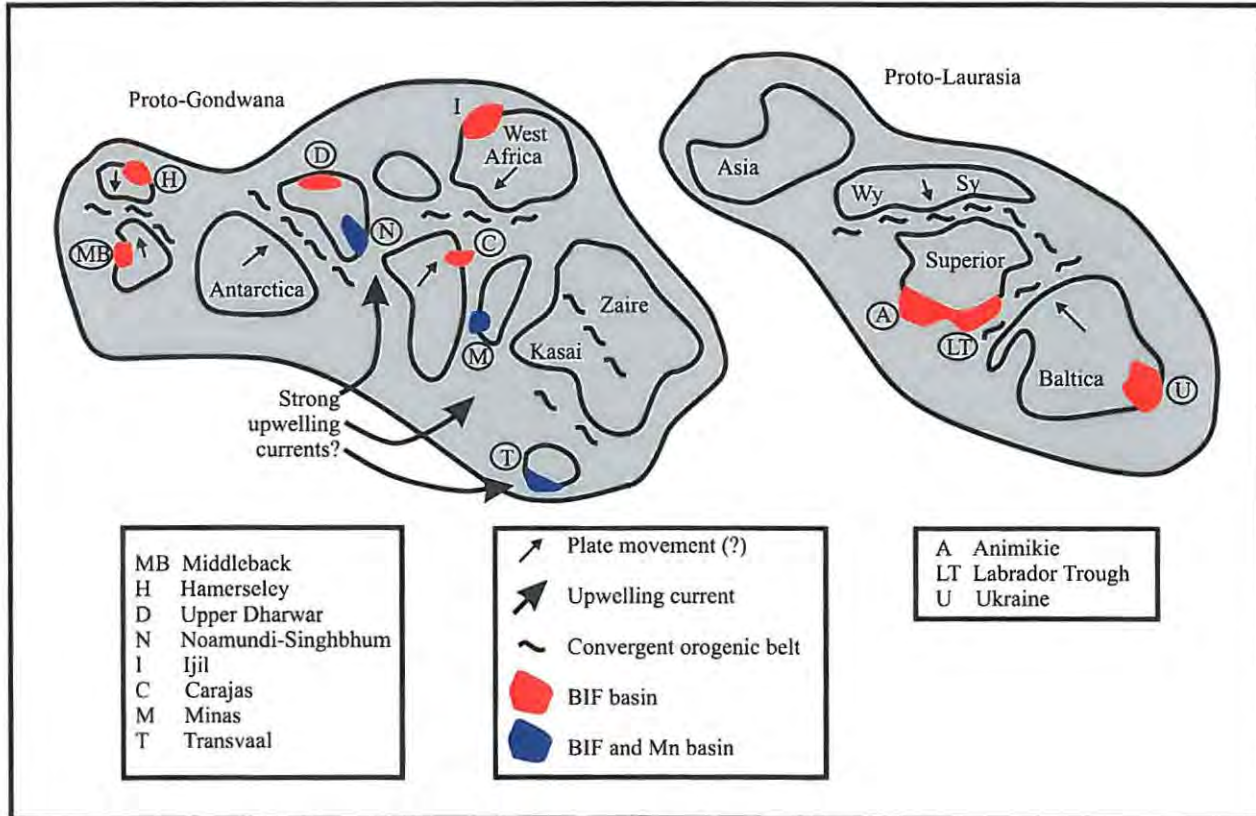
Figure V.7. Distribution of Early Proterozoic basins with major iron-manganese formations on a continental reconstruction prior to Proterozoic supercontinent disaggregation (from Schissel and Aro, 1992).

Figure V.7 (from Schissel and Aro, 1992) shows the distribution of the different Early Proterozoic basins and their major iron and manganese deposits. Manganese deposits are located in areas of strong upwelling currents located preferentially in the lower proto-Gondwanaland (Schissel and Aro, 1992). In contrast, the northern supercontinent does not have any occurrences of manganese deposits within associated BIFs. According to Schissel and Aro (1992), the Early Proterozoic paleogeography controlled the formation of BIFs and manganese and they postulated that strong upwelling currents, bringing large volumes of deep anoxic waters onto the shallow continental shelves, promoted the giant manganese accumulations, such as the Kalahari Manganese Field.

The Makganyene glacial episode is responsible for the transport, accumulation and preservation of manganese and iron in solution in the anoxic glacial ocean, and deglaciation triggered the massive manganese precipitation of the Kalahari Manganese Field 2.4 Ga ago.

This Slushball Earth model is a compromise of the Snowball Earth hypothesis, and the precise geological and geochemical processes that were active during the first Proterozoic major glaciation in the Transvaal Supergroup. It explains:

➤ the apparent association of BIFs with Early Proterozoic glacial deposits;

➤ recorded rise of oxygen that triggered glaciation;

➤ a process to allow the continued production of oxygen (i.e. open waters);

➤ the transport and deposition of the diamictites;

➤ low-latitude glaciation;

➤ a simple process to terminate a glacial event (CO_2 increase together with accumulation of heat-absorbing black ash on the ice).

V.4. Conclusions and suggestions for further studies

This study provides significant new interpretations of the stratigraphy of the Transvaal Supergroup by examining the Makganyene Formation, a poorly studied and controversial portion of the sedimentary succession across the Griqualand West Basin. In the main mining areas located on the Maremane Dome, the Transvaal Supergroup has been thrusted on itself. The sole of the thrust fault commonly consists of the Makganyene Formation. This situation resulted in an incorrect interpretation of the stratigraphy that was based primarily on borehole logging at the Sishen Iron Mine. This led to the inclusion in the Transvaal Supergroup, of a younger unit, the Gamagara Formation of the Olifantshoek Supergroup. Field work is usually motivated by economic interest, and since the Makganyene Formation does not directly bear significant ore deposits, little work has been done to clarify its stratigraphic attributes.

Previous research done by the author (Polteau, 2000) was restricted to the Rooinekke Mine area. The localities investigated showed that the Makganyene was resting conformably and gradationally on the Koegas Subgroup. A similar study has been carried out regionally, examining the basal contact and facies changes of the Makganyene Formation and of the Koegas Subgroup.

The Koegas Subgroup consists mainly of clastic sediments that are characteristic of submarine fan deposition and distal turbidites. The Nagaras Formation, with its alternating shales and siltstones, represents the submarine fan facies. The Rooinekke Formation

corresponds to turbidites associated with stromatolitic bioherms and has mixed chemical/clastic characteristics. The Griquatown Hinge Zone is generally interpreted as a fault zone. It has been proposed that the Koegas Subgroup ended abruptly against one of these normal faults that were active during the Campbellrand carbonate deposition (Altermann, 1997). However, the Koegas Subgroup appears to pinch out in this zone, which is interpreted as representing the edge of the basin. In other words, the Griquatown Fault Zone corresponds rather to a hinge zone during the Koegas Subgroup and Postmasburg Group period. On the carbonate Ghaap platform, lacustrine deposits have been described by Beukes (1983) and are located at the Griquatown BIFs-Koegas Subgroup transition. South of the Griquatown Hinge Zone, the Koegas Subgroup has progressively deeper submarine facies and rests conformably on the Asbestos Hills BIFs (Beukes, 1983). A diamictite lens has been mapped near the base of the Koegas Subgroup indicating an early glacial influence.

The Makganyene Formation rests conformably on the Koegas Subgroup wherever it is present. In the Sishen area, the base of the diamictite is clearly interbedded with some BIFs that are assigned to the Koegas Subgroup. The Griquatown Hinge Zone is a key locality since it is the place where the entire Koegas Subgroup pinches out, placing the Makganyene Formation on an unconformity with the underlying Asbestos Hills Subgroup. The unconformity present on the Ghaap platform represents the entire Koegas package and corresponds to the erosional event (possibly subglacial ice scouring) that affected the Vryburg Arch during Koegas times. In the Hotazel area, the diamictite rests unconformably on peloidstone BIFs of the Asbestos Hills Subgroup, characteristic of a shallow high-energy environment of deposition, but representing also the unconformity surface.

The stromatolitic bioherms within the Makganyene diamictite are only present south of the Griquatown Hinge Zone. They are best preserved in the southern localities as bioherms with/without clasts. Further north, these calcareous bodies thin out and are replaced by clastic sheets, until they completely disappear about 20 kilometres south of the Griquatown Hinge Zone to be replaced by sandstone lenss on the Ghaap platform. The Ongeluk Formation is interbedded with the topmost portion of the diamictite, thus implying contemporaneous volcanism and glaciation.

The base of the Voëlwater Subgroup, the Hotazel Formation, marks the final glacial retreat with fine diamictites that are interbedded with BIFs and hyaloclastites. The rest of the Hotazel Formation contains BIFs that are interbedded with the world's largest sedimentary manganese deposit, the Kalahari Manganese Field. The Mooidraai Formation of the upper

Voëlwater Subgroup consists of carbonates and represents the end of the Transvaal Supergroup deposition in the Griqualand West Basin.

Petrographic studies have been carried out on the different rock types of the Makganyene Formation and the base of the Hotazel Formation. All lithologies described reveal mineral assemblages that are diagnostic of early to late diagenetic crystallisation and of low-grade metamorphism not exceeding the very low green-schist facies.

The Asbestos Hills BIFs display facies deepening from allochtonous graded peloidstones of the Hotazel area to more typical autochtonous band-rhythmites to pillow-rhythmites southward. The BIFs from the base of the Hotazel Formation define the following cycle of deposition below the first manganese ore bed: hematite band-rhythmite – greenalite-magnetite rhythmites – calcite-magnetite rhythmites – hematite band-rhythmite.

Both the Makganyene and Hotazel diamictites consist of heterogeneous clasts set in a very fine-grained matrix. The Makganyene diamictite contains clasts of volcanic tuffs, stromatolites, chert, peloidstone and sulphide. The Makganyene diamictite contains clasts of Asbestos Hills rock types that could indicate transport from northeast to southwest. In the Matsap area, the presence of dropstones implies the presence of floating ice-shelves.

The Hotazel diamictite is stilpnomelane-rich giving the rock its characteristic brown colour. It contains small clasts that outline the bedding, as well as abundant dropstones indicating a glacial origin.

The Makganyene volcanic tuffs consist of 2-3 cm thick stacked fine-grained graded cycles. They are interpreted as being deposited after distal subaerial volcanic eruptions. They also cover virtually the entire surface area of the Griqualand West Basin. The Hotazel volcanic tuffs are more proximal and consist of volcanic shards and spherules set in a glassy matrix. They are interpreted as being hyaloclastites.

All the BIFs from the Transvaal Supergroup in the Griqualand West Basin share similar geochemical compositions that are characteristic of Superior-type BIFs. The genetic implication is that iron (and Mn) in BIFs did not derive from a proximal hydrothermal source.

Whole-rock geochemical compositions allowed direct comparisons between the Makganyene diamictites from different localities and also comparisons between the diamictites from below and above the Ongeluk Formation. Both diamictites have similar geochemical compositions that reflect the source rocks. The Makganyene diamictite is derived primarily from the weathering and transport of carbonates and BIFs, and contains a

pelitic/granitic component. Compositional variations have been observed at the different localities investigated, and correspond to sorting processes and paleoenvironmental conditions. Diamictites from the Ghaap platform (Hotazel and Sishen area) show the characteristics of a carbonate platform with higher proportions of Ca, Fe, P and Mg than the deeper-water Matsap localities. The Ghaap platform area also contains high Na concentrations related to late Na-metasomatism. On the other hand, the slope facies (Matsap area) is characterised by higher detrital elements, such as Al, Ti, K and most trace elements, all of which belong to the fine clay detrital component. The granitic basement of the Kaapvaal Craton represents the minor crustal component present within the diamictite. A geochemical stratigraphic trend is observed in the Makganyene Formation, by an upward decrease in iron and an increase in carbonate (Ca, Mg), which is interpreted as reflecting carbonate deposition in the uppermost part of the Makganyene Formation, as observed in the southern localities.

The Hotazel diamictite, which occurs at the base of the Hotazel Formation, was deposited in a similar environment to the Makganyene diamictite of the Hotazel area, and is therefore characteristic of the Ghaap platform facies. The Hotazel diamictite has a similar composition to that of the Makganyene diamictite. Both diamictites have similar source rocks, primarily BIFs. Since it is interbedded with hyaloclastites, however, the Hotazel diamictite has incorporated some volcanic material from the Ongeluk Formation and thus shows a partly basic volcanic signature.

The carbon and oxygen stable isotopic curves of the entire Transvaal Supergroup succession in the Griqualand West Basin display a progressive negative incursion centred on the glacial event. This incursion is interpreted as representing the shift from warm to cold and back to warm paleoclimatic conditions.

Sequence stratigraphy is based on the recognition of contacts separating the different systems tracts that compose a depositional sequence. However, the current model (Beukes, 1983) is incorrect because the basal contact of the Makganyene Formation is of a different nature to that described in literature. Therefore any intracratonic basin correlations, specifically between the Griqualand West and the Transvaal basins, based on lithostratigraphic similarities and extrapolations of unconformities, have to be reviewed, especially since newly published radiometric ages (Bau et al., 1999) disagree with previously proposed correlations.

The basal contacts of the Makganyene Formation with the Koegas Subgroup have been re-assessed. In sequence stratigraphic terms, the Asbestos Hills Subgroup represents the

184

Transgressive Systems tract (TST) and Highstand Systems tract (HST). The Koegas Subgroup, identified with its distal facies restricted off the shelf edge, and with its Subaerial Unconformity (SU) and correlative conformity (cc), corresponds to the Falling Stage Systems tract (FSST). The Makganyene Formation forms the Low Stand Systems tract (LST) and the Transgressive Systems tract (TST) corresponds to the Voëlwater Subgroup. Identification of systems tracts has led to the current re-appraisal of the intracratonic basinal correlations. This confirms the correlations of Polteau (2000) as being the most reliable, because they integrate the new radiometric ages of the Mooidraai Formation (2.394 Ga, Bau et al., 1999) and the Koegas Subgroup (2.415 Ga, Kirschvink et al., 2000) with the sequence stratigraphy concept. In this model, only the Ghaap and Chuniespoort Groups are confirmed as time equivalents. It is proposed that the Koegas Subgroup, together with the Postmasburg Group, do not have any equivalent in the Transvaal Basin. The Duitschland Formation, however, could be a potential correlative to the entire Postmasburg Group because it consists, as the Postmasburg Group, of a basal diamictite, andesitic volcanics and carbonates. The immediate consequences are that the Pretoria Group of the Transvaal Basin should not be part of the rest of the Transvaal Supergroup and may be correlated to the younger Gamagara/Mapedi Formation of the Olifantshoek Supergroup (Evans et al., 2002). The Transvaal Supergroup in the Griqualand West Basin represents a single continuous depositional sequence that lasted approximately 200 Ma. This is in contrast with the 450 Ma duration estimated in previous studies.

The Makganyene Formation, and also many Early and Late Proterozoic glacial deposits apparently accumulated within 30° of the equator. Different models have been proposed to explain the development of ice shelves at sea level in low-paleolatitude positions. However, none of the proposed models so far explain all the features observed in the Proterozoic glacial deposits. A literature review of the different Early Proterozoic paleoenvironments, combined with observations made during this project, has led to the proposal of a compromised Snowball Earth model, namely the Softball or Slushball Earth model. The Slushball Earth model corresponds to a frozen Earth with portions of ice-free ocean within the tropics. This model explains all the unusual geological features observed in the Early Proterozoic glacial deposits, especially the Makganyene Formation, but also explains the occurrence of the post-glacial Kalahari Manganese Field.

The data and interpretations presented in this thesis will hopefully be used as a base for future research on the Transvaal Supergroup in the Griqualand West Basin, whilst they can also be tested in other Early Proterozoic basins. However, such an extensive one-man

185

fieldwork based project bears obvious limitations. Researchers in the Griqualand West Basin concentrate their efforts in the study of ore deposits and too often forget the sedimentary basin that hosts them. Because mining activities are centered on the Ghaap platform, the outcrop area of the Koegas Subgroup has been poorly studied (unless there was a mine nearby such as the Rooinekke Mine) and therefore lends itself for further study.

Specifically, the relationship between the base of the Koegas Subgroup with the top of the Asbestos Hills BIFs was not assessed in this thesis, and is assumed to be a correlative conformity (cc). A diamictite lens was observed at the base of the Koegas Subgroup. Therefore additional studies on the Koegas Subgroup are recommended to determine whether or not it corresponds to a distal glacial setting.

REE studies could be important in evaluating more accurately the proportions of the different sources of the Makganyene and Hotazel diamictites. The isotopic composition of organic carbon in the Makganyene and Hotazel diamictites could assess the importance of methane as an important greenhouse gas prior to the Makganyene glacial event and indirectly as a marker for the rise in atmospheric oxygen. Accurate geochronological studies can be carried out on the different Early Proterozoic glacial formations worldwide to determine their synchronicity or not. Finally, to test the contiguity of the Kaapvaal and Pilbara Cratons at around 2.4 Ga, provenance studies on the Turee Creek and Koegas rocks should be carried out in order to compare their respective source rocks. If they share identical origins, then the Kaapvaal and Pilbara Cratons probably were adjacent to each other.

The proposed depositional model, with all the hypotheses involved in its elaboration, may provide a solid framework for further work on Early Proterozoic geological paleoenvironments. Undoubtly many modifications will be needed as soon as new data emerge, but some enigmatic aspects of the Transvaal depositional environment will remain. The Griqualand West Basin, which is a never-ending source of information on the Early Proterozoic paleoenvironmental conditions, will continue to challenge many geologists in the future.

CHAPTER VI

References

Abbott D., and Menke W. (1990) –Length of the Global Plate Boundary at 2.4 Ga- Geology (18), 58-61.

Aitken J.D. (1991) –Two Late Proterozoic Glaciations, Mackenzie Mountains, North-Western Canada- Geology (19), 445-448.

Alley R.B., Balkenship D.D., Rooney S.T., and Bentley C.R. (1989) – Sedimentation beneath Ice Shelves – the View from Ice Stream B- Marine Geology (85), 101-120.

Altermann W. (1996) –Sedimentology, Geochemistry and Paleogeographic Implications of volcanic Rocks in the Upper Archaean Campbell Group, Western Kaapvaal Craton, South Africa- Precambrian Research (79), 73-100.

Altermann W. (1997) –Sedimentological Evaluation of Pb-Zn Exploration Potential of the Precambrian Griquatown Fault Zone in the Northern Cape Province, South Africa- Mineralium Deposita (32), 382-391.

Altermann W., and Herbig H.-G (1991) –Tidal Flats Deposits of the Lower Proterozoic Campbell Group Along the South-western Margin of the Kaapvaal Craton, Northern Cape Province, South Africa- Journal of African Earth Science (13), 415-435.

Altermann W., and Schopf J.W. (1995) –Microfossils from the Neoarchaean Campbell Group, Griqualand West Sequence of the Transvaal Supergroup, and their Paleoenvironmental and Evolutionary Implications- Precambrian Research (75), 65-90.

Altermann W., and Hälbich I.W. (1990) –Thrusting, Folding and Stratigraphy of the Ghaap Group Along the South-western Margin of the Kaapvaal Craton- South African Journal of Geology (93), 553-566.

Altermann W., and Hälbich I.W. (1991) –Structural History of the South-western Corner of the Kaapvaal Craton and the Adjacent Namaqua Real: New Observations and a Reappraisal- Precambrian Research (52), 133-166.

Altermann W., and Nelson D.R. (1998) –Sedimentation rates, Basin Analysis and regional Correlations of Three Neoarchaean and Paleoproterozoic Sub-Basins of the

Kaapvaal Craton as Inferred From Precise U-Pb Zircon Ages from Volcaniclastic Sediments- Sedimentary Geology (120), 225-256.

Anbar A.D., and Holland H.D. (1992) -The Photochemistry of Manganese and the Origin of Banded Iron Formations- Geochimica et Cosmochimica Acta (56), 2595-2603.

Anderson J.B., and Ashley G.M. (1991) –Glacial Marine Sedimentation; Paleoclimatic Significance; a Discussion- *In*: Glacial Marine Sedimentation: Paleoclimatic Significance, Anderson J.B., and Ashley G.M. Editors, Geological Society of America Special Paper 261, 223-226.

Anderson J.B., and Domack F.W. (1991) –Foreword- *In*: Glacial Marine Sedimentation: Paleoclimatic Significance, Anderson J.B., and Ashley G.M. Editors, Geological Society of America Special Paper 261, v-viii.

Anderson J.B., Kennedy D.S., Smith M.J., and Domack E.W. (1991) – Sedimentary Facies Associated with Antarctica's Floating Ice Masses- *In*: Glacial Marine Sedimentation: Paleoclimatic Significance, Anderson J.B., and Ashley G.M. Editors, Geological Society of America Special Paper 261, 1-26.

Anderson J.B., Kurtz D.D., Domack E.W., and Balsaw K.M. (1980) –Glacial and Glacial Marine Sediments of the Antarctic Continental Shelf- Journal of Geology (88), 399-414.

Andrews J.E., Brimblecombe P., Jickells T.D. and Liss P.S. (1996) -An Introduction to Environmental Chemistry- Blackwell Science, 209pp.

Armstrong R.A., Compston W., and Retief EA (1991) –Zircon Ion Microprobe Studies Bearing on the Age and Evolution of the Witwatersrand Triad- Precambrian Research (53), 243-266.

Ashley G.M., Boothroyd J.C., and Borns W.Jr. (1991) –Sedimentology of Late Pleistocene (Laurentide) Deglacial Phase Deposits, Eastern Maine; an Example of a temperate Marine Grounded Ice-Sheet Margin- *In*: Glacial Marine Sedimentation: Paleoclimatic Significance, Anderson J.B., and Ashley G.M. Editors, Geological Society of America Special Paper 261, 107-126.

Aspler L.B., and Chiarenzelli J.R. (1997) –Initiation of ≈2.45-2.1 Ga Intracratonic Basin Sedimentation of the Hurwitz Group, Keewatin Hinterland, Northwest Territories, Canada- Precambrian Research (81), 265-297.

Aspler L.B., and Chiarenzelli J.R. (1998) –Two Neoarchaean Supercontinents? Evidence from the Paleoproterozoic- Sedimentary Geology (120), 75-104.

Barnola J.M., Raynaud D., Korotkevich Y.S., and Lorius C. (1987) –Vostok Ice Core Provides 160,000-Year Record of Atmospheric CO_2- Nature (329), 408-414.

Bartek L.R., and Anderson J.B. (1991) –Facies Distribution Resulting from Sedimentation Under Polar Interglacial Climatic Conditions Within High-Latitude Marginal Basin, McMurdo Sound, Antarctica- *In*: Glacial Marine Sedimentation: Paleoclimatic Significance, Anderson J.B., and Ashley G.M. Editors, Geological Society of America Special Paper 261, 27-50.

Bau M., and Dulski P. (1996) –Distribution of Yttrium and rare-Earth Elements in the Penge and Kuruman Iron-Formations, Transvaal Supergroup, South Africa- Precambrian Research (79), 37-56.

Bau M., Romer R.L., Lüders V., and Beukes N.J. (1999) –Pb, O, and C Isotopes in Silicified Mooidraai Dolomite (Transvaal Supergroup, South Africa): Implications for the Composition of Paleoproterozoic Seawater and 'Dating' the Increase of Oxygen in the Precambrian Atmosphere- Earth and Planetary Science Letters (174), 43-57.

Beaumont V., and Robert F. (1999) –Nitrogen Isotope Ratios of Kerogens in Precambrian Chert: a Record of the Evolution of Atmosphere Chemistry?- Precambrian Research (96), 63-82.

Becker R.H., and Clayton R.N. (1972) –Carbon Isotopic Evidence for the Origin of a Banded Iron-Formation in Western Australia- Geochimica et Cosmochimica Acta (36), 577-595.

Bekker A., Kaufman A.J., Karhu J.A., Beukes N.J., Swart Q.D., Coetzee L.L., and Eriksson K.A. (2001) –Chemostratigraphy of the Paleoproterozoic Duitschland Formation, South Africa: Implications for Coupled Climate Change and Carbon Cycling- American Journal of Science (301), 261-285:

Beukes N.J. (1980) –Lithofacies and Stratigraphy of the Kuruman and Griquatown Iron Formations, Northern Cape Province, South Africa- Transactions of the Geological Society of South Africa (83), 69-86.

Beukes N.J. (1983) –Palaeoenvironmental Setting of Iron-Formations in the Depositional Basin of the Transvaal Supergroup, South Africa- *In*: Trendall A.F. and Morris S.C. Editors, Iron-Formations, Facts and Problems, Elsevier, Amsterdam, 131-209.

Beukes N.J. (1984) –Sedimentology of the Kuruman Iron-Formations, Transvaal Supergroup, Griqualand West, South Africa- Precambrian research (24), 47-84.

Beukes N.J. (1986) –The Transvaal Sequence in Griqualand West- *In:* Mineral deposits of Southern Africa, Anhaeusser C.R., and Maske S. Editors, Geological Society of South Africa, Johannesburg, 819-828.

Beukes N.J., and Smit C.A. (1987) –New Evidence for Thrust Faulting in Griqualand West, South Africa: Implication for Stratigraphy and the Age of Red Beds- Transactions of the Geological Society of South Africa (90), 378-394.

Beukes N.J., and Klein C. (1990) -Geochemistry and Sedimentology of a Facies Transition -from Microbanded to Granular Iron-Formation- in The Early Proterozoic Transvaal Supergroup, South Africa- Precambrian research (47), 99-139.

Beukes N.J., Klein C., Kaufman A.J., and Hayes J.M. (1990) –Carbonate Petrography, Kerogen Distribution, and Carbon and Oxygen Isotope Variations in an Early Proterozoic Transition from Limestone to Iron-Formation Deposition, Transvaal Supergroup, South Africa- Economic Geology (85), 663-690.

Beukes N.J., Burger A.M., and Gutzmer J. (1995) –Fault-Controlled Hydrothermal Alteration of the Paleoproterozoic Manganese Ore in Wessels Mine, Kalahari Manganese Field- South African Journal of Geology (4), 430-451.

Bhatia M.R., and Crook K.A.W (1986) -Trace Element Characteristics of Graywackes and Tectonic Setting Discrimination of Sedimentary Basins- Contributions to Mineralogy and Petrology (92), 181-193.

Bills B.G. (1998) –An Oblique View of Climate- Nature (396), 405-406.

Bond G.C., Nickeson P.A., and Kominz M.A. (1984) –Breakup of a Supercontinent between 625 Ma and 555 Ma: New Evidence and Implications for Continental Histories- Earth and Planetary Science Letters (70), 325-345.

Braterman P.S., Cairns-Smith A.G., and Sloper R.W. (1983) –Photo-Oxidation of Hydrated Fe^{2+} -Significance for Banded Iron Formations- Nature (303), 163-164.

Brown D.A., Gross G.A., and Sawicki J.A. (1995) –A Review of the Microbial Geochemistry of Banded Iron-Formations- Canadian Mineralogist (33), 1321-1333.

Buick I.S., Uken R., Gibson R.L., and Wallmach T. (1998) – High-δ^{13}C Paleoproterozoic Carbonates from the Transvaal Supergroup, South Africa- Geology (26), 875-878.

Bühn B., and Stanistreet I.G (1997) – Insight Into the Enigma of Neoproterozoic Manganese and Iron Formations From the Perspective of Supercontinental Break-up and Glaciation- *In*: Manganese Mineralisation: Geochemistry and Mineralogy of

Terrestrial and Marine Deposits; Nicholson K., Hein J.R., Bühn B., and Dasgupta S. Editors, Geological Society Special Publication NO 119, The Geological Society of London, 81-90.

Bühn B., Stanistreet I.G., and Okrusch M. (1992) –Late Proterozoic Outer Shelf Manganese and Iron Deposits at Otjosondu (Namibia) Related to the Damaran Oceanic Opening- Economic Geology (87), 1393-1411.

Burdett J.W., Grotzinger J.P., and Arthur M.A. (1990) –Did Major Changes in the Stable-Isotope Composition of Proterozoic Seawater Occur?- Geology (18), 227-230.

Button A. (1986) –The Transvaal Sub-Basin of the Transvaal Sequence- In: Anhaeusser C.R., Maske S. Editors, Mineral Deposits of Southern Africa, Geological Society of South Africa, Johannesburg, 811-817.

Cairns A. (2001) –Snowball Fight in Edinburgh- http://www.eurekalert.org/pub8releases/2001-06/GsoA-SfiE-2006101.php

Cameron E.M. (1982) –Sulphate and Sulphate Reduction in the Early Precambrian Oceans- Nature (296), 145-148.

Carlson P.R. (1989) –Seismic Reflection Characteristics of Glacial and Glaciomarine Sediment in the Gulf of Alaska and Adjacent Fjords- Marine Geology (83), 391-416.

Carrigan W.J., and Cameron E.M. (1991) –Petrological and Stable Isotope Studies of carbonate and Sulfide Minerals from the Gunflint Formation, Ontario: Evidence for the Origin of Early Proterozoic Iron-Formation- Precambrian Research (52), 347-380.

Catuneanu O., and Eriksson P.G. (1999) –The Sequence Stratigraphic Concept and the Precambrian Rock Record: an Example from the 2.7-2.1 Ga Transvaal Supergroup, Kaapvaal Craton- Precambrian Research (97), 215-251.

Chan M.A., Kvale E.P., Archer A.W., and Sonett C.P. (1994) –Oldest Direct Evidence of Lunar-Solar Tidal Forcing Encoded in Sedimentary Rhythmites, Proterozoic Big Cottonwood Formation, Central Utah- Geology (22), 791-794.

Cheney E.S. (1996) –Sequence Stratigraphy and Plate Tectonic Significance of the Transvaal Succession of Southern Africa and Its Equivalent in Western Australia- Precambrian Research (79), 3-24.

Cheney E.S., and de la Winter H. (1995) –The Late to Mesoproterozoic Major Unconformity-Bounded Units of the Kaapvaal Province of Southern Africa- Precambrian Research (74), 203-223.

Cheney E.S., Roering C., and de la Winter H. (1990) –The Archaean-Proterozoic Boundary in the Kaapvaal Province of Southern Africa- Precambrian Research (46), 329-340.

Chumakov N.M., and Elston D.P. (1989) –The Paradox of Late Proterozoic Glaciations at Low Latitudes- Episodes (12), 115-120.

Clemmey H., and Badham N. (1982) –Oxygen in the Precambrian Atmosphere: an Evaluation of the Geological Evidence- Geology (10), 141-146.

Clendenin C.W., Charlesworth E.G., and Maske S. (1988) –An Early Proterozoic Three-Stage Rift System, Kaapvaal Craton, South Africa- Tectonophysics (145), 73-86.

Clendenin C.W. (1989) –Tectonic Influence on the Evolution of the Early Proterozoic Transvaal Sea, Southern Africa- Unpublished PhD thesis, University of Witwatersrand, Johannesburg.

Coetzee L. L. (2002) - Genetic stratigraphy of the Paleoproterozoic Pretoria Group in the Western Transvaal- Unpublished M.Sc. thesis, Rand Afrikaans University, South Africa, 212pp.

Condie K.C. (1986) -Geochemistry and Tectonic Setting of Early Proterozoic Supracrustal Rocks in the Southwestern United States- Journal of Geology (94), 845-864.

Condie K.C., and Wronkiewicz D.J. (1990) -The Cr/Th Ratio in Precambrian Pelites From the Kaapvaal Craton as an Index of Craton Evolution- Earth and Planetary Science Letters (97), 256-267.

Condie K.C., Des Marais D.J., and Abbott D. (2001) –Precambrian Superplumes and Supercontinents: a Record in Black Shales, Carbon Isotopes, and Paleoclimates?- Precambrian Research (106), 239-260.

Conybeare C.E.B., and Crook K.A.W. (1968) –Manual of Sedimentary Structures- Bureau of Mineral Resources, Geology and Geophysics, Canberra, Bulletin 102, 327pp.

Cornell D.H., and Schütte S.S. (1995) -A Volcanic-Exhalative Origin for the World's Largest (Kalahari) Manganese Field- Mineralium Deposita (30), 146–151.

Cornell D.H., Schütte S.S., and Eglington B.L. (1996) –The Ongeluk Basaltic Andesite Formation in Griqualand West, South Africa: Submarine Alteration in a 2222 Ma Proterozoic Sea- Precambrian Research (79), 101-123.

Cowan E.A., and Powell R.D. (1991) –Ice-Proximal Sediment Accumulation Rates in a Temperate Glacial Fjord, South-Eastern Alaska- *In*: Glacial Marine Sedimentation: Paleoclimatic Significance, Anderson J.B., and Ashley G.M. Editors, Geological Society of America Special Paper 261, 61-74.

Cowen R. (2002) –Planktonic Paradise on Slushball Earth: a Scenario for the Metazoan Radiation- http://quartz.ucdavis.edu/~GEL3/slushball.htlm

Crockett R.N. (1972) –The Transvaal System in Botswana: its Geotectonic and Depositional Environment and Special Problems- Transactions of the Geological Society of South Africa (75), 275-292.

Crossing A.R., and Gostin V.A. (1994) –Isotopic Signatures of Carbonates Associated with Sturtian (Neoproterozoic) Glacial Facies, Central Flinders Ranges, South Australia- *In* :Earth's Glacial Record; Deynoux M., Miller J.M.G., Domack E.W., Eyles N., Fairchild I.J., and Young G.M. Editors, Cambridge University Press, 165-175.

Crowley T.J., and Baum S.K. (1993) –Effect of Decreased Solar Luminosity on Late Precambrian Ice Extent- Journal of Physical Research (98), 16723-16732.

Dalziel I.W.D. (1995) –Earth before Pangea- Scientific American (January) 58-63.

Dalziel I.W.D. (1997) –Neoproterozoic-Paleozoic Geography and Tectonics: Review, Hypothesis, Environmental Speculation- Geological Society of America Bulletin (109), 16-42.

Dehler C.M., Elrick M., Karlstrom K.E., Smith G.A., Crossey L.J., and Timmons J.M. (2001) –Neoproterozoic Chuar Group (~800-742 Ma), Grand Canyon: a Record of Cyclic Marine Deposition during Global Cooling and Supercontinent Rifting- Sedimentary Geology (141-142), 465-499.

Derry L.A., Kaufman A.J., and Jacobsen S.B. (1992) –Sedimentary Cycling and Environmental Change in the Late Proterozoic: Evidence from Stable and Radiogenic Isotopes- Geochimica et Cosmochimica Acta (56), 1317-1329.

Des Marais D.J. (1994) –Tectonic Control of the Crustal Organic Carbon Reservoir during the Precambrian- Chemical Geology (114), 303-314.

Des Marais D.J., Strauss H., Summons R.E., and Hayes J.M. (1992) – Carbon Isotope Evidence for the Stepwise Oxidation of the Proterozoic Environment- Nature (359), 605-608.

De Villiers J.E. (1983) –The Manganese Deposits of Griqualand West, South Africa: Some Mineralogic Aspects- Economic Geology (78), 1108-1118.

De Villiers P.R. (1967) –New Stratigraphic Correlation and Interpretation of the Geological Structure of the Postmasburg-Sishen Area- Geological Survey Annals of South Africa (6), 39-42.

De Villiers P.R., and Visser J.N.J. (1977) –The Glacial Beds of the Griqualand West Supergroup as Revealed by Four Deep Boreholes Between Postmasburg and Sishen-Transactions of the Geological Society of South Africa (80), 1-8.

De Wit J. M., Roering C., Hart R.J., Armstrong R.A., De Ronde C.E.J., Green R.W.E., Tredoux M., Peberdy E., and Hart R.A. (1992) –Formation of an Archaean Continent- Nature (357), 553-562.

Deynoux M., Miller J.M.G., Domack E.W., Eyles N., Fairchild I.J., Young G.M. (1994) –Preface- *In*: Earth's Glacial Record; Deynoux M., Miller J.M.G., Domack E.W., Eyles N., Fairchild I.J., Young G.M. Editors, Cambridge University Press, 226pp.

Dixon R.D. (1985) –Sugilite and Associated Minerals from Wessels Mine, Kalahari Manganese Field- Transactions of the Geological Society of South Africa (88), 11-17.

Domack E.W., and Lawson D.E. (1985) –Pebble Fabric in an Ice-Rafted Diamicton-Journal of Geology (93), 577-591.

Donnadieu Y., Fluteau Y., Ramstein G., Ritz C., and Besse J. (2003) –Is There a Conflict Between the Neoproterozoic Glacial Deposits and the Snowball Earth Interpretation: an Improved Understanding With Numerical Modeling- Earth and Planetary Science Letters (208), 101-112.

Donnelly T.H. (1979) –Discussion: Sedimentology, Stable-Isotope Geochemistry and Paleoenvironment of Dolostones Capping Late Precambrian Glacial Sequences in Australia- Journal of the Geological Society of Australia (28), 99-101.

Dreimanis A. (1983) –Quaternary Glacial Deposits: Implications for the Interpretation of Proterozoic Glacial Deposits- Geological Society of America Memoirs (161), 299-307.

Drewry D. (1986) -Glacial Geologic Processes- Edward A. Publisher, British Library.

Dunn P.J., Brummer J.J., and Belsky H. (1980) –Sugilite, a Second Occurrence: Wessels Mine, Kalahari Manganese Field, Republic of South Africa- Canadian Mineralogist (18), 37-39.

Du Toit A.L. (1954) –Geology of South Africa- Oliver and Boyd Editors, Edinburgh, 611pp.

Embleton B.J.J., and Williams G.E. (1986) –Low Paleolatitude of Deposition for Late Precambrian Periglacial Varvites in South Australia: Implications for paleoclimatology- Earth and Planetary Science letters (79), 419-430.

Eriksson P.G. (1999) –Sea Level Changes and the Continental Freeboard Concept: General Principles and Application to the Precambrian- Precambrian Research (97), 143-154.

Eriksson P.G., and Reczko B.F.F. (1995) –The Sedimentary and tectonic setting of the Transvaal Supergroup Floor Rocks to the Bushveld Complex- Journal of African Earth Sciences (21), 487-504.

Eriksson P.G., Schweitzer J.K., Bosch P.J.A., Schreiber U.M., Van Deventer J.L., and Hatton C.J. (1993) –The Transvaal Sequence: an Overview- Journal of African Earth Sciences (16), 25-51.

Eriksson P.G., Hattingh P.J., and Altermann W. (1995) –An Overview of the Geology of the Transvaal Sequence and Bushveld Complex, South Africa- Mineralium Deposita (30), 98-111.

Eriksson P.G., Condie K.C., Tirsgaard H., Mueller W.U., Altermann W., Miall A.D., Aspler L.B., Catuneanu O., and Chiarenzelli J.R. (1998) –Precambrian Clastic Sedimentation Systems- Sedimentary Geology (120), 5-53.

Eriksson P.G., Bose P.K., and Altermann W. (1999) –Variation in Sea Level and Continental Freeboard: Evidence from the Precambrian Volcano-Sedimentary Record- Precambrian Research (97), 137-141.

Eriksson P.G., Mazumder R., Sarkar S., Bose P.K., Altermann W., and Van der Merwe R. (1999) –The 2.7-2.0 Ga Volcano-Sedimentary Record of Africa, India and Australia: Evidence for Global and Local Changes in Sea Level and Continental Freeboard- Precambrian Research (97), 269-302.

Eriksson P.G., Altermann W., Catuneanu O., van der Merwe R., and Bumby A.J. (2001) -Major Influences on the Evolution of the 2.67-2.1 Ga Transvaal Basin, South Africa- Sedimentary Geology (141-142), 205-231.

Eriksson P.G., Martins-Neto M.A., Nelson D.R., Aspler L.B., Chiarenzelli J.R., Catuneanu O., Sarkar S., Altermann W., and Rautenbach C.J. de W. (2001) -An Introduction to Precambrian Basins: Their Characteristics and Genesis- Sedimentary Geology (141-142), 1-35.

Evans D.A.D. (1997) –Stratigraphic, Geochronological, and Paleomagnetic Constraints upon the Neoproterozoic Climatic Paradox- Tectonics (16), 161-171.

Evans D.A.D., Beukes N.J., and Kirschvink J.J. (1997) –Low-Latitude Glaciation in the Paleoproterozoic Era- Nature (386), 262-266.

Evans D.A.D., Li Z.X., Kirschvink J.L., and Wingate M.T.D. (2000) –A High-Quality Mid-Neoproterozoic Paleomagnetic Pole From South China, With Implications For Ice Ages and the Breakup Configuration of Rodinia- Precambrian Research (100), 313-334.

Evans D.A.D., Beukes N.J., and Kirschvink J.J. (2002) –Paleomagnetism of a Lateritic Paleoweathering Horizon and Overlying Paleoproterozoic Red Beds from South Africa: Implications for the Kaapvaal Apparent Polar Wander Path and a Confirmation of Atmospheric Oxygen Enrichment- Journal of Geophysical Research (107, N0.B12), EPM2.1-EPM2.22.

Eyles N., and Clark B.M. (1985) –Gravity-Induced Soft-Sedimentation in Glaciomarine Sequences of the Upper Proterozoic Port Askaig Formation, Scotland-Sedimentology (32), 789-814.

Eyles N., and McCabe A.M. (1989) –Glaciomarine Facies Within Subglacial Tunnel Valleys: the Sedimentary Record of Glacio-Isostatic Downwarping in the Irish Basin-Sedimentology (36), 431-448.

Eyles N., and Young G.M. (1994) –Geodynamic Controls on Glaciation in Earth History- *In*: Earth's Glacial Record; Deynoux M., Miller J.M.G., Domack E.W., Eyles N., Fairchild I.J., Young G.M. Editors, Cambridge University Press, 1-28.

Eyles C.H., and Eyles N. (2000) –Subaqueous Mass Flow Origin for the Lower Permian Diamictites and Associated Facies of the Grant Group, Barbwire terrace, Canning Basin, Western Australia- Sedimentology (47), 343-356.

Eyles N., Eyles C.H., and Miall A.D. (1983) –Lithofacies Types and Vertical Profile Models; an Alternative Approach to the Description and Environmental Interpretation of Glacial Diamict and Diamictite Sequences- Sedimentology (30), 393-410.

Eyles C.H., Eyles N., and Miall A.D. (1985) –Models of Glaciomarine Sedimentation and their Application to the Interpretation of Ancient Glacial Sequences- Paleogeography, Paleoclimatology, Paleoecology (51), 15-84.

Fairchild I.J., Bradby L., and Spiro B. (1994) –Reactive Carbonate in Glacial Systems: a Preliminary Synthesis of it Creation, Dissolution and Reincarnation- *In*: Earth's Glacial Record- Deynoux M, Miller J.M.G., Domack E.W., Eyles N., Fairchild I.J., Young G.M. Editors, Cambridge University Press, 176-192.

Fedo C.M., Eriksson K.A., and Krogstad E.J. (1996) -Geochemistry of the Shales from the Archean (~3.0 Ga) Buhwa Greenstone Belt, Zimbabwe: Implications for Provenance and Source-Area Weathering- Geochimica et Cosmochimica Acta (60), 1751-1763.

Fedo C.M., Young G.M., and Nesbitt H.W. (1997) -Paleoclimatic Control on the Composition of the Paleoproterozoic Serpent Formation, Huronian Supergroup, Canada: a Greenhouse to Icehouse Transition- Precambrian Research (86), 201-223.

Feng R., and Kerrich R. (1990) -Geochemistry of Fine-Grained Clastic Sediments in the Archean Abitibi Greenstone Belt, Canada: Implications for Provenance and Tectonic Setting- Geochimica et Cosmochimica Acta (54), 1061-1081.

Frakes L., and Bolton B. (1992) -Effects of Ocean Chemistry, Sea Level, and Climate on the Formation of Primary Sedimentary Manganese Ore Deposits- Economic Geology (87), 1207-1217.

Gaál G. (1990) -Tectonic Styles of Early Proterozoic Ore Deposition in the Fennoscandian Shield- Precambrian Research (46), 83-114.

Gaál G. (1992) -Global Proterozoic Tectonic Cycles and Early Proterozoic Metallogeny- South African Journal of Geology (95), 80-87.

Gaidos E.J., Nealson K.H., and Kirschvink J.L. (1999) -Life in Ice-Covered Oceans- Science (284), 1631-1633.

Geerthsen K., Maher M.J., and Meyer R. (1991) -The Western Edge of the Griqualand West Basin- A Geophysical Perspective- South African Journal of Geology (94), 96-103.

Genthon C., Barnola J.M., Raynaud D., Lorius C., Jouzel J., Barkov N.I., Korotkevich Y.S., and Kotlyakov V.M. (1987) -Vostok Ice Core: Climatic Response to CO2 and Orbital Forcing Changes over the Last Climatic Cycle- Nature (329), 414-418.

Geobulletin (1995) -Task Group for the Griqualand West Supergroup- (38), 5.

Glasby G.P. (1997) -Fractionation of Manganese from Iron in Archaean and Proterozoic Sedimentary Ores- *In*: Manganese Mineralisation: Geochemistry and Mineralogy of Terrestrial and Marine Deposits; Nicholson K., Hein J.R., Bühn B., and Dasgupta S. Editors, Geological Society Special Publication NO 119, The Geological Society of London, 29-42.

Goodwin A.M., Monster J., and Thode H.G. (1976) –Carbon and Sulfur Isotope Abundances in Archaean Iron-Formations and Early Precambrian Life- Economic Geology (71), 870-891.

Gould D., Rathbone P.A., Kimbell G.S. (1987) –The Geology of the Molopo Farm Complex, Southern Botswana- Bulletin of the Geological Survey of Botswana (23), 178.

Grieve R.A.F. (1994) –Impact: a Natural Hazard in Planetary Evolution- Episodes (17), 9-17.

Griffith T.W., and Anderson J.B. (1989) Climatic Control of Sedimentation in Bays and Fjords of the Northern Antarctic Peninsula- Marine Geology (85), 181-204.

Grobbelaar W.S., Burger M.A., Pretorius A.I., Marais W., and van Niekerk I.J.M. (1995) –Stratigraphic and Structural Setting of the Griqualand West and Olifantshoek Sequences at Black Rock, Boshoek and Rooinekke Mines, Griqualand West, South Africa- Mineralium Deposita (30), 152-161.

Grobler N.J., and Botha B.J.V. (1976) –Pillow-Lavas and Hyaloclastite in the Ongeluk Andesite Formation in a Road-Cutting West of Griquatown, South Africa- Transactions Geological Society of South Africa (79), 53-57.

Gross G.A. (1972) –Primary Features in Cherty Iron-Formations- Sedimentary Petrology (7), 241-261.

Gross G.A., and McLeod C.R. (1980) –A Preliminary Assessment of the Chemical Composition of Iron-Formations in Canada- Canadian Mineralogist (22), 223-229.

Grotzinger J.P., and Kasting J.F. (1993) –New Constraints on Precambrian Ocean Composition- Journal of Geology (101), 235-243.

Grotzinger J.P., and Reed J.F. (1983) –Evidence for Primary Aragonite Precipitation, Lower Proterozoic (1.9 Ga) Rocknest Dolomite, Wopmay Orogen, Northwest Canada- Geology (11), 710-713.

Gurnis M. (1988) –Large-Scale Mantle Convection and the Aggregation and Dispersal of Supercontinents- Nature (332), 695-699.

Gutzmer J., and Beukes N.J. (1995) –Fault-Controlled Metasomatic Alteration of Early Proterozoic Sedimentary Manganese Ores in the Kalahari Manganese Field, South Africa- Economic Geology (90), 823-844.

Gutzmer J., and Beukes N.J. (1996) –Mineral Paragenesis of the Kalahari Manganese Field, South Africa- Ore Geology Reviews (11), 405-428.

Gutzmer J., and Beukes N.J. (1997) –Effects of Mass Transfer, Compaction and Secondary Porosity on Hydrothermal Upgrading of Paleoproterozoic Sedimentary Manganese Ore in the Kalahari Manganese Field, South Africa- Mineralium Deposita (32), 250-256.

Gutzmer J., Beukes N.J., and Yeh H.-W (1997) –Fault-Controlled Metasomatic Alteration of Early Proterozoic Sedimentary Manganese Ore at Mamatwan Mine, Kalahari Manganese Field, South Africa- South African Journal of Geology (100-1), 53-71.

Hälbich I.W., Lamprecht D., Altermann W., and Horstmann U.E. (1992) –A Carbonate-Banded Iron Formation Transition in the Early Proterozoicum of South Africa- Journal of African Earth Science (15), 217-236.

Halliday A.N. (2000) –Terrestrial Accretion rates and the Origin of the Moon- Earth and Planetary Science Letters (176), 17-30.

Hambrey M.J., and Harland W.B. (1981) –Earth's Pre-Pleistocene Glacial Record- Cambridge University Press, Cambridge, 1004pp.

Harland W.B. (1981) –Chronology of Earth's Glacial and Tectonic Record- Journal of the Geological Society, London (138), 197-203.

Harland W.B. (1983) –The Proterozoic Glacial Record- In: Proterozoic Geology: Selected Papers from an International Proterozoic Symposium, Medaris, Byers, Mickelson, Shanks Editors, Geological Society of America Memoirs 161, 279-288.

Harland W.B., and Bidwood D.E.T. (1959) –Paleomagnetism in some Norwegian sparagmites and the Late PreCambrian Ice Age- Nature (134), 1860-1862.

Harland W.B., Herod K.N., and Krinsley D.H. (1966) –The Definition and Identification of Tills and Tillites- Earth-Science Reviews (2), 225-256.

Hart J.K., and Roberts D.H. (1994) –Criteria to Distinguish between Subglacial Glaciotectonic and Glaciomarine Sedimentation, I. Deformation Styles and Sedimentology- Sedimentary Geology (91), 191-213.

Hart J.K., and Roberts D.H. (1998) –Comings and Goings of Global Glaciations on a Neoproterozoic tropical Platform in Namibia- GAS Today (8), 1-9.

Hartnady C.J.H. (1991) –About Turn For Supercontinents- Nature (352), 476-478.

Hoffman P.F. (1999) –Snowball Earth Theory Still Stands- Nature (400), 708.

Hoffman P.F., and Maloof A.C. (1999) –Glaciation: the Snowball Theory Still Holds Water- Nature (397), 384.

Hoffman P.F., and Schrag D.P. (2000) –Snowball Earth- Scientific American (January), 68-75.

Hoffman P.F., and Schrag D.P. (2002) –The Snowball Earth Hypothesis: Testing the Limits of Global Change- Terra Nova (14), 129-155.

Hoffman P.F., Schrag D.P., Halverson G.P., and Kaufman A.J. (1998) –An Early Snowball Earth – Response- Science (282), 1645-1646.

Hoffman P.F., Kaufman A.J., Halverson G.P., and Schrag D.P. (1998) –A Neoproterozoic Snowball Earth- Science (281), 1342-1346.

Hoffman P.F., Kaufman A.J., Halverson G.P., and Schrag D.P. (1998) –A Neoproterozoic Snowball Earth: Response- Science (282), 1345-1346.

Holland H.D. (1972) –The Geologic History of Sea Water-An Attempt to Solve the Problem- Geochimica et Cosmochimica Acta (36), 637-651.

Holland H.D., Lazar B., and McCaffrey M. (1986) –Evolution of the Atmosphere and Ocean- Nature (320), 27-33.

Holland H.D. (2002) –Volcanic Gases, Black Smokers, and the Great Oxidation Event- Geochimica et Cosmochimica Acta (66), 3811-3826.

Horstmann U.E., and Hälbich I.W. (1995) –Chemical Composition of Banded Iron Formations of the Griqualand West Sequence, Northern Cape Province, South Africa, in Comparison With Other Precambrian Iron Formations- Precambrian Research (72), 109-145.

Houston R.S., Lanthier L.R., Karstrom K.K., and Sylvester G.G. (1981) –Early Proterozoic Diamictite of Southern Wyoming- *In*: Hambrey and Harland Editors, Earth's Pre-Pleistocene Glacial Record, Cambridge University Press, Cambridge, 795-799.

Hunt B.G. (1979) –The Effects of Past Variations of the Earth's Rotation Rate on Climate- Nature (281), 188-191.

Hyde W.T., Crowley T.J., Baum S.K., and Peltier W.R. (2000) –Neoproterozoic 'Snowball Earth' Simulations With a Coupled Climate/Ice-Sheet Model- Nature (405), 425-429.

Ingri J., and Pontér C. (1986) –Iron and Manganese Layering in Recent Sediments in the Gulf of Bothnia- Chemical Geology (56), 105-116.

Jahn B., Bertrand-Sarfati J., Morin N., and Macé J. (1990) –Direct Dating of Stromatolite Carbonates from the Schmidtsdrif Formation (Transvaal Dolomite),

South Africa, with Implications on the Age of the Ventersdorp Supergroup- Geology (18), 1211-1214.

JCPDS – Joint Comity on Powder Diffraction Standards (1st Edition) (1974) – Selected powder diffraction data for minerals, Philadelphia, USA, 833pp.

JCPDS – Joint Comity on Powder Diffraction Standards (Search Manual) (1980) – International Center for Diffraction Data, USA, 484pp.

Jenkins G.S., and Frakes L.A. (1998) –GCM Sensitivity test using Increased Rotation rate, Reduced Solar Forcing and Orography to Examine Low Latitude Glaciation in the Neoproterozoic- Geophysical Research Letters (25), 3525-3528.

Jenkins G.S., and Scotese C.R. (1998) –An Early Snowball Earth?- Science (282), 1644-1645.

Karhu J.A., and Holland H.D. (1996) – Carbon Isotopes and the Rise of Atmospheric Oxygen- Geology (24), 867-870.

Kasting J.F. (1987) –Theorical Constraints on Oxygen and Carbon Dioxide Concentrations in the Precambrian Atmosphere- Precambrian Research (34), 205-229.

Kasting J.F. (1991) –Box Models for the Evolution of Atmospheric Oxygen: and Update- Paleogeography, Paleoclimatology, Paleoecology (Global and Planetary Change Section) (97), 125-131.

Kasting J.F., Eggler D.H., and Raeburn S.P. (1993) –Mantle Redox Evolution and the Oxidation State of the Archaean Atmosphere- Journal of Geology (101), 245-257.

Kaufman A.J., Hayes J.M., and Klein C. (1990) –Primary and Diagenetic Control of isotopic Compositions of Iron-Formation Carbonates- Geochimica et Cosmochimica Acta (54), 3461-3473.

Kempf O., Kellerhals P., Lowrie W., and Matter A. (2000) –Paleomagnetic Directions in the Late Precambrian Glaciomarine Sediments of the Mirbat Sandstone Formation, Oman- Earth and Planetary Science Letters (175), 181-190.

Kennedy M.J., Christie-Blick N., and Sohl L.E. (2001) –Are Proterozoic Cap Carbonates and Isotopic Excursions a Record of Gas Hydrate Destabilization Following Earth's Coldest Intervals?- Geological Society of America (29), 443-446.

Kennedy M.J., Christie-Blick N., and Prave A.R. (2001) –Carbon Isotopic Composition of Neoproterozoic Glacial Carbonates as a Test of Paleoceanographic Models for Snowball Earth Phenomena- Geological Society of America (29), 1135-1138.

Kennedy M.J., Christie-Blick N., and Sohl L.E. (2002) –Are Proterozoic Cap Carbonates and Isotopic Excursions a Record of Gas Hydrate Destabilization Following Earth's Coldest Intervals?: Comment and Reply: Reply to Shapiro- Geology (30), 763.

Kennedy M.J., Christy-Blick N., and Sohl L.E. (2002) –Are Proterozoic Cap Carbonates and Isotopic Excursions a Record of Gas Hydrate Destabilization Following Earth's Coldest Intervals?: Reply to Max and Dillon- Geology (30), 762-763.

Kennedy M., Runnegar B., Prave A.R., Hoffman K.H., and Arthur M.A. (1998) – Two or Four Neoproterozoic Glaciations?- Geology (26), 1059-1063.

Kerr R.A. (2000) –An Appealing Snowball Earth That's Still Hard to Swallow- Science (287), 1734-1736.

Key R.M. (1983) –The Geology of the Area Around Gaborone and Lobatse, Kweneng, Kgatleng, Southern and South East Districts- District Memoir Geological Survey Botswana 5, 230pp.

Kiehl J.T., and Dickinson R.E. (1987) –A Study of the Radiative Effects of Enhanced Atmospheric CO_2 and CH_4 on Early Earth Surface Temperatures- Journal of Geophysical Research (92), 2991-2998.

Kimberley M.M. (1989) –Exhalative Origin of Iron Formations- Ore Geology Reviews (5), 13-145.

Kimura H., Abe Y., and Abe-Ouchi A. (2002) –Role of Ocean on Planetary Climate: an Implication for Ancient Mars- Lunar and Planetary Science (33).

Kirschvink J.L. (1992) –Late Proterozoic Low-Latitude Glaciations: the Snowball Earth- *In:* The Proterozoic Biosphere: a Multidisciplinary Study, Schopf J.W. and Klein C. Editors., Cambridge University Press, Cambridge, 51-52.

Kirschvink J.L. (1992) –A Paleogeographic Model for the Vendian and Cambrian Time- *In:* The Proterozoic Biosphere: a Multidisciplinary Study, Schopf J.W. and Klein C. Editors., Cambridge University Press, Cambridge, 569-583.

Kirschvink J.L. (2002) –Quand Tout les Océans étaient Gelés- La Recherche (355), 26-30.

Kirschvink J.L., Gaidos E.J., Bertani L.E., Beukes N.J., Gutzmer J., Maepa L.N., and Steinberger R.E. (2000) –Paleoproterozoic Snowball Earth: Extreme Climatic and Geochemical Change and its Biological Consequences- PNAS (97), 1400-1405.

Klein C. (1983) –Diagenesis and Metamorphism of Precambrian Iron-Formations- *In*: Iron-Formations: Facts and Problems, Trendall A.F., and Morris R.C. Editors Developments in Precambrian Geology 6, Elsevier Science Publication, 417-469.

Klein C., and Beukes N.J. (1989) –Geochemistry and Sedimentology of a Facies Transition from Limestone to Iron-Formation Deposition in the Early Proterozoic Transvaal Supergroup, South Africa- Economic Geology (84), 1733-1774.

Klein C., and Beukes N.J. (1992) –Models for Iron Formation Deposition- *In*: The Proterozoic Biosphere, a Multidisciplinary Study, Schopf J.W. and Klein C. Editors; Cambridge University Press, 147-152.

Klein C., and Beukes N.J. (1993) –Sedimentology and Geochemistry of the Glaciogenic Late Proterozoic Rapitan Iron-Formation in Canada- Economic Geology (88), 542-565.

Klein C, and Bricker O.P. (1977) –Some Aspects of Sedimentary and Diagenetic Environment of Proterozoic Banded Iron-Formation- Economic Geology (72), 1457-1470.

Kleyenstrüber A.S.E. (1984) –The Mineralogy of the Manganese-Bearing Hotazel Formation of the Proterozoic Transvaal Sequence in Griqualand West, South Africa- Transactions Geological Society of South Africa (87), 257-272.

Knoll A.H., Hayes J.M., Kaufman A.J., Swett K., and Lambert I.B. (1986) – Secular Variation in Carbon Isotope Ratios from Upper Proterozoic Successions of Svalbard and East Greenland- Nature (321), 832-838.

Kuhn W.R., Walker J.C.G., and Marshall H.G. (1989) –The Effect on Earth's Surface Temperature from Variations in Rotation rate, Continent Formation, Solar Luminosity, and Carbon Dioxide- Journal of Geophysical Research (94), 11129-11136.

Kump L.R., and Holland H.D. (1992) –Iron in the Precambrian Rocks: Implications for the Global Oxygen Budget of the Ancient Earth- Geochimica et Cosmochimica Acta (56), 3217-3223.

Kurtz D.D. (1981) –Early Proterozoic Diamictites of the Black Hills, South Dakota- *In*: Hambrey and Harland Editors, Earth's Pre-Pleistocene Glacial Record, Cambridge University Press, Cambridge, 800-802.

Lasaga A.C., and Ohmoto H. (2002) - The Oxygen Geochemical Cycle: Dynamics and Stability- Geochimica et Cosmochimica Acta (66), 361-381:

Levin I. (1994) –The Recent State of Carbon Cycling Through the Atmosphere- *In*: Carbon Cycling in the Glacial Ocean: Constraints on the Ocean's Role in Global Change; Zahn R., Pedersen T.F., Kaminski M.A., and Labeyrie L. Editors, NATO ASI Series, Series I: Global Environmental Change, Volume 17, 1-13.

Levrard B., and Laskar J. (2000) –Climate Friction and the Earth's Obliquity-Geophysical Journal International (142), 1-22.

Levrard B. (2003) –Is High Obliquity a Still Plausible Explanation for the Neoproterozoic Low-Latitude Glaciations?- Geophysical Research Abstracts (5).

Li Z-X., Zhang L., Powell C.McA. (1995) –South China in Rodinia: Part of the Missing Link Between Australia-East Antarctica and Laurentia?- Geology (23), 407-410.

Link P.K., Miller J.M.G., Christie-Blick N. (1994) –Glacial-Marine Facies in a Continental Rift Environment: Neoproterozoic Rocks of the Western United States Cordillera- *In*: Earth's Glacial Record; Deynoux M., Miller J.M.G., Domack E.W., Eyles N., Fairchild I.J., Young G.M. Editors, Cambridge University Press, 29-46.

Mackiewicz N.E., Powell R.D., Carlson P.R., Molnia B.F. (1984) –Interlaminated Ice-Proximal Glaciomarine Sediments in Muir Inlet, Alaska- Marine Geology (57), 113-147.

Mangini A., Rutsch H-J., Frank M., Eisenhauer A., and Eckhardt (1994) –Is There a Relationship Between Atmospheric CO2 and Manganese in the Ocean?- *In*: Carbon Cycling in the Glacial Ocean: Constraints on the Ocean's Role in Global Change, Zahn R., Pedersen T.F., Kaminski M.A., and Labeyrie L. Editors, NATO ASI Series, Series I: Environmental Global Change, (17), 87-104.

Manikyamba C., Naqvi S.M., Moeen S., Gnaneshwar Rao T., Balaram V., Ramesh S.L., and Reddy G.L.N. (1997) –Geochemical Heterogeneities of Metagraywackes from the Sandur Schist Belt: Implications for Active Plate Margin Processes- Precambrian Research (84), 117-138.

Marmo J.S., and Ojakangas R.W. (1984) –Lower Proterozoic Glaciogenic Deposits, Eastern Finland- Geological Society of America Bulletin (95), 1055-1062.

Marshall H.G., Walker J.C.G., and Kuhn W.R. (1988) –Long-Term Climate Change and the Geochemical Cycle of Carbon- Journal of Geophysical Research (93), 791-801.

Marthur S.M. (1981) –The Middle Precambrian Gangau Tillite, Bijawar Group, Central India- *In*: Hambrey and Harland Editors, Earth's Pre-Pleistocene Glacial Record, Cambridge University Press, Cambridge, 428-430.

Martin D.McB., Powell C.McA., George A.D. (2000) –Stratigraphic Architecture and Evolution of the Early Paleoproterozoic McGrath Through, Western Australia- Precambrian Research (99), 33-64.

Martin D.McB., Clendenin C.W., Krapez B., and McNaughton (1998) –Tectonic and Geochronological Constraints on Late Archaean and Paleoproterozoic Stratigraphic Correlation Within and Between the Kaapvaal and Pilbara Cratons- Journal of the Geological Society, London (155), 311-322.

Martini J.E.J. (1979) –A Copper-Bearing Bed in the Pretoria Group in Northeastern Transvaal- Geocongress 77: Geological Society of South Africa Special Publications (6), 65-72.

Matsch C.L., and Ojakangas R.W. (1991) –Comparisons in Depositional Style of "Polar" and "Temperate" Glacial Ice: Late Paleozoic Whiteout Conglomerate (West Antarctica) and Late Proterozoic Mineral Fork Formation (Utah)- *In*: Glacial Marine Sedimentation: Paleoclimatic Significance, Anderson J.B., and Ashley G.M. Editors, Geological Society of America Special Papers 261, 191-206.

Max M.D., and Dillon W.P. (2002) –Are Proterozoic Cap Carbonates and Isotopic Excursions a Record of Gas Hydrate Destabilization Following Earth's Coldest Intervals? Comment- Geology (30), 762.

McKay C.P. (2000) –Thickness of Tropical Ice and Photosynthesis on a Snowball Earth- Geophysical Research Letters (27), 2153-2156.

McKerrow W.S., Scotese C.R., and Brasier M.D. (1992) –Early Cambrian Continental Reconstructions- Journal of the Geological Society, London (149), 599-606.

McLennan S.M., and Taylor S.R. (1985) - The Continental Crust: Its Composition and Evolution- Oxford, Blackwell, 312pp.

McLennan S.M., and Taylor S.R. (1991) -Sedimentary Rocks and Crustal Evolution: Tectonic Setting and Secular Trends- Journal of Geology (99), 1-21.

McLennan S.M., Taylor S.R., and Eriksson K.A. (1983) – Geochemistry of Archaean Shales From the Pilbara Supergroup, Western Australia- Geochimica et Cosmochimica Acta (47), 1211-1222.

McLennan S.M., Hemming S.R., Taylor S.R., and Eriksson K.A. (1995) -Early Proterozoic Crustal Evolution : Geochemical and Nd-Pb Isotopic Evidence From Metasedimentary Rocks, South-western North America- Geochimica et Cosmochimica Acta (59), 1153-1177.

Meert J.G., and van der Voo R. (1994) –The Neoproterozoic (1100-540 Ma) Glacial Intervals: No More Snowball Earth?- Earth and Planetary Science Letters (123), 1-13.

Meert J.G., and van der Voo R. (1995) –The Neoproterozoic (1100-540 Ma) Glacial Intervals: No More Snowball Earth?: Reply- Earth and Planetary Science Letters (131), 123-125.

Mertanen S., Halls H.C., Vuollo J.I., Pesonen L.J., and Stepanov V.S. (1999) – Paleomagnetism of 2.44 Ga Mafic Dykes in Russian Karelia, Eastern Fennoscandian Shield- Implications for Continental Reconstructions- Precambrian Research (98), 197-221.

Miall A.D. (1985) –Sedimentation of an Early Proterozoic Continental Margin under Glacial Influence: the Gowganda Formation (Huronian), Elliot Lake Area, Ontario, Canada- Sedimentology (32), 763-788.

Miyano T., and Beukes N.J. (1987) –Physicochemical Environments for the Formation of Quartz-Free Manganese Oxide Ores from the Early Proterozoic Hotazel Formation, Kalahari Manganese Field, South Africa- Economic Geology (82), 706-718.

Moore J.M., Tsikos H., and Polteau S. (2001) –Deconstructing the Transvaal Supergroup, South Africa: Implications for Paleoproterozoic Paleoclimate Models- Journal of African Earth Sciences (33), 437-444.

Morel P., and Irving E. (1978) –Tentative Paleocontinental Maps for the Early Phanerozoic and Proterozoic- Journal of Geology (86), 535-561.

Morris W.A. (1977) –Paleomagnetism of the Gowganda and Chibougamau Formations: Evidence for 2,200 My Old Folding and Remagnetization Event of the Southern Province- Geology (5), 137-140.

Morris R.C. (1993) Genetic Modelling for Banded Iron-Formation of the Hamersley Group, Pilbara Craton, Western Australia- Precambrian Research (60), 243-286.

Mustard P.S., and Donaldson J.A. (1987) –Early Proterozoic Ice-Proximal Glaciomarine Deposition: the Lower Gowganda Formation at Cobalt, Ontario, Canada- Geological Society of America Bulletin (98), 337-387.

Myers R.E., Cawthorn R.G., McCarthy T.S., and Anhaeusser C.R. (1987) Fundamental Uniformity in the Trace Element Patterns of the Volcanics of the Kaapvaal Craton from 3000 to 2100 Ma: Evidence for the Lithospheric Origin of These Continental Tholeiites- Geological Society of South Africa Special Publications (33), 315-326.

Nel C.J., Beukes N.J., and De Villiers J.P.R. (1986) -The Mamatwan Manganese Mine of the Kalahari Manganese Field- *In*: Anhaeusser C.R. and Maske S. Editors, Mineral deposits of Southern Africa : Johannesburg, Geological Society of South Africa, 963-978.

Nel L.T. (1929) -The Geology of the Postmasburg Manganese Deposits and the Surrounding Country- Geological Survey of South Africa, an Explanation of the Geological Map, 109pp.

Nelson D.R., Trendall A.F., and Altermann W. (1999) –Chronological Correlations between the Pilbara and Kaapvaal Cratons- Precambrian Research (97), 165-189.

Nesbitt H.W., and Young G.M. (1982) -Early Proterozoic Climates and Plate Motions Inferred from Major Element Chemistry of Lutites- Nature (299), 715-717.

Nesbitt H.W., Young G.M., McLennan S.M., Keays R.R. (1996) -Effects of Chemical Weathering and Sorting on the Petrogenesis of Siliclastic Sediments, with Implications for Provenance Studies- Journal of Geology (104), 525-542.

Newman M.J., and Rood R.T. (1977) –Implications of Solar Evolution for the Earth's Early Atmosphere- Science (198), 1035-1037.

Nichols G. (1999) –Sedimentology and Stratigraphy- Blackwell Science Ltd, 355pp.

Norrish K., and Hutton J.T. (1969) –An Accurate X-Ray Spectrography Method for the Analysis of a Wide Range of Geological Samples- Geochimica et Cosmochimica Acta (33), 431-453.

Oberholzer J.D., and Eriksson P.G. (2000) –Subaerial Volcanism in the Paleoproterozoic Hekpoort Formation (Transvaal Supergroup), Kaapvaal Craton- Precambrian Research (101), 193-210.

Oglesby R.J., and Ogg J.G. (1998) –The Effect of Large Fluctuations in Obliquity on Climates of the Late Proterozoic- Paleoclimates (264), 293-336.

Ovenshine A.T. (1970) –Observations of Iceberg Rafting in Glacier Bay, Alaska, and the Identification of Ancient Ice-Rafted Deposits- Geological Society of America Bulletin (81), 891-894.

Pais M.A., Le Mouël J.L., lambeck K., and Poirier J.P. (1999) –Late Precambrian Paradoxical Glaciation and Obliquity of the Earth – A Discussion of Dynamical Constraints- Earth and Planetary Science Letters (174), 155-171.

Park J.K. (1994) –Paleomagnetic Constraints on the Position of Laurentia from Middle Neoproterozoic to Early Cambrian Times- Precambrian Research (69), 95-112.

Park J.K. (1997) –Paleomagnetic Evidence for Low-Latitude Glaciation During Deposition of the Neoproterozoic Rapitan Group, Mackenzie Mountains, N.W.T., Canada- Canadian Journal of Earth Sciences (34), 34-49.

Perry E.C., and Ahmad S.N. (1981) –Oxygen and Carbon Isotope Geochemistry of the Krivoy Rog Iron Formation, Ukrainian SSR- Lithos (14), 83-92.

Pickard A.L. (2003) –SCHRIMP U-Pb Zircon Ages for the Paleoproterozoic Kuruman Iron Formation, Northern Cape Province, South Africa: Evidence for Simultaneous BIF Deposition on Kaapvaal and Pilbara Cratons- Precambrian Research (125), 275-315.

Pisarevsky S.A., Li Z.X., Grey K., and Stevens M.K. (2001) –A Paleomagnetic Study of Empress 1A, a Stratigraphic Drillhole in the Officer Basin: Evidence for a Low-Latitude Position of Australia in the Neoproterozoic- Precambrian Research (110), 93-108.

Polteau S. (2000) –Stratigraphy and Geochemistry of the Makganyene Formation, Transvaal Supergroup, South Africa- unpublished M.Sc. Thesis, Rhodes University, Grahamstown, South Africa, 146pp.

Polteau S., and Moore J.M. (1999) –Stratigraphy and Geochemistry of the Makganyene Formation, Transvaal Supergroup, South Africa- Journal of African Earth Sciences (28A), 65.

Polteau S., and Moore J.M. (2002) –Genetic Relationships Between the Glacial Makganyene Formation and the Kalahari Manganese Field in the Transvaal Supergroup, Griqualand West Basin, South Africa- 16th International Sedimentological Congress Abstract Volume, 296.

Poulsen C.J., Jacob R.L., Pierrehumbert R.T., and Huynh T. (2002) –Testing Paleogeographic Controls on a Neoproterozoic Snowball Earth- Geophysical Research Letters (29), 1-4.

Powell R.D. (1984) –Glacimarine Processes and Inductive Lithofacies Modelling of Ice Shelf and Tidewater Glacier Sediment Based on Quaternary Examples- Marine Geology (57), 1-52.

Powell R.D. (1991) –Grounding-Line Systems as Second-Order Controls on Fluctuations of Tidewater Termini of Temperate Glaciers- *In*: Glacial Marine Sedimentation: Paleoclimatic Significance, Anderson J.B., and Ashley G.M. Editors, Geological Society of America Special Paper 261, 75-94.

Powell R.D., and Molnia B.F. (1989) –Glaciomarine Sedimentary Processes, Facies Morphology of the South-Southeast Alaska Shelf and Fjords- Marine Geology (85), 359-390.

Prévot M., Mattern E., Camps P., and Daignières M. (2000) –Evidence for a 20° tilting of the Earth's Rotation Axis 110 Million Years Ago- Earth and Planetary Science Letters (179), 517-528.

Raymo M.E. (1991) –Geochemical Evidence Supporting Chamberlin, T., C. Theory of Glaciation- Geology (19), 344-347.

Reczko B.F.F., Oberholzer J.D., Res M., Eriksson, P.G., and Schreiber U.M. (1995) -A Re-Evaluation of the Volcanism of the Palaeoproterozoic Pretoria Group (Kaapvaal Craton) and a Hypothesis on Basin Development- Journal of African Earth Sciences (21), 505–519.

Rogers A.W., and du Toit A.L. (1909) –An Introduction to the Geology of the Cape Colony- Longmans, Green, and Co. Editors, 491pp.

Romer R.L., and Bau M. (1998), Chinese Science Bulletin Supplement (43), 109.

Roser B.P., and Korsch R.J. (1988) –Provenance Signatures of Sandstone-Mudstone Suites Determined Using Discriminant Function Analysis of Major-Element Date- Chemical Geology (67), 119-139.

Roy S. (1988) -Manganese Metallogenesis: a Review- Ore Geology Reviews (4), 155-170.

Roy S. (1992) –Environments and Processes of Manganese Deposition- Economic Geology (87), 1218-1236.

Runnegar B. (2000) –Loophole for Snowball Earth- Nature (405), 403-404.

Rye R., Kuo P.H., and Holland H.D. (1995) –Atmospheric Carbon Dioxide Concentrations before 2.2 Billion Years Ago- Nature (378), 603-605.

SACS (1980) -Stratigraphy of South Africa- Part 1 (Comp. L.E.Kent). Lithostratigraphy of the Republic of South Africa, South West Africa/Namibia and

the Republic of Bophuthatswana, Transkei and Venda. Handbook Geological Survey South Africa (8), 690pp.

Schidlowski M. (1988) –A 3,8000-Million-Year Isotopic Record of Life From Carbon in Sedimentary Rocks- Nature (333), 313-318.

Schissel D., and Aro P. (1992) –The Major Early Proterozoic Sedimentary Iron and Manganese Deposits and Their Tectonic Settings- Economic Geology (87), 1367-1374.

Schmidt P.W., and Williams G.E. (1995) –The Neoproterozoic Climatic Paradox: Equatorial Paleolatitude for Marinoan Glaciation Near Sea Level in South Australia-Earth and Planetary Science Letters (134), 107-124.

Schreiber U.M. (1990) –A Paleoenvironmental Study of the Pretoria Group in the Eastern Transvaal- Unpublished PhD Thesis, University of Pretoria.

Schreiber U.M., Eriksson P.G., van der Neut M., and Snyman C.P. (1992) – Sedimentary Petrography of the Early Proterozoic Pretoria Group, Transvaal Sequence, South Africa: Implications for Tectonic Setting- Sedimentary Geology (80), 89-103.

Schwarzbach M. (1963) –Climates of the Past: an Introduction to Paleoclimatology-Fairbridge R.W. Editor, The University Series in Geology, D. Van Nostrand Company, Ltd, 328pp.

Shapiro R.S. (2002) –Are Proterozoic Cap Carbonates and Isotopic Excursions a Record of Gas Hydrate Destabilization Following Earth's Coldest Intervals?: Comment and Reply- Geology (30), 761.

Simonson B.M., and Hassler S.W. (1996) –Was the Deposition of Large Precambrian Iron Formations Linked to Major Marine Transgressions?- Journal of Geology (104), 665-676.

Spencer A.M. (1985) –Mechanisms and Environments of Deposition of Late Precambrian Geosynclinal Tillites: Scotland and East Greenland- Paleogeography, Paleoclimatology, Paleoecology (51), 143-157.

Sohl L.E., Christie-Blick N., and Kent D.V. (1999) –Paleomagnetic Polarity reversals in the Marinoan (ca. 600 Ma) Glacial Deposits of Australia: Implications for the Duration of Low-Latitude Glaciation in the Neoproterozoic Time- Geological Society of America Bulletin (111), 1120-1139.

Sonnett C.P., Kvale E.P., Zakharian A., Chan M.A., Demko T.M. (1996) –Late Proterozoic and Paleozoic Tides, Retreat of the Moon, and Rotation of the Earth- Science (273), 100-104.

Stewart T.G. (1991) –Glacial Marine Sedimentation from Tidewater glaciers in the Canadian High Arctic- *In*: Glacial Marine Sedimentation: Paleoclimatic Significance, Anderson J.B., and Ashley G.M. Editors, Geological Society of America Special Paper 261, 95-106.

Stowe C.W. (1986) –Synthesis and Interpretation of Structures Along the North-Eastern Boundary of the Namaqua Metamorphic Province, South Africa- South African Journal of Geology (89), 185-198.

Strand K.O., and Laajoki K. (1993) –Paleoproterozoic Glaciomarine Sedimentation in an Extensional Tectonic Setting: the Honkala Formation, Finland- Precambrian Research (64), 253-271.

Styvinski J.P.M. (1989) –On the Deposition of Sediment within Glacier-Influenced Fjords: Oceanographic Controls- Marine Geology (85), 301-329.

Symons D.T.A. (1975) –Huronian Glaciation and Polar Wander from the Gowganda Formation, Ontario- Geology (June), 303-306.

Sumner D.Y., and Bowring S.A. (1996) –U-Pb Geochronologic Constraints on the Deposition of the Campbellrand Subgroup, Transvaal Supergroup, South Africa- Precambrian Research (79), 25-36.

Taussig D., and Maiden K. (1986) –Stratabound Copper Mineralisation in the Duitschland Formation, Transvaal Basin- Geocongress 86 (Johannesburg, South Africa), Abstracts, 545-547.

Taylor G., Eggleton R.A., Holzhauer C.C., Maconachie L.A., Gordon M., Brown M.C., and McQueen K.G. (1992) –Cool Climate Lateritic and Bauxitic Weathering- Journal of Geology (100), 669-677.

Thatcher E.C., and associates (1993) –Photogeology and Landsat-TM Interpretation Sishen-Postmasburg-Wolhaarkop-Rooinekke Area, Northern Cape Province- on behalf of Associated Manganese Mines of South Africa LTD, 128pp.

Tinker J., de Wit M., and Grotzinger J. (2002) –Seismic Stratigraphic Constraints on Neoarchaean-Paleoproterozoic Evolution of the Western Margin of the Kaapvaal Craton, South Africa- South African Journal of Geology (105), 107-134.

Towe K.M. (1991) –Aerobic Carbon Cycling and Cerium Oxidation: Significance for Archaean Oxygen Levels and Banded-Iron Formation Deposition- Global and Planetary Changes (5), 113-123.

Trendall A.F. (1976) –Striated and Faceted Boulders from Turee Creek Formation – Evidence for a Possible Huronian Glaciation on the Australian Continent- Western Australian Geological Survey Annual Report (1975), 88-92.

Trendall A.F. (1981) –The Lower Proterozoic Meteorite Bore Member, Hamersley Basin, Western Australia- *In*: Hambrey and Harland Editors, Earth's Pre-Pleistocene Glacial Record, Cambridge University Press, Cambridge, 555-559.

Trendall A.F., and Blockley J.G. (1970) –The Iron Formations of the Precambrian Hamersley Group, Western Australia- Western Australian Geological Survey Bulletin (119), 366pp.

Trendall A.F., Nelson D.R., de Laeter J.R., and Hassler S. (1998) –Precise U-Pb Zircon Ages from the Marra Mamba Iron Formation and the Wittenoom Formation, Hamersley Group, Western Australia- Australian Journal of Earth Sciences (45), 137-142.

Truter F.C., Wasserstein B., Botha P.R., Visser D.L.J., Boardman L.G., and Paver G.L. (1938) –The Geology and Mineral Deposits of the Oliphant Hoek Area-Geological Survey of South Africa, Explanation Sheet No173, 144pp.

Tsikos H. (1994) –The Mineralogy and Geochemistry of the Voëlwater Banded Iron-formation, Northern Cape Province Unpublished M.Sc. Thesis, Rhodes University, Grahamstown, South Africa.

Tsikos H. (1999) –Petrographic and Geochemical Constraints on the Origin and Post-Depositional History of the Hotazel Iron-Manganese Deposits, Kalahari Manganese Field, South Africa- PhD Thesis unpublished, Rhodes University, Grahamstown, South Africa, 217pp.

Tsikos H., and Moore J.M. (1997) –Petrography and Geochemistry of the Paleoproterozoic Hotazel Iron-Formation, Kalahari Manganese Field, South Africa: Implications for Precambrian Manganese Metallogenesis- Economic Geology (92), 87-97.

Tsikos H., and Moore J.M. (1998) –The Kalahari Manganese Field: an Enigmatic Association of Iron and Manganese- South African Journal of Geology (101), 287-290.

Tsikos H., Moore J.M., and Harris C. (1998) –Geochemistry of the Paleoproterozoic Mooidraai Formation: Fe-Rich Limestone as End Member of Iron Formation Deposition, Kalahari Manganese Field, Transvaal Supergroup, South Africa- Journal of African Earth Sciences (32), 19-27.

Urban H., Stribrny B., and Lippolt H. (1992) –Iron and Manganese Deposits of the Urucum District, Mato Grosse do Sul, Brazil- Economic geology (87), 1375-1392.

Veizer J. (1992) –Life and the Rock Cycle- Nature (359), 587-588.

Visser D.J.L. (1944) –Stratigraphic Features and Tectonics of Portions of Bechuanaland and Griqualand West- Transactions Geological Society of South Africa (47), 197-254.

Visser D.J.L. (1958) –The Geology and Mineral Deposits of the Griquatown Area, Cape Province- Geological Survey of South Africa, Explanation Sheet No175, 72pp.

Visser J.N.J. (1971) –The Deposition of the Griquatown Glacial Member in the Transvaal Supergroup- Transactions of the Geological Society of South Africa (74), 187-199.

Visser J.N.J. (1981) –The Mid-Precambrian Tillite in the Griqualand West and Transvaal Basins, South Africa- *In*: Hambrey and Harland Editors, Earth's Pre-Pleistocene Glacial Record, Cambridge University Press, Cambridge, 180-184.

Visser J.N.J. (1994) –The Interpretation of Massive Rain-Out Debris-Flow Diamictites from the Glacial Marine Environment- *In*: Earth's Glacial Record; Deynoux M., Miller J.M.G., Domack E.W., Eyles N., Fairchild I.J., Young G.M. Editors, Cambridge University Press, 226pp.

Visser J.N.J. (1999) –Lithostratigraphy of the Makganyene Formation (Postmasburg Group)- South African Committee for Stratigraphy, Lithostratigraphic Series No 34, 1-7.

Von Brunn V., and Gold D.J.D. (1993) –Diamictite in the Archaean Pongola Sequence of Southern Africa- Journal of African Earth Sciences (74), 187-199.

Walker J.C.G. (1982) –Climatic Factors on the Archaean Earth- Paleogeography, Paleoclimatology, Paleoecology (40), 1-11.

Walker J.C.G., and Brimblecombe P. (1985) –Iron and Sulfur in the Pre-Biologic Ocean- Precambrian Research (28), 205-222.

Walker J.C.G., and Zahnle K.J. (1986) –Lunar Nodal Tide and Distance to the Moon during the Precambrian- Nature (320), 600-602.

Walter M.R., and Bauld J. (1983) –The Association of Sulphate Evaporites, Stromatolitic Carbonates and Glacial Sediments: Examples from the Proterozoic of Australia and the Cainozoic of Antarctica- Precambrian Research (21), 129-148.

Walvaren F., and Martini J. (1995) –Zircon Pb-Evaporation Age Determinations of the Oak Tree Formation, Chuniespoort Group, Transvaal Sequence: Implications for Transvaal-Griqualand West Basin Correlations- South African Journal of Geology (98), 58-67.

Williams G.E. (1975) –Late Precambrian Glacial Climate and the Earth's Obliquity-Geological Magazine (112), 441-465.

Williams G.E. (1979) –Sedimentology, Stable-Isotope Geochemistry and Paleoenvironment of Dolostones Capping Late Precambrian Glacial Sequences in Australia- Journal of the Geological Society of Australia (26), 377-386.

Williams G.E. (1989) –Late Precambrian Tidal Rhythmites in South Australia and the History of the Earth's Rotation- Journal of the Geological Society, London (146), 97-111.

Williams G.E. (1993) –History of the Earth's Obliquity- Earth Science Reviews (34), 1-45.

Williams G.E. (1994) –The Enigmatic Late Proterozoic Glacial Climate: an Australian Perspective- *In* :Earth's Glacial Record; Deynoux M., Miller J.M.G., Domack E.W., Eyles N., Fairchild I.J., and Young G.M. Editors, Cambridge University Press, 146-164.

Williams G.E. (1997) –Precambrian length of Day and the Validity of Tidal Rhythmite Paleotidal Values- Geophysical Research Letters (24), 421-424.

Williams G.E. (1998) –Precambrian Tidal and Glacial Clastic Deposits: Implications for Precambrian Earth-Moon Dynamics and Paleoclimate- Sedimentary Geology (120), 55-74.

Williams G.E. (2000) –Geological Constraints on the Precambrian History of Hearth's Rotation and the Moon's Orbit- Reviews of Geophysics (38), 37-59.

Williams G.E., Schmidt P.W., and Embleton B.J.J. (1995) –Comments on 'The Neoproterozoic (1000-540 Ma) Glacial Intervals: No More Snowball Earth?' by Joseph G. Meert and Rob van der Voo- Earth and Planetary Science Letters (131), 115-122.

Williams G.E., Kasting J.F., and Frakes L.A. (1998) –Low-Latitude Glaciation and Rapid Changes in the Earth's Obliquity Explained by Obliquity-Oblateness Feedback- Nature (396), 453-455.

Wingate M.T.D. (1998) –A Paleomagnetic Test of the Kaapvaal Craton-Pilbara (Vaalbara) Connection at 2.78Ga- South African Journal of Geology (101), 257-274.

Winter H. de la (1989) –A Tectonic Classification of Certain South African Depositional Basins and Criteria for Recognition of Major Unconformity-Bounded Sequences- South African Journal of Geology (92), 167-182.

Woodhead J.D., Hergt J.M., and Simonson B.M. (1998) –Isotopic Dating of an Archaean Bolide Impact Horizon, Hamersley Basin, Western Australia- Geology (26), 47-50.

Wronkiewicz D.J., and Condie K.C. (1987) -Geochemistry of Archean Shales from the Witwatersrand Supergroup, South Africa: Source-Area Weathering and Provenance- Geochimica et Cosmochimica Acta (51), 2401-2416.

Worsley T.R., Nance D., and Moody J.B. (1984) –Global Tectonics and Eustasy for the Past 2 Billion Years- Marine Geology (58), 373-400.

Wronkiewicz D.J., and Condie K.C. (1989) -Geochemistry and Provenance of Sediments from the Pongola Supergroup, South Africa: Evidence for a 3.0-Ga-Old Continental Craton- Geochimica et Cosmochimica Acta (53), 1537-1549.

Yanjing C., and Yongchao Z. (1997) –Geochemical Characteristics and Evolution of REE in the Early Precambrian Sediments: Evidence from the Southern Margin of the North China Craton- Episodes (20), 109-116.

Young G.M. (1976) –Iron-Formation and Glaciogenic Rocks of the Rapitan Group, Northwest Territories, Canada- Precambrian Research (3), 137-158.

Young G.M. (1991) –The Geological Record of Glaciation; Relevance to the Climatic History of Earth- Geoscience Canada (18), 100-108.

Young G.M. (1995) –Are Neoproterozoic Glacial Deposits Preserved on the Margins of Laurentia Related to the fragmentation of Two Supercontinents?- Geology (23), 153-156.

Young G.M. (2002) –Stratigraphic and Tectonic Settings of Proterozoic Glaciogenic Rocks and Banded Iron-Formations: Relevance to the Snowball Earth Debate- Journal of African Earth Sciences (35), 451-466.

Young G.M., and McLennan S.M. (1981) –Early Proterozoic Padlei Formation, Northwest Territories, Canada- *In*: Hambrey and Harland Editors, Earth's Pre-Pleistocene Glacial Record, Cambridge University Press, Cambridge, 790-794.

Young G.M., and Nesbitt H.W. (1985) –The Gowganda Formation in the Southern Part of the Huronian Outcrop Belt, Ontario, Canada: Stratigraphy, Depositional Environments and Regional Tectonic Significance- Precambrian Research (29), 265-301.

Zieliński T., and Loon van A.J. (1996) –Characteristics and Genesis of Moraine-Derived Flowtill Varieties- Sedimentary Geology (101), 119-143.